

Two Methods for Three - Dimensional Culture: Addition of
Exogenous ECM Components and Capture of Endogenous
ECM Components

Sarah McGinlay

Student ID: 14316277

Supervisors: Prof C Merry

Prof A Mata

Dr V Sottile

ABSTRACT

The culture of cells in hydrogels and scaffolds that mimic *in vitro* tissue has become increasingly popular now there is an understanding of how important the role of ECM is in supporting and directing the behaviour of cells. As such there is a wide range of culture methods varying in complexity, that are available, each of which varies in complexity. From synthetic hydrogels with tuneable mechanical properties or natural (polysaccharide or protein) hydrogels that allow for natural interactions with ECM components, that more accurately represent the composition of tissues and cells. This thesis looks at two different models of hydrogels, with opposite approaches. First, was an adipogenic model that used a top-down approach, where a native ECM protein (collagen) was used to form a natural hydrogel. Research into adipogenesis is important as obesity becomes more prevalent. Models that represent adipogenesis are important to combat the rise in obesity as they can become high content screening models for anti-obesity drugs. This model used an alginate fibre surrounding a collagen I core with mouse mesenchymal stem cells. Over the course of two weeks, this was found to be a viable model, that supported adipogenesis of mesenchymal stem cells. The creation of the fibre was simple, but requires optimisation to prevent alginate from blocking equipment.. The second model was developed using a bottom-up approach where synthetic self-assembling peptides were selected for the presence of a charge and then used to make a hydrogel. The peptide amphiphiles were designed to have increasing lysine residues (K2, K3 and K4) or a negative glutamic acid residue for a PA with a negative charge (E3). The presence of a charge was theorised to sequester native ECM components. Human induced pluripotent stem cells were in clusters on top of the range of PA hydrogels, a neutral hydrogel (FEFEFKFK) and Matrigel. This synthetic PA hydrogels (K2 and K3) sequestered a glycosaminoglycan secreted by human induced pluripotent stem cells. There was a change in cellular behaviour when cultured on hydrogels with different charges, there was increased attachment to the hydrogel on the negative PA (E3) hydrogel, than all others except Matrigel. There was also increased proliferation on the most positive PA (K4) hydrogel than all other hydrogels except Matrigel.

Together this suggested that differently charged hydrogels may be able to create different ECM environments through the sequestration of natively secreted ECM components. The charged PA hydrogels have the potential to form a complex ECM with a large range of ECM components, that cannot be replicated by human design. In addition, the synthesised ECM components will be able to be modified by the cells throughout their lifetime, thereby replicating natural processes. This model could therefore be used to produce representative models for use in a wide range of systems many applications, for example drug testing, disease research and tissue regeneration.

Table Of Contents

Chapter 1. Introduction	1
1.1.1 Human Induced Pluripotent Stem Cells.....	3
1.2 The extracellular matrix.....	5
1.3 Three-dimensional cell cultures.....	11
1.4 Thesis aims objectives	22
Chapter 2. Alginate fibre to culture stem cells during adipogenic differentiation.	24
2.1 Introduction.....	25
2.1.1 Obesity.....	25
2.1.2 Adipocytes.....	25
2.1.3 Mesenchymal stem cells.....	29
2.1.4 Adipogenesis	29
2.1.5 Extra cellular matrix of adipose tissue.....	31
2.1.6 Current 2D culture of adipocytes	35
2.1.7 The 3D culture of Adipocytes.....	36
2.1.8 Alginate.....	39
2.1.9 Fibres as an adipogenic culture model	43
2.1.10 Chapter aims	46
2.2 Materials and methods	47
2.2.1 Cell Culture.....	47
2.2.2 Laminar flow soft-core fibre production.....	47
2.2.3 Cell Seeding.....	49
2.2.4 Cell Metabolic Assays	50
2.2.5 Live and dead imaging	50
2.2.6 Lipid staining.	51
2.2.7 Removing cells from fibres.....	51

2.2.8 Cryosectioning.....	53
2.2.9 Total corrected fluorescence intensity using Fiji ImageJ	54
2.2.10 Statistics	54
2.2.11 Data collection.....	55
2.3 Hypothesis	58
2.4 Results	60
2.4.1 Characterisation of the fibre for the technical requirements.....	61
2.4.2 Viability of Mesenchymal stem cells in a soft-core fibre.	64
2.4.3 Proliferation in the fibres.....	70
2.4.4 Adipogenesis within the fibre	72
2.4.5 Cryosectioning to assess the lipid content within the fibres	79
2.4.6 Optimisation of the alginate removal method.....	82
2.4.7 Conclusions	89
2.5 Discussion	90
2.5.1 Production of alginate fibre	90
2.5.2 Viability of MSCs within the fibre	92
2.5.3 Proliferation of MSCs within the fibre	93
2.5.4 Adipogenesis in fibres.....	94
2.5.5 Swelling of the fibres	96
2.5.6 Removal of MSCs from fibres.....	97
2.6 Future work	99
2.6.1 Optimisation production method.....	99
2.6.2 Analysis of adipocytes within fibre	100
2.6.3 Rheology	101
2.6.4 Expansion of the fibre's applications.....	102
2.6.5 Co-culture within the fibre.....	103
2.6.6 The fibre as a high content screening model	104

2.7 Conclusion	106
-----------------------------	------------

Chapter 3. Peptide amphiphile scaffolds and human induced pluripotent stem cells

.....	107
-------	------------

3.1 Introduction	108
-------------------------------	------------

3.1.1 Peptide amphiphiles	109
---------------------------------	-----

3.1.2 Native expression of ECM and sequestration	116
--	-----

3.1.3 ECM proteins expressed by hiPSCs.....	118
---	-----

3.1.4 Hyaluronic Acid.....	119
----------------------------	-----

3.1.5 Biosynthesis of GAGs	120
----------------------------------	-----

3.1.6 GAGs in stem cells	122
--------------------------------	-----

3.1.7 Chapter aims	123
--------------------------	-----

3.2 Materials and methods	126
--	------------

3.2.1 Peptide amphiphiles	126
---------------------------------	-----

3.2.2 E3 hydrogel for the encapsulation of hiPSC clusters	126
---	-----

3.2.3 hiPSC culture on vitronectin with E8	127
--	-----

3.2.4 hiPSC cluster formation	127
-------------------------------------	-----

3.2.5 Optimisation of hiPSC encapsulation in E3 hydrogel.....	127
---	-----

3.2.6 The creation of heatmaps	128
--------------------------------------	-----

3.2.7 Optimisation of PA hydrogels.....	129
---	-----

3.2.8 Self-assembling peptide FEFEKFK	129
---	-----

3.2.9 Size test of Cell Clusters	130
--	-----

3.2.10 Preparation of PA, FEFEKFK, and Matrigel Hydrogels.....	131
--	-----

3.2.11 Culture of hiPSCs on top of PA, FEFEKFK and Matrigel hydrogels	132
---	-----

3.2.12 Cross-sectional area of the hiPSC	132
--	-----

3.2.13 Distance from the hiPSC clusters to the furthest cell removed	132
--	-----

3.2.14 Retention of clusters on hydrogel	132
--	-----

3.2.15 Immunostaining of PA gels.....	133
---------------------------------------	-----

3.2.16 Statistics	133
3.3 Hypothesis	137
3.4 Results	142
3.4.1 Optimisation of cell clusters encapsulated in E3 hydrogels.....	142
3.4.2 Optimization of PA hydrogels for 2D culture	156
3.4.3 Optimisation K PAs	159
3.4.4 Optimisation E3 PA hydrogel	167
3.4.5 PA hydrogels their pH values	173
3.4.6 Optimisation of cell cluster size	175
3.4.7 Observations of the clusters cultured upon differently charged hydrogels	187
3.4.8 Observed differences in cells escaping from the clusters between hydrogels.	201
3.4.9 Identification of ECM components secreted by hiPSCs cultured on hydrogels	210
3.5 Discussion	214
3.5.1 The encapsulation of hiPSC clusters in E3 PA.....	214
3.5.2 Toxicity of E3 to the hiPSCs	214
3.5.3 Gelation by CaCl ₂	219
3.5.4 Formulations of PA hydrogels	220
3.5.5 pH of PA hydrogels	222
3.5.6 Size for hiPSC clusters	223
3.5.7 Viability of hiPSC clusters on the hydrogels.....	225
3.5.8 The sequestration of GAGs and ECM proteins and differences in behaviour.....	225
3.6 Further work.....	237
3.6.1 Broader investigation into the sequestered matrix components	237
3.6.2 Rheology	239
3.6.3 Spontaneous differentiation	240
3.6.4 Additional complexity to the PA hydrogel	242
3.6.5 Encapsulation of hiPSC clusters in PA hydrogels.....	243

3.7 Conclusion	243
Chapter 4. References	245
Chapter 5. Appendix	290

Figure List

Figure 1. Embryonic stem cells before differentiation into the three germ lineages.	3
Figure 2. Overview of Human Induced Pluripotent Stem Cells (hiPSCs).....	4
Figure 3. A graphical representation of an ECM surrounding the endothelial cells.	7
Figure 4. Three dimensional hydrogels methods that can be used to replicate the ECM for cell culture.	15
Figure 5. The differing approaches to hydrogel design and development, within this work.	23
Figure 6. Graphical representation of the three adipocytes types.....	26
Figure 7. A simplified representation of the control of adipogenesis.....	30
Figure 8. A graphical representation of the ECM surrounding the adipocytes during a month long culture in male mice.	34
Figure 9. The structure of alginate residues and their bonds with calcium ions.	41
Figure 10. Diagrammatic representation of extrusion or laminar flow hydrogel production.	45
Figure 11. A graphical depiction of the creation of the fibre.	49
Figure 12. A flow chart detailing the method to optimise the removal of the cells from the fibres.	53
Figure 13. Flow chart demonstrating the collection of data points	57
Figure 14. A graphical representation of the benefits to a soft-core fibre to culture adipocytes.	59
Figure 15. The technical requirements the hydrogel fibre needs to meet to be a potential 3D model for adipogenesis.	61
Figure 16. Live and dead staining of the cells cultured in fibres (3D – lower panel) and culture plastic (2D – upper panel.	67
Figure 17. Fluorescence quantification of live and dead staining.	68
Figure 18. Metabolic assay assessing the effect of culture type.	69
Figure 19. The fibres produced lipid filled adipocytes and with an increasing number of adipocytes and lipids over the days cultured.	74
Figure 20. Enlarged images of the increasing number of adipocytes and lipids over the days cultured.	75
Figure 21. Adipogenesis in the fibres when the inner core containing MSCs was interrupted.	76
Figure 22. ORO assessment of lipid content was not a viable measure for use on the fibres.	78
Figure 23. MSCs were stained within the sectioned fibres, but lipid drop-lets could not be.	81

Figure 24. Optimisation of sodium citrate concentrations for alginate removal.	83
Figure 25. Optimisation of MSC removal from fibre.	86
Figure 26. The use of 75mM sodium citrate and manual pipetting was the current optimised cell retrieval method for maintaining adipogenic differentiation.	87
Figure 27. Graphical representation of the nano organisation of PAs to form hydrogels.	114
Figure 28. The methods to produce the 3D hydrogels in use.	115
Figure 29. The building blocks of GAGs.....	122
Figure 30. A diagramic representation showing the hypothesis that charged PAs can capture proteins and glycans secreted by hiPSC clusters.	125
Figure 31. Overview of all protocols with hiPSC clusters.	136
Figure 32. The experimental composition for the optimisation of hiPSC cluster viability when encapsulated in E3 droplet hydrogels.....	144
Figure 33. Categorisation of hiPSC Clusters.	146
Figure 34. Cell viability in phenotype1 and 2 clusters.	147
Figure 35. Optimisation of hiPSCs viability when encapsulated in E3 hydrogels.	149
Figure 36. The protocol for further optimisation of E3 hiPSC cluster encapsulation.....	151
Figure 37. Further optimisation of hiPSCs viability.....	155
Figure 38. Specifications for the creation of the PA hydrogels.....	158
Figure 39. Optimisation of method of mixing PBS and PA solutions.	163
Figure 40. Representative bright field images, showing the physical differences in the PA hydrogels.	167
Figure 41. Optimisation of method for E3 hydrogels.	171
Figure 42. Graphical representation of the process to make the various hydrogels after optimisation.	172
Figure 43. The K PAs showed a decreasing pH that was still present after gelation.....	175
Figure 44. The specifications for the optimisation of the cell clusters.	178
Figure 45. Optimisation of cell cluster size.	185
Figure 46. The retained cultures across all cultured day.....	186
Figure 47. Flow chart detailing the experimental set-up.....	187
Figure 48. Observed impact of culture on hiPSC clusters grown on hydrogels.	188

Figure 49. Observation of hiPSC clusters merging.	190
Figure 50. The difference in cross-sectional area per hydrogel.	193
Figure 51. The difference in cross-sectional area per day.	194
Figure 52. The percentage loss of cell clusters over the culture time.	195
Figure 53. A summary of the cross-sectional area and retention data.	201
Figure 54. Live/dead staining of all the clusters on hydrogels.	203
Figure 55. Observations of the cells extending from the surface of the cluster.	204
Figure 56. The distance of cells surrounding the clusters per day.	205
Figure 57. The distance of cells surrounding the clusters per hydrogel.	206
Figure 58. Representative images of Chondroitin Sulphate and HA binding protein immunostaining on day 4.	212
Figure 59. Enlarged representative images of CS immunostaining in K3 and K4 on day 4.	213
Figure 60. Potential differences in SNMC sequestration between K and E3 hydrogels.	234
Figure 61. Anti-laminin immunostaining upon differently charged hydrogels.	290

Table List

Table 1. Overview of ECM proteins, including collagen, laminin, fibronectin and elastin. Not every isoform if the protein is included here. Genes expressed per protein, their general structure, location, function and the matrix metalloproteinases that degrade the protein. This table shows the variation in ECM proteins and the wide range of functions they provide. *There are limitations for identifying the spatial location of laminins due to differing chains appearing in multiple isopforms, for example chain $\alpha 5$ in both laminin 511 and 521.	10
Table 2. Differences in youngs modulus between tissues. The stiffness values shown between organs (Handorf et al., 2015, Butcher et al., 2009).	10
Table 3. The variety of natural and snythetic hydrogel materials. The advantages and disadvantages of various natural and snythetic hydrogels. Edited from (Leberfinger et al., 2017).	17
Table 4. The locations of WAT and BAT in human newborns and adults. There is a reduction in BAT as humas age (Zoico et al., 2019). Adapted from (Zoico et al., 2019).	27
Table 2. An assessment of the fibres' characteristics, including the production and culturing.	62
Table 3. The Optimisation of the removal methods for the alginate layer.	84
Table 4. Description of categories used to assess viability of hiPSC clusters.	128
Table 5. A table of the cell concentrations and droplet size to make a range of cell cluster sizes. ...	131
Table 6. Description of peptides showing amino acid sequence, molecular formulae, and mass.	140
Table 7. Graphical representation of the peptides used, highlighting their structure and key features.	141
Table 8. The CaCl_2 concentrations in the 10 μl droplets and once 250 μl medium was added for overnight culture.	145
Table 9. The CaCl_2 concentrations used.	152
Table 10. Observations of K3 formulations.	162
Table 11. Optimisation of pH for K2, K3 and K4 gelation.	166
Table 12. Optimisation of the formulation for the E3 hydrogels.	170
Table 13. Comparison of the different size of cluster (starting cell number clusters during production and handling.	180
Table 14. The median cross-sectional area of the hiPSC clusters across all days of culture (μm^2). ..	184
Table 15. The significant differences found between cluster cross-sectional areas on day 0.	191

Table 16. The median cross-sectional areas (μm^2) for the hiPSC clusters on all hydrogels for 4 days of culture.	192
Table 17. The median values for the furthest cell distance from the cluster (μm).	202

Abbreviations

2D	2-Dimensional
3D	3-Dimensional
BAT	Brown Adipose Tissue
C/EBPs	CCAAT Enhancer Binding Proteins
CD44	Cluster Determinate 44
CS	Chondroitin Sulfate
CtBP	C-Terminal Binding Protein
CTCF	Corrected Total Cell Fluorescence
DS	Dermatan Sulfate.
ECM	Extra Cellular Matrix
EGF receptor	Epidermal Growth Factor Receptor
ERK	Extracellular Signal-Regulated Kinases
FAK	Focal Adhesion Kinases
FGF	Fibroblast Growth Factor
GAG	Glycosaminoglycans
HA	Hyaluronic Acid

HEPES	4-(2-hydroxyethyl)-1-piperazineethanesulfonic acid
hESCs	Human Embryonic Stem Cells
hiPSCs	Human Induced Pluripotent Stem Cells
HS	Heparin Sulfate
KLF	Kruppel Like Factors
KS	Keratan Sulfate,
LOX	Lysyl Oxidase
mESCs	Human Embryonic Stem Cells
MMP	Matrix Metalloproteinases
MSCs	Mesenchymal Stem Cells
ORO	Oil Red O
PA	Peptide Amphiphile
PBS	Phosphate-buffered saline
PG	Proteoglycans
PGC-1γ	PPAR γ Co-Activator 1 Alpha

PPARγ	Peroxisome Proliferator- Activated Receptor Gamma
PRDM16	Pr Domain Containing 16
RHAMM	Hyaluronan-Mediated Mobility
SNMC	Secreted Native Matrix Components
TGF-β	Transforming Growth Factor Beta
VEGF	Vascular Endothelial Growth Factor

WAT	White adipose tissue
β3-ARs	β 3-adrenoreceptors
CCP	Cell penetrating peptides
SNMC	Secreted native matrix components
NDSTS	N-deactylases and sulfotranferases
EXT	Exostosin glycosyltransferase

Acknowledgments

To my parents, who always believed in me even when I didn't, and my granddad who I know so wished to be here to see it finished.

To my friends who have supported me throughout this journey.

And finally, my thanks to Cathy and Alvaro, without whom there would have been no final thesis.

COVID-19 impact statement

Over the last (2.5 years), there has been a major change in the direction of my research. This is largely due to the departure of both supervisors. When COVID-19 was highlighted as a potential concern in November 2019, my primary supervisor had just left the university. While the supervisor in question did seem eager to remain a secondary supervisor and was happy to advise from afar, it became clear that there would still be a detrimental effect upon my research as any supervisory contact was sporadic and delayed. While we were able to find another professor to take over as main supervisor, unfortunately there was not enough space in their lab to accommodate me. As such, there was an expectation that a post-doctorate researcher from my previous lab would become my first point of contact, placing me in a separate research space. This delayed my research considerably (Nov 2019 – March 2020) as this was not university policy and several different members of staff had to agree to the arrangement. By the time this was resolved, the post-doctorate researcher had moved to their secondary PI's group. Therefore, we were no longer in the same group. This meant that, while she had access to the laboratories, there was a delay in the organisation of lab space and access to the necessary equipment. To compound this, in July 2020 during lockdown my remaining supervisor decided to retire, leaving me without a main supervisor once again. These delays to my research and data collection left me already in an extremely difficult position to then mitigate the effects of COVID.

Attempts were made by both supervisors to find replacements over the course of several months (July 2020 - Sept 2020), but all attempts failed. The School of Medicine eventually intervened. While new supervisors were found, there was no possibility to continue the research I had previously undertaken as the only supervisors that the school of Medicine could find focused upon a completely different method of 3D culture. This change in focus has meant I must now start from scratch to gain the depth of knowledge and practical expertise to complete my PhD within the limited timeframe remaining.

On top of this, another factor that reduced my ability to mitigate the impact of the pandemic upon my research were delays in data collection caused by the University's decision to move the group into a new building (move to BDI3). This interrupted data collection in the 6 weeks (Oct - Dec 2020) before the move and for several months after the move, as there were inevitable teething problems with the new building that had to be prioritised. These delays in data collection were then compounded by the COVID lockdown. The obvious use of such time during lockdown would be to analyse any previously collected data, However, due to the move, I had not been able to generate enough data. This meant there was limited data analysis to be completed, and as such the impact of lockdown was only further compounded.

Once students were able to restart research within the COVID safe space, I was considerably delayed (Sept 2020 – Oct 2020), as due to the change in supervisors I had to undergo induction and training to work in BDI3. There were further delays (Oct 2020 – Nov 2020) in accessing some labs and training while COVID safety measures were being altered and put in place. While obviously necessary, this meant there were several additional weeks without data collection.

In addition, COVID safety rules are severely restricting the laboratory space necessary to maintain the required social distance thereby reducing the time to collect data. This has now been compounded by limitations or delays in stock supply from personal protective equipment to cell culture flasks as a result of Brexit/COVID.

These situations listed above make it clear that it was practically impossible to maintain the original thesis hand in date.

CHAPTER 1. INTRODUCTION

There is a long history of animals being used in modern medicine, whether to model disease or in early-stage drug testing. For examples, rats used to create a model for cardiac hypertrophy (enlargement) through surgical intervention. This allowed for the study of the remodelling events or contractile properties using the progression of enlargement till heart failure (Gs et al., 2014). Mouse models have also been used to model infections such as *Helicobacter pylori*, which allows for further study into treatments to combat antibiotic resistance (Dey et al., 2021). In as recently as 2023 an anti-malaria drug was tested for use in preventing amyloid- β pathology (found in Alzheimer's disease) with the use of a transgenic mouse model (Kisler et al., 2023). Untill now, there has been no practical alternative to animals in medicine, however questions are now being raised into the ethics of such practices (Svendsen et al., 1997, Akkaya and GÜngör, 2022). While great care has been taken to reduce harm and stress during animal *in vivo* experiments, it is impossible to entirely prevent this. Animal models do not reliably replicate human diseases (Hackam and Redelmeier, 2006, Perel et al., 2007). For example, patient-derived xenograft tumour models (Abdolahi et al., 2022) and transgenic murine models for autoimmune liver diseases (Trzos et al., 2022)) lack this capacity. Cancer xenografts in mice can provide a complex system for studying tumours but the model has limitations. The model is not designed to replicate the matrix environment of the tumour or immune response in a human, which would provide more accurate data about the tumour in humans. (Denayer et al., 2014). Therefore highlighting the need for complex models with human cell types. Animal models result in limited translational reach for the research, with many animal models failing to fulfil their basic requirements – replicating human conditions.

In vitro cell culture is used for a wide variety of applications, including reprogramming of somatic cells to pluripotent stem cells (Takahashi et al., 2007), which can be used for the

Introduction

The extracellular matrix

development of organoids (e.g. optic vesicle-containing brain organoids that could become a promising tool for research into eye development) (Kozlowski et al., 2021, Gabriel et al., 2021), as well as in the large-scale production of medicines (e.g. Chinese hamster ovary cells are used to produce Epoetin a biopharmaceutical used to treat anaemia) (Zhu et al., 2017) and vaccines (e.g. for severe acute respiratory syndrome coronavirus 2 (SARS-CoV-2) were produced in Chinese hamster ovary cells) (Fang et al., 2022). In the move away from using animal models, there is great potential to optimise *in vitro* cell cultures to better mimic the environments required for testing. Such potential is currently the focus of intense research (Lutolf and Hubbell, 2005). Stem cells are of great focus in particular due to their ability to differentiate into multiple cell types in a controllable manner.

All stem cells have the ability to self-renew and maintain a level of pluripotency (Weissman, 2000). The cells within mammalian embryos are totipotent from fertilisation and differentiate progressively into specialised cells (pluripotent to multipotent to unipotent). The pluripotent stem cells in an embryo at the blastocyst stage (within the inner cell mass) can be isolated to generate embryonic stem cells (ESCs) (Smith, 2001). ESCs were first derived from fertilised zygotes by *Thomson et al* (Thomson et al., 1998). The ESCs are derived from the inner cell mass of the blastocyst stage of an embryo (Rippon and Bishop, 2004b) as shown in Figure 1, and have the ability to differentiate into all three germ layers that will then form all the cell types found throughout the adult body (Evans and Kaufman, 1981, Martin, 1981). In addition, there are adult stem cells within the body that can self-renew, for example hematopoietic stem cells, but these stem cells are only multipotent and cannot differentiate into all cell types like the embryonic stem cells, only a smaller range of cell types (Spangrude et al., 1988). The somatic differentiated cells can be reprogrammed to form induced pluripotent stem cells (Takahashi et al., 2007).

Introduction

The extracellular matrix

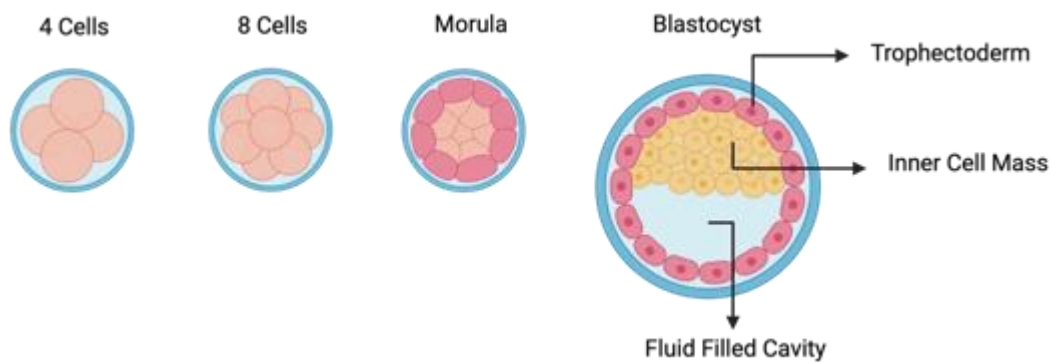


Figure 1. Embryonic stem cells before differentiation into the three germ lineages.

A fertilised egg divides and forms a blastocyst from which pluripotent (embryonic) stem cells can be isolated. As the zygote ages cells differentiate into cell types becoming less pluripotent. At the morula stage the formation of the trophectoderm (red) is located around the outer surface, this layer will become the extraembryonic material (placenta) that will support the embryo. The embryonic stem cells (ESCs) that were isolated by *Thomson et al* were derived from the inner cell mass (yellow) when at the early blastocyst stage, as identified by the presence of a fluid filled cavity (Thomson et al., 1998, Niwa, 2007). Created with BioRender.com.

1.1.1 Human Induced Pluripotent Stem Cells

Human induced pluripotent stem cells (iPSCs) are somatic cells reprogrammed into a pluripotent state, through the stimulation of reprogramming factors (Oct4, Sox2, Klf4 and c-Myc) (as seen in Figure 2) (Takahashi and Yamanaka, 2006). Human iPSCs have been shown to be like human ESCs (Maherali et al., 2007, Wernig et al., 2007, Guenther et al., 2010). However, there are some differences; in differentiation potential (Hu et al., 2010a), DNA methylation (Doi et al., 2009) and gene expression (Chin et al., 2009). All stem cells are able to self-renew without senescence and have the potential to differentiate into a range of cell types (Rippon and Bishop, 2004a). The ability to reprogram somatic cells into pluripotent cells has created a new field in enabling research into personalised medicine (Tabar and Studer, 2014) and optimisation of unique personal treatments using the patient's own cells. iPSCs are also a resource for specific human disease modelling (Lee et al., 2009a) as the iPSCs can be differentiated to all cells within the body. There are ethical concerns associated with the

Introduction

The extracellular matrix

destruction of viable embryos to create ESCs, therefore ESCs are not ideal for use in research or for regenerative medicine (Nwigwe, 2019) and hiPSCs do not have such problems.

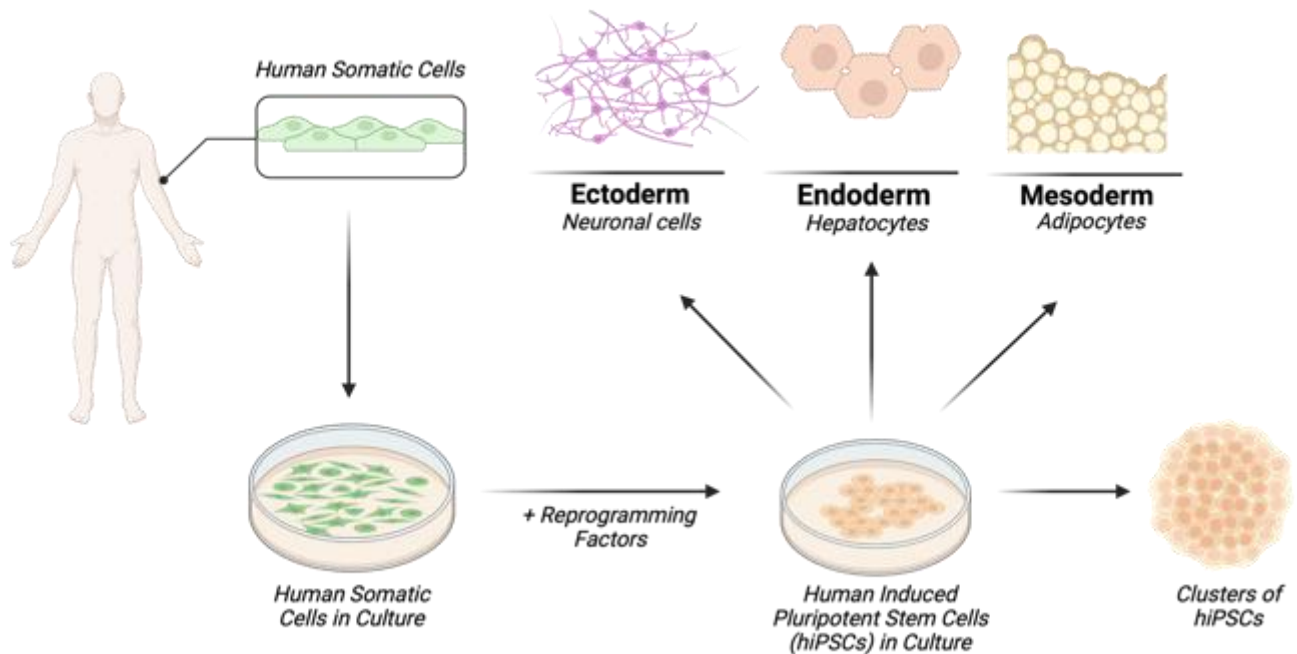


Figure 2. Overview of Human Induced Pluripotent Stem Cells (hiPSCs).

hiPSCs were created from somatic cells using critical reprogramming factors (Oct4, Sox2, Klf4, c-Myc) found by (Takahashi and Yamanaka, 2006). hiPSCs are pluripotent and able to differentiate into all three lineages (ectoderm, endoderm and mesoderm). The hiPSCs can be cultured on 2D culture plastic in the presence of a suitable substrate (e.g. vitronectin) but have also been cultured in spheroids to form clusters. Created with BioRender.com.

An enormous benefit to hiPSCs is the future where patients with diseases (i.e., cancer) can get personalised medicine. As hiPSCs can be taken from health and diseased patients and then be cultured to create disease models that can replicate human pathophysiology (Chun et al., 2011). In the future it may even be possible for hiPSCs to be used to differentiate into organs that could replace damaged organs (Sayed et al., 2016).

Introduction

The extracellular matrix

1.2 The extracellular matrix

If animal models cannot be used whether due to the ethical issues or due to the lack of translatability to human systems, then stem cell or primary cell (derived from tissues) models could take their place. Primary cells are the best for replicating the original tissues they were taken from but there are some limitations (Zhao, 2023). For example, primary cells proliferate less, vary depending upon the donor and have a limited life span (Li, 2019). In fact, there is a downside to both primary and stem cell culture as much of the initial work developing these models has been carried out using 2-dimensional (2D) tissue culture plates or flasks. These do not truly represent physiological tissue, as most cell types are not found in an environment like culture plastic. The tissue culture plastic forces a single layer of cells into a flat and stiff environment, which is not found in most cell environments *in vivo*. The cells grown on tissue culture plastic are typically flattened (Von Der Mark et al., 1977), given a forced polarity (Mseka et al., 2007) and have reduced interactions with extracellular components (Kapałczyńska et al., 2018).

The extra cellular matrix (ECM) is secreted by and surrounds cells. It fulfils several essential functions, acting as a support for the cells (e.g. collagen networks provide structural support for cells (Theocharis et al., 2016)), as well as providing tissue-specific mechanical signals (the stiffness of ECM varies between tissues and controls differentiation, for example adipogenesis is reduced on stiff substrates (Kuroda et al., 2017) (Humphrey et al., 2014)), ligands of cell membrane receptors (several ECM components bind to cell membrane receptors, e.g. laminin and integrins (Yue, 2014, Hynes, 2009)) and a source of growth factors (growth factors bind to a range of ECM components providing a localised gradient of growth factors, e.g. fibronectin and vascular endothelial growth factor (Wijelath et al., 2006)).

Introduction

The extracellular matrix

ECM composition is tissue-specific (Padhi and Nain, 2020) and can alter during progression of disease (Lu et al., 2011) and ageing (Birch, 2018). The ECM composition varies between tissues, for example, elastin (an ECM protein) in lung tissues has ~20–50 µg/mg, whereas heart tissue has 90–110 µg/mg (Padhi and Nain, 2020). In disease the ECM changes for example, in breast cancer there is an increased deposition of collagen during tumour formation (Egeblad et al., 2010). Furthermore, as humans age the ECM alters, there is a decrease in the collagen in the ECM, which reduces the density and toughness of the bone (Nyman et al., 2007). Typically, the ECM is comprised of around 300 distinct proteins and glycans and, due to the negative charge associated primarily with these glycans, it also contains a large volume of water (Hynes and Naba, 2012). The ECM is therefore a dynamic cell-specific microenvironment, which acts to keep the chemical, mechanical and topographic environment in ideal balance to support a multitude of cellular functions, from maintaining the stem cell niche to stimulating differentiation (Rozario and DeSimone, 2010, Yue, 2014).

Figure 3 shows a graphical representation of one example ECM surrounding endothelial cells as a simplified example, with many of the components commonly found throughout ECMs. The ECM itself contains situationally specific proteins and polysaccharides to create a unique environment. It is composed of fibrous structural proteins, adhesive proteins, and proteoglycans as well as the glycosaminoglycan (GAG), hyaluronic acid (HA) (Stevens and George, 2005, Yue, 2014).

Introduction

The extracellular matrix

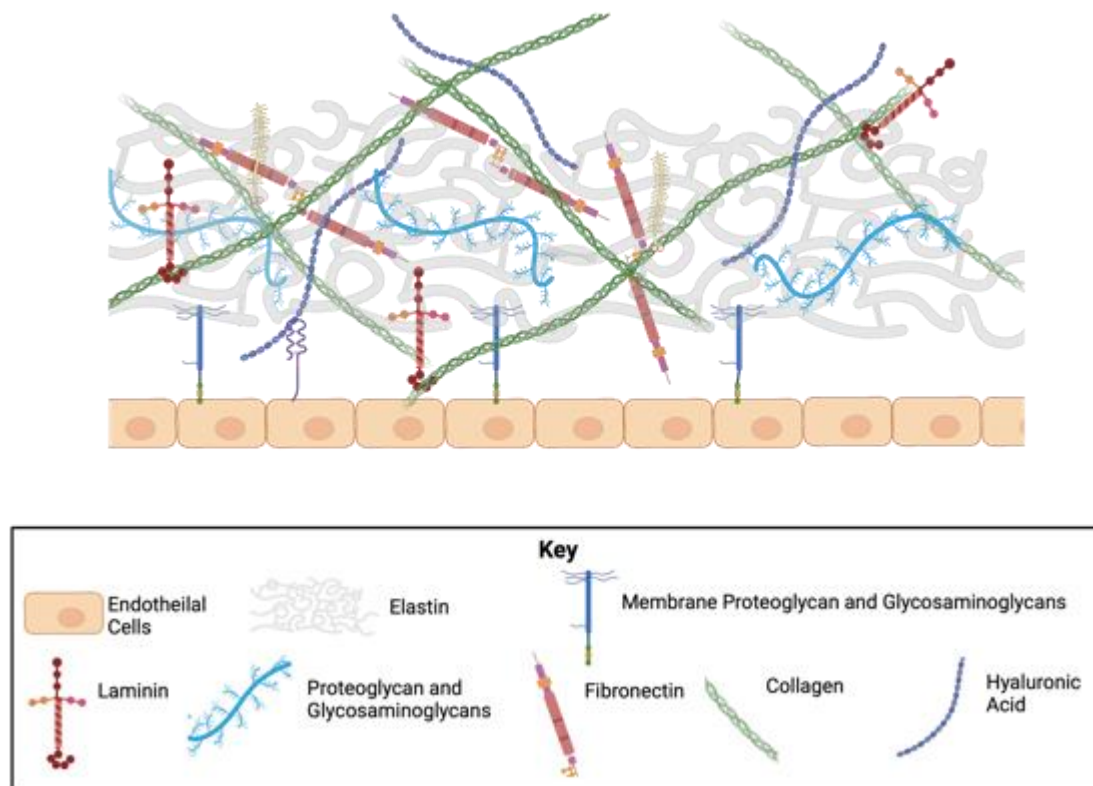


Figure 3. A graphical representation of an ECM surrounding the endothelial cells. The ECM is a network of molecules including proteins and polysaccharides, that are organized around cells. The ECM is dynamic and confers the cells with anchorage, biomechanical stiffness, receptor binding, and growth factor reservoirs. The ECM can control such factors as proliferation, adhesion, differentiation, and migration. The example above is a simplified example of the ECM surrounding endothelial cells, this is only one of many differing ECMs. There are several cell membrane anchored proteoglycans with glycosaminoglycans. Collagens, laminin, fibronectin, and elastin are the major components of the ECM. Extracellular proteoglycans are also displayed. Figure made in Biorender.

Collagen

Collagen is the most abundant ECM protein in the body, in mammals it is approximately 30% of their total protein content and is formed from three chains of polypeptides that assemble together to form a triple helix (Frantz et al., 2010). There are 28 different types of collagen currently identified (Wu et al., 2022); with collagens I, II, and III being the most abundant with 80 – 90% of the collagens found within the body (Zeugolis and Raghunath, 2011). The amino

Introduction

The extracellular matrix

acid sequence of collagen is conserved throughout collagen types, with a glycine-proline-X or glycine-X-hydroxyproline, with X being any other amino acids, sequence (Wu et al., 2022). Glycine is the smallest amino acid thereby allowing a triple helix to be a close configuration, able to withstand stress (Shoulders and Raines, 2009). Collagens provide the tensile strength in tissues including muscles (Kovanen, 2002), promotes differentiation (e.g. Mesenchymal stem cells into osteoblasts) (Akhir and Teoh, 2020) and cell adhesion of the ECM through the interactions with the $\alpha1\beta1$ integrin (Zeltz and Gullberg, 2016) (Rozario and DeSimone, 2010).

Collagens are required for life and the natural development of tissues during embryogenesis of mammals. When loss of function experiments were completed by removing a selected collagen type there was a range of defects, reviewed by (Rozario and DeSimone, 2010). When collagen I was removed it was embryonic lethal due to aortic rupture in the *M. musculus* (Liu et al., 1995), this lethality was seen in the removal of other collagens (collagens III (Brachvogel and Mayer, 2004), IV (Brachvogel and Mayer, 2004), V (Wenstrup et al., 2004)). The removal of other collagen types were not lethal but produced defects in several tissues, for example collagen VIII produced notochord and eye defects in *M. musculus* and *D. rerio* (Hopfer et al., 2005). The importance of collagen is further shown as mutations in collagen genes (COL1A1 and COL1A2) have been linked to clinical pathologies, including osteogenesis imperfecta (Semler et al., 2019) and Ehlers-Danlos syndrome (Cortini et al., 2019).

Collagens can be either fibril forming (a small or fine fibre) (Collagen type I, II, III), fibril-associated collagens (collagen IX, XII), network forming collagens (collagens IV), membrane-associated collagens (collagens XIII, XVII), or anchoring fibrils collagen (collagen VII) (Mecham, 1998, Ricard-Blum, 2011), see **Error! Reference source not found..** Fibril collagens are staggered to form fibrils and are responsible for the tensile strength of the ECM (Kadler et al., 2007). Network-forming collagens have interruptions in the triple helix that make

Introduction

The extracellular matrix

these collagens flexible to form networks, a requirement for molecular filtering in basement membranes and interacting with other ECM components (Than et al., 2002). Fibril-associated collagens are relatively shorter collagens with interruptions in the triple helix, thereby allowing fibril-associated collagens to interact with the fibrillar collagens, linking collagen fibres to each other and with other ECM components, thereby creating an interconnected network within the ECM (Wu et al., 1992). Membrane-associated collagens are transmembrane proteins that act as cell surface receptors. For example, membrane-associated collagens (MACITs) with interrupted triple helices are responsible for the anchoring fibrils beneath the *lamina densa* of basement membrane (Kadler et al., 1996).

Table 1. Overview of ECM proteins, including collagen, laminin, fibronectin and elastin.

Not every isoform of the protein is included here. Genes that transcribe each protein, their general structure, location, function and the matrix metalloproteinases that degrade the protein are listed. This table shows the variation in ECM proteins and the wide range of functions they provide.

*There are limitations for identifying the spartial location of laminins due to differing chains appearing in multiple isopforms, for example chain $\alpha 5$ in both laminin 511 and 521.

Protein	Genes	Structure	Location	Function	Matrix Metalloproteinase
Collagen I	COL1A1 COL1A2 (Shoulders and Raines, 2009)	Heterotrimer to form into collagen fibrils (Ramachandran and Kartha, 1955)	Widespread throughout the body, i.e., bone, dermis, and tendons (Shoulders and Raines, 2009)	Structural support and tensile strength (Theocharis et al., 2016)	MMP 1, MMP 8, MMP 14 and MMP 12 (Jabłońska-Trypuć et al., 2016)
Collagen II	COL2A1 (Theocharis et al., 2016)	Homodimer into fibril Collagen (Theocharis et al., 2016)	Majority located in cartilage (Shoulders and Raines, 2009)	Structural support and tensile strength (Theocharis et al., 2016)	MMP1, MMP8 and MMP 14 (Jabłońska-Trypuć et al., 2016)
Collagen IV Network	COL4A1, COL4A2, COL4A3, COL4A4, COL4A5, COL4A6	Three heterotrimers forms of collagen IV. All form a network with interruptions in	Basement membranes (Shoulders and Raines, 2009)	Basement membrane structural support (Wu and Ge, 2019)	MMP2, MMP9, MMP7 and MMP12

Introduction

The extracellular matrix

	(Shoulders and Raines, 2009)	their triple helix (Theocharis et al., 2016)			(Jabłońska-Trypuć et al., 2016)
Collagen XII FACIT	COL12A1 (Theocharis et al., 2016)	Short homotrimer with interruptions in the helix. Associates with collagen I and II (Theocharis et al., 2016)	Dermis and tendons (Shoulders and Raines, 2009)	Interacts with other collagen fibrils together (Theocharis et al., 2016)	MMP 12 (Didangelos et al., 2011)
Collagen XIII MACIT	COL13A1 (Logan et al., 2015)	Transmembrane homotrimer (Theocharis et al., 2016)	Skin, eyes, and endothelial cells (Shoulders and Raines, 2009)	Cell surface receptors, when cleaved soluble collagen (Theocharis et al., 2016)	-
Laminin 332	LAMA3, LAMB3 and LAMC2 (Tzu and Marinkovich, 2008)	Cross-shaped trimer (Tzu and Marinkovich, 2008)	Skin (Rousselle et al., 1991) and mammary glands (Doliana et al., 1997, Champlaud et al., 1996)	Cellular migration (Tzu and Marinkovich, 2008)	MMP1, MMP3, MMP 7 MMP 11, MMP14 and MMP 15 (Didangelos et al., 2011)

Introduction

The extracellular matrix

Laminin 511	LAMA5, LAMAB1 and LAMC1(Tzu and Marinkovich, 2008)	Cross-shaped trimer (Tzu and Marinkovich, 2008)	Vascular endothelial cells, skin and embryos (Champlaud et al., 2000)	Basement membrane support, embryogenesis (Tzu and Marinkovich, 2008)	MMP1, MMP3, MMP 7 MMP 11, MMP14 and MMP 15 (Didangelos et al., 2011)
Laminin 423	LAMA4, LAMB2 and LAMC3 (Tzu and Marinkovich, 2008)	Cross-shaped trimer (Tzu and Marinkovich, 2008)	Central nervous system (Libby et al., 2000) and hippocampus (Egles et al., 2007)	Central nervous system organisation (Egles et al., 2007)	MMP1, MMP3, MMP 7 MMP 11, MMP14 and MMP 15 (Didangelos et al., 2011)
Fibronectin	FN1 (Schwarzbauer and DeSimone, 2011, Hynes and Naba, 2012)	Can be soluble fibronectin or fibrils (To and Midwood, 2011)	Ubiquitous (Schwarzbauer and DeSimone, 2011, Hynes and Naba, 2012)	Adhesion [(Singer et al., 1987), and cell migration (Veevers-Lowe et al., 2011), differentiation (Samuel et al., 1994)	MMP2, MMP 3, MMP7, MMP 8, MMP15 and MMP 17 (Didangelos et al., 2011)

Introduction

The extracellular matrix

Elastin	ELN (Fazio et al., 1988)	Self-assemble into aggregates that can form elastic fibres (Visconti et al., 2003)	Major blood vessels, lungs, elastic ligaments, skin (Uitto, 1979)	Provides the elastic ability of the ECM (Kristensen and Karsdal, 2016),	MMP 2, MMP 9, AND MMP 12 (Rabkin, 2017)
---------	--------------------------	--	---	---	---

Therefore, the varied nature of collagen and its importance for life requires a highly controlled biosynthesis. When the biosynthesis is not tightly controlled, during tumorigenesis, there is an increased production of collagen which can lead to increased promotes tumour progression, in for example lung cancer (Zhuang et al., 2013). Collagen genes (i.e., COLA1) are transcribed within cells, using a range of transcription initiation sites and alternative splicing (Ramshaw and Glattauer, 2019). The mRNA is then translated into pre-pro-collagen molecules containing a signalling domain protruding from the endoplasmic reticulum (Wu et al., 2022). Once the signalling domain is removed through the activity of a signal peptidase the molecule, the molecule is now classed as procollagen undergoes post-translational modifications (Wu et al., 2022). The post translational modifications upon collagen are complex, varied and allow for heterogeneity in collagen molecules, which can alter the characteristics of collagen depending upon the niche, expanded on below (Wu et al., 2022). The differing collagen types are expressed in a pattern determined by location and time. For example, collagen type II is found predominantly in cartilage while type I is located in skin, organs and bone (Shoulders and Raines, 2009). During embryogenesis there is more type III collagen than in adults, (18% -21% than 8% - 11%) while type I collagen is reduced during the same time when compared to the collagen content in adult skin (70% -75% than 85% - 90%) (Anttinen et al., 1977).

Hydroxylation is one of the post-translational modifications that collagens undergo. This modification is upon the proline and lysine residues (Gjaltema and Bank, 2017). The 4-hydroxylysine is required for the assembly of collagen triple helixes (Berg and Prockop, 1973). The amount of hydroxylation is species dependent, for example 3-hydroxyproline is found in the A1 section of collagen III in chicken skin but not in mammals (Hudson et al., 2011) and are dependent upon the type of collagen, collagen IV has the highest number of 3-hydroxyproline residues (RISTELI et al., 1980). The amount of hydroxyproline differs between tissues for example, it is highest in the cornea and lowest in articular cartilage (Eyre et al., 2011).

Introduction

The extracellular matrix

After hydroxylation of lysine residues, glycosylation, the addition of monosaccharide or disaccharide on hydroxylated lysine residues, occurs (Wu et al., 2022). Similar to hydroxylation, this process is also dependent upon the type of collagen and the niche the collagen is synthesised in. The glycosyl transferases are tissue dependent for example, glycosyl transferase 25 domain 2 is located specifically in the nervous system (Schegg et al., 2009). Glycosylation can determine the diameter of the collagen fibres when formed, more glycosylation the thinner the collagen fibril diameter (Brinckmann et al., 1999).

Following the post-translational modification, three pro-collagen chains assemble into a triple helix, and it is secreted into the intracellular space. Where collagen peptidases cleave the N- and C-terminuses of the pro-collagen to form tropo-collagen. Lysyl oxidase (LOX) then forms a collagen fibril from several tropo-collagen molecules (Wu et al., 2022). These post-translation modifications highlight the variation in collagen molecules despite collagen being the most abundant protein in the human body. Thereby demonstrating the variable nature of ECM is differing locations throughout the body.

Laminin

Collagen is only one component of the ECM, another component is laminin, a cross-shaped glycoprotein with up to three short arms and a long arm (shown in Figure 3) (Cheng et al., 1997). Laminin forms a lattice-type network with itself (Cheng et al., 1997). Laminins are heterotrimers formed from three chains, one alpha (α), one beta (β), and one gamma (γ) (Durbeej, 2010). Each chain is transcribed from individual genes, with several isoforms per chain, LAMA5 transcribes the RNA for laminin chain α 5. For example, there are five different chains in vertebrates, and two isoforms for α chain 3 (α 3A and α 3B), allowing for 6 different α chains (Miner and Yurchenco, 2004). Currently there have been sixteen laminin trimers

Introduction

The extracellular matrix

found and these sixteen laminin trimers have a spatial distribution within tissues (see table for examples) (Aumailley et al., 2003). Laminin trimers are named based on to the composition of the chains, laminin 111 is comprised of the α 1 chain, β 1 chain and the γ 1 chain (Aumailley et al., 2005).

The three chains that comprise a laminin glycoprotein form the cross-shaped structure assemble into an α helical coiled coil (the long chain), till the c-termini of the β and γ chains, the α chain has five laminin G-like (LG) domains following the coil structure (Colognato and Yurchenco, 2000). Above the coiled coil long tail, the short arms of each chain form the short arms and thereby the cross shape. The short arms share domains between chains; the globular laminin N-terminal (LN) domain, repeated laminin-type epidermal growth factor-like (LE) and within the LE domain are globular domains (one in chains β and γ or two in the α chain (Beck et al., 1990).

Laminin biosynthesis begins with the transcription of all three laminin chains (Lissitzky et al., 1986). There are splice variants of laminin chains, as the two isoforms of α chain 3 is controlled though the use of differing promoters to start transcription (Ferrigno et al., 1997). The RNA is then translated. The N-terminal signal peptides are removed from the translated chain proteins (Lissitzky et al., 1986). The chains then undergo glycosylation (post translational modification) while in the endoplasmic reticulum (ER), this increases the variation of laminin throughout the body in addition of the multiple isoforms of laminin (Cooper et al., 1981). Glycosylation of laminin can be up to 30% of the total molecular weight (Fujiwara et al., 1988). The glycosylation varies from chain to chain, for example the α chain 1 has more than α chain 5 (Champlaud et al., 2000). The glycosylation is believed to protect against degradation (Morita et al., 1985). The laminin trimer forms within the ER of the cells, the β and γ chains LG domains

Introduction

The extracellular matrix

associate first followed by the α chain (Yurchenco et al., 1997). Once the trimer is assembled, it can undergo further glycosylation in the Golgi organelle (Morita et al., 1985).

The laminin glycoproteins are the adhesion proteins of the ECM (Tzu and Marinkovich, 2008). Laminin molecules provided the anchorage of cells to the ECM specifically the basement membrane (a thin ECM between epithelial tissues and connective tissues) (Tzu and Marinkovich, 2008). The laminin forms a network between itself through the short arms (Cheng et al., 1997). In addition to this, laminin also provides some structure or anchorage to the ECM through the interactions they make with other ECM components, including collagen VII (Sasaki et al., 2004). Laminin provides anchorage for cells through interactions with integrins upon the cell surface (Tzu et al., 2005).

Further, laminin also plays a role in maintaining pluripotency (Rodin et al., 2010) and migration (Hintermann et al., 2005). Laminin 511 and 521 maintain embryonic stem cells in pluripotency (Rodin et al., 2010). Laminin 332 is thought to favour cell migration through the binding with the $\alpha 3\beta 1$ and $\alpha 6\beta 1$ integrins (Hintermann et al., 2005), and has been implicated in wound healing perhaps due to cell migration (Frank and Carter, 2004).

Fibronectin

Fibronectin is a ubiquitous ECM protein and is a second adhesion protein of the ECM (Walters and Gentleman, 2014), it is an important component of the ECM, for example when mice have inactive fibronectin, they have a lethal phenotype due to vascular deformities (George et al., 1993). Fibronectin is functional when in fibrils, therefore the fibronectin molecules must assemble into interconnected fibres (Dalton and Lemmon, 2021). Fibronectin organises the ECM, as the assembly of other matrix components (i.e., collagen) are dependent upon a

Introduction

The extracellular matrix

provisional fibronectin network (Singh et al., 2010). Fibronectin is also able to bind to the ECM members, for example collagen (Leikina et al., 2002).

Fibronectin has several roles in differentiation (Martino et al., 2009), cell adhesion (Ruoslahti and Pierschbacher, 1986), and cell migration (Veevers-Lowe et al., 2011). Fibronectin is required for the differentiation of several tissues (skeletal, limb, neural tube, and cardiac) during fetal development (Samuel et al., 1994). In addition, Fibronectin has been found to promote the differentiation of adult stem cells to skeletal lineages (Martino et al., 2009). Fibronectin can bind to many integrins found upon the cell surface, this provides a cell adhesion role as well as an interface with the ECM, reviewed by (Plow et al., 2000). An important cell binding domain on fibronectin is the RGDS motif sequence. RGDS provides attachment between the cells and the ECM (Ruoslahti and Pierschbacher, 1986), including through interactions with integrins ($\alpha 5\beta 1$ and $\alpha 5\beta 3$) (Singer et al., 1987). The interactions with cell surface integrins promote cell migration through the cross talk between the receptor tyrosine kinase platelet-derived growth factor receptor β and the $\alpha 5\beta 1$ integrin in stem cells (Veevers-Lowe et al., 2011).

Fibronectin is comprised of two subunits connected by disulphide bonds (Zollinger and Smith, 2017). The fibronectin subunits are formed from a series of three repeating domains (I, II, III) (Hynes and Naba, 2012). Differing from collagen and laminin, fibronectin is encoded by a single gene and the variation in isoforms are produced due to alternative splicing to produce 20 isoforms of fibronectin (Schwarzbauer and DeSimone, 2011, Hynes and Naba, 2012). The fibronectin alternative splicing can integrate extra domains; extra domains A (EDA), extra domain B (EDB) and a variable region (V region) into the fibronectin structure (Ffrench-

Introduction

The extracellular matrix

Constant, 1995). The splicing is cell type dependent, for example neither EDA or EDB are found in plasma fibronectin (Gehris et al., 1996).

The heterogeneity of fibronectin is achieved through the alternative splicing (Veevers-Lowe et al., 2011) and through post-translational modifications (such as, glycosylation, and phosphorylation) (Yalak et al., 2019). The glycosylation of fibronectin has been suggested to prevent the degradation of fibronectin (Liu et al., 2021) and the glycation can modify ligand binding during liver regeneration (Sano et al., 2008). The phosphorylation of fibronectin has been found to increase cell attachment (Veevers-Lowe et al., 2011).

Elastin

Elastin, shown in Figure 3 in grey, is another ECM component as a structural protein (Eckes et al., 2010). It provides the majority of elasticity to the ECM, and it is 1000 times more elastic than collagen (Kristensen and Karsdal, 2016), particularly in tissues such as the arterial wall and the lining of the lungs (Kozel et al., 2011). Elastin is a hydrophobic monomer with no defined secondary structure but instead forms random coils that can then be connected via intermolecular cross-linking, a process which is catalysed by lysyl oxidase (LOX) (Kozel et al., 2011). In the arterial wall elastin is structured to form thin lamina, thereby allowing the blood vessel to expand (Glagov et al., 1992). Whereas in the skin elastin fibres are rich in the dermis so that the skin can be flexible (Roten et al., 1996). Mutations in elastin can result into several diseases for example Williams-Beuren syndrome, a developmental disorder of the central nervous system (Ewart et al., 1993) and supravalvular aortic stenosis, a disease characterised by the narrowing of arteries (Curran et al., 1993).

Introduction

The extracellular matrix

Elastin is only produced during late embryonic development till the end of adolescence, with the produced elastin having to last the remainder of the adult animal's (Myers et al., 1983). Elastin is transcribed from a single gene (ELN) (Fazio et al., 1988) and in humans is subject to splice variants (Reichheld et al., 2019). The elastin gene is translated into tropoelastin monomers, and then moved to the ER (Swee et al., 1995). While in the ER tropoelastin interacts with elastin binding protein resulting in the secretion of tropoelastin to the cell surface (Hinek et al., 1995). The tropoelastin then aggregates are then cross-linked with LOX (Umeda et al., 2001). The aggregates then get deposited upon the elastin fibres, comprised of multiple proteins including fibrillin (Visconti et al., 2003). A post translation modification found on elastin is the hydroxylation of prolines residues (occurs on 1% of residues) (Jacob and Hornebeck, 1985). The hydroxylation is species and tissue dependent, for example, intervertebral disc has the highest hydroxylation (Schmelzer et al., 2016).

PGs and GAG

In addition to the proteins in the ECM there are also proteoglycans (PGs) and GAG present. As well as being found within the ECM itself, PG are found on the surface of cells, (Iozzo and Schaefer, 2015a) and are capable of interacting with cell surface receptors cytokines and growth factors (Balasubramanian and Zhang, 2016). Because of this flexibility, PGs are commonly classified by location and structural type (Gao et al., 2018). Structurally, they can be grouped into small leucine-rich PGs, aggrecan family PGs, or basement membrane PGs. The intracellular PG is Serglycin, while the membrane-bound PGs are considered transmembrane, or glycosylphosphatidylinositol (GPI) anchored PGs. Transmembrane PGs have a cytoplasmic section, a transmembrane domain, and an extracellular domain. This is where GAGs are located (Iozzo and Schaefer, 2015b). While PGs can interact with cell surface receptors, cytokines, and growth factors through the core protein, the large majority of possible reactions take place through the GAGs (Iozzo and Schaefer, 2015b).

Introduction

The extracellular matrix

PGs are comprised of a core protein that GAGs can covalently bind to (Karamanos et al., 2018). GAGs are therefore an important part of cell functions as they provide pathways to proliferation, adhesion and differentiation, through the interactions with other proteins (Izumikawa et al., 2014). Chondroitin sulfate a GAG, stimulates the proliferation and migration of human chondrocytes through β -catenin and the suppression of MMPs (Hsu et al., 2022) and is required for pluripotency and differentiation of stem cells (Izumikawa et al., 2014). Thereby demonstrating some of the pathways GAGs can alter cell behaviour.

GAGs are polysaccharides of varying lengths, with repeating disaccharides of acetyl-galactosamine or acetyl--glucosamine (hexosamines) and glucuronic acid or iduronic acid (hexuronic acids), GAGs are therefore extremely distinctive (Mikami and Kitagawa, 2017). GAGs are also highly negatively charged which helps to attract and maintain the water content of the ECM (Ikemoto et al., 2017). GAGs are substituted in a location specific manner with sulfate groups to the hydroxyl groups of the hexosamines, hexuronic acid and galactose or to the amino group of glucosamine (Gao et al., 2018, Karamanos et al., 2018). GAGs can be sub-divided. The Galactosaminoglycans: Chondroitin Sulfate (CS) and Dermatan Sulfate. The Glucoaminoglycans: Heparin Sulfate (HS), Heparin, Keratan Sulfate, and HA. More detail is provided on GAGs in Chapter 3.

Growth factor reservoir

In addition to the interactions between ECM components and cells, the ECM can hold a range of growth factors as a biochemical gradient or reservoir for growth factors, thereby controlling cell behaviours (Flaumenhaft and Rifkin, 1991). Several different components of the ECM have growth factor binding motifs, allowing for the localisation of soluble factors (Kirkpatrick et al., 2004). An example of this is the process through which fibroblast growth factor (FGF) 2

Introduction

The extracellular matrix

binds to HS (Rapraeger et al., 1991). The lack of FGF2 binding to HS reduces the fibroblast growth and FGF2 binding to the cell surface FGF receptor 1 (FGFR 1) (Rapraeger et al., 1991, Yayon et al., 1991). However not all FGF2 bound to HS, activates the FGFR, differing HS structures prevent FGF binding to FGFR1 while FGF is bound to HS (Guimond et al., 2006). Fibronectin can bind vascular endothelial growth factor (VEGF) (Hynes and Naba, 2012). When Fibronectin is bound to VEGF and the integrin $\alpha 5\beta 1$, there is a promotion of migration and proliferation in endothelial cells (Wijelath et al., 2006). Collagen type II has a domain capable of binding to transforming growth factor $\beta 1$ (TGF- $\beta 1$) and bone morphogenetic protein 2 (BMP-2) resulting in negative regulation of these growth factors, which are important for the dorso-ventral axis in embryology (Garcia Abreu et al., 2002). The ability of the ECM to interact with the soluble growth factors is therefore an important function of the ECM.

Cell anchorage and mechanosensing

The ECM interacts with cells as well as physically anchoring them through cell surface receptors. Such receptors include integrins (Barczyk et al., 2010) and other families such as dystroglycans (Barresi and Campbell, 2006) and the syndecan PGs (Woods, 2001). Integrins are transmembrane proteins with two subunits (α and β) (Barczyk et al., 2010). The principal integrin pairs that interact with the ECM are those with the $\beta 1$ subgroup. These interact with collagen, laminins, and fibronectin, the latter two of which are the adhesive proteins in the ECM (Barczyk et al., 2010, Humphrey et al., 2014). Integrins activate downstream signalling through focal adhesion kinases (FAK) (Vicente-Manzanares and Horwitz, 2011). The connectivity formed by the interaction of the cellular cytoskeleton via integrins out to the ECM through fibronectin forms a critical pathway which the cells use to interact with their environment, and forms part of the cellular mechanosensing process (Jansen et al., 2017). The physical forces exerted on cells embedded within the ECM can therefore alter the

Introduction

The extracellular matrix

cytoskeleton of that cell, changing its shape (Heer and Martin, 2017) and behaviour, for example a reduction in adipogenesis in stiff substrates (Kuroda et al., 2017).

A major force sensed by cellular mechanotransduction (the conversion of mechanical stimulus to the cell) is the stiffness of the ECM. This relative stiffness is dependent on both the composition of the ECM and its organisation, the stiffness of the ECM, therefore differs between tissues (Muiznieks and Keeley, 2013). This value is typically expressed as the elastic modulus or Young's modulus as shown in Table 2, the measure of tensile or compressive strength when a known force is applied (Jastrzebski, 1959). During embryogenic development (e.g., head-tail axis development) (Petzold and Gentleman, 2021), wound healing (e.g., myofibroblast differentiation) (Rosińczuk et al., 2016) and disease, such as cancer (Seewaldt, 2014), the elasticity of the surrounding ECM has a direct impact on cell behaviour. The use of *Caenorhabditis elegans* embryos demonstrated that during embryogenesis the elongation in the head-tail axis relies upon tissue stiffness and mechanical stress (Vuong-Brender et al., 2017). In 32 – 112 cell chordate embryos the single cell stiffness differs depending upon the hemisphere of the embryo (Fujii et al., 2021). In wound healing the myofibroblasts contract and stiffen the matrix, causing a positive feedback loop that results in stimulating the differentiation of myofibroblasts (Wipff et al., 2007), myofibroblasts produce and organise the ECM during wound healing (Hinz, 2016). In breast cancer the stiffening of the ECM results in increased microRNA 18a that reduces tumour suppressant pathways (Mouw et al., 2014), showing a direct line to between the stiffness of the ECM and disease progression.

Introduction

The extracellular matrix

Table 2. Differences in Young's modulus between tissues. The stiffness values shown between organs. Adapted from (Handorf et al., 2015, Butcher et al., 2009).

Tissue	Youngs Modulus (Elastic Modulus) (kPa)
Fat	0.5 – 1.5
Brain	1 - 4
Kidney	5 - 10
Heart	10 -15
Intestine	20 - 40
Cartilage	1000 - 1500
Bone	15000 - 20000

Changes to the ECM composition

However, despite this, the ECM itself does not remain static, and is constantly remodelled in response to specific triggers e.g., during development (Lee et al., 1984), wound repairing (Schilling, 1976, Li et al., 2007), disease (Lu et al., 2011) and tissue development (Simon-Assmann et al., 1995). The ECM is continuously produced with distinct components and the ECM is degraded by specialist enzymes such as matrix metalloproteinases (MMPs) (Lu et al., 2011). Examples of this include, MMP 1, MMP 8, MMP 14 and MMP 12 that can degrade collagen I (**Error! Reference source not found.**) (Jabłońska-Trypuć et al., 2016), see Table 2.

The synthesis of ECM proteins can be complex with the production of precursors and then crosslinking to form the matrix as seen above. The creation of the ECM components is

Introduction

Three-dimensional cell cultures

therefore complex and well controlled by the cells. The degradation of the ECM components (e.g., collagen by MMPs) are tightly controlled to avoid abnormal degradation of the ECM.

Error! Reference source not found. demonstrates the range of different MMPs that degrade ECM proteins. Excess ECM production and degradation has been found to be present during tumour formation reviewed by (Winkler et al., 2020). The reverse condition where there was an excess of MMPs (ECM degradation) have been described in cancer (Zucker and Vacirca, 2004), osteoarthritis (Burrage et al., 2006), and emphysema (Gharib et al., 2018).

1.3 Three-dimensional cell cultures

The creation of three-Dimensional (3D) cell culture is an important aim as there is a shift from animal models and the 2D culture method to 3D cell culture models. The large interest in 3D cell culture can be seen through the publication of over 43,500 research articles published in the last year alone. The search to gather this figure included the words hydrogels, “3D culture”, 3D, scaffolds, or synthetic matrix, (pubmed.gov). This demonstrates that there is an accepted need for 3D models throughout the scientific community. The main goal of 3D cell culture is to create the most accurate model systems, of disease (e.g., tumour models breast cancer (Casey et al., 2017)), tissues (e.g., pancreatic organoids (Candiello et al., 2018)) and specific cell types (e.g., adipocytes (Louis et al., 2019)) for a variety of applications. Some key applications are tissue regeneration (Chuah et al., 2017), disease modelling (Sidhaye and Knoblich, 2021), drug testing (Wang and Jeon, 2022) all of which enable for greater understanding of life. Cartilage regeneration is one such example of an applications for hydrogels, where research is ongoing into using hydrogels to repair cartilage defects. Tissue regeneration could occur though either cartilage replacement grown on a 3D model or through a 3D culture within the defect that stimulated tissue regeneration (Wei et al., 2021). 3D models have been designed to model disease, for example a methacrylated hyaluronic acid system,

Introduction

Three-dimensional cell cultures

with a controllable stiffening ability was used to model fibrosis (Caliari et al., 2016). A 3D model of pancreatic ductal adenocarcinoma found that the patient specific response to anti-cancer drugs was replicated more accurately in the 3D model than previously used models (Osuna de la Peña et al., 2021). This highlights the potential of 3D culture methods to function as model for drug testing and the benefit of personal-derived primary cells that can be used within hydrogels for personalised models.

Due to the complex nature of physiology, no one model will be able to replicate all in vivo ECM environments and 3D culture systems therefore must be tailored to the situation and desired aim. The physical characteristics of the ECM varies among tissues and as detailed above, has a huge effect on the cells the ECM surrounds. Therefore, when designing systems to culture cells in 3D several physical characteristics need to be considered: the composition and concentration of the ECM components, porosity, stiffness (due to crosslinking or material selection), presence of any artificial biochemical gradients and the potential for remodelling.

These 3D culture methods offer a multitude of benefits over 2D; cells either encapsulated in or seeded on to 3D culture methods can form cellular interactions in all planes surrounding themselves. Cells in 3D models can interact with a typically softer environment than tissue culture plastic, and the presence of ECM proteins (improved cell – ECM interactions) typically either provided by the scaffold or ‘captured’ as they are secreted by the cells. These factors make the 3D models more representative of the ECM found in human tissues and therefore provide greater use as accurate model systems (Tibbitt and Anseth, 2009).

Introduction

Three-dimensional cell cultures

Substrates for 3D cultures

The characteristics of each 3D culture method must be selected for the desired cell type, outcome, or complexity. As the understanding of how important the reciprocal nature of the ECM and the cells it surround has grown, more work has incorporated ECM components into *in vitro* culture methods. There are several different methods to include ECM components, decellularised ECM tissue or hydrogels with natural components or epitopes.

Decellularized ECM tissues that are sterilised have been reused for culture cells (Zhang et al., 2022b, Morissette Martin et al., 2018) (see **Error! Reference source not found.**). Decellularized ECM has been selected to culture cells since 1995 where decullarilised small intestinal submucosa was used model for Achilles tendon repair (Badylak et al., 1995). Decellularized whole lungs have been used to culture pulmonary epithelium and vascular endothelium cells to create a hierarchical organization within the matrix that could participate in gas exchange (Petersen et al., 2010). The matix lungs were not without problems as the alveolar barrier function was insufficient to prevent blood from entering the airways (Petersen et al., 2010). This decellularized ECM has the benefit of replicating the compositiion, structure and even vascularisation of native ECM in the lungs. However, the decellurization methods can vary and each have their disadvantages, reviewed by (Moffat et al., 2022). For example, physical methods like freeze thaw cycles which may disrupt the ECM structures and chemical methods such as ionic detrgents can reduce GAGs and alter ECM structures (Liu et al., 2017b). Another example of decellularized ECM is extracted from rat livers and used to form hydrogels where human adipose-derived stem cells were differentiated into functional hepatocytes (Lee et al., 2014). This process provides a complex network of natural ECM components for cell culture with a large range of ECM components that can not be replicated

Introduction

Three-dimensional cell cultures

in full by artificially produced hydrogels but does not replicate the mechanical properties of the native tissue.

However, decellularized ECM is the ECM from a specific spatiotemporal point of a tissue and may not be representative of the desired conditions for the wanted experiment. As the ECM varies in composition and structure depending upon the location and processes occurring (e.g., differentiation or migration) any decellularized ECM needs to be selected for a situation as close to the wanted experimental conditions. An example of this is the study of adipogenesis (formation of adipocytes), during the early adipogenesis there is a different ECM composition to late adipogenesis (e.g., there is a reduction in fibronectin (Kubo et al., 2000)). A decellularized scaffold from late adipogenesis will therefore be functionally different from an early adipogenesis scaffold, that will result in differing behaviour. Chen et al. (2019) used a poly-(dl-lactic-co-glycolic acid) and collagen construct to culture human mesenchymal stem cells to produce cultures of either no adipogenesis, early adipogenesis or late adipogenesis. These constructs were then decellularized and used as scaffolds to assess the effect of ECM from different stages of adipogenesis. Both the no adipogenesis and late stage adipogenesis scaffolds inhibited the adipogenic differentiation of human mesenchymal stem cells (Chen et al., 2019). Similar results were found by others where early adipogenesis ECM stimulated the more adipogenesis than late adipogenesis ECM (Hoshiba et al., 2010, Cai et al., 2016). The use of decellularised scaffold is therefore a viable option for cell culture due to their high complexity and replication of native ECM environments but it is not always preferable if the ECM does not match the wanted experimental ECM. In addition, if studying the ECM produced or the effect of specific components of the ECM on the behaviour of cell the complexity of the decellurlsed scaffolds becomes a hindrance. As it will become more difficult to determine the effect of a specific ECM component, Therefore, other 3D methods of culture have been created, see Figure 4.

Introduction

Three-dimensional cell cultures

Introduction

Three-dimensional cell cultures

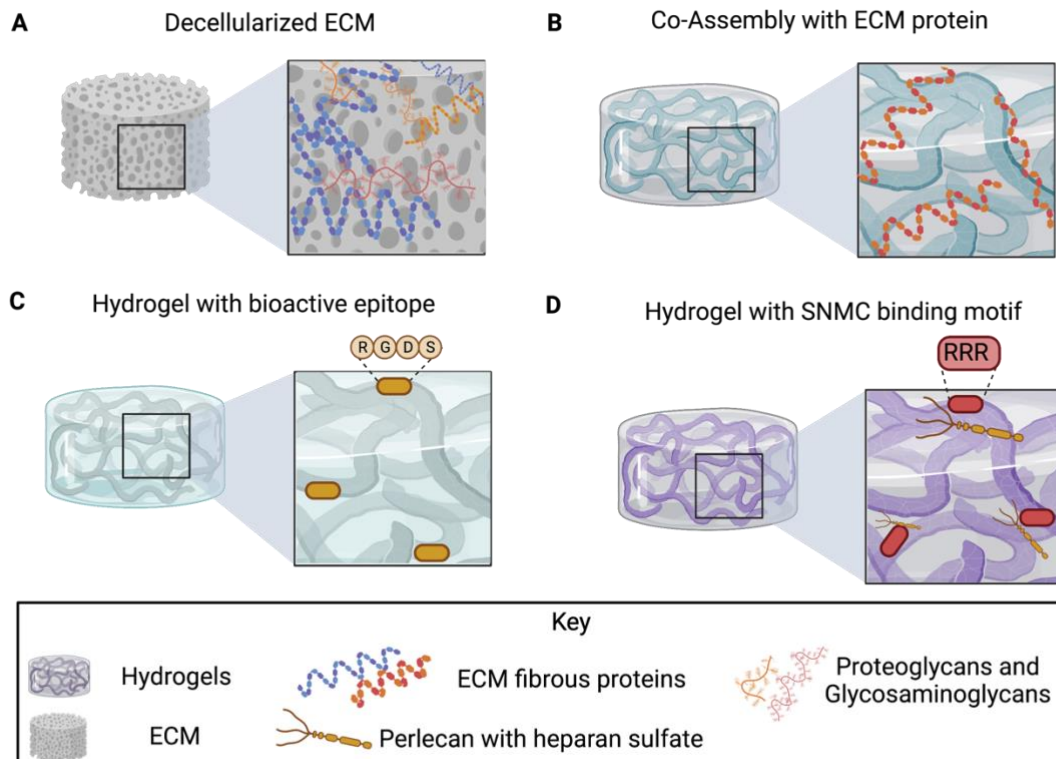


Figure 4. Three dimensional hydrogels methods that can be used to replicate the ECM for cell culture.

A Decellularized ECM has the whole ECM of a tissue and can be sterilised and reseeded with cells (Zhang et al., 2022b, Morissette Martin et al., 2018). However, it is the ECM isolated from a specific time and place. **B** Synthetic hydrogels have been mixed with selected ECM components to form a more representative model of the native ECM (Osuna de la Peña et al., 2021, Ahmad et al., 2022). **C** Synthetic hydrogels displaying cell-binding peptide motifs, present on ECM proteins can be used to support interactions between the biomaterial in a fully synthetic hydrogel. (Anderson et al., 2009, Ferreira et al., 2013b). **D** The hydrogels containing binding motifs that can sequester secreted natural matrix components (SNMC) to direct cells towards the required cell fate (Shah et al., 2010, Tomaszewski et al., 2021). Figure made in Biorender.

Introduction

Three-dimensional cell cultures

Hydrogels are meshwork of polymers, peptides, or polysaccharides; either natural or synthetic, see Table 3, that trap and retain water. The meshwork of polymers creates a porous substrate with high permeability for oxygen and nutrients. The stiffness of hydrogels can be tuned, through increases in the concentration of the substrate being used, for example increasing alginate or gelatin concentrations (Giuseppe et al., 2018), as can its porosity, through several methods depending on the hydrogel, an example is freeze-drying can increase pore size (Annabi et al., 2010). Synthetic hydrogels can be edited to present ECM epitopes (i.e. RGDS) (Ishida et al., 2020) or combined with ECM components. The polymers used to make the hydrogels can be synthetic (e.g., polyallylamine and polyethylene glycol) (Pandala et al., 2022), natural (e.g., collagen) (Torabizadeh et al., 2022) (see Table 3) or a mixture of both, for example designed peptides with keratin or fibronectin for a model of ovarian tumours (Hedegaard et al., 2020).

The natural hydrogels have several benefits in that they have good biocompatibility and physical characteristics (viscoelastic, pore size and bioactive interactions) reviewed by (Ho et al., 2022). In addition, natural hydrogels are often bioactive and can direct cellular behaviour. For example, the presence of RGDS motif found on collagen in collagen hydrogels, can enhance cellular attachment (Davidenko et al., 2016). Collagen is a commonly used hydrogel for the culture of stem cells (human mesenchymal stem cells) (Kuo and Tuan, 2008) to cancer cells (e.g., human colon carcinoma cells) (Ali et al., 2014). Hydrogels made from collagen have a low stiffness, degradability and batch to batch variability reviewed by (Caliari and Burdick, 2016). HA is another natural hydrogel that is extensively used (Lou et al., 2018, Goodarzi and Rao, 2021). To control the physical characteristics of HA hydrogels work has been completed to modify HA and allow for a range of crosslinking (Burdick and Prestwich, 2011).

Table 3. The variety of natural and synthetic hydrogel materials. The advantages and disadvantages of various natural and synthetic hydrogels and the interactions that form the hydrogel. Edited from (Leberfinger et al., 2017).

		Advantages	Disadvantages	Bonding	Reference
Natural	Collagen I	Bioactive, and cell attachment through RDGS	Low stiffness (<1kPa), easily clogs, limited stability, and batch to batch variation	Electrostatic interactions	(Walters and Stegemann, 2014, Caliri and Burdick, 2016, Duarte Campos et al., 2014)
	Chitosan	Antibacterial, antifungal	Slow gelation, easily clogs, weak mechanical properties therefore often mixed with other ECM components	Electrostatic interactions	(Qu et al., 2018, Pellá et al., 2018)
	Alginate	Fast gelation, low cost, stable	Poor attachment, clogs, and no cell attachment	Electrostatic interactions	(Caliri and Burdick, 2016, Leberfinger et al., 2017)

Introduction

Three-dimensional cell cultures

	HA	Bioactive, results in proliferation, angiogenesis, has fast gelation, and the stiffness can be modified through the molecular weight of HA used	Rapid degradation, often requiring chemical modification (hydroxyl group modified by an ester bond)	Covalent crosslinking	(Li et al., 2019, Leberfinger et al., 2017, Xu et al., 2012)
Synthetic	PEG	Blank slate hydrogel, low cost, mechanical properties can be specified	No adhesion, bioinert and requires chemical modification or combination with ECM components for bioactive ability	Physical or chemical crosslinking	(Caliari and Burdick, 2016, Della Sala et al., 2020, Cao et al., 2021)
	Methacrylate gelatin	As a modified gelatin, it is bioactive, high mechanical strength and its mechanical properties can be altered (i.e., UV intensity for cross linking)	Slow gelation, and UV light can cause cell death	UV light	(Caliari and Burdick, 2016, Leberfinger et al., 2017, Klotz et al., 2016)

Introduction

Three-dimensional cell cultures

	Peptides (e.g., PA)	User designed for wanted properties (i.e., stiffness or bioactive epitopes)	Weak long-term stability, and expensive to produce	Electrostatic interactions	(Caliari and Burdick, 2016, Matson and Stupp, 2012)
	Polyvinyl alcohol (PVA)	High elastic modulus and high strength, low cost, mechanical properties can be managed	No adhesion, bioinert and requires chemical modification or combination with ECM components for bioactive ability	Physical or chemical crosslinking	(Ho et al., 2022, Wang et al., 2021)

Synthetic polymers used in creating hydrogels include polyethylene glycol (PEG), an easily modified polymer (Lin and Anseth, 2009) and polyvinyl alcohol (PVA) (Okita et al., 2021), used in a range of research. PEG hydrogels with oligopeptide substrates for MMPs have been researched for bone regeneration and proangiogenic ability (Lutolf et al., 2003, Moon et al., 2010), and organoid culture, where a PEG hydrogel that supports intestinal organoids (Cruz-Acuña et al., 2017). I

Synthetic hydrogels have been mixed with selected ECM components. For example, peptides and ECM proteins (collagen type I, fibronectin, laminin and hyaluronan) model create for pancreatic cancer (Osuna de la Peña et al., 2021). In addition, natural polysaccharides have been added to synthetic models. A PEG and HA hydrogel has been created for bone marrow organoids (Vallmajo-Martin et al., 2020). The blending of natural and synthetic components form a more accurate representation of the true environment being modelled while still being able to control the physical characteristics of the hydrogel, (shown in Figure 4)**Error! Reference source not found.** (Osuna de la Peña et al., 2021, Ahmad et al., 2022). Synthetic hydrogels have also been designed to express epitopes, that are normally present on ECM components. These can add interactions between the ECM and cells in the hydrogel without adding the ECM components, therefore allowing the research into a specific role or function completed by the ECM protein or motif. This allows for cells to interact with the motif, resulted in an alteration in behaviour. For example two of the most common bioactive motifs that have been added to synthetic hydrogel materials, are the RGDS (from fibronectin) and IKVAV (derived from laminin) (Kleinman et al., 1991) motifs, for increased attachment (Storrie et al., 2007) and neuronal differentiation respectively (Silva et al., 2004). This is an approach to build scaffolds from the nano scale to the micro, the characteristics can be dependent upon the individual building blocks (Hedegaard et al., 2020, Derkus et al., 2020). The model can be made as complex as needed with the presence of one to multiple bioactive epitopes. Another method by which synthetic hydrogels can also be made to mimic the natural interacts within

Introduction

Three-dimensional cell cultures

the ECM is to express binding motifs that can sequester desired ECM components and growth factors to direct a selected cell fate (Shah et al., 2010, Tomaszewski et al., 2021) (see Figure 4).

Introduction

Thesis aims objectives

1.4 Thesis aims objectives

Despite much interest and progress in the application of synthetic environments, for 3D cell culture to mimic *in vivo* tissues, there remains a real need for improved replication of the ECM *in vitro*. To accurately replicate the role of the ECM in supporting, directing, and maintaining the functions of multiple cell types, new models must be explored. The interest in this research is due in part due to an understanding of the vital role the ECM has supporting, directing, and maintaining the actions of cells that maintain all life.

This thesis will cover work on two independent models, which can be seen as attempts to tackle similar aims from opposite directions, see Figure 5. Objective 1 was to provide a natural 3D hydrogel to support cells during adipogenesis. This was an example of top-down engineering, where an ECM component (collagen), enriched in the native ECM being replicated. Objective 2 was to influence cells by capturing, and maintaining them in a matrix enriched with their own ECM components. This was a bottom-up approach where specific peptides were used to build a synthetic hydrogel with selected physical characteristics (more specifically charge). In both settings, the aim was to alter the behaviour of cells in culture, influenced by their environment.

Introduction

Thesis aims objectives

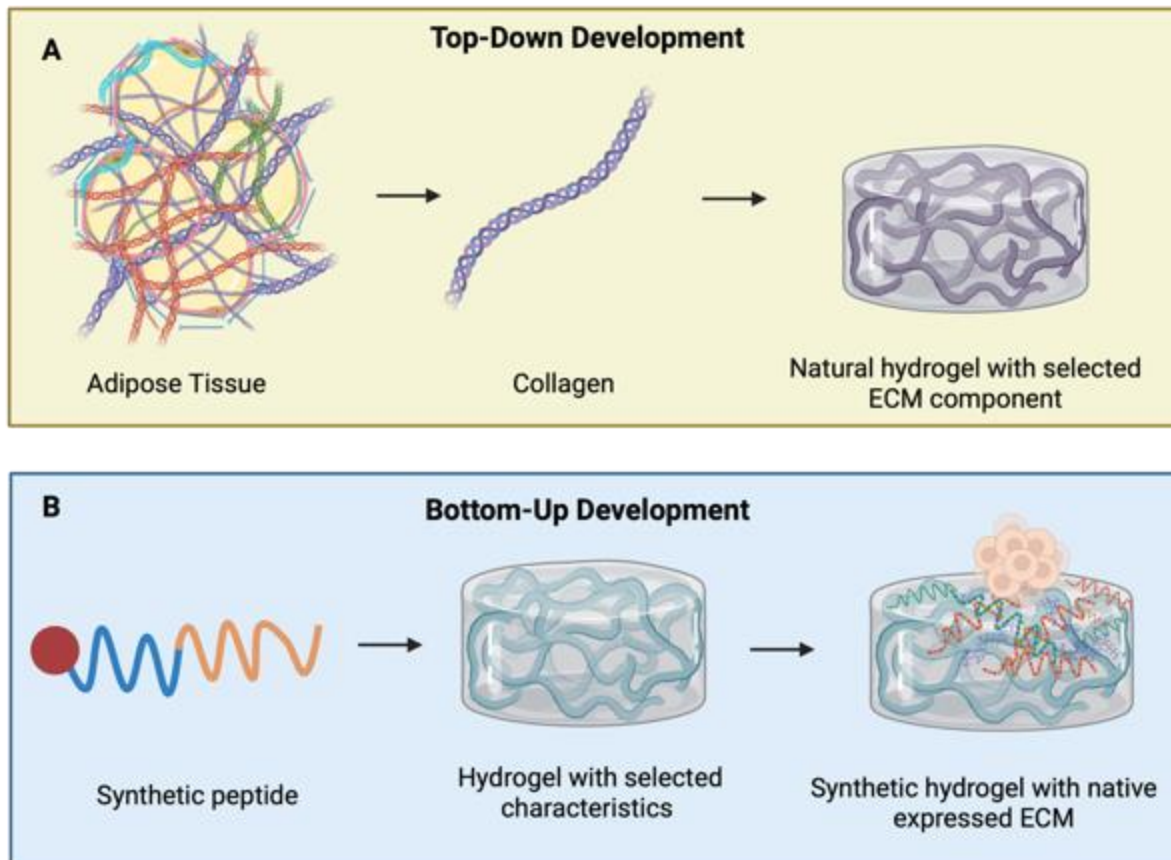


Figure 5. The differing approaches to hydrogel design and development, within this work. **A** The first hydrogel system will show a potential model for the differentiation of fat cells (Adipogenesis). This was a top-down model, a selected ECM protein found in fat (adipose) tissue (collagen) was combined with alginate to make a natural hydrogel, with ECM interactions. **B** The second hydrogel designed from the bottom-up. Synthetic peptides were selected with wanted characteristics, the presence of charge, to capture native expressed ECM proteins. The ball of cells upon the hydrogel are expected to have expressed native ECM (shown in orange and green) captured within the synthetic hydrogel. Figure produced in Biorender.

**CHAPTER 2. ALGINATE FIBRE TO CULTURE STEM CELLS DURING
ADIPOGENIC DIFFERENTIATION.**

Alginate fibre to culture stem cells during adipogenic differentiation.

Introduction

2.1 Introduction

2.1.1 Obesity

One of the most prevalent problems currently facing the world is the sharp rise in obesity, specifically in adults. In the UK 63% of adults are overweight and half of these people are classified as obese and 1 in 3 children leave primary school (11 years old) are overweight (UK Government, 2020). It is well known that obesity leads to an increase in life-threatening secondary conditions, such as cancer (Assumpção et al., 2022), type 2 diabetes (Golay and Ybarra, 2005), and heart disease (Csige et al., 2018). The burden of obesity and obesity-related diseases was calculated to cost the tax payer in 2021 £58 Billion (Frontier, 2022), and as such the British government has made reducing obesity levels an important aim for the next few decades (UK Government, 2020). It has therefore never been more important to expand upon research in adipogenesis, specifically the modelling of adipogenesis, in order to provide a model to test potential therapeutic drugs that could be used, in combination with lifestyle changes, to reduce obesity.

Obesity is the result of an energy imbalance in the body, where more calories are consumed than the body metabolises. The excess energy is stored as triglycerides in adipocytes, more specifically white adipocytes (Mescher, 2016). Therefore, a key target of obesity research is in the differentiation and characterisation of adipocytes.

2.1.2 Adipocytes

White adipose tissue (WAT) is an endocrine organ and connective tissue which helps to maintain energy homeostasis in mammals by storing excess lipids and releasing energy in the form of free fatty acids when needed, for example, during fasting or exercise (lipolysis)

Alginate fibre to culture stem cells during adipogenic differentiation.

Introduction

(Trayhurn and Beattie, 2001). However, this homeostasis is not always maintained, and excess WAT can form, leading to metabolic dysfunction (Al-Goblan et al., 2014). White adipocytes are circular cells with a large singular lipid droplet (unilocular) with a low number of mitochondria, see Figure 6 (Richard et al., 2020). In adults, WAT is mainly located subcutaneously and visceraally around the internal organs (Park et al., 2014).

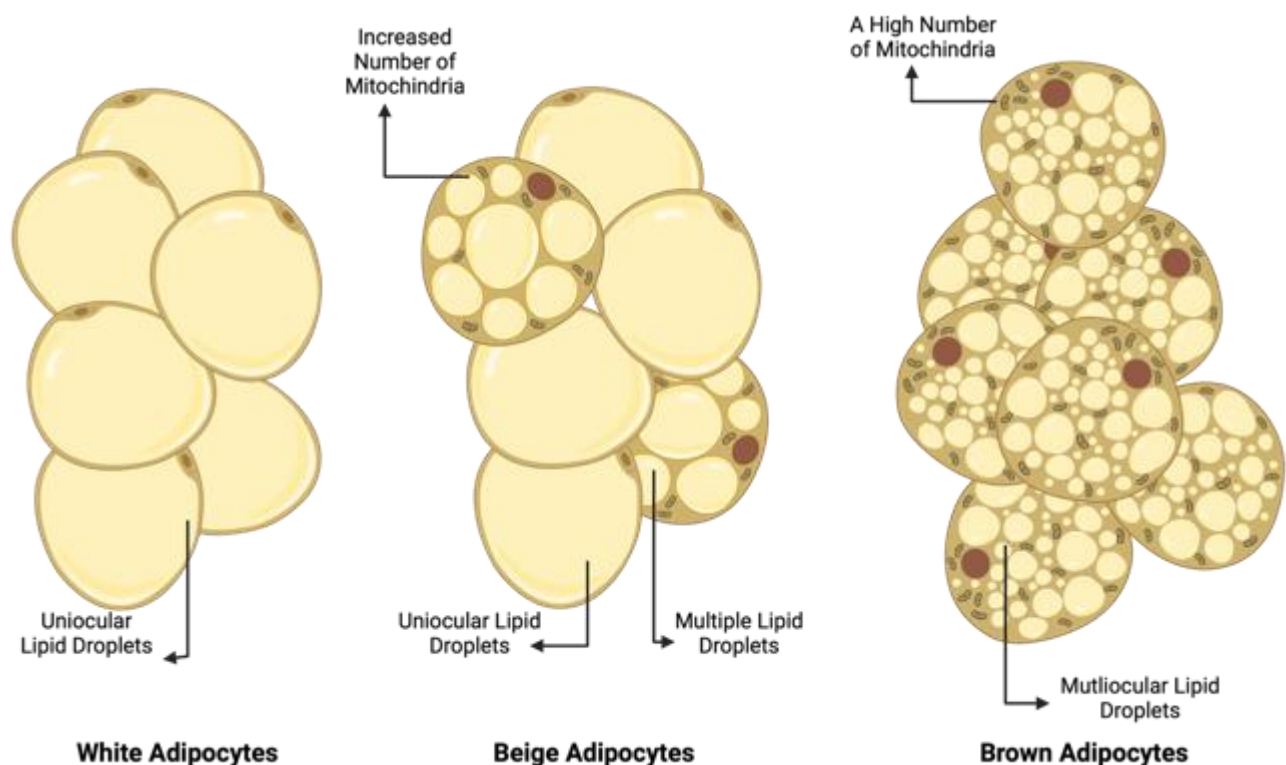


Figure 6. Graphical representation of the three adipocytes types.

White adipocytes are represented on the left with large unilocular droplets, lower number of mitochondria and the nucleus located at the periphery. The cells in centre display a mixture of white and beige adipocytes. The beige adipocytes are adipocytes that derived from white adipocytes but have some of the characteristics of brown adipocytes. The beige cells have an increased number of lipid droplets, and an increased number of mitochondria present. The brown adipocytes on the right are multilocular with many smaller lipid droplets, and many mitochondria. Figure made in Biorender.

Brown adipose tissue (BAT) contains a second type of adipocyte composed of several smaller lipid droplets (multilocular), and a greater number of mitochondria than WAT (Baba et al., 2010) (see Figure 6). BAT maintains the body temperature in rodent (Ghorbani et al., 1997)

Alginate fibre to culture stem cells during adipogenic differentiation.

Introduction

and human new-borns in hypothermic conditions through non-shivering thermogenesis (Lidell, 2019). Thermogenesis is activated by cold temperature, through the metabolism of the stored lipids resulting in the production of heat. (Brychta and Chen, 2017, Nedergaard and Cannon, 2013). Thermogenesis requires the expression of UCP1 (expressing uncoupling protein 1) (Brychta and Chen, 2017, Nedergaard and Cannon, 2013) and as such the expression of UCP1 is a major characteristic of brown adipocytes (Park et al., 2014).

Table 4. The locations of WAT and BAT in human newborns and adults. There is a reduction in BAT as human age (Zoico et al., 2019). Adapted from (Zoico et al., 2019).

	WAT	BAT
New-born	<ul style="list-style-type: none"> ○ Visceral (around organs) ○ Mesenteric ○ Perirenal (around kidneys) ○ Subcutaneous (under skin) ○ Abdominal ○ Gonadal (around reproductive organs) 	<ul style="list-style-type: none"> ○ Interscapular
Adult	<ul style="list-style-type: none"> ○ Visceral (around organs) ○ Mesenteric ○ Perirenal (around kidneys) ○ Subcutaneous (under skin) ○ Abdominal ○ Gonadal (around reproductive organs) 	<ul style="list-style-type: none"> ○ Supraclavicular ○ Scapular

Alginate fibre to culture stem cells during adipogenic differentiation.

Introduction

The brown in white adipocytes or beige adipocytes are the third known adipocyte type, these cells have a brown-like function and are found within WAT depots (as seen in Figure 6. Beige cells are white adipocytes activated by β 3-Adrenoreceptors (β 3-Ars) or cold exposure (Harms and Seale, 2013). Despite BAT characteristics being expressed in beige cells, there are numerous differences between the two, the most obvious being lower amounts of UCP1 and less mitochondria (Wang and Seale, 2016, Wu et al., 2012). On top of this, brown cells are autonomous while beige cells must be activated by cold exposure (Wang and Seale, 2016). Beige cells also have a flexible phenotype able to store lipids or undergo thermogenesis (Wu et al., 2012).

Alginate fibre to culture stem cells during adipogenic differentiation.

Introduction

2.1.3 Mesenchymal stem cells

Adipocytes are derived from mesodermal cells (Sebo and Rodeheffer, 2019). Therefore, Mesenchymal stem cells (MSC) are used to model adipogenesis (Velickovic et al., 2019). MSC are adult stem cells that can be found in several different parts of the body including adipose tissues (Bianco, 2014), bone marrow (Li et al., 2016) and the umbilical cord (McElreavey et al., 1991). In 2006, The International Society for Cellular Therapy defined the features of mesenchymal stem cells. First, MSC in culture conditions are attached to culture plastic. Second, the MSC express CD90, CD73 and CD105 surface markers but no hematopoietic or endothelial surface markers (i.e., CD45, CD14). Finally, MSCs are multipotent and are capable of differentiation into adipocytes, osteoblasts and chondroblasts (Dominici et al., 2006).

2.1.4 Adipogenesis

The two main transcription factors during adipogenesis are peroxisome proliferator-activated receptor gamma (PPAR γ) and CCAAT enhancer binding proteins (C/EBPs) (Tontonoz et al., 1994). Though there is an overlap in the expression of PPAR γ and C/EBP, PPAR γ on its own is able to stimulate adipogenesis, while C/EBPs cannot achieve this when PPAR γ is absent (Tontonoz et al., 1994, Rosen et al., 2002).

PPARs are a nuclear hormone receptor super family of ligand-activated transcription factors that can either increase or decrease DNA transcription (Tyagi et al., 2011). PPAR γ can be activated by insulin (Rieusset et al., 1999) and both mRNA and protein can be down-regulated with fasting (Kajita et al., 2008). PPAR γ is also required for the maintenance of differentiated adipocytes. Without PPAR γ the adipocytes die (Schoonjans et al., 1995).

Alginate fibre to culture stem cells during adipogenic differentiation.

Introduction

C/EBPs are leucine zipper transcription factors and the first transcription factors induced during the first wave of adipogenesis including the stimulation of PPAR γ (Wedel and Ziegler-Heitbrock, 1995), see Figure 7. There are several members of the family which are expressed during adipogenesis α , β and δ . Once PPAR γ is induced a feedback loop is created by stimulating C/EBP α and thereby itself (Kajita et al., 2008). The activation of C/EBP α and PPAR γ can then promote adipogenesis through the activation of over 3000 target genes (Lefterova et al., 2008). For example, C/EBP α stimulates the transcription of glucose transport 4 (GLUT4), thereby increasing the glucose present in the cell, the glucose can then be turned into fatty acids stored in lipid droplets in adipocytes (Lefterova et al., 2008, Wang, 2010).

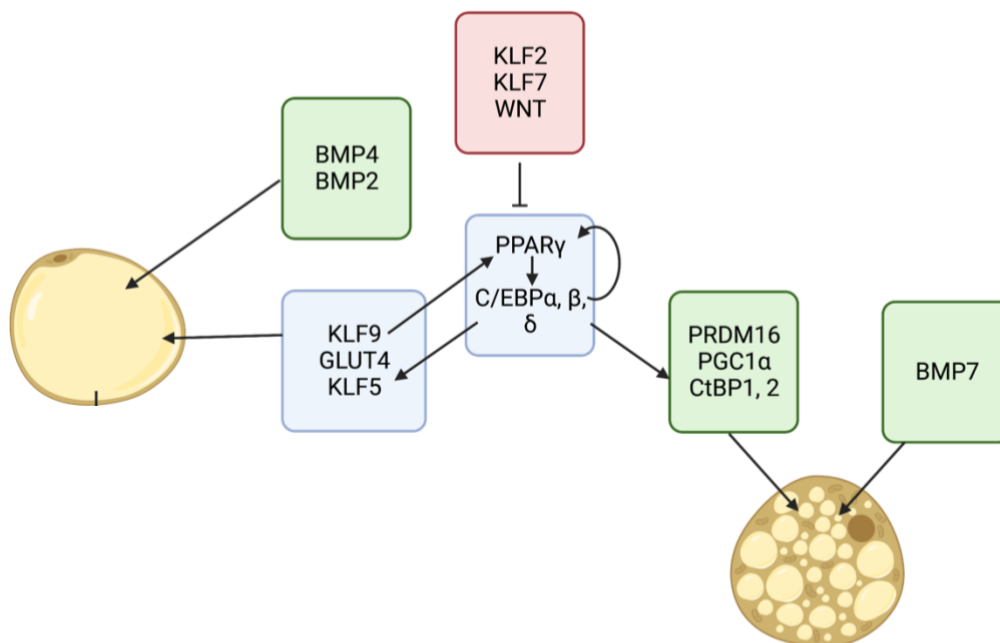


Figure 7. A simplified representation of the control of adipogenesis.

The key genes required for adipogenesis are shown in the centre (PPAR γ , C/EBP α , β and δ). C/EBP α stimulates the expression of PPAR γ generating a feedback loop. These genes then activate up to 3000 target genes for adipogenesis, including KLF9, GLUT4 and KLF5. KLF9 also stimulates the expression of PPAR γ . KLF2, 7 and wingless (WNT) inhibit the adipogenesis process (in red). Different genes or conditions stimulate the production of specific adipocytes. For the production of white adipocytes BMP4 (bone morphogenic protein) and BMP2 are required. While the brown adipocytes requires PRDM16, PGC1 α and CtBP1 and 2. BMP7 has also been found to stimulate brown adipocytes.

Alginate fibre to culture stem cells during adipogenic differentiation.

Introduction

C/EBPs can induce Kruppel like factors (KLF). KLFs are zinc finger transcription factors, which also play a large role in adipogenic differentiation (McConnell and Yang, 2010, Uchida et al., 2000). KLF5 is induced early in adipogenesis by C/EBP β and C/EBP δ and can bind directly to the PPAR γ 2 promoter to activate transcription (Oishi et al., 2008) thereby promoting adipogenesis. KLF9 is upregulated in the middle of adipogenesis and indirectly activates PPAR γ by activating C/EBP α (Pei et al., 2011). KLF can also down regulate adipogenesis with KLF2 and 7 repressing the PPAR γ promoter (Wu et al., 2005, Cho et al., 2007, Wu and Wang, 2013).

Several of the above genes are required for the formation of both white and brown adipocytes however, there are specific genes that are only required for the creation of brown adipocytes. Transcription factor PR Domain Containing 16 (PRDM16) is a transcriptional co-regulator of PPAR γ that determines brown adipocytes, and when mice are deficient in PRDM16 (through the crossing of knockout mice) there is a reduction of thermogenic gene expression (Harms et al., 2014). This is because it forms a complex with C/EBP β that controls the initial process in brown adipocyte development (Kajimura et al., 2009). PRDM16 represses the expression of WAT genes by interacting with CtBP1 and CtBP2 (C-Terminal Binding Protein 1 and 2) (Vernochet et al., 2009), while at the same time inducing BAT genes by interacting with the coactivator PGC-1 α (PPAR γ Co-Activator 1 alpha) (Hondares et al., 2011). PGC-1 α is raised during cold exposure, it induces the expression of UCP1, and is not required for brown adipocyte differentiation (Puigserver et al., 1998).

2.1.5 Extra cellular matrix of adipose tissue

As mentioned in the introduction (section 1.3 p11) the ECM differs dependent upon the location and requirements for the cells. An example of this would be, the differing locations of adipose tissue depots (Strieder-Barboza et al., 2020). In particular, it was found that altering the ECM can alter the thermogenic ability of such adipocytes, LAMA4 knockout mice were seen to be

Alginate fibre to culture stem cells during adipogenic differentiation.

Introduction

more obesity resilient and expressed more thermogenic markers (Gonzalez Porras et al., 2021).

Collagens (types I-VII present), laminin, fibronectin, elastin and glycosaminoglycans (GAGs) are found in adipose tissue (Napolitano, 1963, Chun et al., 2019). The largest contributor to the ECMs are the Collagens which make up 30% of any tissue found within the body (Frantz et al., 2010) and provide the tissue with vital tensile strength (Kadler et al., 1996). The proportion of the collagen types differs between lean people and the obese, collagen VI increased with obesity (Pasarica et al., 2009). Immunostaining of stromal vascular preadipocytes from black cattle showed that all collagen types except type II stained intensely, collagen II is therefore present in smaller amounts (Nakajima et al., 2002a). Collagen VI is enriched within adipose tissue (Scherer et al., 1998). Type I collagen surround adipocytes to provide the structure required for the tissue, it does this by forming either thin fibres or thick bundles of heterodimer in triple helix (Nakajima et al., 2002a). *Kubo et al.* immunostained for ECM components of the adipogenesis of stromal vascular cells of male F1 (C57BL/6 • C3H) mice, for a period of a month (Kubo et al., 2000). In the experiment collagen I was kept to the cytoplasm while the cells were pre-adipocytes. After induction, the collagen I network covering the cell surface began to form, becoming dense and well organised, see Figure 8 (Kubo et al., 2000).

Collagen III, on the other hand is located around the unilocular adipocytes but showed no network formation (Kubo et al., 2000). Collagen V forms a similar network that covered the whole adipocyte resembling a cobweb pattern. Microfibrils (heterodimers) comprised of Collagen V and Collagen VI form between the collagen I bundles forming a cobweb style network (Kubo et al., 2000, Nakajima et al., 2002a). Collagen IV serves as a basement

Alginate fibre to culture stem cells during adipogenic differentiation.

Introduction

membrane (a thin sheet of ECM underneath the epithelium) for adipose tissue located under the vascular endothelial layer (Brown et al., 2011).

Fibronectins have been found to be most present during preadipogenic stage of long term culture of stromal-vascular cells from mice and decay during adipogenesis (Antras et al., 1989). During the immunostaining the fibronectin network was most organised and larger during the early stage of adipogenesis (Kubo et al., 2000). Figure 8 highlights the changes in ECM proteins through adipogenesis. Laminin formed balloon like structures around adipocytes (Kubo et al., 2000).

When the deposition of ECM was quantified, there was an increase in the mentioned ECM proteins in the early days of adipogenesis (Nakajima et al., 2002a). More specifically, fibronectin production decreased after day 4 (Nakajima et al., 2002a), in line with the immunostaining in *Kubo et al* (Kubo et al., 2000). The laminin production increased before reaching a plateau by day 4 (Nakajima et al., 2002a). There was a decrease in all collagen production by day 10 (Nakajima et al., 2002a). The ECM is therefore produced and laid down during early adipogenesis. Collagen types were altered differently throughout the adipogenesis, with collagen V and VI increasing and becoming denser by day 10. This suggested that as the triglycerides increase in the lipid droplets the ECM forms a differing structure to maintain and support the lipid swollen adipocytes (Nakajima et al., 2002a).

Alginate fibre to culture stem cells during adipogenic differentiation.

Introduction

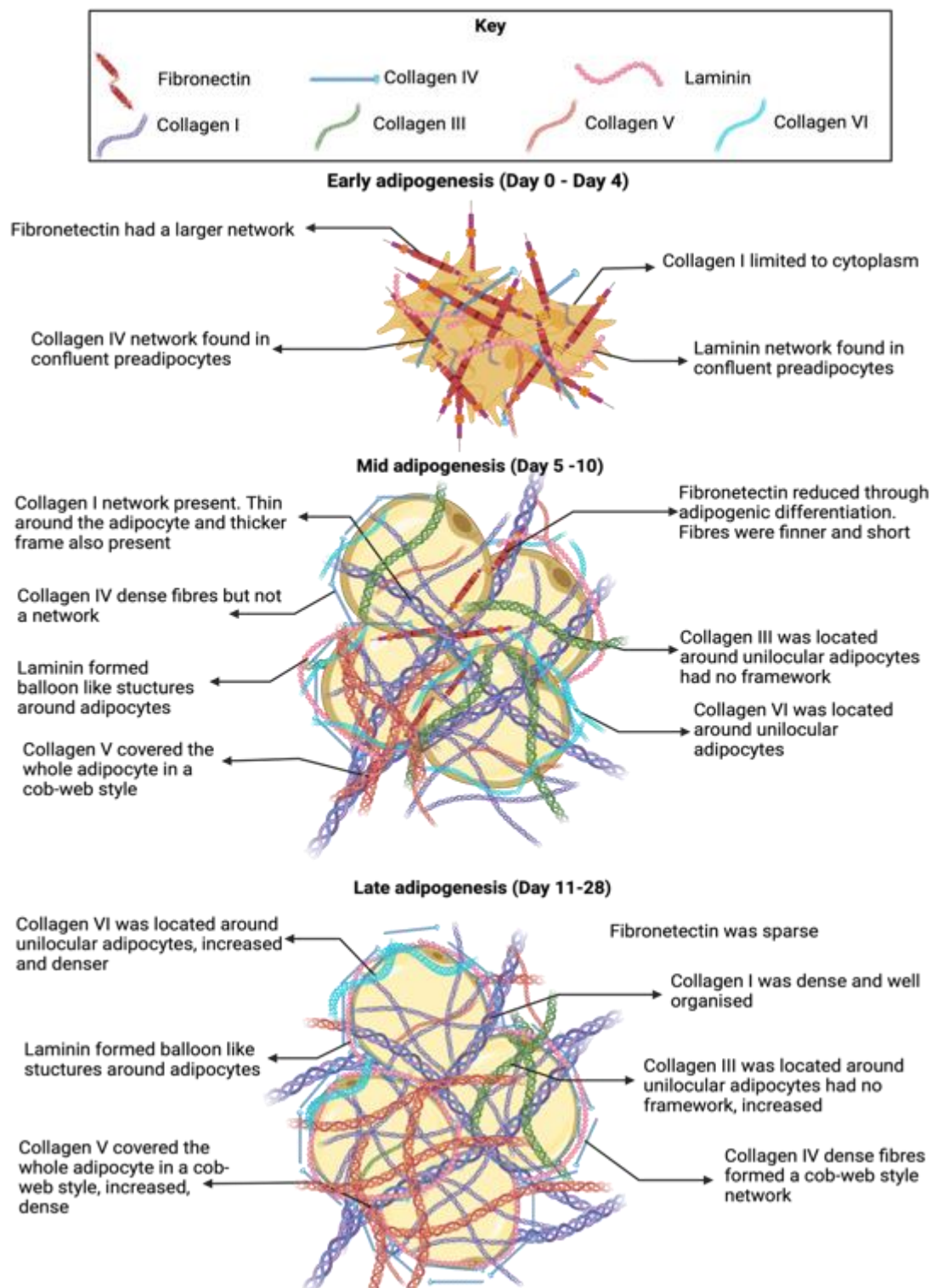


Figure 8. A graphical representation of the ECM surrounding the adipocytes during a month long culture in male mice.

The change ECM is shown above, with 7 ECM proteins based off immunostaining (Brown et al., 2011, Kubo et al., 2000). The presence of ECM proteins is required for adipogenesis, and they may play a role in physically supporting and maintaining the lipid filled adipocytes. Not drawn with correction proportions. Figure made in Biorender.

Alginate fibre to culture stem cells during adipogenic differentiation.

Introduction

2.1.6 Current 2D culture of adipocytes

The majority of research into adipogenesis is completed on flat 2D surfaces (i.e., flasks or culture plates) allowing for the growth of monolayers of cells in an easily controlled environment. 2D culture methods have been seen to grow and maintain viable cells through a multitude of differentiation media and cell types (Ahmad et al., 2017, France et al., 2014, De Melo et al., 2019). 2D culture methods have also shown themselves as a highly repeatable methodology allowing for confidence in the research.

However, 2D cultures are not representative of the in vivo configuration of adipose tissue (Turner et al., 2017) as they miss the multidimensional cell-to-cell connections, which can impact cell signalling. Cell signalling is an important process for the differentiation of adipocytes (Yeganeh et al., 2012, Azarnia and Russell, 1985) and as such the monolayer formation used in 2D cultures does not fully recapitulate the in vivo structure. The 2D tissue culture products have flat stiff surfaces, and are thought to have a low elastic ability and do not bend (Fekete et al., 2018). This may be detrimental for studying adipogenesis as adipocytes fill with lipid droplets as they mature; in particular white adipocytes filling with large amounts of lipids, which go on to eventually fill the whole cytoplasmic space (Mescher, 2016). The increase in lipids causes the cells to become rounder and to lose their contact to the culture plate, as well as more buoyant (Lee and Fried, 2014, Zhang et al., 2000). This could also result in mature adipocytes progressively losing their attachment.

The stiffness of the 2D culture may have a negative effect upon adipogenesis as adipocytes are mechanosensitive and cyclic stretching has been observed to reduce adipogenesis in 3T3-L1 mouse pre-adipocytes (Sen et al., 2008). The stiffness of 2D is determined by the tissue culture plastic, which has been reported to have a Young's modulus of >1GPa (Travers et al.,

Alginate fibre to culture stem cells during adipogenic differentiation.

Introduction

2016). Whereas in hydrogels as mentioned the stiffness can be altered to suit wanted conditions. This mechanosensing could also determine the MSCs differentiation into the type of adipocyte (white or brown) (Rahaman et al., 2014, Lin and Farmer, 2016) Static force also reduces adipogenesis through the down regulation of PPAR γ 2 (Tanabe et al., 2004). The stresses and strains of the 2D culture plastic may in addition change the shape of differentiating cells; if the cells become more spread then less adipogenesis is seen and osteogenesis is more likely (Ang et al., 2014). Therefore, the stretching of multipotent progenitors such as MSC during 2D culture may inhibit adipogenesis.

Additionally, the stiffness of the culture plates themselves may also be a problem as soft substrates (2-3kPa) have been reported to promote adipogenesis even without the addition of adipogenic media (Young et al., 2013), while stiff hydrogels (around 59kPa) have been seen to make MSCs preferentially differentiate into osteoblasts (Darnell et al., 2018, Högberg et al., 2018). The elasticity of adipocytes is much lower than that of osteoblasts (0.9+0.8 kPa and 6.5+2.7 kPa, respectively) (Darling et al., 2008). Adipocytes have recently been shown to decrease in stiffness as the lipid volume increases (Abuhattum et al., 2022). Therefore, a model for adipogenesis may benefit from using a softer or more elastic surface.

2.1.7 The 3D culture of Adipocytes

To achieve a more realistic working 3D model for adipogenesis, different 3D culture models are currently being investigated in many forms. For example, hydrogels (Louis et al., 2017, Albrecht et al., 2022), fibres (more in depth discussion below) (Unser et al., 2016b), microfluidic systems (Compera et al., 2022, Chen et al., 2022) and decellularized scaffolds (DeBari et al., 2021). A recent example of hydrogels used, include a bio-printed gellum gum (a polysaccharide produced by the bacterium *Sphingomonas elodea*) to culture human

Alginate fibre to culture stem cells during adipogenic differentiation.

Introduction

primary adipose stem cells. The adipose stem cells were viable over 98 days and there was an increase in adipogenesis (differentiation rate of 78%) (Albrecht et al., 2022). While the gellum gum was a natural hydrogel, it is not a polysaccharide found in human adipose tissue as such there was no reported interaction between the gellum gum and the primary adipose stem cells, the differentiation rate may be due to the soft stiffness of the gellum gel (Young et al., 2013). This research didn't analysis the native expressed ECM by the adipose stem cells, which would have provided evidence of the hydrogels ability to replicate adipose tissue. A modified HA with the RGDS epitope was combined with collagen I and collagen VI, was used to culture the preadipocyte cell lines (3T3-L1 and 3T3-F442A) and human white preadipocytes were cultured (Louis et al., 2017). This hydrogel was therefore comprised of natural ECM components found in adipose tissue and had a low stiffness (0.45 ± 0.05 kPa) that is required for adipogenesis. The cells were encapsulated were viable and underwent adipogenesis with increased and earlier differentiation than 2D, when gene analysis was completed (Louis et al., 2017). This model is a demonstrates the usefulness of hydrogels from natural ECM components.

The microfluidic systems are small on chip culture comprised of microfluidic channels to supply small amounts of fluids to the cell cultured. One example of microfluidic systems for adipocyte culturing was created by Chen et al. (2022). It was a simple three channel chip with a central channel for a hydrogel mixture containing mouse preadipocytes (3T3-L1). The hydrogel was comprised of collagen I mixed with a range of decellularized matrix components (subcutaneous or visceral adipose tissue from mice with either a high fat-diet or low-fat diet). The adipocytes did differentiate in the model and demonstrated a more representative morphology (than 2D) (e.g., more spherical) (Chen et al., 2022). This model provided a complex mix of ECM components to culture cells. However, there was no identification of any differences in the proteomics between the different decellularized ECMs. In addition, there

Alginate fibre to culture stem cells during adipogenic differentiation.

Introduction

was no analysis of whether the different decellularized ECM produced any difference in the cultured adipocytes.

A more complex microfluidic model used a multichannel chip with 96 3D cell cultures within 32 fluidically individually units (Compera et al., 2022). The human adipogenic stem cells formed aggregated spheroids from single cells in a suspension culture, the lack of ECM was chosen to allow for mass spectrometry without interference from all exogenous ECM components. The adipocytes were successfully differentiated and maintained for two weeks and demonstrated a change in proteomics depending of glucose alterations (Compera et al., 2022). While this model has the advantages of many samples per chip and reduced reagent needs, the suspension culture has no mechanical stimulation for the cells.

Scaffolds used to culture adipocytes include decellularized lung tissue, due to the presence of collagen I, VI and VI in the lung tissue (DeBari et al., 2021). The human adipose stem cells were viable and able to differentiate within the decellularized lungs (DeBari et al., 2021). However, this research was completed with the aim of creating an adipocyte tissue graft for filling large defects, the aims therefore differed from other 3D models of adipocyte culture. In this case the aim was a pre-vascularised high density adipocytes from patient derived adipose cells, such a model could not be used to model adipose tissue for research purposes (DeBari et al., 2021).

A popular model for adipogenesis has been the creation of spheroid cultures; where the 3D cultures show a higher adipogenic gene expression (e.g., CCAAT/enhancer-binding protein (C/EBP) β , peroxisome proliferator-activated receptor (PPAR) γ , fatty acid-binding protein 4 (FABP4)), than those seen in standard 2D culture (Wolff et al., 2022, Mandl et al., 2022). While

Alginate fibre to culture stem cells during adipogenic differentiation.

Introduction

there has been works to investigate the ECM nativity expressed in the spheroid cultures (Christiane Hoefner et al., 2020, Shen et al., 2021) this ECM data was assessed to show how successful the model was not to assess the effect of the ECM component and 3D culture.

When cultured in Matrigel, a hydrogel comprised of several ECM proteins (Hughes et al., 2010), the adipocytes demonstrated a higher level differentiation by 3T3-L1 cells (Josan et al., 2021). The potential benefits of these models are the ability of cells to maintain more natural cell-cell adhesions, as well as the formation of an environmental niche with the 3D distribution of extracellular matrix (ECM) components (Unser et al., 2016b). The inclusion of ECM components provides support, ligands for cell membrane receptors, and a source for signalling factors required for cell migration and differentiation. Specific examples of ECM factors include collagen I and VI, which are required for ECM structure and remodelling (Bonnans et al., 2014). The use of ECM components is also more likely to have a softer and/or more elastic culture environment which will also benefit adipogenesis (Jin, Rozario and DeSimone, 2010).

2.1.8 Alginate

The use of biomaterials, such PEG and collagen has also been reported to model adipogenesis in 3D, for example through the creation a PEG and collagen hydrogel, where PEG allowed for mechanical control and collagen a bioactive ability (Lee et al., 2023). Hydrogels can be similar to native extracellular matrix in terms of biocompatibility and 3D properties (Unser et al., 2015). A common natural material used for hydrogel formation is alginate; a polysaccharide extracted from brown seaweed (Helgerud et al., 2009). Alginate is found naturally in brown seaweeds (i.e. Ascophyllum) as part of the cell wall and is then extracted using alkali solutions (i.e. NaOH) (Helgerud et al., 2009). Alginate is a biomaterial currently used in wound healing, (alginate has anti-microbial and regenerative features)

Alginate fibre to culture stem cells during adipogenic differentiation.

Introduction

(Barbu et al., 2021), cell culture (3D cell culture hydrogels) (Kang et al., 2021) and bone tissue regeneration, reviewed by (Venkatesan et al., 2015) due to its biocompatibility.

Alginate can form a stable hydrogel when interacting with Ca^{2+} , Ba^{2+} , Mg^{2+} and Sr^{2+} (Helgerud et al., 2009, Machida-Sano et al., 2012). It is a polyanionic (negativity charged at several sites) polysaccharide formed from linear residues β -D-Mannuronic acid (M) and α -L-Guluronic acid (G) (Haug, 1964). G is an epimer of M or in other words, M and G are isomers where one of the carbon atoms is asymmetric (Haug, 1964). The variation the organisation and amount of G or M residues alters the chemical characteristics, including hydrogel formation (Haug, 1964). Alginate has been used in a range of cell culture (Liu et al., 2017c), and can be used in many forms from layers on chips (Workman et al., 2007), microbeads (Patel et al., 2016) and micro-strands (Raof et al., 2011).

Alginate in solution is highly viscous due to the intramolecular electrostatic repulsion from its polyanionic nature, the viscosity of chitosan was found to be 187.2 mPa s at 1 s⁻¹ while alginate was 797.2 mPa s at 1 s⁻¹ (Purwanti et al., 2018). To form a hydrogel, the alginate needs to create cross-links of divalent or multivalent cations to the carboxylates and hydroxyls on the residues, thereby producing an intermolecular hydrogel network (Haug, 1964, Haug et al., 1970) (Figure 9). This cross-linking takes place instantaneously. A hydrogel of alginate can be reversed and then returned to a solution, using chelating agents for divalent cations, for example sodium citrate and ethylenediaminetetraacetic acid (EDTA), (EDTA is used to passaging mesenchymal stem cells) (Smidsrød and Skjåk-Bræk, 1990, Soleimani and Nadri, 2009). The other benefit to using alginate as a 3D culture method is that the gentle release of cells entrapped in alginate hydrogels allows for further downstream processing including serial passaging in 3D (Ikeda et al., 2017).

Alginate fibre to culture stem cells during adipogenic differentiation.

Introduction

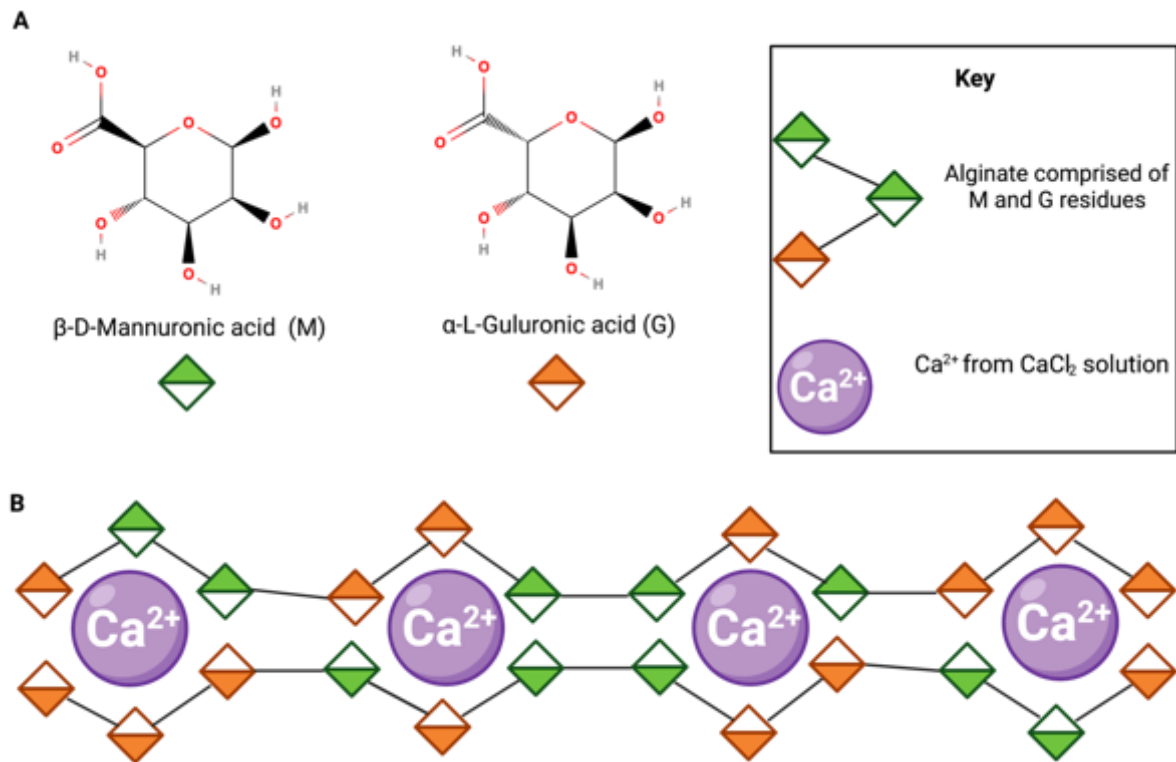


Figure 9. The structure of alginate residues and their bonds with calcium ions.

A The structure of Alginate residues β -D-Mannuronic acid (M) and α -L-Guluronic acid (G). The residues drawn, show that they are epimers of each other. **B** The intramolecular interaction between the cation calcium and the carboxylates or hydroxyls on the alginate, results in the formation of an alginate hydrogel. Figure made in Biorender.

Alginate is a biocompatible material able to be physically manipulated, allowing easier movement when in the laboratory (Tam et al., 2011). Another benefit of alginate is that small molecules (\sim <60kDa) can pass through the pore sizes present in alginate hydrogels allowing for nutrient exchange (Li et al., 1996). In addition, alginate hydrogels are soft, the young's modulus can be as low as 2kPa, though this is dependent upon concentration of alginate, cross-linker and the molecular weight of the alginate (Dalheim et al., 2019, Freeman and Kelly, 2017), potentially allowing for better culturing of adipocytes. Alginate hydrogels have been used as an encapsulating agent for cell culture but with the exception of neural cells, most cell

Alginate fibre to culture stem cells during adipogenic differentiation.

Introduction

types can not adhere to the surface of alginate hydrogels (Kang et al., 2012). To counteract this alginate hydrogels have been formulated with ECM components, such as alginate-gelatin (Sakai et al., 2008), and by the addition of ECM component motifs, for example alginate-RDGS (Alsberg et al., 2001). The alginate-gelatin fibre hydrogel supported smooth muscle cells on the surface and endothelial cells in the core, before being encased in collagen and the alginate degraded, to form channels of cells within the collagen hydrogel. In the preliminary testing on 2D alginate did not allow for cell attachment (Sakai et al., 2021). An RDGS modified alginate was studied with the aim of bone regeneration, when unmodified alginate was used there was a minimal cell adhesion but the modified alginate was found to increase cell adhesion, cell proliferation and cell differentiation into osteoblasts (MC3T3-E1 cells) (Alsberg et al., 2001).

These mixed alginate hydrogels mentioned above have to be used to make 'surface type' hydrogels where cells are seeded upon the external surface of the fibres and as such are still a version of 2D culturing as there is a monolayer of cells on the surface of the fibre (Lee et al., 2010, Hirayama et al., 2013). For a true 3D approach with 360° of culturing the cells need to be seeded within the fibre (encapsulation). To encapsulate cells, the cells are re-suspended in the pre-gel solutions, if the pre-gel solution is alginate by itself then the cells will still have problems adhering. A solution to this was to create soft-core fibres, which use an ECM component as a core for the fibre. Cells are re-suspended into an ECM component to which the cells can adhere. The alginate hydrogel is then created around the soft-core containing the cells (Trebbin et al., 2013, Bouhleb et al., 2022).

Alginate fibre to culture stem cells during adipogenic differentiation.

Introduction

2.1.9 Fibres as an adipogenic culture model

Alginate cell encapsulating hydrogel fibres, also named 'core shell hydrogel fibres', are formed by a laminar flow device or co-axle needle (Onoe et al., 2010). This is where a collagen solution core containing cells is first surrounded by sodium alginate solution and then by a calcium chloride solution. The use of calcium chloride, results in crosslinking of the alginate around the collagen/cell solution. The fibre can then be wrapped around a cylinder or weaved (Onoe et al., 2010). Different cell types (cortical cells and the HepG2 cells) trialled in this method were able to fill the space within the core for up to 18 days and kept the shape of the fibre after the alginate shell was removed due to cell-cell adhesion and interactions with the collagen (Onoe et al., 2010). The cell types tested in this model maintained their metabolic activity in the fibres even when weaved. This work has been suggested as a method to build 3D functional artificial tissues (Onoe et al., 2010).

Human induced pluripotent stem cells have also been cultured within hydrogel alginate fibres, without the presence of Matrigel, collagen or collagen present or Matrigel present in the core. The fibres were assed as a more viable system for stem cell expansion (Ikeda et al., 2017). They allowed for cells to proliferate while maintaining a small aggregate cell thickness. It was also shown that the fibres had the ability to expand the number of stem cells greatly, as the cells proliferated up to 14-fold in 8 passages. The expansion was done by passaging the cells from the fibres after removing the alginate shell and entering back into a collagen solution to have more fibres produced (Ikeda et al., 2017). The human stem cells remained pluripotent even after the serial passaging for 44 days (11 passages) shown in the high levels of pluripotent associated marker genes (i.e., Nanog and Oct3/4). The cells within the fibre were able to differentiate into all three germ layers again showing pluripotency remains (Ikeda et al., 2017). Therefore, the alginate fibres were a viable system to maintain and expand several cell lines while maintaining their ability to differentiate.

Alginate fibre to culture stem cells during adipogenic differentiation.

Introduction

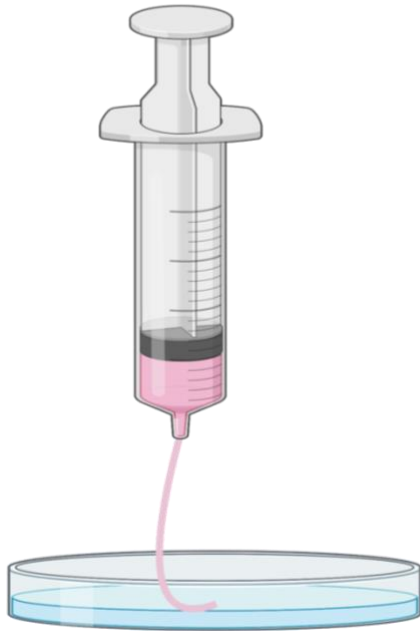
An alteration to the above method created fibres with a liquid centre made by creating alginate fibres covered in 0.05% poly-L-lysine (PLL) and incubating in 1.6% sodium citrate to liquidise the alginate with the PLL (Raof et al., 2011, Unser et al., 2016b). The Murine WT-1 preadipocytes within the fibre then differentiated into adipocytes and remained viable for the 27 days of culture (Unser et al., 2016b). The presence of adipocytes, specifically brown adipocytes was confirmed using ORO, though images were not clear, and the presence of PPAR γ 2, Perilipin (present on the surface of lipid droplets) and UCP1 were identified using immunochemistry. There was an increase in relative expression (fold change) of UCP1, PGC1 alpha and Ap2 (fatty acid binding protein 4) compared to 2D culture of the same cells (Unser et al., 2016b). This model did not have any addition of ECM proteins which as mentioned are an important component of adipogenesis.

There are two methods available to create hydrogel fibres: extrusion and laminar flow, see Figure 10 (Zhang et al., 2010, Kiriya et al., 2012). The extrusion method simply extrudes a pre-gel solution in a syringe needle or micro-nozzle (i.e. alginate) into a gelling solution (i.e. CaCl₂) (Zhang et al., 2010). Laminar flow is the most commonly used method where embedded syringe needles or glass capillaries are used to form a laminar flow within a microfluidic channel and when the two fluids interact gelation occurs (Kiriya et al., 2012). Laminar flow allows for a more controlled creation of hydrogel fibres as the flow rates and dimensions of the needles or capillaries can be altered depending on desired characteristics of the fibre (Kiriya et al., 2012, Trebbin et al., 2013).

Alginate fibre to culture stem cells during adipogenic differentiation.

Introduction

A



B

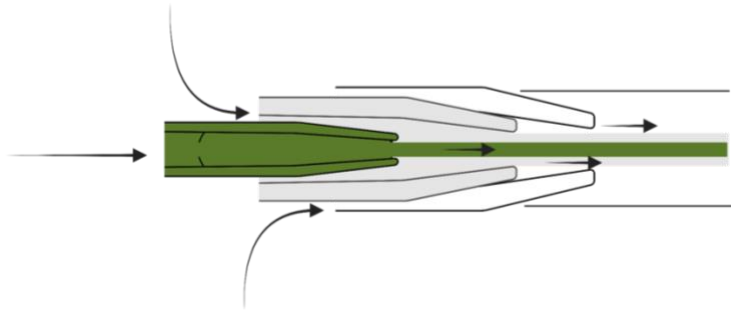


Figure 10. Diagrammatic representation of extrusion or laminar flow hydrogel production.

A In extrusion printing the polymer is extruded out of the nozzle under pressure to form a continuous fibre or filament. This method can be used for simple hydrogel fibre production or can be present in bio-printing with a movable platform to create more complex structures, reviewed in (Zhang et al., 2022c). **B** Laminar flow is the flow of solutions in smooth paths with little to no mixing. In fibre creation a core (green) is surrounded by a secondary solution, often a biomaterial, such as alginate, and then surrounded by the gelator for the biomaterial. Thereby creating a layered fibre that forms continuously from the needle or pipette tip (Onoe et al., 2013).

Alginate fibre to culture stem cells during adipogenic differentiation.

Introduction

2.1.10 Chapter aims

The increasing levels of obesity have raised need for adipogenesis research in recent years. The current method of culture tends to be 2D which is not representative of adipose tissue, thereby reducing the efficiency of this research. This pilot study will describe the initial assessment of a collagen I core fibre and whether it has the capabilities to be an accurate 3D model for mouse mesenchymal stem cell adipogenesis and proliferation. The mouse cells will be used as they have been used often in the research of adipogenesis (Velickovic et al., 2018). In further work after a pilot study human cells would be more presentative. First, the production method of the fibre will be assessed for it to be a reliably produced and that the model can be manipulated and stable throughout culture. Second, the ability of the fibre to maintain viable cells throughout a culture time of 14 days will be investigated. Third, the ability of the cells within the fibre to undergo adipogenesis will be researched, also through 14 days. The final aim will be to assess any changes in the differentiation ability of the cells cultured within the soft-core fibre once removed from the fibre.

Alginate fibre to culture stem cells during adipogenic differentiation.

Materials and methods

2.2 Materials and methods

2.2.1 Cell Culture

Mouse mesenchymal stem cells (D1) (MSCs) (ATCC CRL-12424) were maintained at 37°C with 5% CO₂ in control Medium; low glucose Dulbecco's modified Eagle's medium (DMEM) (ThermoFisher, UK) supplemented with 1% penicillin/streptomycin (ThermoFisher, UK), 1% non-essential amino acid (ThermoFisher, UK), 1% L-Glutamine (ThermoFisher, UK) and 5% foetal bovine serum (ThermoFisher, UK) (Velickovic et al., 2018, De Melo et al., 2019). Adipogenesis was induced when the MSCs were at 80% confluency with adipogenic medium; standard maintenance medium supplemented with 1µM Rosiglitazone (Cayman Chemicals, USA), 100µM isobutylmethylxanthine (IBMX) (Sigma-Aldrich, UK), 1µM Dexamethasone (Cayman Chemicals, USA), and 10µg/mL Insulin (Sigma-Aldrich, UK), previously used (Velickovic et al., 2018). The Medium was changed every 48 hours.

2.2.2 Laminar flow soft-core fibre production

The MSCs cells were removed from the culture flasks with trypsin and re-suspended (5 million cells per mL) in collagen I solution (3mg/mL) comprised of Dulbecco's Modified Eagles Medium (DMEM), NaOH (0.79%) (1N) (Corning, UK) and collagen I (Sigma-Aldrich, UK). A mixture of 2% w/v alginate solution (FMC Agro Ltd, Flintshire, UK) and 2% w/v CaCl₂ (Sigma-Aldrich, UK) were prepared and loaded into 50mL syringes. The alginate solution was first pushed through the co-axel needle (18G) (Electrospinning, China) at a rate of 0.4mL/min to make sure the alginate flows through the needle in the correct direction. The CaCl₂ solution was then pushed through at a rate of 0.4mL/min to surround the alginate, thereby allowing the CaCl₂ to form crosslinks with the alginate and form the fibre. The needle was set 16cm away from a roller and the fibre was then placed upon the roller spinning at a rate of 60 RPM: creating a fibre bundle. Once a solid fibre is produced the collagen I (3mg/mL)/cell solution (5

Alginate fibre to culture stem cells during adipogenic differentiation.

Materials and methods

million cell/mL) was flushed through the smaller needle (27G) in the centre, at a rate of 0.08mL/min; creating a soft-core cell laden fibre. A new fibre was pulled every minute during this process. See Figure 11 for a representation of fibre creation.

After pulling, the fibres were further cross-linked for 2 minutes in warm crosslinking medium: dH₂O supplemented with HEPES buffer (10x stock) (10%) (Sigma-Aldrich, UK), 1mL 2% Antibiotic-Antimycotic (AB/AM) (ThermoFisher, UK), CaCl₂ (100mM) and NaOH (1N) until pH ~7.4. The fibres were then transferred to washing medium, comprised of DMEM with 2% AB/AM in an incubator set at 37°C and 5% CO₂ for 2 hours, in 6-well plates (1 fibre per well). The time in the washing media allowed the collagen I to polymerise. The final fibres had a calculated radius of 0.727mm with the alginate layer being 0.622mm thick and the radius of the inner collagen core was 0.105mm. Method similar to previous work (Onoe et al., 2013).

Alginate fibre to culture stem cells during adipogenic differentiation.

Materials and methods

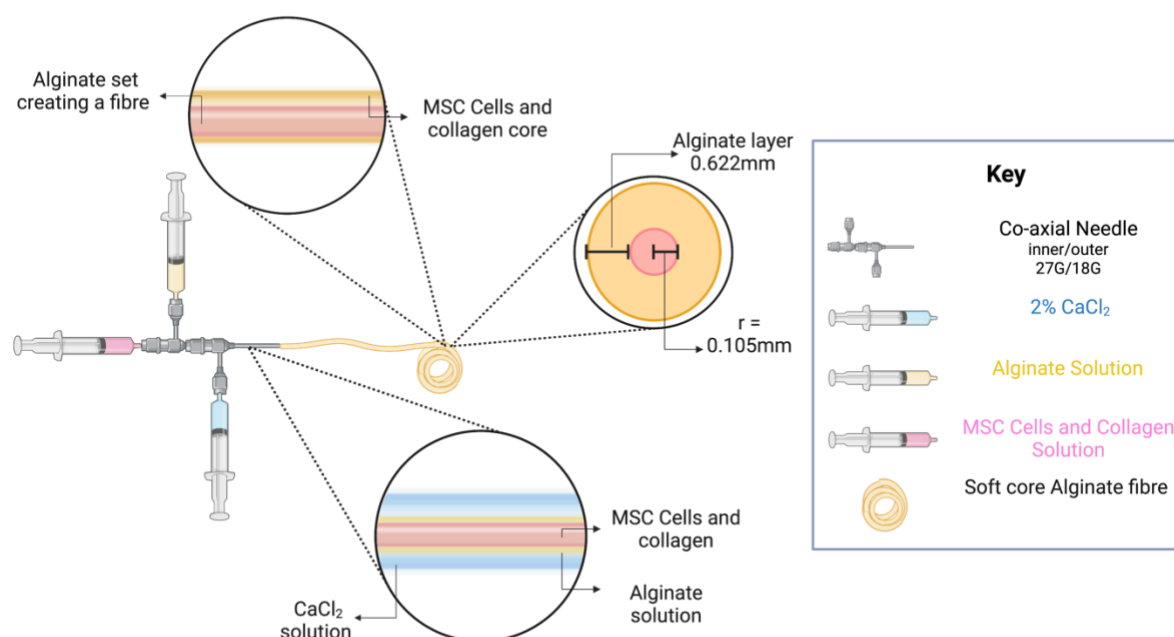


Figure 11. A graphical depiction of the creation of the fibre.

The fibre was created by co-axial needles (inner/outer 27G/18G) through which a core of MSC stem cells (5 million cell/mL) and collagen I solution (3mg/mL) (pink) was surrounded by 2% w/v alginate solution (yellow). The alginate was then set into a hydrogel by surrounding it with 2% w/v CaCl₂ solution (blue). The set alginate hydrogel fibre was then coiled for a minute and then a new fibre was made. The alginate fibres were further cross linked for 2 minutes in cross linking solution with 100mM CaCl₂. The collagen was polymerised in DMEM for 2 hours. Figure made in Biorender.

2.2.3 Cell Seeding

MSCs (D1) (ATCC CRL-12424) cells were seeded on top of 2D culture plastic with the same number of cells as a fibre. Therefore, 400'000 cells per 3.5 cm² were seeded (12-well plate; Fisher Scientific, Leicestershire, UK). Adipogenesis was then induced in selected plates and fibres with the addition of adipogenic medium added to 2D cultured cells and the fibres. The medium was changed every 72 hours for the fibres.

Alginate fibre to culture stem cells during adipogenic differentiation.

Materials and methods

2.2.4 Cell Metabolic Assays

The cell viability was assessed using a measure of metabolic activity from the resazurin-based Presto Blue reagent (10% w/v) (ThermoFisher, UK), based off a metabolic assay previously used (Velickovic et al., 2019).. Cells were cultured in 10% v/v Presto Blue in control medium (presto blue solution) and incubated for 40 minutes at 37°C. The 2D wells were incubated in 500µl of presto blue solution per well, but as the fibres were physically larger the volume of presto blue solution used was 2mL per fibre. 100µl of the Presto Blue medium was taken to have the fluorescence measured. The fluorescent signals were measured in triplicate using an Infinite M200 PRO plate reader and i-control software (Tecan, Switzerland). The signal measured was at an excitation of 560nm and emission of 590nm and then expressed in arbitrary units (AU). The reaction between the preston blue solution and the cells within the fibre was therefore four times more diluted than the reaction in 2D (2mL of presto blue solution than 500µl), to compensate the measured signal from the fibres (AU) was multiplied by four. Data shown as mean +/- SEM.

2.2.5 Live and dead imaging

Calcein AM (2µM) and Ethidium homodimer (4µM) (R&D Systems, UK) were supplemented in the maintenance medium. The fibres were incubated in 2mL and the 2D in 500µl of the staining solution for 30 minutes at room temperature. Both were then live imaged on a Nikon Eclipse TS2 microscope coupled with a Nikon D3300 camera (Nikon Instruments Inc, USA). Calcein AM has an excitation of 494nm and an emission of 517nm (green), while ethidium homodimer has an excitation of 528nm and an emission of 617nm (red) (Bradley et al., 1998).

Alginate fibre to culture stem cells during adipogenic differentiation.

Materials and methods

2.2.6 Lipid staining.

Bodipy 493/503 (4,4-Difluoro-1,3,5,7,8-Pentamethyl-4-Bora-3a,4a-Diaza-s-Indacene) (ThermoFisher, UK) was used to show the presence of lipids. Maintenance medium was supplemented with 1 μ l/mL of Bodipy as used by *De Melo* and others (Velickovic et al., 2018, De Melo et al., 2019). Live fluorescent images were taken on the Nikon Eclipse TS2 microscope and Nikon D3300 camera.

For the ORO staining of the plates the previously used protocol was used (Velickovic et al., 2019, De Melo et al., 2019). For the staining the fibres were washed in HEPES buffer (25mM) (pH 7) not Phosphate buffered saline (PBS) and then fixed in 4% paraformaldehyde (in HEPES buffer) (ThermoFisher, UK) for 20 minutes. Once washed again with the HEPES buffer the fibres were covered in 1mL per well of 60% ORO solution (Sigma-Aldrich, UK) for 15 minutes. The fibres were then washed in phenol free medium (ThermoFisher, UK) to remove ORO stain trapped in the fibre itself not the cells. The fibres were placed in 60% isopropanol for 30 seconds to remove non-specific staining, then placed back into the phenol free medium. The 60% isopropanol washes and medium washes were repeated until as much as possible of the non-specific ORO stain was removed. The fibres were then imaged using Nikon Eclipse TS 100 microscope with a Nikon coolpix S10 VR camera (Nikon Instruments Inc, USA). Data collected over several days kept the settings within the plate reader for the measurement of ORO absorption.

2.2.7 Removing cells from fibres

The alginate surrounding the fibres was removed using a chelating agent, sodium citrate (Sigma-Aldrich, UK). The fibres were placed into two concentrations of sodium citrate (150mM and 75mM) with 5mL per fibre. The dissociated fibre mixture containing the cells were then

Alginate fibre to culture stem cells during adipogenic differentiation.

Materials and methods

spun down to remove the fibre components (centrifuged at 2000rpm for two minutes). The cells were re-suspended in maintenance medium or trypsin before reseeding. The cells re-suspended in 0.5mL of trypsin (ThermoFisher) for two minutes at 37°C were then spun down, the trypsin was removed, and the cells re-suspended in standard maintenance media. All the cells were then seeded onto 2D culture plates (24 well) (ThermoFisher, UK), and each fibre was split 1:12. On the second day of culture, the cells were stained with medium supplemented with Calcein AM (2 μ M) and Ethidium homodimer (4 μ M) (ThermoFisher, UK) and live imaged on a Nikon Eclipse TS2 microscope coupled with a Nikon D3300 camera, as done above. The cells did not reach 80% confluency until 4 days after seeding, when adipogenic medium was added. The ORO imaging and extraction of the reseeded plates followed previously used methods (Velickovic et al., 2019, Velickovic et al., 2018), after 7 days of culture.

Alginate fibre to culture stem cells during adipogenic differentiation.

Materials and methods

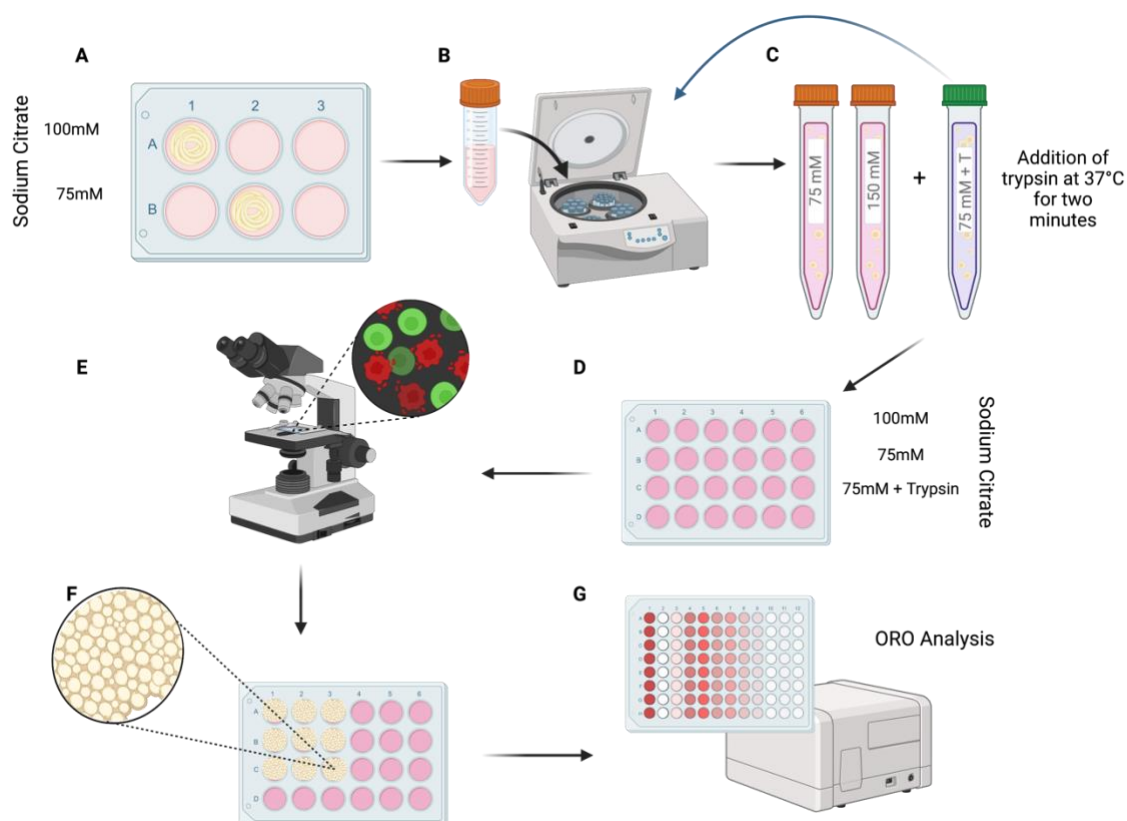


Figure 12. A flow chart detailing the method to optimise the removal of the cells from the fibres. **A** The cells were placed into two concentrations of sodium citrate (100mM and 75mM) till the alginate was seen to be dissolved. **B** The sodium citrate solution was centrifuged to form a cell pellet. **C** Once the supernatant was removed the cells were resuspended in control medium, except for one group which had used 75mM sodium citrate, 0.5 mL trypsin was added for two minutes at 37°C. The solution was spun again and the cell resuspended in control medium. **D** All conditions (100mM, 75mM and 75mM + trypsin) were plated onto a 24 well plate. **E** After 48 hours the cells were imaged using Calcein AM (2mM) and Ethidium homodimer (4mM). **F** Once the cells had reached 80% confluency, they were stimulated to undergo adipogenesis. **G** After 7 days the lipids were removed and quantified (ORO analysis) through absorbance at 510nm on a plate reader.

2.2.8 Cryosectioning

Fibres were fixed in HEPES 4% Paraformaldehyde for 15 minutes before being surrounded by OCT (optimum cutting temperature) compound (ThermoFisher, UK) and frozen at -25°C (Liyanage et al., 2017) upon a cryostat (Leica CM2018) (Leica Biosystems Lab Solutions, UK). The fibres were then sectioned at a 10µm thickness. Sections were taken as cross-sections through a bundled fibre or longitudinally along a bundled fibre. The sections were placed upon

Alginate fibre to culture stem cells during adipogenic differentiation.

Materials and methods

gelatine coated slides (Sigma-Aldrich, UK), left to dry in at room temperature for 48 hours, then washed in HEPES buffer (25mM) to remove the OCT compound while keeping the alginate fibre on the side. Hoechst 33342 (2,5'-Bi-1H-benzimidazole, 2'-(4-ethoxyphenyl)-5-(4-methyl-1-piperazinyl)- 23491-52-3) (ThermoFisher, UK) staining was added to HEPES buffer (25mM) and added to the slide, covering all sections at room temperature for 30 minutes. The slides were then covered with coverslips (Fisher Scientific, UK) using Fluoro-shield mounting media (Abcam, UK). The slides were then imaged on the Nikon Eclipse TS2 microscope coupled with a Nikon D3300 camera.

2.2.9 Total corrected fluorescence intensity using Fiji ImageJ

ImageJ (version:2.0.0-rc-69/1.52p) was used to measure the fluorescence intensity of all the live and dead staining completed. The intensity of the cells was measured in 3 images for each stain per each sample. The intensity was measured in both the areas of each image with visible signal and areas without signal (background). The corrected total cell fluorescence (CTCF) was calculated to remove the background signal to get an accurate measure of the true signal. $CTCF = \text{Measured intensity of visible signal} - (\text{Area of visible signal} \times \text{mean fluorescence of the background})$ (McCloy et al., 2014, Bhavsar et al., 2019). However, several images had negative CTCF values due to no visible signal and high background. The negative numbers were removed and indicated within Figure 17.

2.2.10 Statistics

All data was assessed by MANOVA, and ANOVAs with post hoc tukey testing when there was a significant difference in an independent condition. Significant results shown indicated by p-value *P<0.05, **P<0.005, ***P<0.001. Data was analysed using SPSS statistics software version 28.0.0.0(190).

Alginate fibre to culture stem cells during adipogenic differentiation.

Materials and methods

Due to the loss of supervisors and COVID the number of repeats for this work is too low to have complete confidence in the results. The live dead analysis of the fluorescence used images. There was a biological repeat of $n = 2$, for each biological repeat 3 images were measured per sample. Except in the ethidium homodimer staining for the 2D plate where only one image could be used due to the difficulties in measuring the background staining (days 3, 7, 10). For each image taken three measurements were taken. For the metabolic assay there was a variation in the number of biological repeats with an $n = 1$ for all measurements taken on day 0 and day 14 and $n = 2$ for days 3, 7 and 10. On all days for each condition (2D or fibre, control or adipogenic) there were three replicates taken. For the assessment of ORO there was a biological repeat of $n = 2$, for each sample 3 replicates were taken. The quantification of lipid content between the fibre and 2D, had an $n = 2$ biological repeats, with three replicates per sample. The corrected total fluorescence live dead analysis for the removal methods, had a biological repeat $n = 1$, and three images were taken, for each image three measurements were used. Finally, the assessment of lipid content after removal from the fibres, had a biological repeat of $n = 1$ and three replicates per condition.

2.2.11 Data collection

The time points and analysis are shown in Figure 13. The repeats for all experiments are listed in results as numbers varied due to the number of fibres that could be produced. CTFI was always calculated for any images of live and dead. There was first the assessment of viability (live dead staining, metabolic activity assay) and adipogenesis (bodipy, ORO) completed upon cell cultured on 2D plates or fibres and in both maintenance medium and adipogenic medium. ORO was not completed on day 14 for in adipogenic medium or in maintenance medium on days 3 and 7 due to limited fibre production. Fibres were cultured in maintenance and adipogenic medium till day 7 for cryosectioning. The analysis of the best removal method was

Alginate fibre to culture stem cells during adipogenic differentiation.

Materials and methods

assessed after 7 days in culture and reseeded on to tissue culture plates, 2 days later live and dead staining was completed with CTFI calculated. 2 days after that the cells reached 80% confluency and a 7-day adipogenic differentiation was started, after which the cells were stained with ORO.

Alginate fibre to culture stem cells during adipogenic differentiation.

Materials and methods

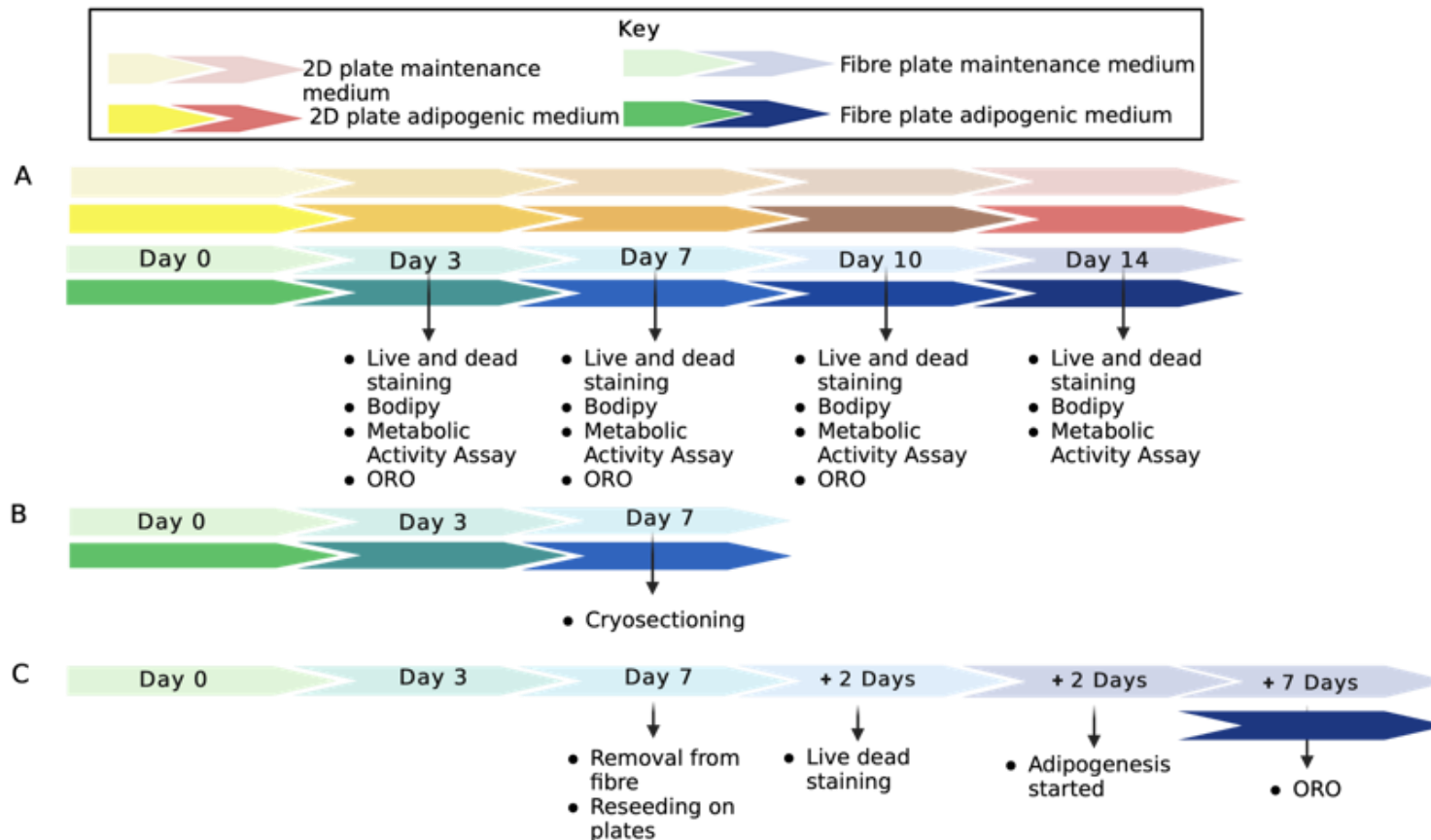


Figure 13. Flow chart demonstrating the collection of data points

A The data collection for all comparison between the 2D cell culture and the fibre, viability and adipogenesis. Data points were not all collected on the same fibres but were set up to collect data at the same time points to allow for comparison. The 2D plates and fibres were treated to the same tests each time. **B** Fibres fixed and then cryosectioned. **C** The assessment of the removal methods from the fibres and the cytotoxic effect upon MSCs, followed by an assessment of adipogenic differentiation ability. The 2D are shown in the yellow to red day arrows, while the fibres are green to blue. The paler arrows are cells kept in maintenance medium and the brighter colours are cells cultured in adipogenic medium. Figure made in Biorender.

Alginate fibre to culture stem cells during adipogenic differentiation.

Hypothesis

2.3 Hypothesis

This preliminary study set out to investigate the feasibility of soft-core fibres containing mouse MSC cells as a 3D model for the differentiation of adipocytes. As the most common method currently used to grow adipocytes is on a flat 2D surface of tissue culture plastic (Ahmad et al., 2017, France et al., 2014). While the 2D culture is suitable in many ways - cell attachment, viability, and differentiation ability, it is not representative of *in vivo* tissues, nor is the best representation of adipose tissue, as shown in

Figure 14. The 2D culture methods adversely alter the cells due to the cell adhesions only being present on one plane, which leads to forced polarity and unnatural stretching of the cells. There was also reduced cell to cell interaction and limited cell interaction with ECM components. The tissue culture plastic was very stiff (~1 GPa) (Buxboim et al., 2010), which is completely different to adipocytes and white adipose tissue which have been found to be very elastic (0.9+0.8 - 2 kPa) (Young et al., 2013, Darling et al., 2008).

This fibre had the potential to be a more reliable approach to modelling the differentiation of adipocytes as it allowed the MSCs to make cell-cell connections in 360° as well as interacting with the extracellular matrix component collagen. The fibre may have provided other benefits for adipocyte culture as shown in

Figure 14, as it may have been less rigid which, may have provided a better environment to keep the rounding adipocytes in the culture and to reduce the cell stresses and strains which can prevent adipocyte differentiation (Sen et al., 2008, Tanabe et al., 2004). A three-dimensional model for adipogenesis as closer to the true process may then allow for a more accurate platform to test the upcoming weight lose drugs or treatments. A platform able to do this would then provide a model that could be used in place of or before animal testing.

Alginate fibre to culture stem cells during adipogenic differentiation.

Hypothesis

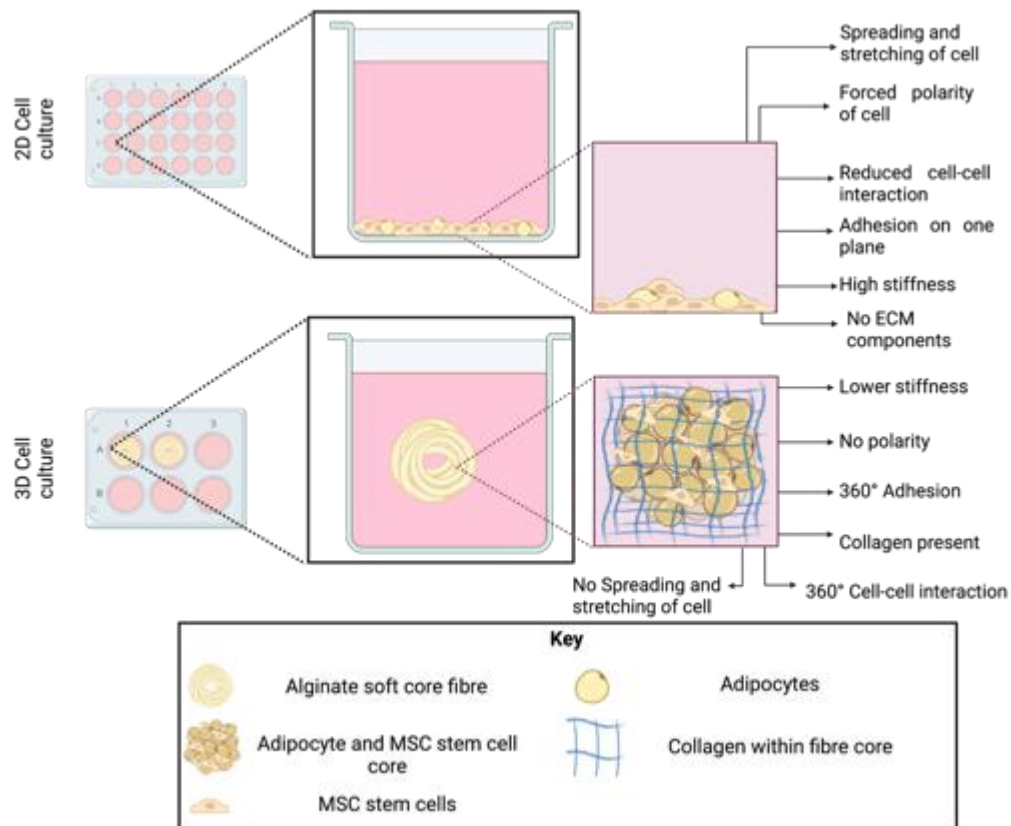


Figure 14. A graphical representation of the benefits to a soft-core fibre to culture adipocytes. The 2D culture methods commonly used to culture adipocytes, shown above were tissue culture plastic. This culture method was used as a control to compare adipocyte viability and differentiation ability against an alginate fibre with a core of collagen and cells. When cultured on the tissue culture plates the adipocytes were forced to endure disadvantageous conditions, which may prevent adipocyte differentiation and were less representative to actual adipose tissue. The disadvantages to 2D tissue culture include: the stiffness of the plate, forced polarity and spreading upon the cells and reduced cell to cell interaction. The proposed fibre study attempted to create an improved environment for adipocyte culture. The fibre model above presents a fibre post differentiation and a visualisation of the core of a fibre. The adipocytes and undifferentiated MSC are present in 360° cluster interwoven with collagen. Figure made in Biorender.

Alginate fibre to culture stem cells during adipogenic differentiation.

Results

2.4 Results

As detailed in the methods (See section 2.2.2 and page 47), the alginate fibres were created first without the inner core; the alginate solution and CaCl_2 solution were pushed through a co-axial needle and then pulled from the needle with twisters to be placed upon a rotating roller where it was wound around to form a coil of fibre, as shown in Figure 11. Once a fibre was completely formed, there was no blockage and the fibres retained their shape upon the roller, the collagen and MSC solution was pushed through the needle. The cell solution entered the needle first (Figure 11), the alginate solution, and then CaCl_2 surrounded both. The alginate is set by the CaCl_2 , and the collagen polymerised when heated from ice cold.

A 3D hydrogel was likely to be beneficial for many of the reasons mentioned above (Figure 14) but the 2D culture methods were undoubtedly easier and simpler to use. Therefore, it was important to assess the fibre production method for several factors. These factors were the technical aspect and for the viability and differentiation ability of the MSCs. First, the assessment technical production methods and the fibres' ability to be cultured.

The materials used to make the fibre were a major reason for the selection of this 3D model. As shown in Figure 11 the outer layer was created from alginate. Alginate was known to make hydrogels with a softer stiffness than culture plastic (Andersen et al., 2015). The internal core of this 3D model was comprised of collagen I and MSCs, this was an ideal ECM protein as collagen I located in adipose tissue surrounding the lipid filled adipocytes (as seen in Figure 8). During adipogenesis the collagen I network forms to provide support for the adipose tissue. The presence of one ECM component may allow for a more natural and representative model.

Alginate fibre to culture stem cells during adipogenic differentiation.

Results

2.4.1 Characterisation of the fibre for the technical requirements

For the fibres to be used as a culture method for adipogenesis the fibres must meet both technical/physical specifications and cellular specifications. Firstly, the fibres' ability to meet the technical requirements shown in Figure 15 was assessed. The technical specifications have been separated into those needed for production and those for culturing.

<u>Production</u>	<u>Culture</u>
<ul style="list-style-type: none">• Time taken to produce fibres was not extremely long	<ul style="list-style-type: none">• Remained stable through culture
<ul style="list-style-type: none">• Reliably made	<ul style="list-style-type: none">• Could be physically manipulated
<ul style="list-style-type: none">• Production of >20 samples in one process	<ul style="list-style-type: none">• Cells can be monitored throughout

Figure 15. The technical requirements the hydrogel fibre needs to meet to be a potential 3D model for adipogenesis.

The requirements are split into two categories, the materials used to make the fibres, the production method, and the fibres ability to be cultured.

Assessment of production methods

The fibre production itself had several benefits as shown in Table 5 when running successfully the system was able to produce a fibre a minute. Provided the fibres remained intact, this extremely quick formation process allowed the production of a large number of fibres in one process, a benefit for larger scale experiments. In addition, as the alginate is clear and the collagen and MSC solution contained phenol adulterated medium, and the inner core was seen through the alginate. This was particularly helpful to make sure that the collagen cell solution was present within the fibre and allowed for quality control through the production time. The time taken to set up the production process including collecting the cells was around an hour.

Alginate fibre to culture stem cells during adipogenic differentiation.

Results

Table 5. An assessment of the fibres' characteristics, including the production and culturing.

	Advantages	Disadvantages
Production	<p>One fibre made per minute once formed</p> <p>Large number of fibres can be made in one attempt</p> <p>Cell and collagen solution can be seen through fibre</p>	<p>Pulling the alginate fibre from the needle could be difficult</p> <p>Needle got blocked from alginate and the collagen and MSC solution (reduced cell loading). Occurred at least once everytime fibres were made.</p> <p>Cell and collagen solution did not form a continuous core (reduced cell loading)</p> <p>Time taken can be unexpectedly long</p>
Culturing	<p>Can be handled with ease using tweezers</p> <p>Cells were easily seen and imaged through alginate surface</p> <p>Remained stable in medium culture</p>	<p>Fibre can be damaged or broken if sucked up though pipette tip</p> <p>Cannot be placed into PBS, as the alginate will partially disintegrate</p>

However, the production time itself varied depending upon how well the alginate layer formed and could be pulled from the needle. This was a major disadvantage to the protocol and required optimisation (Table 5). The gelling of the alginate occurred within the needle; it therefore could become hard to pull the alginate fibre from the needle tip. The pulling of the fibre took time and the longer this took the more likely the needle would become blocked,

Alginate fibre to culture stem cells during adipogenic differentiation.

Results

potentially increasing the time needed to produce the fibres. As the MSCs and collagen were kept on ice, the longer the production process takes the more potential damage to the cells. The inability to accurately predict the time of production protocol reduced the efficiency of this production method. Once blocked the needle was unlikely to be unblocked, though attempts were made by disassembling the equipment. There were instances where there was no unblocking the needle without risking the needle becoming unsterile and as such no fibres were produced.

As the core of collagen and MSC was visible through the alginate, it was clear that the core was not always present during fibre production. While there was plenty of collagen and MSC within the syringe the pink colour from the medium would fade within the fibre till none was present. In others cases the core was interrupted temporarily, and the colour would return. As the alginate fibre surrounding the core continued to be expressed without interruption, it was the collagen and MSC solution itself that blocked the needle. Whether this was due to the collagen polymerising due to heat or the cells clumping and forming a block was not known. If the interruption was temporary then the fibres would have a reduced cell load, which produced fibres with a range of cell number. A range of fibres with differing cell numbers would make some experiments or downstream analysis more difficult. If the blockage was not able to be removed without risking compromising the sterility of the needle, then production of the fibre was stopped. The fibres were often unable to meet the reliability requirements listed in Figure 15 and as such require further optimisation.

Assessment of fibres during culturing

When the fibres produced were placed into culture medium and adipogenic medium, there was no visible swelling or disintegrating of the fibre. The fibres were easily imaged as the

Alginate fibre to culture stem cells during adipogenic differentiation.

Results

alginate was optically clear. (Table 5). In addition, the fibres were moved from well to well without trouble as manipulation with tweezers could be done without damaging the fibres. While tweezers did not damage the fibre, no suction or aggressive pipetting could be used as the fibre would break. This was not detrimental to culture but should be noted for further experiments. More problematic for cell culturing was the fibres' reaction to being in PBS, where the fibres swelled till they began to disintegrate though not completely (Table 5). Therefore, any protocol that required washing steps or the use of PBS needed to be altered; for example, the 4% PFA solution used for fixation was produced using HEPES buffer instead of PBS. The fibres did meet the technical specifications for culturing listed in Figure 15.

The characterisation of the fibres' ability to meet the technical requirements to be a 3D model for adipogenesis showed that the fibres were able to meet most of the specifications required. There was still optimisation to be completed to make the fibres production more reliable both in terms of actual fibre production and the constant presence of the inner core.

2.4.2 Viability of Mesenchymal stem cells in a soft-core fibre.

In addition, to the technical requirements for the fibres, the fibres must be non-toxic to the MSCs and able to support the differentiation of adipocytes and their lipid droplets. While alginate and collagen have not been found to be toxic to cells when used in other models (Bouhlef et al., 2022), the inner core of MSC and collagen need to be assessed as there was a risk of a necrotic core. There was the possibility of detrimental effects from the production method; the cells were on ice for up to several hours, the stresses and strains imposed and the time the MSCs were not within an incubator. The viability of MSCs was assessed post fibre production through bright field images (on days 3, 7, 10 and 14) and stained with calcein AM and ethidium homodimer to show the live and dead cells present. The images were then

Alginate fibre to culture stem cells during adipogenic differentiation.

Results

live imaged on a Nikon Eclipse TS2 microscope coupled with a Nikon D3300 camera. Higher magnification images were not possible as the confocal imaging was not available due to logistical problems. The fluorescent intensity levels of the live/dead staining was completed. The images from the live dead staining were taken in image J with the background intensity measured to calculate the corrected total fluorescence intensity (CTFI) as explained in the method section (section 2.2.9). CTFI takes a measurement of the intensity, the background intensity was then measured and removed. The CTFI measurements in Figure 17 were assessed by a MAOVA test. To define where the statistical differences were Tukey post hoc testing was completed. However, the measurements of the dead cell fluorescence were not always possible in some of the images due to an inability to detect any real signal out of the background signal using CTCF formula (Figure 17), therefore on certain days all the values for dead cell fluorescence were from one image. This could reduce the accuracy of the dead fluorescence intensity of the 2D plates, and it lowers the statistical power of the MANOVA. The assessment of the dead fluorescent intensity on the 2D plates would need further repeats to be certain of the result. However, the 2D plates have been used for long term culture and were not likely to be toxic.

Metabolic activity assays have been used to assess the health of cells; it was also able to provide information on the number of cells within a fibre (Thermo Fisher Scientific, 2019). As such the metabolic activity was measured over several days along with 2D controls. The measurements were taken in both control (maintenance) medium and adipogenic medium. While Figure 18 displays the same data but focusing on the effect of culture type. The metabolic activity measurements have a variation in the number of independent repeats. The measurements for days 0 and 14 were the result of the one repeat while the measurements for days 3, 7 and 10 were from two repeats. Therefore, these results must be interpreted with care.

Alginate fibre to culture stem cells during adipogenic differentiation.

Results

Viability assessment

The live and dead staining in Figure 16 showed there was visibly more live (green) MSCs than dead (red) MSCs across all days imaged for both the 2D and fibre culture methods (Figure 16 and Figure 17) in agreement with the bright field images. The 2D MSCs and the MSCs in fibres had a higher fluorescence intensity than dead as expected for a culture model widely used. The fibres did not seem to show any decrease in cell viability (Figure 16), there was no evidence that the cells within the centre of the fibre were stressed or dying. However, the microscope did not allow for images in the core of the fibre, therefore images from a confocal microscope or dissection of the fibre would be needed to better see the centre part of the fibres. There was no reduction in metabolic activity of MSCs within the fibres by the end of culture, indicating that the fibres were not toxic (Figure 18). It is, therefore, clear that the fibres are non-toxic and offer a possible option for the culturing of MSCs over two weeks, in structure that allows for co-culture with ECM proteins and the ability of MSCs to cluster.

Alginate fibre to culture stem cells during adipogenic differentiation.

Results

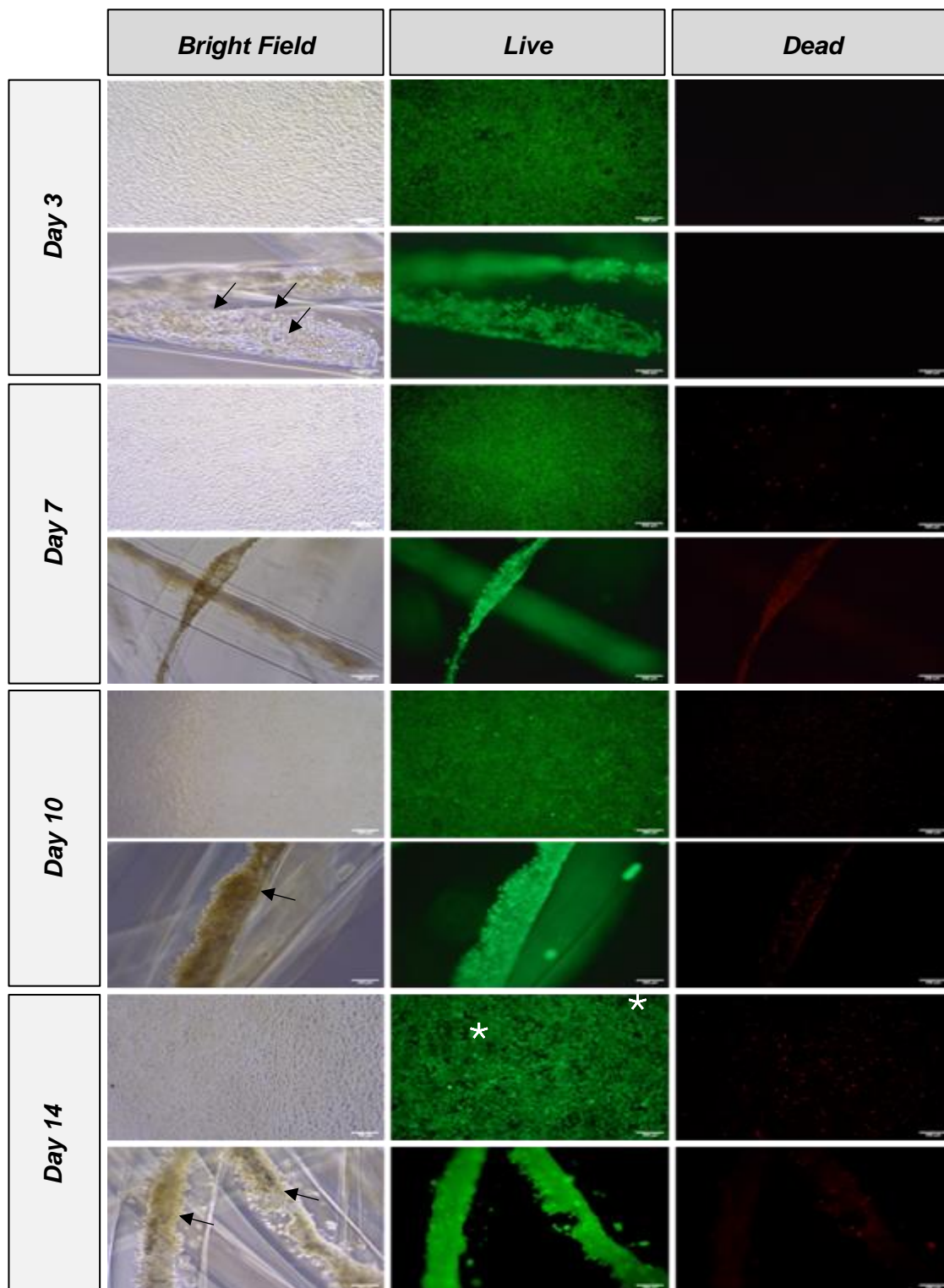


Figure 16. Live and dead staining of the cells cultured in fibres (3D – lower panel) and culture plastic (2D – upper panel).

Showing that the fibres are not toxic. Calcein AM and Ethidium Homodimer staining of both fibres and culture plastic, there is a small number of dead cells seen in both conditions. The two conditions are non-toxic to the MSCs. Arrows display the cells present within the fibre, on day 3 the MSCs were visible as single cells and on day 10 and 14 the inner core of fibre was much denser. The star shows the space present between some cells due to the loss of MSCs. N = 2, three images were taken per condition. Scale bars: 500µm.

Alginate fibre to culture stem cells during adipogenic differentiation.

Results

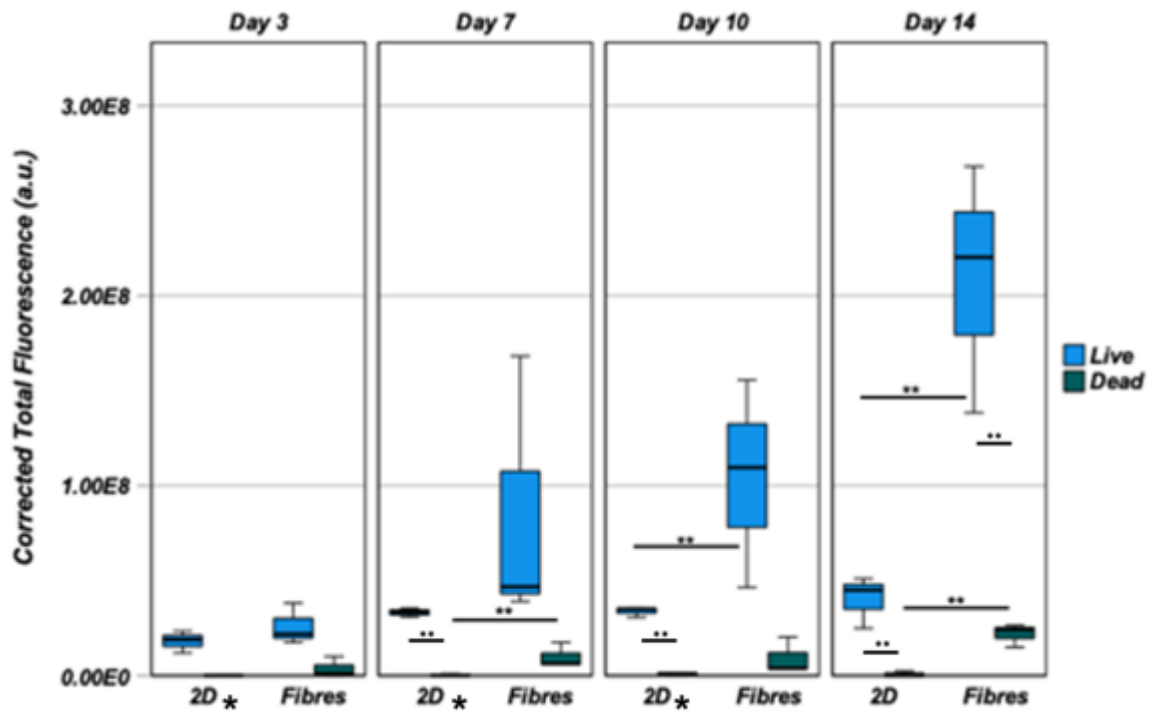


Figure 17. Fluorescence quantification of live and dead staining.

The corrected total fluorescence intensity for live and dead staining shown in a box and whisker plot. The data displayed the differences between the culture methods. The cells within the fibre were viable over 14 days when compared to the 2D control. In the later culture days, there is a significant increase in fluorescence intensity of the live and dead staining by the fibres. N = 2, with 3 images measured per sample except upon the ethidium homodimer staining for the 2D plate where only one image could be used due to the difficulties in measuring the background staining (days indicated by *). For each image three measurements were taken. All data was assessed through MANOVA. * P < 0.05, ** P < 0.001.

Alginate fibre to culture stem cells during adipogenic differentiation.

Results

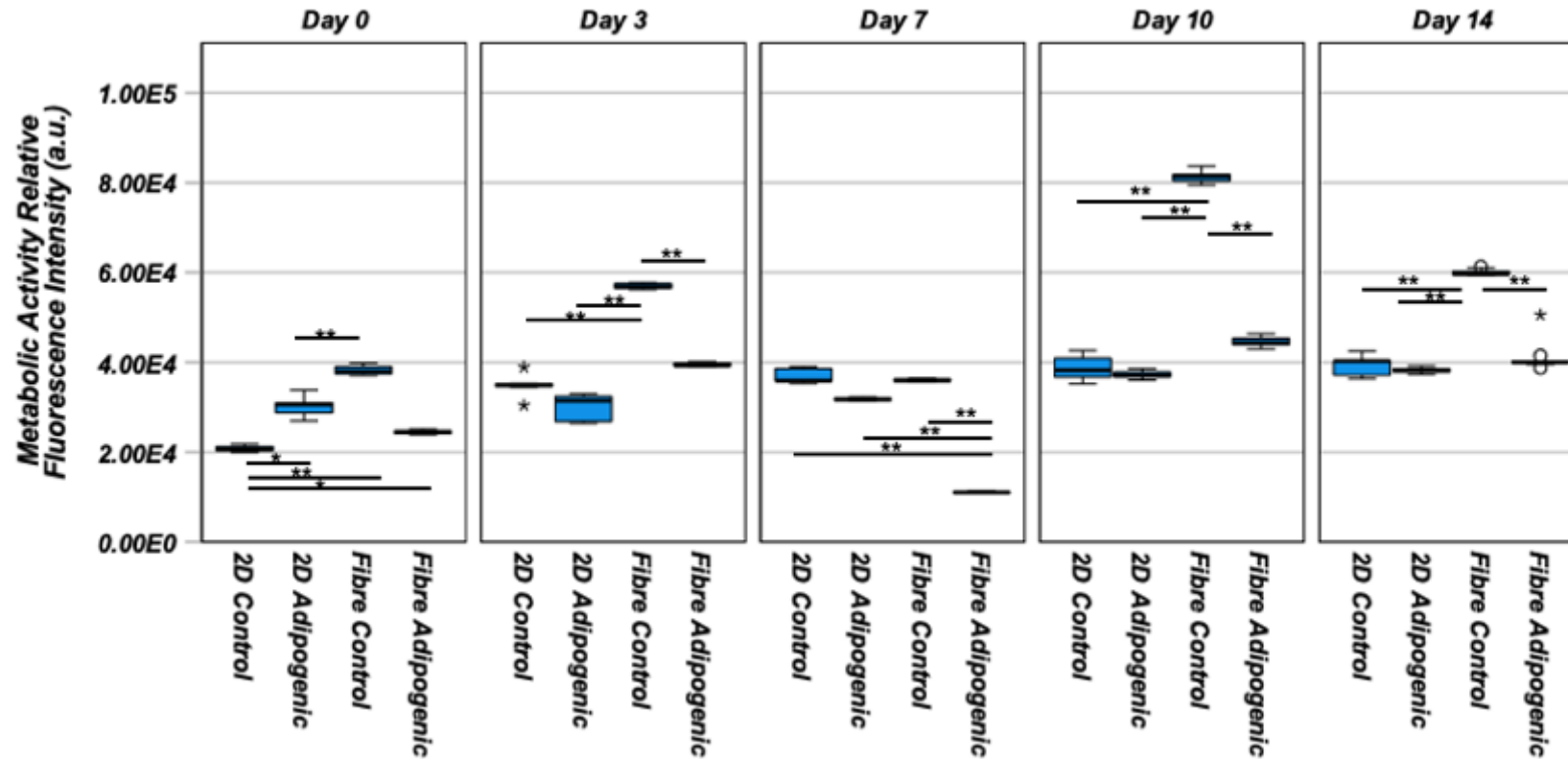


Figure 18. Metabolic assay assessing the effect of culture type.

The MSCs with the fibres in the control medium consistently had a higher metabolic rate than the MSCs on the 2D plates. The MSCs upon the 2D plates and the adipogenic fibres had similar metabolic activity except for day 7. The box and whisker plot display the median and interquartile ranges. The data was analysed by ANOVAs. The post hoc Tukey testing was completed. * $p < 0.005$ and ** $p < 0.0001$. The number of repeats varies $n = 1$ for all measurements taken on day 0 and day 14 and $n = 2$ for days 3, 7 and 10. There were three replicates per condition.

Alginate fibre to culture stem cells during adipogenic differentiation.

Results

2.4.3 Proliferation in the fibres

The CTFI values found to be higher than the 2D could indicate proliferation within the fibres, this was also suggested by the bright field images taken in Figure 16. The bright field images show that within the fibres the MSCs were more distributed throughout the fibre and single cells were visible (Figure 16 day 3). The MSCs were denser in the fibre on day 10 and 14 (Figure 16), this suggested that the cells were healthy and proliferating in the control medium and that they had the space within the fibre to proliferate.

While the fibres imaged on each day were created on the same day, some fibres showed a reduced MSC core due to reduced cell loading during production as mentioned in Table 5 and as seen in the day 7 fibre (Figure 16 bright field images). Therefore, the increase in density seen could be representative of inequality in cell loading. This problematic cell loading was also seen in the metabolic activity both the culture methods on day 0 (Figure 18). The data collected on day 0 was representative of the seeding density of 2D plates and the cell loading of the fibres as it was taken on the day production. Day 0 metabolic activity measurement was one repeat and may not be representative, but it does show the variation metabolic activity. It also highlights the differences in cell seeding for the 2D plates where the wells in the control medium was found to have a lower metabolic rate (Figure 18). Due to uncontrollable external problems further repeats were not completed though they are needed.

The significant reduction in metabolic activity for the fibre on day 7 in adipogenic medium and all other measurements (Figure 18) and the reduced cell density seen in the bright field images (Figure 16) indicated that a reduced cell density. As the reduction was not due to any toxic effect, there was no increase in dead cell CTFI in Figure 17 The fibre culturing MSCs in the control medium was not toxic but the metabolic activity measure was lower than on other days

Alginate fibre to culture stem cells during adipogenic differentiation.

Results

suggesting it was adversely affected by cell number. This difference in cell number could be due to the cell loading encapsulated in the fibres on day 0.

There was proliferation in the 2D culture as by day 3 there was no longer any difference in metabolic activity between the 2D plate in either the control medium or adipogenic medium. This suggests proliferation in the 2D control medium as the day 0 value was lower than the 2D adipogenic value (Figure 18). However, the MSCs on the 2D plates were less densely packed on day 14 with more space between the cells (Figure 16 shown by *), as some of the cells started to lift off from the culture plastic (observation). This was a major limitation of 2D plate; the MSCs lifting from the plate reduced the cells present for downstream analysis (i.e., RNA collection or immunostaining).

The fibres in the control medium, showed a trend in that it consistently had a higher metabolic rate than all other culture types (Figure 18). This suggested that there was an increase in metabolic activity in the control medium fibre, which was likely due to an increase in the cell number as the MSC proliferate more in the fibre due to the space allowed in the fibre compared to the 2D plates. The adipogenic fibres' metabolic rates were similar with the 2D plate conditions throughout (Figure 18), which may indicate limited proliferation due to most cells differentiating into adipocytes instead. There was an increase in CTCI levels from the 2D to fibres, this may imply that the fibres contain more cells than the 2D wells (Figure 17). While the plates and fibres were seeded with the same number of cells there is variation in the fibres, therefore, either the fibres have more cells due to a variation on the seeding level or a higher level of proliferation in the fibre than the culture on the 2D plastic plates. It is possible that the cells may proliferate more as the fibre could provide a larger surface area than the 2D wells. The fibres fluorescence intensity was higher than the 2D, which may indicate that the fibres had an increased number of cells.

Alginate fibre to culture stem cells during adipogenic differentiation.

Results

It was therefore, suggested that while in the fibre (in control medium) the MSCs were able to proliferate into the space in the fibre. The limited space of the 2D plates has been shown to limit the retention of the MSCs, the fibres provide an alternative for longer term culture. This could provide a better culture for the culture of adipocytes over culture times of a month.

2.4.4 Adipogenesis within the fibre

Once it became clear that culturing MSCs in the fibres were not toxic to the cells and that it allowed for the proliferation of the MSCs in control medium, the ability of the cells to undergo adipogenesis was assessed. The fibres and 2D plates that had been cultured in adipogenic medium were stained with Bodipy, a commonly used lipid stain to show the droplets within the adipocytes (Gocze and Freeman, 1994). Both the fibres and the 2D cells produced adipocytes, marked by their lipid droplets throughout the culture (Figure 19, Figure 20, Figure 21, Figure 22).

The comparison of adipogenesis between the 2D and fibre culture methods

Figure 19 showed that the lipids were produced by day 3 when the MSCs were cultured on the 2D plastic plates and the fibres (3D), suggesting that the fibre does not stimulate the adipocytes faster than the 2D plate. The apparent volume of adipocytes in the fibres increased over time, much like in the 2D (Figure 20) therefore the fibres maintained the adipocytes created and continued to support adipogenesis throughout the 14 culture days. Further work will be needed to show whether there is an increase in the amount of lipids or adipocytes compared to current 2D plate cultures.

Alginate fibre to culture stem cells during adipogenic differentiation.

Results

The lipid droplets on the 2D plates seemed to be spread across the entire well, which was due to the single plane that the cells were forced to attach to (Figure 19). The lipid droplets within the fibre were clustered closer together and often on top of one another (Figure 20). This was likely due to the narrow inner core of the fibres and the ability of the adipocytes to grow in multiple planes and directions. The ability of the fibres to produce this clustered formation of adipocytes was a benefit to the fibre as a model for adipose tissue, as it was more reminiscent to adipose tissue. The clustering of the adipocytes in the fibre and their location within the fibre, was difficult to see. As the Bodipy stain lipid droplets in several planes the fluorescence formed a green blur in images, shown in Figure 19 and Figure 20. As the images were only taken in one plane, the surface level it was impossible to image the measure the diameters of the lipid droplet or to see the spread of adipocytes completely. Sectioning was attempted (below) to counteract this problem.

The reduced cell loading noted in Table 5 produced areas with limited cell numbers, these produced spheroids of MSCs as seen in Figure 21. This was most likely from sections of fibres isolated from the main soft-core mixture perhaps due to a temporary blockage in the needle used to make the fibres (as stated in Table 5). The MSCs were able to produce adipocytes in a small number of cells in the sphere. The adipocytes present were located towards the surface of the cluster and there was no green blurring to suggest any within the centre of the fibre. There was also a reduction in the amount of lipids seen in the cluster when compared to the fibre day 7 images in Figure 19 and Figure 20. The reduction in cell numbers prevented adipogenesis to the same degree. Therefore, the variability of the cell seeding on day 0 from interruptions in the inner core proved to be a major problem for the ability of the fibre to be a model for adipogenesis or adipose tissue.

Alginate fibre to culture stem cells during adipogenic differentiation.

Results

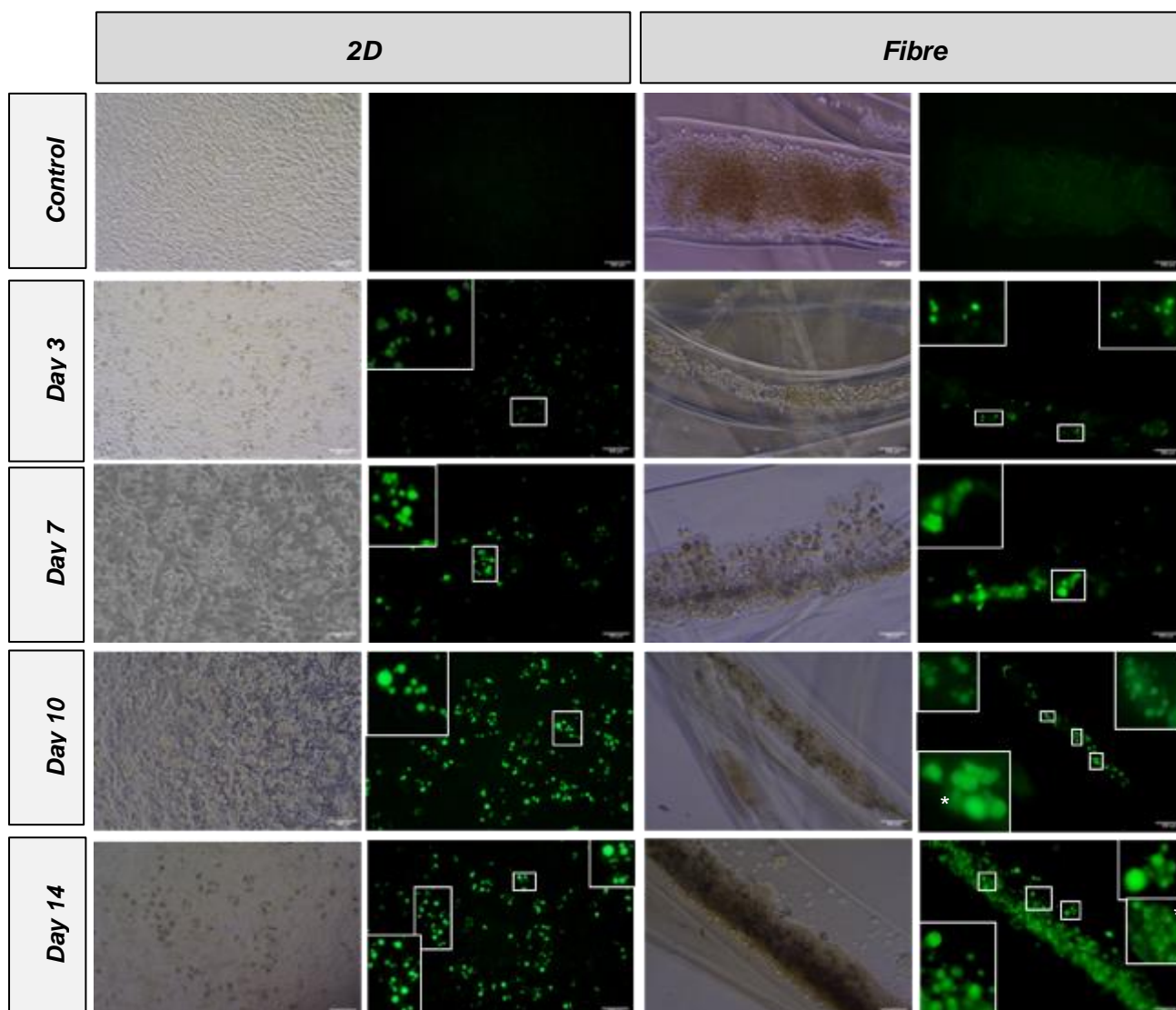


Figure 19. The fibres produced lipid filled adipocytes and with an increasing number of adipocytes and lipids over the days cultured.

Representative images comparing the adipogenic differentiation between the 2D plates and the fibres. The adipogenic differentiation was assessed through images stained with the lipid stain Bodipy here shown in green. The control images were stained with bodipy after they were cultured in the control medium, there was no non-specific staining or autofluorescence from the alginate layer of the fibre, image taken on day 7. The lipid containing adipocytes began on day 3 for both culture methods and there was an increase in lipid containing adipocytes across the culture days. *Demonstrate areas of lipid droplets that cannot be fully imaged due to the 3D clustering, this meant the images cannot be used to measure the size of the droplets. N = 3, with three replicate images taken per condition. Scale bars 500 μ m.

Alginate fibre to culture stem cells during adipogenic differentiation.

Results

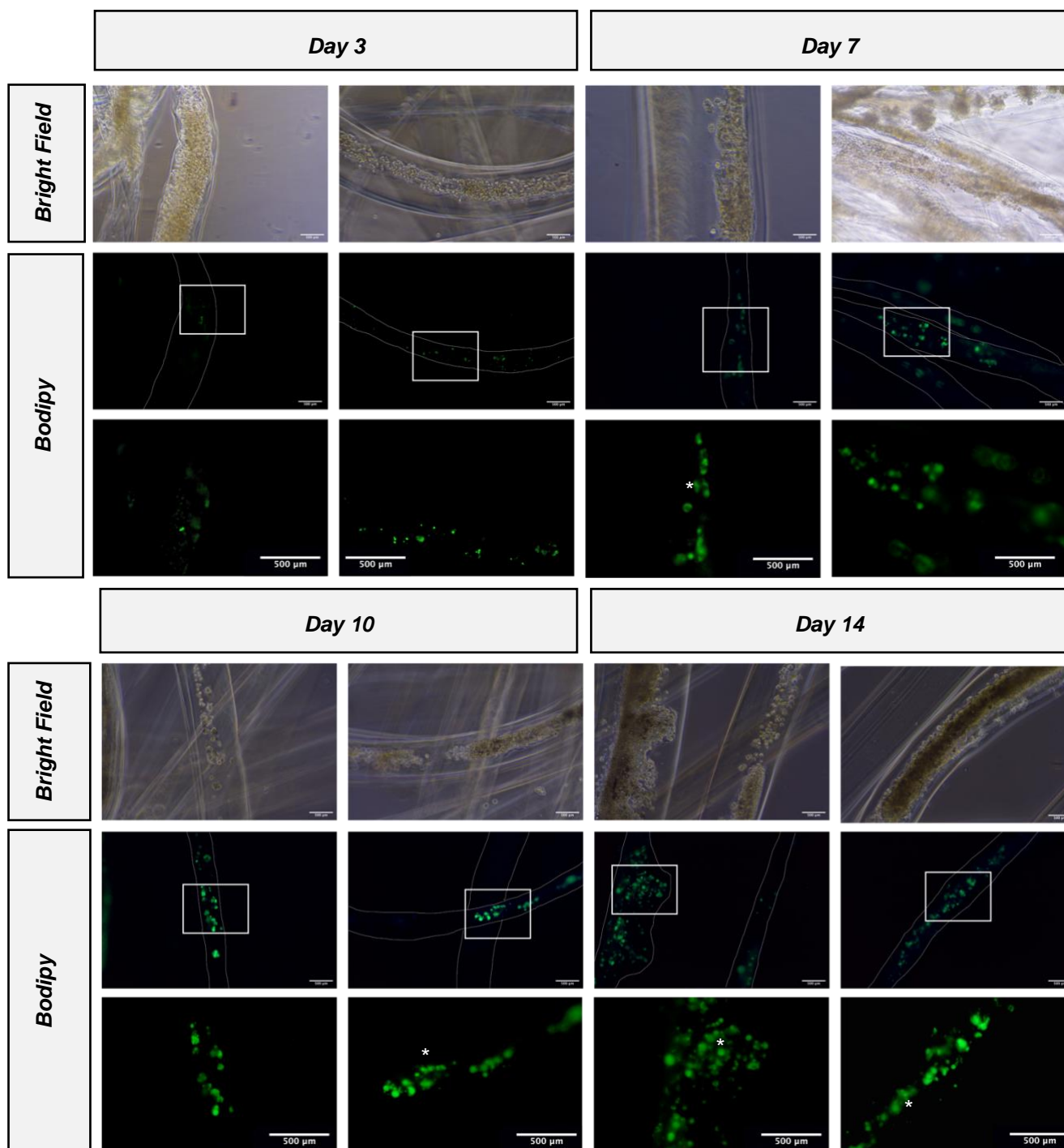


Figure 20. Enlarged images of the increasing number of adipocytes and lipids over the days cultured.

Representative images of the lipid droplets with the adipocytes stained with the lipid stain Bodipy here shown in green. The lipid containing adipocytes began on day 3 and there was an increase in lipid containing adipocytes across the culture days. *Demonstrate areas of lipid droplets that cannot be fully imaged due to the 3D clustering, this meant the images cannot be used to measure the size of the droplets. N = 3, with three replicate images taken per condition. Scale bars 500μm.

Alginate fibre to culture stem cells during adipogenic differentiation.

Results

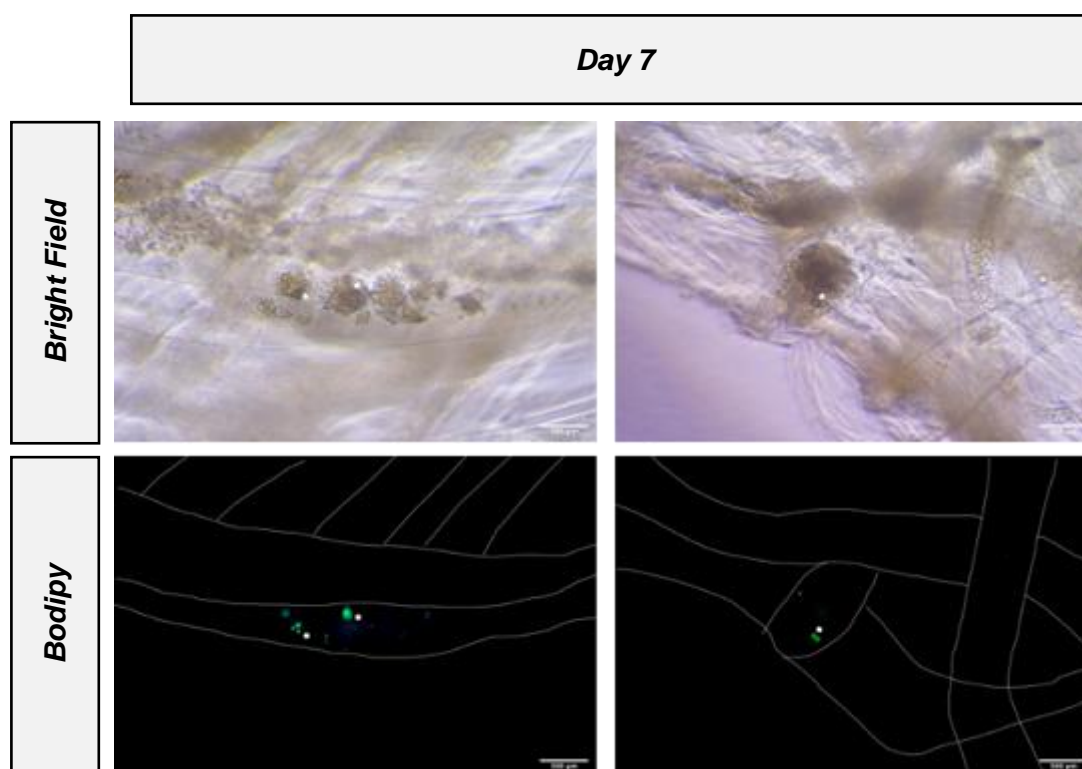


Figure 21. Adipogenesis in the fibres when the inner core containing MSCs was interrupted. The production of clusters of MSCs and collagen were found in some of the fibres, when the inner core had been interrupted during the production of the fibre. Images taken from day 7 and the scale bars shows 500 μ m. The fibres were outlined in white and the lipid droplet locations were indicated by white stars. When compared to the day 7 images in Figure 19 and Figure 20 the reduction in density of MSCs and a reduction of adipogenesis demonstrated by a lower lipid content. Table 5 detailed the interruption of the inner core during processing but the reduction in adipogenesis as indicated by the lipid content show how detrimental this problem in fibre production was.

Adipogenesis quantified by lipid content

When assessing the visible amount of lipids within adipocytes the commonly used method was O Red Oil (ORO). ORO stains lipids within the adipocytes and background staining in the samples was removed through several washes within isopropanol. Once the background staining was removed the samples were washed again in isopropanol till no staining remains. The isopropanol (100%) was then used to remove all ORO staining and this isopropanol sample was assessed for the level of absorbance for the 510nm wavelength, as ORO was red. The more lipids present the higher the presence of absorbance (A.U).

Alginate fibre to culture stem cells during adipogenic differentiation.

Results

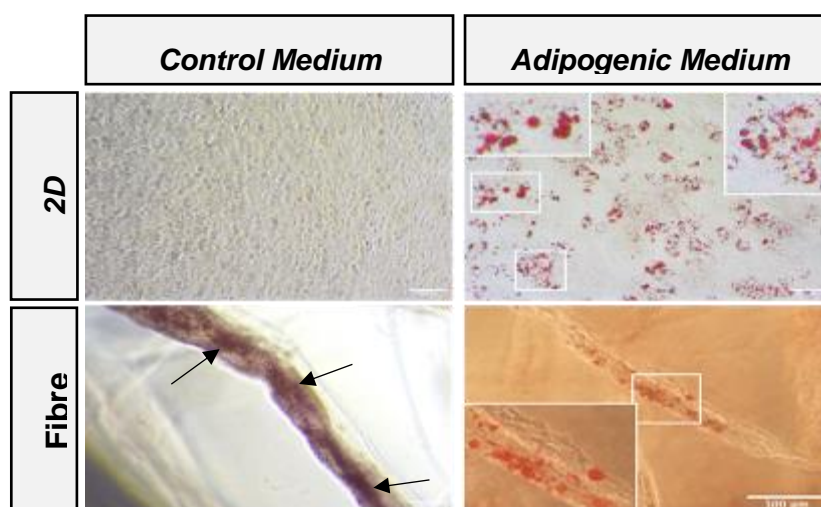
The ORO stained the lipid droplets within the fibre (Figure 22A). However, when it came to wash out the background staining, the fibres swelled dramatically when added to the 60% isopropanol washes. The ORO stain then became difficult to remove. As such attempts were made to move the fibre from the isopropanol into medium then back to the isopropanol, to prevent the fibre from swelling. This protocol did lower the swelling of the fibres, but it did not completely remove the stain as shown in the control fibre (Figure 22B). While removing the fibre was hypothesised to remove this problem, the inner MSCs and collagen core would not be easily moved from well to well for the washing steps and the final ORO removal. Figure 22A showed the ORO stain when completed on the 2D plate with no stain visible in the control and the lipid droplets in the differentiated MSCs are visible. The trapped ORO stain may be due to the density of the MSCs within the fibre as well as the swelling of the fibre.

The 2D MSCs in adipogenic medium produced a significant increase in lipid content when compared to the 2D control (in control medium). This demonstrates an adipogenic differentiation. However, the lipid content was significantly reduced in the adipogenic fibre when compared to the 2D in adipogenic medium (Figure 22B). This was despite the presence of ORO lipid droplets in the fibre and the non-specific trapped ORO in the control fibres (Figure 22A). This decrease in the lipid content measured was also at odds with the increase lipid content seen in Figure 19 and Figure 20. There was no significant difference between the fibres in control medium and the fibres in adipogenic medium (Figure 22B). Due to the problems in production of the fibres (Table 5) there were not enough fibres to have fibres in the control medium on days 3 and 7, which would have been ideal. The reduction of expected ORO staining could be due to the ORO not being removed by isopropanol for the absorption analysis, due to the swelling or the extra washes needed to remove the background staining in the control fibre. Therefore, ORO was not accurate.

Alginate fibre to culture stem cells during adipogenic differentiation.

Results

A



B

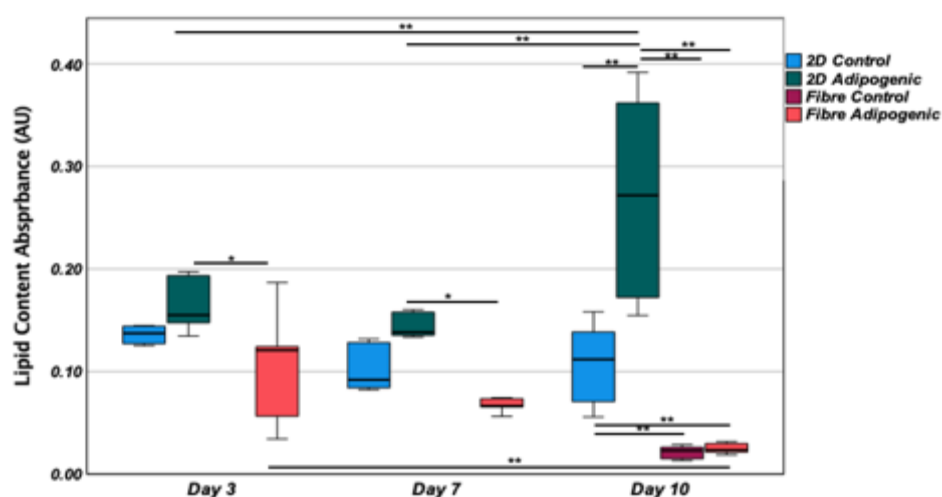


Figure 22. ORO assessment of lipid content was not a viable measure for use on the fibres.

A Representative images of ORO staining on both 2D plates and the fibre in control medium and adipogenic medium, taken on day 10. There was ORO staining retained in the control medium fibre, highlighted by the arrows. The scale bars were 500µm **B** The lipid content absorbance (a.u) taken across several days. When analysed with a ANOVA there was a significant difference across the days of culture. The post hoc Tukey tests show specific differences, * p < 0.05 and ** p < 0.001. The fibre lipid content decreased through the days despite the clear increase in lipids across the culture days in Figure 19 and Figure 20. The lipid content within the fibre can not be assessed through the ORO protocol. N = 2, with three replicate taken per condition.

Alginate fibre to culture stem cells during adipogenic differentiation.

Results

2.4.5 Cryosectioning to assess the lipid content within the fibres

The fibres were shown to produce viable MSCs (Figure 16, Figure 17), that were able to proliferate (Figure 18 and Figure 18) and differentiate into adipocytes (Figure 19 and Figure 20) dependent upon the medium conditions. However, the images taken of the fibres were on one plane and as the adipocytes, shown by the lipid droplets, were densely clustered (Figure 19 and Figure 20) it was impossible to measure the size of lipid droplets. Therefore, the fibres needed to be sectioned to allow for the imaging of the inner core of the fibre. In addition, sectioning the fibres allows for the further experimentation including immunostaining which cannot be completed on the fibre due to the large volumes of solutions required to cover the fibres.

Cryosectioning was selected for the sectioning method as the dehydration steps in paraffin sectioning removes the lipid content no longer allowing ORO staining (Liyanage et al., 2017). Cryosectioning was also faster process than paraffin sectioning as the fixation, freezing and sectioning can be completed in the same day. While paraffin sectioning does produce strong more robust blocks to section, the fibres were stable as they were frozen within an inert optimal cutting temperature compound that provided support.

The fibres were oriented, so they were sectioned across the fibre bundle where the fibres were horizontal and then the fibres were sectioned longitudinally, with the sections taken along the fibre (Figure 23A). The cross-section provided a small view through the fibres and would in theory allow for a view of the adipocytes through the depth of the fibre. The longitudinal sectioning allowed for a view of a length of a fibre through one depth, this would allow analysis of the distribution of the adipocytes in a greater area. In Figure 23 the cryosectioning showed a green material surrounding the cell laden core when stained with Hoechst (shown in blue)

Alginate fibre to culture stem cells during adipogenic differentiation.

Results

that was assumed to be the alginate layer of the fibres as it maintained a close contact to the MSCs. The autofluorescence of the alginate was beneficial as it demonstrated all the components of the fibre. However, the alginate's autofluorescence could prove detrimental for further imaging.

When stained with bodipy to identify the lipid droplets and therefore the adipocytes the lipid droplets were not found close to either MSCs or alginate (Figure 23B). No lipids were found within the fibres (Figure 23B). It was clear that while the cryosectioning had kept the lipid droplets they were unable to remain place within the section. This would prevent the bodipy and ORO from assessing the lipid content but other methods including adipocyte staining including H&E and confocal imaging of whole fibres could be used to assess the adipocytes.

Alginate fibre to culture stem cells during adipogenic differentiation.

Results

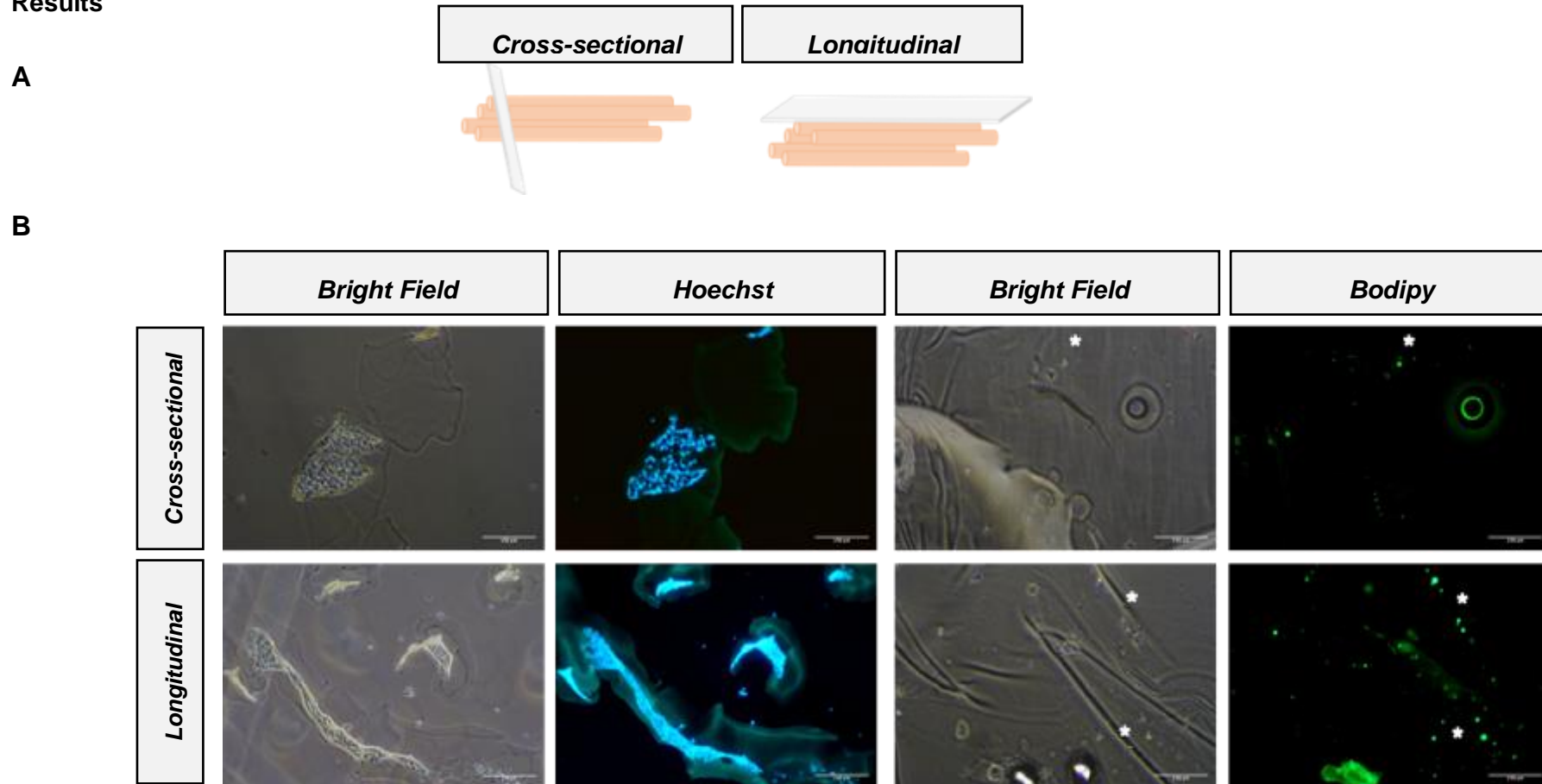


Figure 23. MSCs were stained within the sectioned fibres, but lipid drop-lets could not be.

A A Graphical presentation illustrating the two directions of sectioning. The bundle of fibres was shown in orange and the direction of sectioning was shown in grey. The cross-sectional fibres showed the depth of the fibre, while the longitudinal showed along a fibre. **B** The sections were stained with Hoechst and bodipy. The fibres imaged were from day 7 and the scale bars were 500µm. The Hoechst staining was successful in staining the MSCs but also showed autofluorescence of the alginate layer. The bodipy staining showed that the lipid droplets were not kept in place with the fibres but moved across the section, * showed the lipid droplet location in bodipy and in brightfield images. N = 4. Scale bar 500µm.

Alginate fibre to culture stem cells during adipogenic differentiation.

Results

2.4.6 Optimisation of the alginate removal method

The alginate surface layer kept the inner core protected and easy to handle but it would need to be removed for any downstream processing, for example DNA quantification or RNA extraction. In addition, there was a concern that for experiments over a long period of time it may be necessary to passage the cells within the fibre as the proliferation of the MSC would fill the space in the fibre (Figure 18). As such the removal method needed to be as non-toxic to the MSCs as possible to allow for the MSCs to be seeded into the fibres again. For the MSCs to be removed from the fibre, the alginate comprising the outer wall of the fibre had to be removed.

Optimisation of removal protocols

The alginate outer layer is comprised of crosslinks formed when the negative ions on the carboxylates and hydroxyls on the alginate β -D-Mannuronic Acid (M) and α -L-Guluronic Acid (G) residues that form ionic bonds with Ca^{2+} found in CaCl_2 solutions (Hung and Smidsrod, 1970). These bonds can be removed using a chelating agent, for example sodium citrate (Smidsrød and Skjåk-Bræk, 1990). PBS was the first solution used to remove the outer layer of the fibre; however, PBS was only able to partially remove the alginate wall (Table 6).

Therefore, 150mM sodium citrate was used to remove the alginate fibre wall (Figure 24 and Table 6). The effect of 150mM sodium citrate upon the MSCs was unknown and it was prudent to assess if a lower concentration of sodium citrate would still be able to remove the alginate fibre walls. Figure 24 showed that both concentrations of sodium citrate (150mM and 75mM) were able to remove the outer layer of the fibre; the higher concentration was faster (Table 6). Once the alginate wall was removed, the cells maintained the fibre shape. Attempts to dissociate the soft-core were two-fold: manual pipetting and trypsinisation to remove cell-cell

Alginate fibre to culture stem cells during adipogenic differentiation.

Results

connections. Trypsin was used to remove the cell-cell connections during passaging on 2D flasks (Fong et al., 2017), as such there was an expectation that this would not damage the MSCs. There were groups of cells clumped together in both the manual pipetting and trypsinisation, therefore the clumps were likely to be due to the collagen I in the soft-core. As repeats will be needed, in addition to the current removal protocols used here it could be worth assessing the ability of a collagenase to remove the clumps of cells, as seen in a human pluripotent stem cells fibre model (Ikeda et al., 2017).

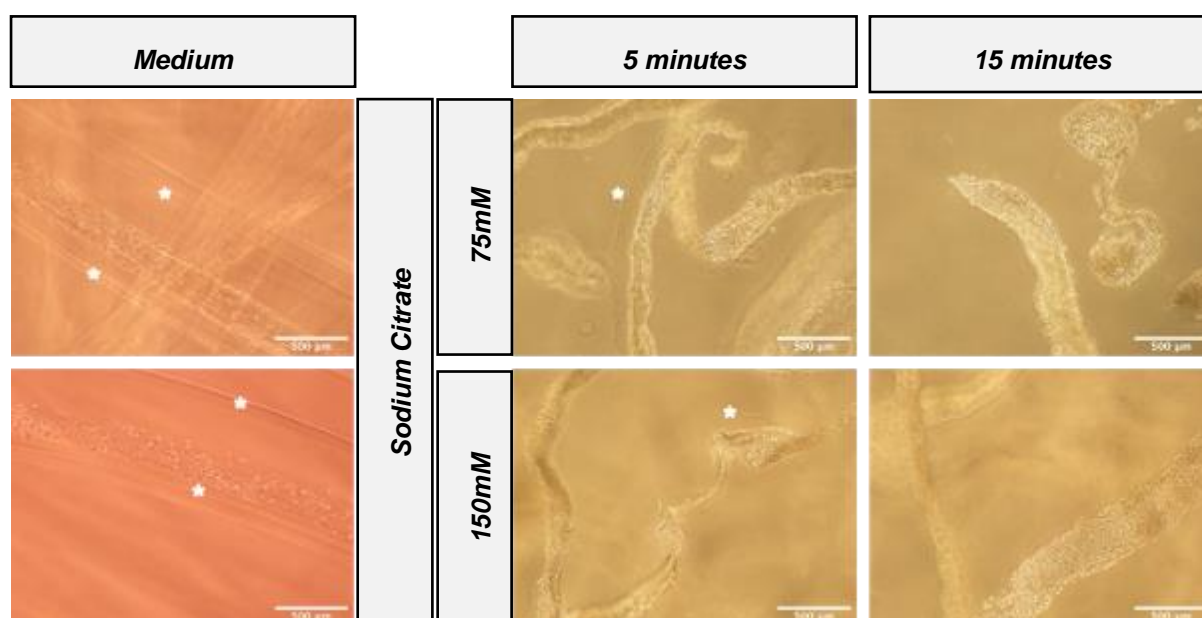


Figure 24. Optimisation of sodium citrate concentrations for alginate removal.

Representative images of the removal of the alginate outer layer around the MSCs and collagen core. While in medium the core was completely surrounded by an outer layer of alginate, highlighted by *. When in the sodium citrate the alginate, layer is dissolved. In the 150mM concentration of sodium citrate showed alginate disintegration after 5 minutes and the alginate was completely disintegrated by 10 minutes as seen in Table 6. The lower concentration of 75mM sodium citrate only had complete disintegration by 15 minutes. Fibres were cultured for 7 days previously. Scale bars 500µm and n = 1.

Alginate fibre to culture stem cells during adipogenic differentiation.

Table 6. The Optimisation of the removal methods for the alginate layer.

Representative images of the alginate removal can be found in Figure 24. The sodium citrate solution at a concentration of 150mM was the most efficient method to remove the alginate layer of the fibre

Removal method	Time (minutes)	Observations	
PBS (1X)	>20	<ul style="list-style-type: none"> The partial disintegration of the alginate formed a viscous solution 	<ul style="list-style-type: none"> Partial removal of the alginate
150mM sodium citrate	10	<ul style="list-style-type: none"> Within 5 minutes there was sections of the alginate layer completely removed After ten the entire alginate layer was removed The solution kept a similar consistency and was easily pipetted 	<ul style="list-style-type: none"> The collagen and cell core produced remained in the fibre shape (Figure 24) The cell collagen core was broken by pipetting, but it stayed in clumps
75mM sodium citrate + manual pipetting	15	<ul style="list-style-type: none"> There was no evidence of alginate removal at 5 minutes After 15 minutes there was a complete removal of the alginate layer The solution kept a similar consistency and was easily pipetted 	<ul style="list-style-type: none"> The collagen and cell core produced remained in the fibre shape The cell collagen core was broken by pipetting, but it stayed in clumps
75mM sodium citrate + trypsin	25	<ul style="list-style-type: none"> There was no evidence of alginate removal at 5 minutes After 15 minutes there was a complete removal of the alginate layer The solution kept a similar consistency and was easily pipetted 	<ul style="list-style-type: none"> The collagen and cell core produced remained in the fibre shape (Figure 24) The addition of trypsin made the clumps of the collagen cell core smaller after pipetting

Alginate fibre to culture stem cells during adipogenic differentiation.

Results

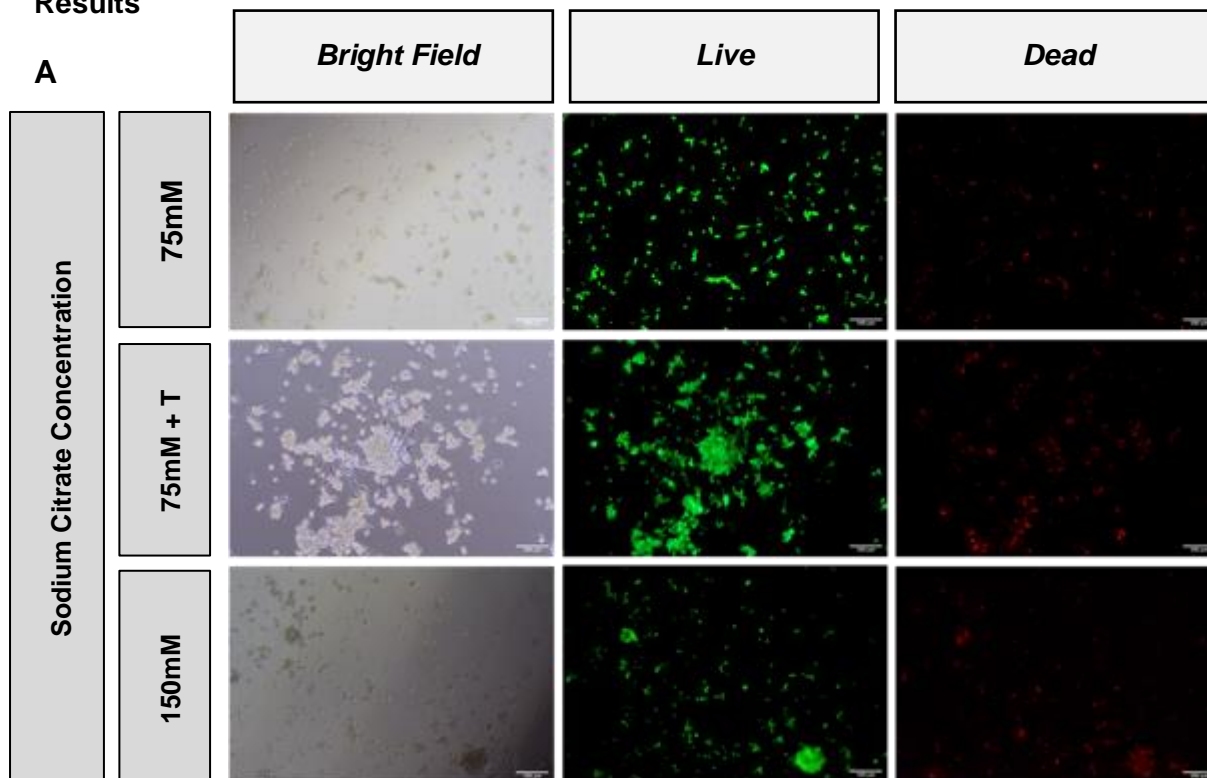
Viability of the MSCs after having been removed from the fibre

The MSCs removed from the fibres (cultured in control medium) and were reseeded onto 2D plates to assess their health. 24 hours later when changing the medium there were clumps of cells that had not managed to attach to the 2D plate and were removed with the medium change. After 48 hours of culture on the 2D plates the MSCs were imaged with live and dead staining (calcein AM and ethidium homodimer). The 48 hours of culture time before live/dead staining allowed for the MSCs to increase in number and get a more complete view of the MSCs viability particularly as there was a lack of some MSCs to remain attached to the plate. The attachment problem may have been due to the presence of the remaining collagen, making the clusters too big to remain on the plate surface or damage to the MSCs from the sodium citrate. The live dead staining was only completed once due to problems producing fibres, and uncontrollable external factors. The results should therefore be taking an indication of the possible optimum removal protocol.

It was also important to check whether the MSCs were adversely affected for example, were the cells still pluripotent MSCs and still able to differentiate. Once the cells removed from the fibres had reached 80% confluency on 2D culture plates adipogenic medium was added to test whether culturing in the fibres had altered the MSCs ability to differentiate into adipocytes. Further work would have differentiated into chondrocytes and osteocytes to assess if the cells were still multipotent. It was expected that the fibres would maintain their multipotency as fibres of this type had kept induced pluripotent stem cells pluripotent when previously assessed (Ikeda et al., 2017). However, the removal methods may have had adverse effects.

Alginate fibre to culture stem cells during adipogenic differentiation.

Results



B

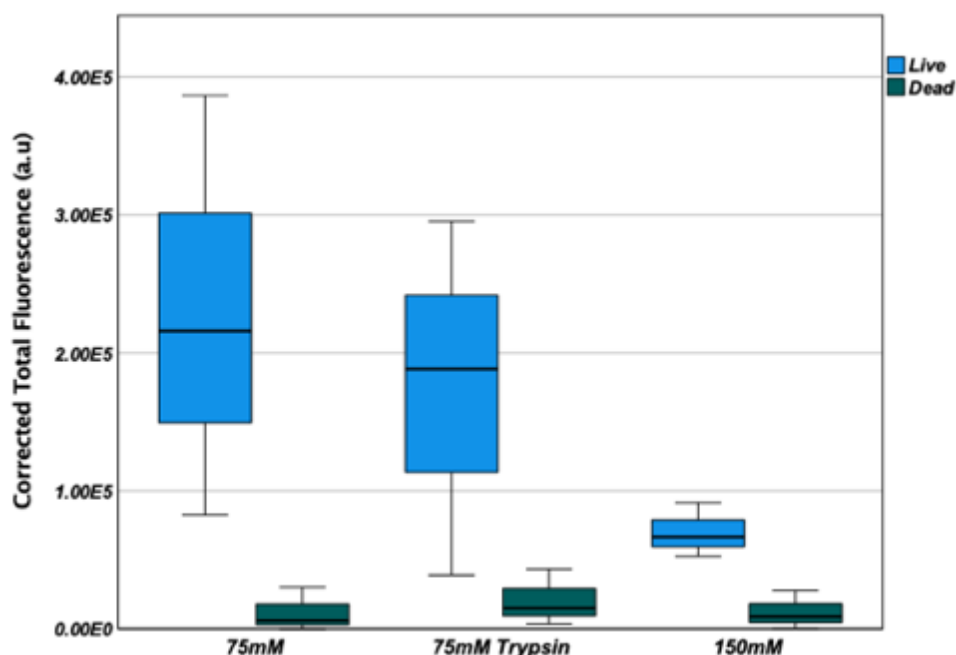


Figure 25. Optimisation of MSC removal from fibre.

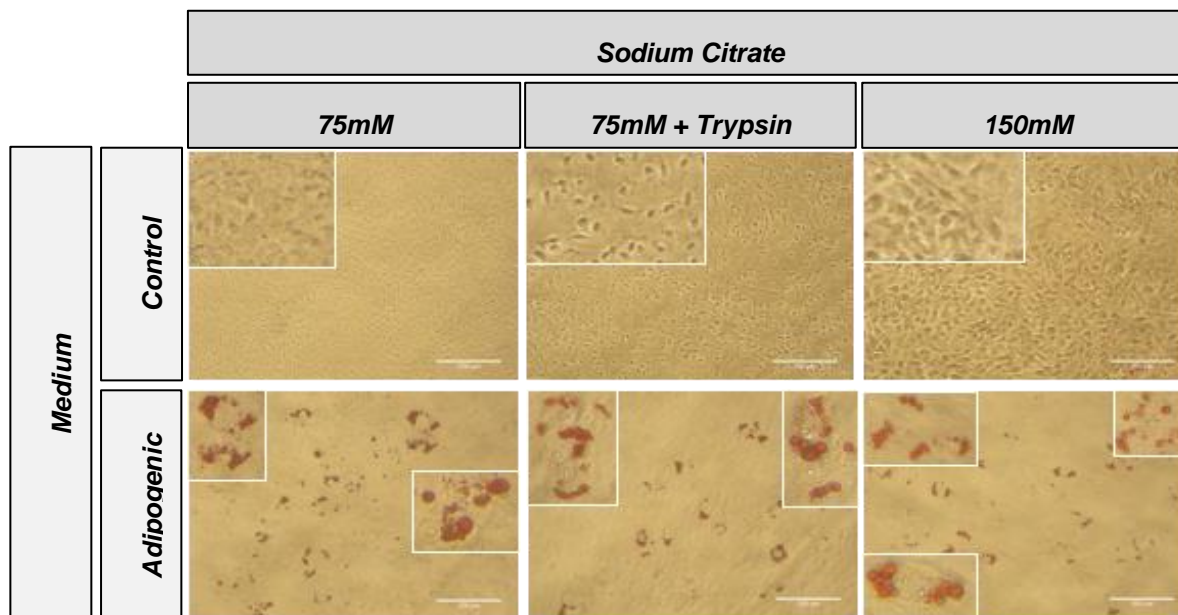
A The live and dead staining (calcein AM and ethidium homodimer) after 48 hours seeded to 2D plates, showed the effect of the three removal methods had upon the MSCs' viability. The addition of trypsin was denoted by "T". Scale bars = 500 μ m. When compared to the Figure 16 2D plate previously imaged there was an increase in toxicity with all the methods. There were more live cells present when the lower concentration of sodium citrate was used with no addition of trypsin..

B The corrected total fluorescence intensity (a.u.) of all the protocols used. There was no statistical difference when MANOVA was used. N = 1, there were three images taken per condition and three measurements.

Alginate fibre to culture stem cells during adipogenic differentiation.

Results

A



B

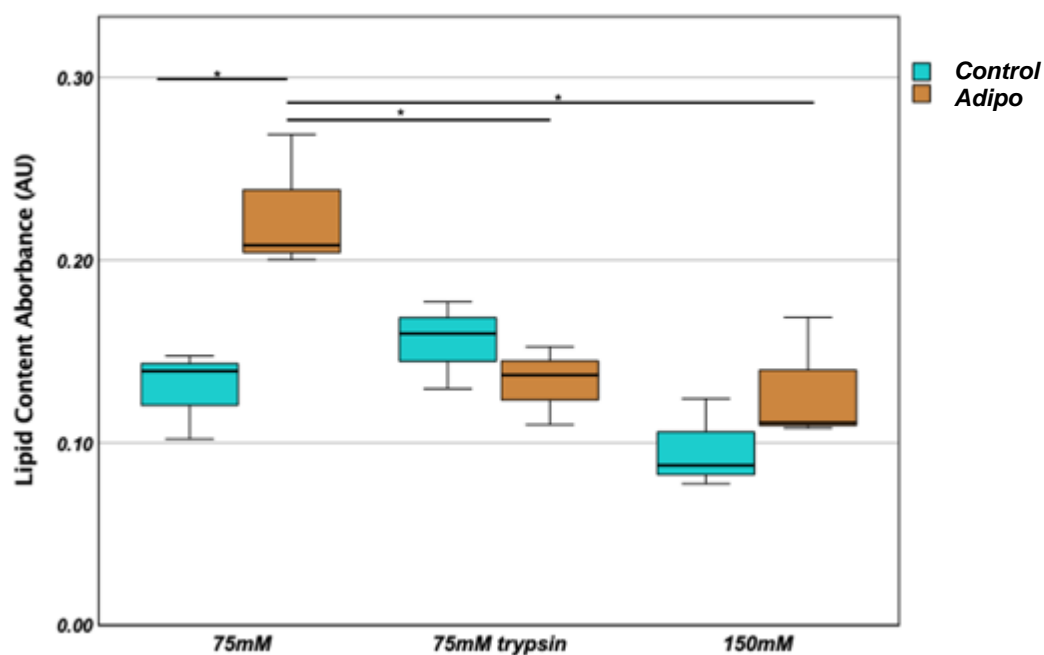


Figure 26. The use of 75mM sodium citrate and manual pipetting was the current optimised cell retrieval method for maintaining adipogenic differentiation.

A The ORO staining on the control medium and adipogenic medium. The control medium showed stressed MSCs when removed from the fibre with 150mM of sodium citrate. All removal methods did allow for the production of lipids. **B** The ORO quantification with an assessment of the lipid content for each removal method. The only true evidence of the presence of adipocytes was in the 75mM sodium citrate with manual pipetting as it was the only one with a difference between the control and adipogenic medium. MANOVA and post hoc Tukey testing showed shown with * $p < 0.05$. $N = 1$, with three replicates per condition. Scale bars = 200 μ m.

Alginate fibre to culture stem cells during adipogenic differentiation.

Results

The MSCs removed from the fibre with 150mM sodium citrate had the lowest number of cells attached to the 2D plate (Figure 25) and though it was not significantly different than the other removal protocols, it had the lowest CTFI for the live cells (Figure 25). After removal from the outer layer of the fibre with 75mM sodium citrate, the manual pipetting and trypsin seemed to have similar levels of dead cell fluorescence intensity and only a slight reduction in live CTFI for when trypsin was used (all non-significant) (Figure 25). The reduction in live cell CTFI may be the result of the extra stress trypsinisation could have on the cells. All the different methods to remove the alginate layer were able to differentiate into lipid filled adipocytes during the 7-day culture in adipogenic medium (Figure 26A). However, the MSCs removed from the fibre with 150mM sodium citrate also showed a reduced ability to differentiate with the lowest level of lipid content (Figure 26B). This does reinforce the conclusion that the cells need to be removed from the fibre with a lower concentration of sodium citrate.

The MSCs that were removed from the fibre with 75mM of sodium citrate, and trypsin showed signs of stress even after being cultured for 11 days (Figure 26A). The cells appeared to be more condensed and darker than those removed from the fibre with 75mM sodium citrate, and the cells seen in Figure 16 that had only ever been cultured on 2D plates in control medium. Taken all together the best current method to remove cells from the fibres is 75mM sodium citrate with manual pipette mixing. The 75mM sodium citrate and manual pipette mixing removal method was the only group to produce enough lipids to have a statistically significant increase of lipids between the control medium and the adipogenic medium which was the true assessment that there was differentiation into adipocytes. This also reinforces the suggestion that the best method, currently tested, of removing the MSCs from the fibres is to use 75mM sodium citrate with manual pipette mixing.

Alginate fibre to culture stem cells during adipogenic differentiation.

Results

The fibres used in this work did not alter the ability of MSCs to differentiate into adipocytes. The fibres culture/retrieval steps did not ablate the capacity for differentiation and the fibre therefore remains a possible 3D model for adipogenesis. The removal method of 75mM sodium citrate with manual pipetting was the optimum removal method currently tested. Neither the fibre nor this removal method prevented the ability of MSCs to differentiate into adipocytes suggesting that both maintained the adipogenic capacity of the MSCs encapsulated. This was only completed with one repeat and may not be a true representation.

2.4.7 Conclusions

To summarise, while pilot study completed here was not comprehensive and in depth but does highlight that there were several important parts of the fibre production method that need optimisation. The blocking of the needle by alginate can prevent fibre production and the interruption of the inner core (collagen and MSCs) results in differing cell loads in fibres which make analysis more complex and prevents adipogenesis. The alginate layer of the fibre made the removal of lipid stains impossible as well as any interaction with PBS, both add complications to experiments. In addition, the removal of the alginate layer needs further optimisation to make sure there was no detrimental effect of sodium citrate. While the technical difficulties involved with this fibre were many, the fibre has been found to be non-toxic. The fibre maintained MSCs ability to differentiate and proliferate after a 14 culture in the fibre and reseeded upon 2D plates.

Alginate fibre to culture stem cells during adipogenic differentiation.

Discussion

2.5 Discussion

2.5.1 Production of alginate fibre

Once produced the fibres formed a robust culture system that can be easily manipulated and cultured over 14 days. This was in line with previous systems that have been able to culture a range of cell types (cardiomyocytes (Wang et al., 2019a), HUVEC, cortical cells, mouse embryonic osteoblast precursor cells (Onoe et al., 2013) and induced pluripotent stem cells (Ikeda et al., 2017)).

The largest problems for this cell culture system tested here are the blockages of both the alginate, and of the collagen MSC core resulting in reduced production and cell loading respectively. The reduced cell loading posed a major problem, as any metabolic activity was subject to the cell loading variability during production and resulted in the aggregates (spheroids) formation. To account for this, any further collected data (i.e., metabolic assay or PCR) gained would have to be normalised to the DNA content in each individual fibre used, which would be time consuming and expensive. As such there needs to be an optimisation of the fibre production method.

A microfluidic device using laminar flow found that the alginate solution clogs their system, which lead to time consuming 'disassemble and repeat setup' cycles (Ghorbanian et al., 2014). *Ghorbanian et al* used the addition of a Ca^{2+} chelator to flush their system when blocked. However, their system was more complex and reminiscent of 3D printing, as the needle producing the hydrogel was mounted upon a motorized stage, which is automatically moved (Ghorbanian et al., 2014). For the work here, the simplest solution would be to alter the rates at which the alginate and CaCl_2 are pushed through the needle during the fibres creation. Currently the rates of both the alginate and CaCl_2 were set to the same rate (0.04mL/min). In

Alginate fibre to culture stem cells during adipogenic differentiation.

Discussion

other alginate CaCl₂ fibres the CaCl₂ solution was faster than the alginate layer (Hu et al., 2010b, Hsiao et al., 2016) and these systems were not reported to have blockages during the formation of alginate fibres. This difference in flow rates then may allow the alginate to be pulled away from the needle due to the force of the CaCl₂ solution surrounding it. It is possible that this would prevent blocking of the system, however alteration to the flow rates can alter the dimensions of the fibres (Wei et al., 2017, Hu et al., 2010b, Lee et al., 2009b).

In addition, when the inner core (collagen and MSCs in this work) was faster, there was instability in the flow and curls formed from the core solution formed (Shin et al., 2007), As others have found that these instabilities can then cause blockages (Ghorbanian et al., 2014), it could be that the blockages were the result of unstable flow due to the lack of difference in flow rates between the collagen/MSc solution and the alginate.

For the blockages caused due to the collagen and MSC solution, optimal concentration of collagen and MSCs for both production and the cell culture should be assessed. However, changes in concentration may not have such an effect upon the core blocking, as others using similar systems with higher concentrations of cells (e.g. Adipose derived stromal cells 1×10^7 cells/mL) and ECM (e.g. 33.3 mg/mL of fibrinogen) components have not reported core blockages (Hsiao et al., 2016, Onoe et al., 2010). It may also be that the collagen has begun to polymerise as the production continues and the core solution raises in temperature. The use of ice bags around the core solution to prevent this could be a simple change to prevent the core blocking. A magnetic spinner (as used when making solutions) could be used to continuously mix the cell and collagen solutions to prevent the cells from clumping.

Alginate fibre to culture stem cells during adipogenic differentiation.

Discussion

2.5.2 Viability of MSCs within the fibre

This work has shown that this particular soft-core fibre was able to maintain viable cells for 14 days with no visible increase in cell death, while using live/dead staining and a metabolic activity assay, to measure the viability cells in 3D models (Kim et al., 2019). However, the images taken for the live/dead staining did not image directly into the centre of the soft-core and as such the viability of the central cells could not be determined. Conclusive evidence that there was no cell death would require imaging live/dead staining by confocal microscopy or imaging after the fibre has been dissected to show the centre of the fibre.

The corrected total fluorescence used here was an attempt to provide a quantification for the live and dead cells within the fibre as seen in section 2.2.9 p54 (McCloy et al., 2014, Bhavsar et al., 2019). This method does come with some problems. When attempting to configure the 2D dead cells there were several days when the background reading was found to be higher than the dead staining, due to the low number of dead cells and weak fluorescent signal (Figure 17, day 3). In addition, the CTFI measured within the fibre could be artificially high as all the cells were condensed into a narrow fibre where the cells must cluster together. There could have been a greater intensity of signal in a condensed area due to the clustering of the adipocytes in the fibre, whereas the 2D wells only have fluorescence from one plane showing a more accurate CTFI measurement.

Collagen I hydrogels (not fibres) have been seen to be a good and viable method to culture visceral preadipocytes to mature adipocytes (Emont et al., 2015). Collagen scaffolds were also able to support MSC differentiation into adipocytes and osteoblasts for 50 days (Neuss et al., 2008).

Alginate fibre to culture stem cells during adipogenic differentiation.

Discussion

The ability of the fibres to maintain viable cells is in line with other similar systems, where cells have been kept viable for up to a total of 91 days (Hsiao et al., 2015b, Campiglio et al., 2019, Hsiao et al., 2016). This is reinforced by the viability of soft-shell micro-capsules that maintain viability through 7 days of culture and keep the cells viable after being removed from the micro-capsules (Louis et al., 2019). Further work would include an extension of the time cultured, increasing for a month or indefinitely to see how long the cells could be cultured for and if there were any detrimental effects.

2.5.3 Proliferation of MSCs within the fibre

The images taken of the fibres over the 14 days suggest there was proliferation in the fibres cultured in the control medium. The CTFI and metabolic activity seemed to show similar trends, although values can be altered by fluorescence of the cells below (CTFI) and the cell loading respectively. Alginate itself is not known to promote proliferation on its own (Pati et al., 2014). However, collagen I (within the soft-core) has been shown to increase proliferation. Similar fibre systems also showed proliferation (Mazari-Arrighi et al., 2022). Not all used collagen as their internal core ECM component (Hsiao et al., 2016), suggesting that the fibre systems could be the reason for proliferation. The increase in proliferation was not due to increased space within the fibre (volume 0.08cm^3) as there were a greater area within the 2D well (3.5cm^2 surface area). The proliferation must be due to the increased cell-cell connections or increased collagen: cell interactions made within the fibre.

Hsiao et al found that after extended culture the fibres' curled/twisted upon themselves (Hsiao et al., 2016). While it was not shown to be detrimental to the cells, it does suggest that the cells within the internal core space of the fibres had proliferated so that the internal core was

Alginate fibre to culture stem cells during adipogenic differentiation.

Discussion

longer than the alginate surrounding it, resulting in curling of the fibre. The proliferation of the cells within the fibre may result in passaging further culture.

Collagen I has also been seen to increase the proliferation of MSCs (Zheng et al., 2022, Yang et al., 2019). *Yang et al* demonstrated that on collagen coated surfaces, the increase in proliferation could be due to nuclear translocation of β -catenin (Yang et al., 2019). While other pathways – such as the ERK (extracellular signal-regulated kinases) and phosphoinositide 3-kinases (PI3)/ protein kinase B (ATK), have been suggested to be responsible for proliferation (Tsai et al., 2010). The direct causes of proliferation in the present system are unknown. To highlight the causes of increased proliferation that may be present here, western blotting for the β -catenin, ATK and ERK signalling pathways should be done. Culturing the fibres with inhibitors for these pathways would allow for the assessment if the removal of a pathway significantly reduced the proliferation within the collagen.

2.5.4 Adipogenesis in fibres

The soft-core fibres were shown to be capable of supporting stem cells adipogenesis throughout the culture days, much like the cells in 2D. This is in line with previous reports describing the culture of adipocytes in similar fibres (Unser et al., 2016a, Hsiao et al., 2015a). A similar soft-core fibre using 3T3-L1 cells found adipocytes growing in the fibre and lipid droplets were seen on the surface of the fibre and were even observed to fuse together (Yokomizo et al., 2019). This is in line with this study, where droplets were seen on the surface of the fibres and assumed to be in the centre. From the work presented here and that from others studies which used Bodipy to identify lipid droplets, there is currently no evidence to show that Bodipy wouldn't reach the centre of the fibres (Yokomizo et al., 2019), therefore confocal imaging should show the lipid droplets throughout the fibre.

Alginate fibre to culture stem cells during adipogenic differentiation.

Discussion

As mentioned above the collagen I in the soft-core does provide a better environment and is beneficial to the extracellular matrix of adipocytes. The collagen may be beneficial for adipocyte culture as it more accurately reflects the extracellular matrix *in vivo* and is required for adipocytes (Yasuaki et al., 2000, Nakajima et al., 1998). Indeed collagen I has been shown to increase the expression of the adipogenesis genes PPAR γ and CEBP β during osteogenic differentiation (Hiew and Teoh, 2022), though this could be due to the presence of Dexamethasone (Dex) in the medium (Ghali et al., 2015). Previously culture with adipogenic medium containing Dex has been seen to produce both adipocytes and osteoblasts (De Melo et al., 2019).

However, collagen I may not be the best core for adipogenesis, despite successful adipogenesis being present in other 3D models that used collagen I (Volz et al., 2019, Venugopal et al., 2017). In 2D systems collagen I has been found to reduce the expression of adipogenic genes (i.e., PPAR γ and CEBP β) and for the adipocytes to have a reduced lipid content (Liu et al., 2020a, Gao et al., 2022). Collagen I has been associated with the increase in osteogenic genes (i.e., RUNX2) (Komatsu et al., 2018, Fernandes et al., 2010).

The images did show the presence of large droplets (though not measured) within the fibre, which could be consistent with the literature as the adipogenesis observed in other fibres and in 3D models showed increases in droplet sizes throughout the culture (Yokomizo et al., 2019) and larger than 2D cultures (Klingelutz et al., 2018, Daquinag et al., 2012).

The method used here to assess the number of adipocytes present mainly relied upon imaging, but this is not quantifiable and as such cannot determine if the adipogenesis in the

Alginate fibre to culture stem cells during adipogenic differentiation.

Discussion

3D model is more than the 2D. The ORO assay attempted could not be used to quantify the lipid content, and unspecific ORO appears to also be found in work by Unser et al. (2016b) perhaps due to a high level of cells present in the fibre or the swelling of the fibre capturing the ORO stain. Sectioning may provide the ability to stain lipids with ORO (quantification not seen) as demonstrated by (Hsiao et al., 2016). Possible routes to quantify the amount of lipids present might be to measure the Bodipy fluorescence signal. The quantification of fluorescence could be completed through the confocal imaging of the fibre, after which image J analysis (e.g., 3D object counter) could be used to estimate the areas of each droplet (Mau et al., 2022, Biltz and Meyer, 2017). Further work will be needed to quantify if there this an increase in adipocytes within the fibre compared to the 2D culture and what type of adipocytes are present (section 2.6.2).

2.5.5 Swelling of the fibres

Oil Red O (a fat soluble, hydrophobic diazo dye) is the standard quantifiable measurement for adipogenesis as the level of lipids (triglycerides) can be measured via absorbance. The fibres were however susceptible to non-specific staining which remained trapped in the fibre despite the use of 60% isopropanol washes. It was during these wash steps that the fibres swelled, and not in any other solution including water. Swelling of hydrogels in water-based solutions or water is not unusual for alginate systems, it is even a desired characteristic for hydrogel systems used for wound healing (Soleimanpour et al., 2022). Alginate concentration increases the swelling of the hydrogels (Wichai et al., 2019). The concentration of CaCl_2 used to gel the alginate and variation in alginate monomers resulted in changes to the swelling ability (Mirabedini, 2018, Okay and Durmaz, 2002). Swelling was not reported by other research groups using alginate fibre systems, whether due to ORO not being attempted or no swelling occurred (Hsiao et al., 2016, Ikeda et al., 2017). Work upon alginate beads has demonstrated that swelling was due to the cation exchange, loosening the alginate-crosslinker (i.e., Ca^{2+})

Alginate fibre to culture stem cells during adipogenic differentiation.

Discussion

bond, allowing for the uptake of Na⁺ buffer solution and causing swelling (Bajpai and Sharma, 2004). It could be that the swelling here was due to electrostatic interactions with the isopropanol or water in the 60% isopropanol solution.

2.5.6 Removal of MSCs from fibres

As the proliferation increases, the fibre may begin to twist upon itself thereby removing any predetermined shape, which could lead to a lack of space. It could therefore be needed to passage the fibres without damaging the MSCs cultured. While only the MSCs within the fibres cultured in control medium were used to assess the removal methods, further work should be done to make sure that adipocytes are not negatively affected by any removal process. More repeats are also required to be certain of the conclusions drawn. The removal method requires further optimisation.

The sodium citrate was able to remove the alginate layer of the fibre in a dose dependent manner, with 150mM being the most efficient. The use of trypsin to remove cell-cell connections was not beneficial and other methods to dissociate the collagen MSC core are required (i.e., collagenase), for instance by trialling collagen lyase.

The live dead staining showed a reduction in viability with the use of sodium citrate. However, likely due to the remaining clumps of collagen I or due to sodium citrate, limited numbers of cells could be seeded onto the 2D tissue culture. The live dead staining was conducted upon the cells after 48 hours, to mitigate the low number of recovered cells at 24 hours. In repeats, if optimisation of the removal method to remove the collagen, was completed improved seeding would allow for live dead staining after 24 hours to see the immediate effect upon cell viability. Sodium citrate has been used to remove encapsulated cells and there has been no

Alginate fibre to culture stem cells during adipogenic differentiation.

Discussion

suggestion that the sodium citrate had any cytotoxic effect (Gillette et al., 2010). After which human adipose derived stem cells underwent live dead and proliferation assays. (Wu et al., 2016) used a weak concentration (55mM) of sodium citrate in medium over several days without any effect upon the human corneal epithelial cells; there was even increased proliferation due to the reduction in hydrogel stiffness. It is therefore clear that if the detrimental effect of sodium citrate is confirmed (repeats needed), then reducing its concentration may prevent further problems. If the reduction in sodium citrate concentration was found to be detrimental at any concentration, to the MSCs, then alginate lyase could be used to remove the alginate layer as seen in the work performed by *Ikeda et al* (Ikeda et al., 2017).

The fibre culture process showed no negative effects upon the ability of cells to differentiate into adipocytes once removed from the fibre (using the lowest concentration of sodium citrate) though this requires repeats to confidently conclude this. Similar maintenance of cell characteristics has been reported for human induced pluripotent stem cells, which also remained pluripotent after several passages consisting of removing the cells from the alginate fibre and then reseeding into a separate fibre (Ikeda et al., 2017). Another report showed MSCs that had been cryo-frozen in the fibres and reseeded on to culture plates. These were still able to differentiate into adipogenic, osteogenic and chondrogenic cells (Tian et al., 2019). Thereby, showing that even under highly stressful conditions (such as freezing or removal from the fibres) the fibres were able to maintain the differentiation ability of the cells. To be completely confident that there was no change in the differentiation ability of the MSCs grown in the soft-core fibres here, cells removed from the fibres should undergo further osteogenic and chondrogenic differentiation, as the MSCs have the ability to differentiate into all.

Alginate fibre to culture stem cells during adipogenic differentiation.

Future work

2.6 Future work

2.6.1 Optimisation production method

The immediate future work will build directly on to the findings of the study outlined above, starting from the optimisation of the fibre production, with a core aim of a reduction in the alginate layer of the fibre to reducing blockages. However, care must be taken to prevent the fibre becoming too large and having cells become necrotic due to a lack of diffused nutrients and oxygen (Valamehr et al., 2008, Van Winkle et al., 2012). In addition, there will need to be an observation of the thickness of the alginate layer and the inner core size as the rate of CaCl_2 , is optimised to prevent alginate blockages. As previous work on hollow tubes have shown the rate of flow can alter the thickness of both the outer layer and inner core (Wang et al., 2019b). Changes in diameter due to alterations in the flow rate can alter the size of adipogenic lipid droplets, (Yokomizo et al., 2019) and as such should be observed, furthering the need to optimise the flow rates used. Work by *Shin et al* found that the blockages in their system were relieved when the flow was allowed to run vertically not horizontally (Shin et al., 2007). While this would be a vast change to the system used here, it would be another option for further assessment.

Further optimisation should include the alterations of the ECM component used to make the core of the fibre. Possible components for the core of the fibre include laminin or collagen IV (Nakajima et al., 2002b, Liu et al., 2017a, Chen et al., 2016). *Hsiao et al* used an internal core of collagen I and fibronectin, but due to the reduction of fibronectin during adipogenesis so the use of fibronectin would not be ideal (Hsiao et al., 2016). *Onoe et al* also used multiple ECM components in the core of an alginate fibre, though not for cells undergoing adipogenesis (Onoe et al., 2013). Multiple ECM components within the core are worth attempting as it would provide the most similar environment to adipose tissue (Yasuaki et al., 2000). Whichever ECM

Alginate fibre to culture stem cells during adipogenic differentiation.

Future work

components are selected will affect the differentiation and even the type of adipocytes (brown, beige or white) (Gonzalez Porras et al., 2021) as the ECM changes during adipogenesis see Figure 8. Therefore, the fibre could be altered for a range of experiments by only altering the inner core components.

2.6.2 Analysis of adipocytes within fibre

The next aim will be to assess the location of the adipocytes within the fibre, (on the surface or throughout) as well as being able to assess the size of the lipid droplets for comparison with adipose tissue and 2D culture. Analysis of the lipid droplets would allow for characterisation of the droplets into unilocular or multilocular. To achieve this, either confocal imaging through the fibre (as mentioned) or by immunostaining for perilipin (Tansey et al., 2004) on the cryo-sections of the fibres could be used. The cryosectioning here indicated that lipid droplets were not found to remain in place, this may be due to the thickness of the sections (10 μ m) (Kwan et al., 2017) which may disrupt the lipid droplets. Larger sections of 30 μ m – 50 μ m and changes to the fixation as per (Nicu et al., 2018, Mehta et al., 2019) may alleviate this problem.

In addition to further imaging, quantification of adipogenesis will need to be performed. The swelling of the fibres makes it difficult to quantify the lipid droplets and instead the presence of adipogenic genes should be assessed. Any qPCR assessment of the adipogenic genes will standardise the RNA content which allows for the comparison between the fibres and 2D even if the problems in cell loading were not corrected in the optimisation of the fibre production. PPAR γ , adiponectin (a hormone secreted by adipose tissue and regulates metabolic progresses, CEBP β and fatty acid binding protein 4 (FABP4, carrier of fatty acids) could be used to assess the amount of adipogenesis (Velickovic et al., 2019, Velickovic et al., 2018).

Alginate fibre to culture stem cells during adipogenic differentiation.

Future work

RNA-seq could also be completed for a more complete view of the adipocytes being cultured (Zhang et al., 2022a)

The identification of the type of adipocytes will need to be completed; imaging can be used (confocal or sections) to measure the size and number of the lipid droplets, while beige or brown adipocytes will be multilocular (Velickovic et al., 2018). Analysis of the genes expressed by the differing types of adipocytes will allow for the identification of the lineage. White adipocytes can be marked by transcription factor 21, leptin and Homeobox protein (HOXC8) (Waldén et al., 2012, Pilkington et al., 2021). Neutral amino acid transporter (Asc-1) has also been suggested to be a marker of white adipocytes (Ussar et al., 2014, Pilkington et al., 2021). As the HOXC8 has also been seen in beige adipocytes (Waldén et al., 2012), to confirm the adipocytes are white there would need to be reduced beige marker genes. These beige marker genes include: CD137, TMEM26, CITED1 and P2RX5 (Velickovic et al., 2019, Garcia et al., 2016). To identify brown adipocyte, the markers include UCP1, CIDEA, or Cox8b (Velickovic et al., 2018).

2.6.3 Rheology

As mentioned in the introduction (section 2.1.6) several cell behaviours (i.e., migration, differentiation, and adherence) are dependent upon the stiffness of the culture material. The stiffness of the fibre could affect the MSC cultured within and as such should be analysed. Adipocytes differentiate better in less stiff conditions (Young et al., 2013, Liu et al., 2020b), reviewed by (Su et al., 2022) and as such the fibres may provide a good environment for differentiation into adipocytes.

Alginate fibre to culture stem cells during adipogenic differentiation.

Future work

The Young's modulus of a recently used collagen scaffold was found to be close to the *in vivo* mouse adipose tissue (~ 1kPa) (Louis et al., 2019). The Young's modulus of an alginate fibre with a collagen core was assessed by atomic force microscopy, with a result if was 6.3 ± 0.4 Pa (Onoe et al., 2013). It is therefore likely that the similar fibres in this work will have a similar Young's modulus. If the fibre was seen to be a stiffer material than adipose tissue, alterations would need to be made to reduce the stiffness. Alterations can be made through changes to the alginate composition (Hung and Smidsrod, 1970) and the concentration of both alginate (Kuo and Ma, 2001) and CaCl_2 (Freeman and Kelly, 2017).

2.6.4 Expansion of the fibre's applications

After optimisation of the fibre is completed, work will need to be done to compare the collagen adipocyte core with adipose tissue, through genes expression, and proteomic analysis (Dohmen et al., 2022). If there are sufficient similarities between the fibre adipocytes and the adipose tissue, then this would be a system that can be used to model adipose tissue in 3D with a controllable ECM component.

For the fibre to be used to model human adipose tissue, there will be a need to make alterations to the cells within the fibre. While the MSCs used here are a robust cell type for adipogenesis, they are from mice and as such may not truly representative of human adipose tissue. Attempts should therefore be made to differentiate human cells into adipocytes. There has been several methods for the differentiation of induced human pluripotent stem cells; including for white (Mohsen-Kanson et al., 2014, Ahfeldt et al., 2012), beige (Singh et al., 2020, Guénantin et al., 2017) and brown (Mohsen-Kanson et al., 2014, Ahfeldt et al., 2012). If successful, the fibre would then be optimised through alterations to the ECM in the core to

Alginate fibre to culture stem cells during adipogenic differentiation.

Future work

be representative of stiffness. This would provide a human 3D and ECM containing adipogenesis models of all the adipocyte types

Adipocyte models have been created to introduce more representative obesity models through the introduction of lipids to the culture medium. The resulting raise in droplet size, increased cytokine secretion, reduced insulin responsiveness and dysfunctional lipolysis are suggested to be marks of adipocyte dysfunction (Ioannidou et al., 2022, Pieters et al., 2022). If adipocytes within the fibre are also seen to show adipocyte dysfunction, this may then form another model for further experimentation.

2.6.5 Co-culture within the fibre

Adipocytes in adipose tissue are not alone, they interact with other cell types including vascular endothelial cells (Sabaratnam and Svenningsen, 2021), and immune cells (Blaszczak et al., 2021). As such, adding them to an adipocyte model would further the complexity of the model and potentially make it more representative of the adipose tissue. During obesity there is an increase in inflammation (Lawler et al., 2016), accompanied by the presence of macrophages and cytokines (Lawler et al., 2016, Di Gregorio et al., 2005). Recent work by *Monk et al* and *Matacchione et al* have demonstrated the use of Transwell co-culture methods for macrophages and adipocytes, which are therefore 2D culture methods (Monk et al., 2020, Matacchione et al., 2022). As previous research has shown that macrophages can “bite” adipocytes (Sárvári et al., 2015), it may be that the optimal placement for any macrophage co-culture would be within the alginate layer, this would allow for the exchange of cytokines without physical interaction.

Alginate fibre to culture stem cells during adipogenic differentiation.

Future work

Previous work has cultured cells within the core and in the alginate layer (Onoe et al., 2010) and it demonstrates the ability of the fibre to have diverse usages. In addition, there has been Janus fibres where two core solutions are surrounded by alginate (Shao et al., 2019), this would allow for enough further flexibility in the design of co-culture experimentation. Co-culture requires different medium components that can be detrimental to one or both cell types; it is another beneficial aspect of the fibre as a culture method if the adipocytes were to be cultured in the fibre first before being removed (in an optimised method) and then reseeded into the fibre with the selected secondary cell type.

2.6.6 The fibre as a high content screening model

Currently there is an increasing need for anti-obesity drugs as in many parts of the world. There are increasing populations of obese people, who will experience the linked health problems that it brings (see section 2.1.1). The creation of high throughput screening models and high content screening models to allow for research into adipogenesis, is of high importance. To date, there multiple models that have been used as high throughput screening for the identification of possible drugs (drug discovery) see review, (Tsui, 2022). While these high throughput/content screening methods have identified many possible drugs, (i.e. Beta-3 -adrenoreceptor agnoists) (Qiu et al., 2018), there has been limited creation of 3D high throughput screening methods for the testing of the drugs themselves (Tsui, 2022, Louis et al., 2022).

High throughput/content screening requires reliable and numerous samples. Recent work had demonstrated a possible adipocyte model using alginate and collagen droplets upon 96 well plates (Louis et al., 2022). Due to the ability of the fibre to be physically manipulated the fibre here could be used to form a high content screening model for the many drugs that are under

Alginate fibre to culture stem cells during adipogenic differentiation.

Future work

investigation (reviews (Wen et al., 2022, Mukherjee et al., 2016)). The length of a fibre (if optimised to have a consistent cell loading) could be cut into small enough sections for a 48 or 96 well plate and would allow for high content screening for anti-obesity drugs. Anti-obesity drugs can target many different aims, such as, increased activation of BAT to increase thermogenesis and energy expenditure (Cypess et al., 2015) or to increase the number of beige cells in white adipocytes (browning) (Zhao et al., 2021). As the fibre may be able to culture a range of adipocyte types, model obesity or in co-culture, there will be a large range of potential samples for anti-obesity drug screening from using this fibre.

High content screening has the benefit of relying upon imaging to collect large quantities of data, including confocal imaging (Antoniou et al., 2022). This would allow assays to be further automated allowing large quantities of data to be analysed (Roper and Coyle, 2022). The data collection would include luciferase-based viability assays (Roper and Coyle, 2022), quantification of the lipids present (3D model may require sectioning) (Yuan et al., 2019), immunostaining and quantification for selected markers (Lau et al., 2019), and glucose and fatty acids uptake measurements (through fluorescent analogues) (Louis et al., 2022). Additional testing may include oxygen consumption rates (OCR), RNA-sequencing data (Singh et al., 2020), and proteomic analysis (Antoniou et al., 2022). An experiment of this nature would provide a model for drug screening in a completely tuneable 3D culture method. This would be particularly true, if the fibre is able to culture a range of human adipocytes (white or brown), to co-culture with other important cell types and able to represent obesity more accurately (due to an increased lipid content). This could be a step towards to a quick and efficient method to find anti-obesity drugs without the use of animal models.

Alginate fibre to culture stem cells during adipogenic differentiation.

Conclusion

2.7 Conclusion

To conclude the soft-core fibre system used in this pilot study contains several of the characteristics required for a good 3D model, in line with other soft-core fibres, fibres and 3D scaffolds used to culture a range of adipogenic cells. The fibre was able to keep cells viable for at least two weeks, possibly longer, while maintaining the ability of the cultured cells to undergo adipogenesis. The fibre is relatively simple to make with simple equipment in laboratory conditions. This fibre could therefore potentially provide a reliable and accurate model to characterise the factors regulating adipose tissue formation. This fibre culture system is a good candidate to produce a range of novel and diverse 3D models of adipogenesis for drug testing through high content screening.

**CHAPTER 3. PEPTIDE AMPHIPHILE SCAFFOLDS AND HUMAN
INDUCED PLURIPOTENT STEM CELLS**

Peptide amphiphile scaffolds and human induced pluripotent stem cells

Introduction

3.1 Introduction

Stem cells in the embryo and the adult require a specific environment to thrive, known as the stem cell niche. The ECM is a component of the stem cell niche along with secreted factors, physical conditions, metabolic regulation, and other cell types (Gattazzo et al., 2014, Li and Xie, 2005). The stem cell niche can interact with the stem cells to maintain pluripotency or to stimulate differentiation (Jha et al., 2011). These stem cell niches are variable depended upon their location and type (Spradling et al., 2008).

The ECM provides structural support and controls the physical conditions (shear stress, oxygen level) need to stimulate stem cell renewal (Rozario and DeSimone, 2010, Humphrey et al., 2014). The composition of adipose tissue in relation to collagen was discussed in Chapter 2. As seen there and in the introduction (1.2 and page 5), the fibrous protein collagen and the adhesive proteins (laminin and fibronectins), proteoglycans (PGs) and glycosaminoglycans (GAGs) (i.e. chondroitin sulphate (CS), hyaluronic acid (HA), and heparan sulphate (HS)) are the major components of the ECM see Figure 3 (Hynes and Naba, 2012).

Natural polymers have often been used to create culture environments for cell culture, as seen in the previous chapter. Another common substrate for culturing cells is Matrigel®, produced by Corning USA (Corning, 2022). Matrigel is a mixture of proteins and glycans from Englebreth-Holm-Swarm tumours grown in mice (Kleinman and Martin, 2005) and has been used to maintain mouse and human embryonic (Xu et al., 2001) and induced pluripotent stem cells (Lam and Longaker, 2012). Work in 2010 detailed the main components in Matrigel as laminin, collagen IV, nidogen and multiple growth factors (fibroblast growth factor, insulin like growth factor TGF β) (Hughes et al., 2010, Kleinman et al., 1982). However, both Matrigel and

Peptide amphiphile scaffolds and human induced pluripotent stem cells

Introduction

other natural hydrogel gels are found to display batch-to-batch variation (Hughes et al., 2010) and their physical characteristics for example variable elastic modulus (Soofi et al., 2009), making Matrigel difficult to manipulate in the lab, particularly when aiming to work at large scale or in an automated setting.

Synthetic hydrogels are often used for cell culture instead as they are typically bioinert (prior to functionalisation) allowing for a fully controlled environment (Breedveld et al., 2004, Caliri and Burdick, 2016). Modification of the synthetic material provides an ability to dictate the physical characteristics of the hydrogel (Xu et al., 2010a), such as the physical stiffness of the hydrogel (Giuseppe et al., 2018), porosity (Annabi et al., 2010), or presence of cell adhesive motifs (i.e. RGDS) (Ishida et al., 2020). One such group of synthetic hydrogels are self-assembling peptides, peptide amphiphiles (PAs), pioneered by the group of Prof. Samuel Stupp (Hartgerink et al., 2001).

3.1.1 Peptide amphiphiles

Peptide Amphiphiles (PAs) are classified as short peptide sequences linked to a hydrophobic tail that can self-assemble to form scaffolds that resemble the fibrous components of ECMs (Webber et al., 2010b, Yu et al., 1996). While this is a broad category, the focus of PAs here will be those with three major structural elements that can affect the self-assembly of the PAs: a hydrophobic alkyl tail, a series of residues capable of forming a beta-sheet secondary structure and charged hydrophilic residues (Mata et al., 2010, Stendahl et al., 2006, Hartgerink et al., 2001), as seen in Figure 27.

Peptide amphiphile scaffolds and human induced pluripotent stem cells

Introduction

The self-assembly of PAs

These PA's self-assemble through three main intermolecular interactions: the hydrophobic interactions of the alkyl tails, the hydrogen bonding involved in beta-sheet formation and electrostatic repulsion of charged amino acids (Cui et al., 2010). When in polar solutions the hydrophobic tail is unable to form hydrogen bonds, which reduces the solution's entropy. To correct this decrease in entropy, the hydrophobic tails aggregate together to reduce the surface area exposed to the polar solution (hydrophilic collapse) (Velichko et al., 2008).

The PAs aggregate together into cylindrical nanofibres due to the hydrogen bonds forming beta-sheets parallel to the long axis of the nanofibre. The beta-sheet forming residues can be altered to change the structure, as weak hydrogen bonding produces micelles and stronger can produce nanofibres. When the residues that result in hydrogen bonding, are hydrophobic then hydrophilic (VVEE) the structures formed are nanofibres (Cui et al., 2010, Jiang et al., 2007). When these residues alternate (VEVE) the structures formed are flatter and described as a nanobelt (Cui et al., 2010, Cui et al., 2009).

Electrostatic repulsion is present due to the charged residues that make up the hydrophilic head of the PA required for dissolving in solutions (see Figure 27). The charges expressed are the same and as such the PAs repel other. The charges must be screened to allow for the hydrophobic and hydrogen bonding to occur (Stendahl et al., 2006). The screening of charges triggers self-assembly, this is achieved through the addition of inorganic salts or a variation in the pH of the solution (Stendahl et al., 2006).

Peptide amphiphile scaffolds and human induced pluripotent stem cells

Introduction

Co-assembly with ECM components

These PA nanofibres produce a porous hydrogel with similar structure to the natural ECM expressed by cells (Hartgerink et al., 2002). PAs can self-assemble when mixed with polymers of opposite charge and suitable proteins have often been selected due to their presence in the ECM (Capito et al., 2008). The GAG HA, with an overall net negative charge, has also been used to form a range of hydrogel shapes from open sacs to continuous strings, with the structure dependent upon HA density and the method of mixing (Capito et al., 2008). This highlights another benefit of PA hydrogels as the physical characteristics can be altered depending on the application (Capito et al., 2008, Derkus et al., 2020). HA and PA hydrogels have been used to create a model of skin tissue ECM (Ferreira et al., 2013a). Other ECM components included heparin (Ferreira et al., 2013a), collagen, fibronectin and keratin (Hedegaard et al., 2018) and recombinant elastin-like-proteins (Inostroza-Brito et al., 2015). However, this method of gelation, adding single ECM components to PAs to drive gelation, leads to simplistic models of the ECM. Recently, multiple components were combined to better mimic the complexity of the natural matrix, creating a model of human pancreatic cancer in a PA hydrogel formed using a range of ECM proteins (Osuna de la Peña et al., 2021) and shown in Figure 4 **Error! Reference source not found.**

Bioactive epitopes on PAs

In addition to using co-assembly between ECM components and PAs to create tissue-relevant ECM models, more direct methods have also been applied. Bioactive epitopes have been incorporated into the PAs adjacent to the charged hydrophilic head. As discussed earlier, short peptide sequences, inspired by cell-binding motifs found in many ECM proteins, can retain their cell-binding properties when displayed on or in biomaterials. Functionalisation of PAs in this way therefore mimics the actions of these ECM proteins (see Figure 4). The most common epitope presented on PA hydrogels was the RGDS motif (Hedegaard et al., 2020, Mata et al.,

Peptide amphiphile scaffolds and human induced pluripotent stem cells

Introduction

2009). As mentioned the RGDS motif is found on the adhesion protein fibronectin (Hynes, 2002), this motif is one that enables the attachment of fibronectin to cells through the integrins on the cell surface (Hynes, 2002). When the RDGS motif is present in PA hydrogels (80% of the PAs had RDGS present and 20% were unmodified PAs) encapsulating human mesenchymal stem cells, cell adhesion was supported (Mata et al., 2009). One of the more complicated models, for ovarian cancer modelling, used PAs modified with RDGS, as well as a PA modified with GHK, for cell proliferation (Hedegaard et al., 2020).

Additional bioactive epitopes have been used to direct the differentiation of cells encapsulated in the hydrogel (Silva et al., 2004, Derkus et al., 2020) or to stimulate a specific receptor (D'Andrea et al., 2005), as shown in Figure 4. For example, the presence of the IKVAV motif (derived from laminin) presented on the PA, directed neural progenitor stem cells into neurons and not astrocytes (Silva et al., 2004). These PA hydrogels can be designed to mimic specific ECM functions and can be used individually or in combination to recreate multiple ECM components. Research by *Derkus et al* created a hydrogel system to represent the ECM of the bone (Derkus et al., 2020). Within these hydrogels, adipose derived stem cells and umbilical vascular endothelial cells were co-cultured and directed to oestrogenic and angiogenic lineages with three different bioactive epitopes present (attachment - RDGS, osteogenic – DGEA, adipogenic - K3SVVYGLR) (Derkus et al., 2020). This approach was a bottom-up design, where the manufacture of the PA itself, with additional ECM protein motifs provided the physical characteristics and bioactive interactions to control cells towards a desired outcome.

The ability of PAs to model the ECM through co-assembly provides a hydrogel containing ECM components, another method has been used to incorporate the functions of ECM components. Bioactive epitopes have been added to the PAs after the charged hydrophilic

Peptide amphiphile scaffolds and human induced pluripotent stem cells

Introduction

head, thereby mimicking the actions of selected ECM proteins (see Figure 4). The epitopes are residues from proteins that have interactions with cells or other proteins. The hydrophilic head remains on the outer surface of the nanofibres, therefore the bioactive epitopes attached to them were expressed on the surface of the nanofibre, allowing interact with any cells encapsulated with it in the PA hydrogels (Guler et al., 2005, Storrie et al., 2007).

Introduction

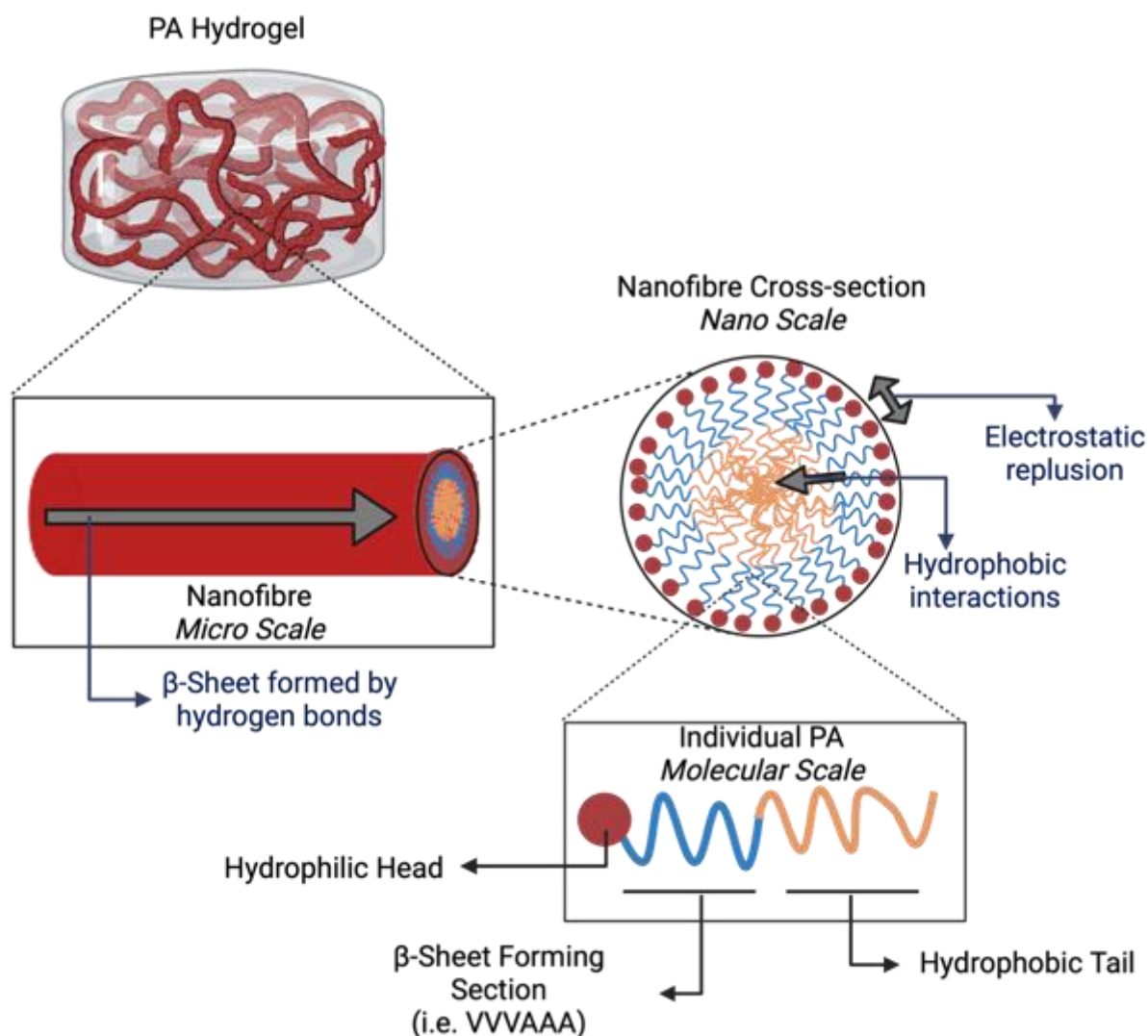


Figure 27. Graphical representation of the nano organisation of PAs to form hydrogels. The PA nanofibres form a porous ECM resembling hydrogels. The structure of the PA controls the formation of the nanofibre and therefore the hydrogel. The PAs are comprised of three major sections, a hydrophobic tail (yellow), beta-sheet forming (blue) and hydrophilic head (red). The fibres form through a range of noncovalent interactions. The beta sheet forms along the length of the fibre creating the cylindrical shape of the fibre. The hydrophobic interactions trigger the alkyl chain to be located internally away from any solution surrounding the PAs while the hydrophilic head of the fibre is external to the solution. The electrostatic repulsion that occurs between these charges' hydrophilic heads of the PA. The charges are identical and as such repel each other, this interaction must be removed before the fibres can be formed. This is known as screening the charges and can be completed through the addition of salts. Created with BioRender.com. (Stendahl et al., 2006, Cui et al., 2010, Cui et al., 2009). Figure made in Biorender.

Peptide amphiphile scaffolds and human induced pluripotent stem cells

Introduction

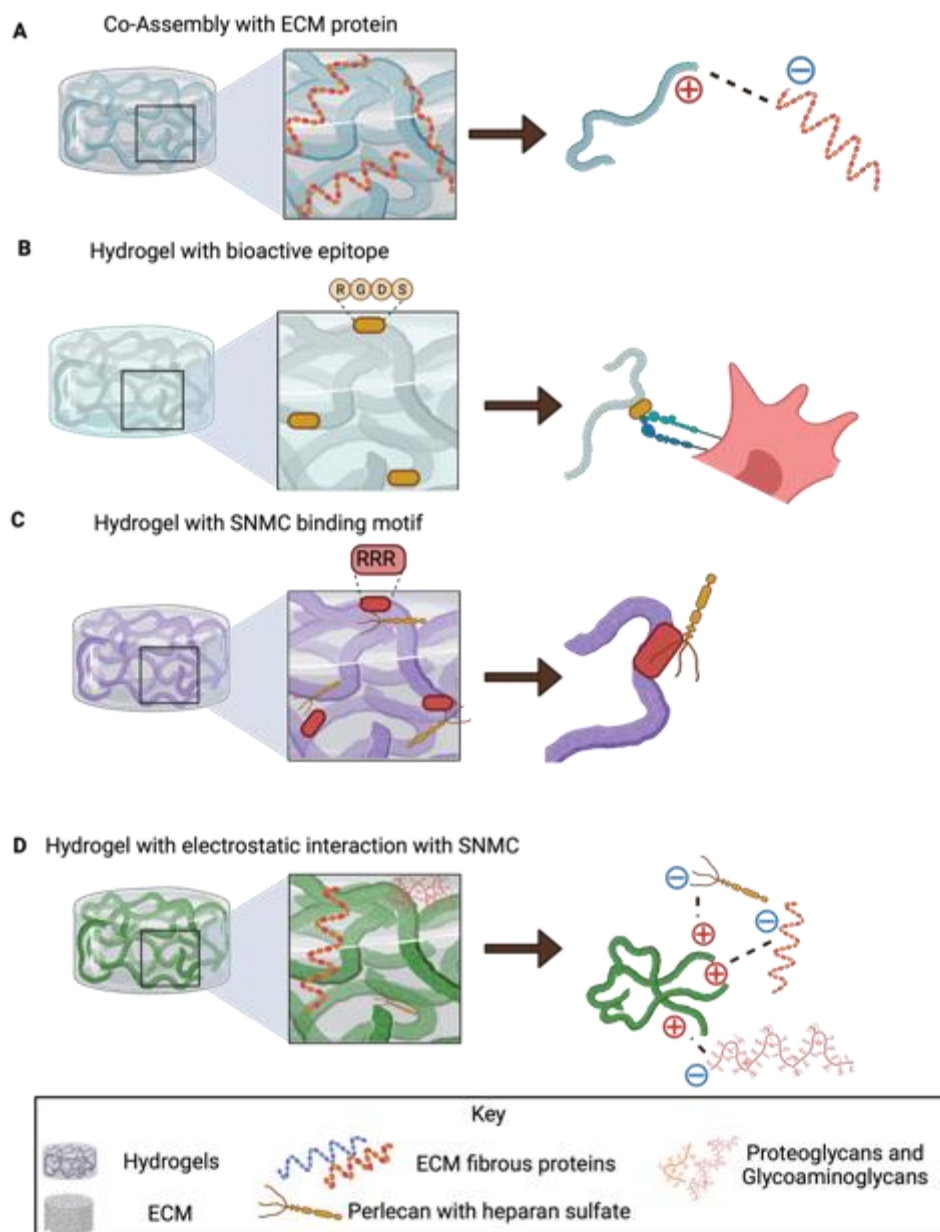


Figure 28. The methods to produce the 3D hydrogels in use.

A The co-assembly of the PA hydrogels is dependent upon the electrostatic integrations of the charged head of the PAs and the opposite charges present upon the ECM component (Ferreira et al., 2013b, Ahmad et al., 2022). **B** The PA hydrogels with bioactive epitopes expressed on the surface of the nanofibres provide an epitope of residues. The residues then bind to proteins on the surface of the cells being cultured. The RGDS epitope here is known to interact with integrins expressed on the surface of cells, thereby providing attachment.(Derkus et al., 2020, Hedegaard et al., 2020, Silva et al., 2004). **C** The hydrogels capable to sequester secreted native matrix proteins (SNMCs), have done so by expressing a SNMC binding motif much like the bioactive motif. The residues are known to bind to selected SNMC, and thereby sequester the SNMP in the hydrogel. (Shah et al., 2010, Tomaszewski et al., 2021). **D** A possible method by which, a physical characteristic could be used to sequester SNMPs in the hydrogel. The possible positive charge expressed by PAs (on the hydrophilic head) may be able to form an electrostatic attraction with any SNMCs (proteoglycans and glycosaminoglycans) with an opposite charge (negative). Figure made in Biorender.

Peptide amphiphile scaffolds and human induced pluripotent stem cells

Introduction

3.1.2 Native expression of ECM and sequestration

The interactions between the stem cells and the ECM are reciprocal; stem cells can remodel and alter the ECM components (Fuchs et al., 2004, Bissell et al., 1982). The reciprocal power that cells have to alter their environment and that the environment has to alter the behaviour of cells was termed “dynamic reciprocity” by *Bissell* (Bissell et al., 1982). The ECM provides an environment that allows for cell viability, the cells can then alter the ECM surrounding them, producing biochemical or physical alterations to the matrix. The cells then respond to these alterations through mechosensing and their behaviour can, in turn, change (Zhou et al., 2022) (section 1.2).

The degradation of ECM has often been exploited in hydrogel design taking full advantage of the relatively good understanding we have of the specificity of matrix-degrading enzymes. Often, gels are engineered to display MMP-cleavable linkers that, following degradation by MMPs released by encapsulated cells, alter cell stiffness, provide increased pore size to promote migration or release immobilised factors (Lutolf et al., 2003, Rosales and Anseth, 2016). However, de novo matrix synthesis can also be used of to engineer scaffolds. This is shown in human bone marrow derived stem cells encapsulated within hydrogels that can remodel their surroundings in the hydrogel by secreting their own native ECM components (Ferreira et al., 2018, Blache et al., 2018). This including recently where *Loebel et al* have labelled the native ECM proteins expressed in hydrogels (Loebel et al., 2019, Loebel et al., 2022). The secreted native matrix components (SNMC) released into hydrogels from cells can be identified as early as 4 hours after encapsulation (Loebel et al., 2019). The MSCs were seen to interact with the SNMC but still interacted with the hydrogel (Ferreira et al., 2018). As the MSCs produce SNMC over time there is a likelihood that the SNMC will overwrite the original characteristics of the hydrogel (Loebel et al., 2019). When exogenous material is

Peptide amphiphile scaffolds and human induced pluripotent stem cells

Introduction

added to a hydrogel it is a controlled variable, but the SNMC will be less controlled and could result in unwanted cellular behaviour for the experiment.

Sequestering secreted native matrix components

The current attempts to use approaches to trap matrix components to direct cells into a specific outcome include the capture and enrichment of SNMCs (see Figure 4 and Figure 28C). Recently there have been several examples of sequestering SNMC through SNMC binding peptides (epitopes) attached to hydrogels (Ding et al., 2022, Abune et al., 2022). Last year *Tomaszewski et al* produced a range of hydrogels that expressed combinations of a heparin binding peptide, two distinct heparan sulphate binding peptides and a less-well defined basement membrane binding peptide. These hydrogels were then used to culture ovarian follicles, and two were found to promote follicle maturation. All the hydrogels were found to sequester and retain laminin, collagen I, perlecan (a heparan sulphate proteoglycan) and fibronectin (these are examples of SNMCs) (Tomaszewski et al., 2021). In another approach, a PA hydrogel was constructed to display a heparin-binding sequence (LRKKLGKA) that was found to sequester heparin (Rajangam et al., 2006, Webber et al., 2010a). In another slightly different example, a PA was engineered to bind to a TGF β binding domain (not a SNMC but sequestered by the ECM) with the aim of promoting chondrogenic regeneration (Shah et al., 2010).

Another method to capture desired SNMC could be through manipulation of the physical characteristics of the hydrogel. There are characteristics that can alter the rate and diffusion ability of SNMC, such as the crosslinking ability and degradability (Bryant and Anseth, 2003, Bryant and Anseth, 2002), alterations to the hydrogel could then allow the sequestration of SNMCs closer to the cells. Several of the SNMCs are charged and may be sequestered if

Peptide amphiphile scaffolds and human induced pluripotent stem cells

Introduction

they can form interactions with the hydrogel. GAGs are highly negatively charged and as such there may be sequestered through ionic bonding with a charged hydrogel, for example a PA hydrogel which, as mentioned above can be gelled via electrostatic interactions with oppositely charged ECM components. In this way, we could consider applying hydrogels as a stem cell niche, using physical characteristics of the hydrogel to trap secreted matrix components and thereby influence stem cell behaviour (Figure 28D). For the sequestration to be directed or targeted we need to understand the cells that will be encapsulated and the ECM they will secrete under specific circumstances.

3.1.3 ECM proteins expressed by hiPSCs

The major components of the ECM expressed during maintained culture of pluripotent hiPSCs (detailed in section 1.1.1) are similar to those expressed by the inner cell mass of an embryo as they share many characteristics (Baldwin et al., 2008). While the inner cell mass is still pluripotent it produces several ECM proteins, the first of which is laminin 111 during the during the two cell stage (Sasaki et al., 1988). Heparan sulphate has been located on the cell surface as early as day 2-4 after fertilisation (Dziadek et al., 1985). Also found was type IV collagen (Leivo et al., 1980) and fibronectin during the blastocyst stage (Wartiovaara et al., 1979). Therefore, all of the ECM proteins are likely but not definitely expressed by hiPSCs.

As one of the ECM proteins expressed by hiPSCs are laminins. Laminins are formed from differing protein chains α , β and γ (Aumailley et al., 2005, Hohenester, 2019). There are 16 different laminin trimers found *in vivo*, located in a range of tissues formed from one chain of each type but with a range of differing isoforms for each chain (Aumailley et al., 2005) The nomenclature for laminins is a set of three numbers denoting the isoform of each chain in the order of α , β and γ . Two laminin isoforms (511 and 521) of are found within the inner cell mass

Peptide amphiphile scaffolds and human induced pluripotent stem cells

Introduction

and an $\alpha 1$ isoform (111) is found in Reichert's membrane, the supporting extraembryonic layer of trophoblasts (Cooper and MacQueen, 1983). Laminins 521 and 511 are expressed in pluripotent ESCs *in vitro*. Mouse and human ESCs have been shown to express $\alpha 1$, $\alpha 5$, $\beta 1$, $\beta 2$ and $\gamma 1$ laminin chains, *in vitro* (Rodin et al., 2010, Laperle et al., 2015). Specifically, the 511 and 521 laminin isoforms maintain pluripotency through binding to the $\alpha 6\beta 1$ integrin on the surface of these pluripotent stem cells. Signalling via $\alpha 6\beta 1$ induces the phosphoinositide 3-kinases (PI3)/ protein kinase B (AKT) signalling pathway maintaining the levels of pluripotent genes (Nanog, Oct4 and Sox2) (Villa-Diaz et al., 2016, Rodin et al., 2014). Laminin 511 and laminin 521 are therefore expressed by hiPSCs and required for self-renewal, but the endogenous expression of the other ECM components is not definitively established. The ability of laminin to keep stem cells pluripotent has led to laminin 521 and 511 being used to support *in vitro* culture of hiPSCs, hESCs and mESCs (Rodin et al., 2014, Lu et al., 2014).

3.1.4 Hyaluronic Acid

HA is a GAG with the repeating disaccharide of glucuronic acid and acetyl-glucosamine, hyaluronan synthases build HA by joining disaccharides (Casale and Crane, 2022). HA differs from the other GAGs as it is not synthesised attached to a core protein and is not sulphated (Heldin and Pertoft, 1993, Laurent and Fraser, 1992). HA is synthesised at the cell membrane in contrast to other GAGs which are synthesised in the Golgi (Park et al., 2008). HA is typically found in the ECM surrounding cells (Laurent and Fraser, 1992) but has also been located intracellularly and in the nucleus (Hascall et al., 2004). HA polysaccharides have been found to accumulate in tissues undergoing remodelling (i.e., during embryonic development) (Toole, 2004), which agrees well with HA's role in wound healing (Lisignoli et al., 2006), differentiation (Roughley et al., 2011) and cell migration (Toole and Gross, 1971). HA has additionally been suggested to have a role in the maintenance of mouse adipose derived stromal cells,

Peptide amphiphile scaffolds and human induced pluripotent stem cells

Introduction

specifically in the proliferation (Chen et al., 2007a). With regards to differentiation, HA has been linked to several different pathways during embryogenesis (Vabres, 2010).

Extracellularly HA participates in various interactions with ECM components including with the PG versican (Park et al., 2008). At the cell surface, HA interacts with and is retained by receptors such as cluster determinate 44 (CD44), and the receptor for hyaluronan-mediated mobility (RHAMM). CD44 is a transmembrane PG that is ubiquitous and an important cell surface receptor (Aruffo et al., 1990). CD44 has been found to have roles in several intracellular pathways including: Rho signalling activate in tumour cell invasion (Bourguignon, 2012), extracellular signal-regulated kinases (ERK) via the epidermal growth factor receptor (EGF receptor) to promote proliferation (Hatano et al., 2011) and PI3K/Akt in cell migration (Singleton and Bourguignon, 2002). RHAMM is a second ubiquitous protein present on the cell membrane, cytoplasm, and nucleus (Assmann et al., 1999, Hall et al., 1994).

3.1.5 Biosynthesis of GAGs

CS is the most abundant GAGs in the human body. It is comprised of alternating acetyl-galactosamine and glucuronic acid and the similar GAG. DS is comprised of acetyl-galactosamine and iduronic acid (Karamanos et al., 2018, Chen et al., 2021) and both CS and DS are tempo-spatially substituted with sulphate. HS is a GAG comprised of acetyl-glucosamine, glucuronic acid and iduronic acid, followed by sulfation. KS is a GAG comprised of galactose and acetyl-glucosamine. The differing GAGs use different linkers between the PG and GAGs.

KS has two differing types (KSI and KSII) and can be identified by the differing linkers to PG. KSI is linked by an asparagine residue on the PG to an acetyl-galactosamine and KSII is linked

Peptide amphiphile scaffolds and human induced pluripotent stem cells

Introduction

by a serine or threonine residue on the PG link to acetyl-galactosamine (see Figure 29). KS is then elongated as galactose and acetyl-glucosamine are added to the growing polymer. After the elongation, acetylglucosaminyl 6-O-sulfotransferases and galactosyl 6-O-sulfotransferases then catalyse the sulfation of KS on the C4, C6 glucosamine and C1, C3 galactose (Merry et al., 2022).

The linker for CS/DS and HS is comprised of a xylose linked by xylosyltransferase to a serine on the PG and two galactose molecules. Following the linker, the addition of acetyl-galactosamine, initiates CS assembly, the addition of acetylglucosamine, initiates HS. CS is then elongated through the alternative addition of galactosamine and glucuronic acid by glucuronyltransferase I. The epimerization of glucuronic acid then occurs to produce iduronic acid, thereby, producing the GAG DS (Merry et al., 2022). The substitution of sulfate groups is completed by sulfotransferases, 2-O-sulfotransferase for iduronic acid sulfation and 4-O-sulfotranferase and 6-O-sulfotranferase for N-acetylgalactosamine sulfation) (Karamanos et al., 2018, Chen et al., 2021).

For HS, several members of the exostosin glycosyltransferase (EXT) family can then elongate the chain by the addition of glucosamine and glucuronic acid residues. HS N-deactylases and sulfotranferases 1-4 (NDSTS) act to replace acetyl groups on N-acetylglucosamine residues to generate N-sulfated glucosamine, see Figure 29, (Karamanos et al., 2018, Chen et al., 2021). HS can also undergo another modification, where a differing epimerase, than those involved with DS synthesis, acts upon the glucuronic acids, producing iduronic acid. 2-O-sulfotransferase then completes iduronic acid sulfation, followed by 2-O-sulfotransferase and 6-O-sulfotransferase to complete sulfation on glucosamine residues. The sulfation and epimerization thereby increase the variation in the structure of GAGs and the tight control of the tempo-spatial control of GAGs (Merry et al., 2022).

Peptide amphiphile scaffolds and human induced pluripotent stem cells

Introduction

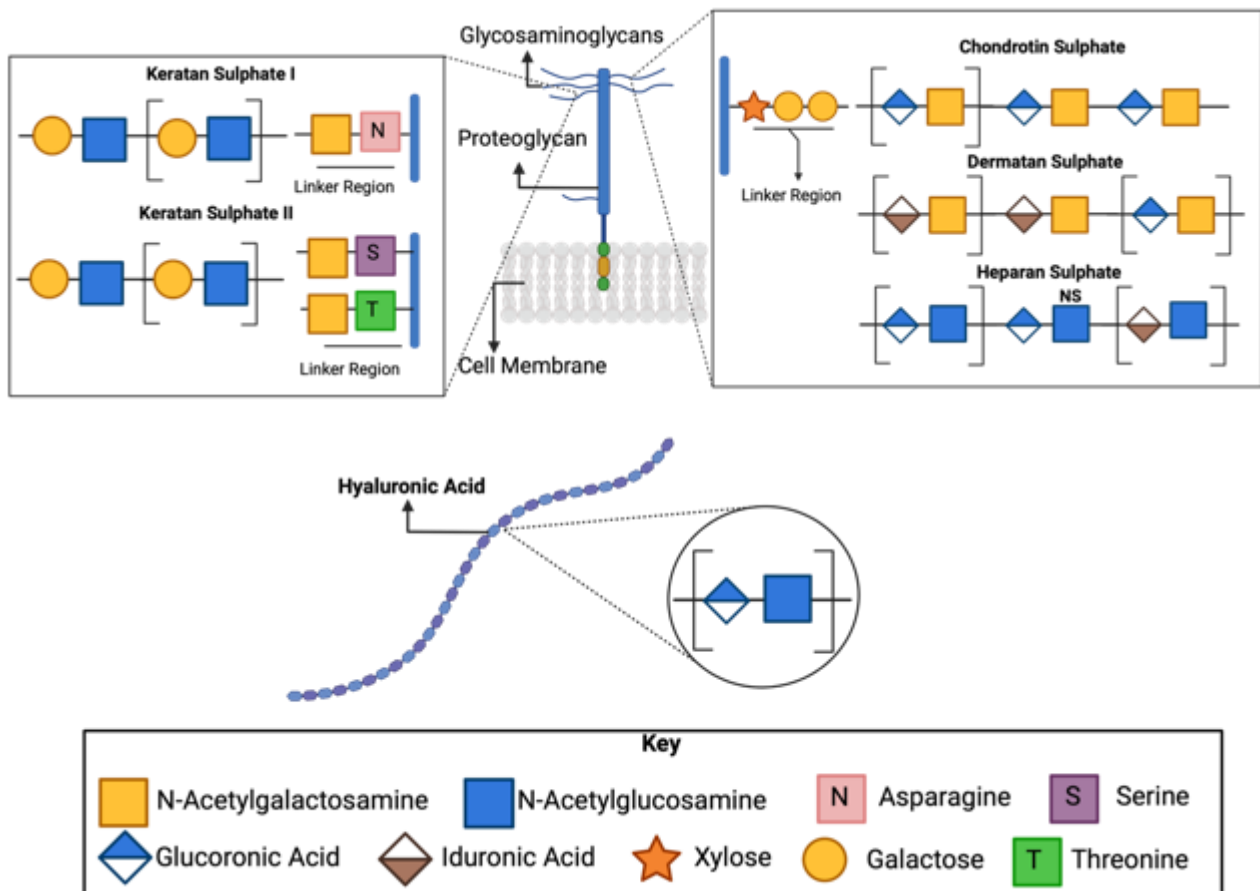


Figure 29. The building blocks of GAGs

Glycosaminoglycans (GAGs) are located upon proteoglycans (PG), except for Hyaluronic acid (HA). The proteoglycans are found on the surface of cells as well as within the ECM. GAGs are polysaccharides comprised of disaccharides of hexosamines and hecuronic acids. The linker to the PG for each GAG and their disaccrides [in brackets] are shown above. The NS denotes the sulation of the N-acetylglucosamine residues to generate N-sulfated glucosamine (Karamanos et al., 2018, Chen et al., 2021, Lin, 2014.).

3.1.6 GAGs in stem cells

HA, CS/DS, KS, and HS have been found in mESCs as well as their differentiated progeny (Nairn et al., 2007, Baldwin et al., 2008). Specifically, there was an increased amount of these GAGs and their sulfation increased when differentiated, to generate embryonic bodies (Nairn et al., 2007). Another study suggested that there were higher levels of low sulphated HS in ESCs and the HS in differentiated progeny were more highly sulphated (Johnson et al., 2007, Hirano et al., 2012). HS analyses in undifferentiated ESCs have shown that N-sulfation can

Peptide amphiphile scaffolds and human induced pluripotent stem cells

Introduction

be as low as 30% (Hirano et al., 2012, Johnson et al., 2007). When hiPSCs, hESCs and various other human cell were analysed there were differences in the presenting GAGs between stem cells and differentiated cells (Fujitani et al., 2013). The GAGs that were increased in the stem cells were non-sulfated CS/HS and low sulfation CS/HS (Gasimli et al., 2014, Fujitani et al., 2013). KS has been found to be present in hiPSCs and hESCs and the KS found was also found to have reduced sulfation (Kawabe et al., 2013, Oguma et al., 2001). The increase in sulfation is lineage specific, which is likely to be the result of the activity of specific sulphotransferases and sulphatases that show lineage-specific expression. For example, during differentiation of mESCs to neural precursors, up-regulation of N-deacetylase N-sulphotransferase 4 was seen as well as two specific 3-O-sulphotransferases (Nairn et al., 2007).

CS has been found to be required for differentiation, following investigation of glucuronyltransferase I null mESCs (Izumikawa et al., 2014). HS has similarly been shown to be required for differentiation. mESCs that are Exostosin glycosyltransferase I null (EXT^{-/-}) result in no HS. The EXT^{-/-} mESCs were unable to differentiate in to neural (Johnson et al., 2007) or mesodermal lineages (Holley et al., 2011) The ability to differentiate was not returned when desulphated HS was added, suggesting a role for sulfation in the determining the ability ESCs to differentiate (Holley et al., 2011, Pickford et al., 2011).

3.1.7 Chapter aims

Whilst there is considerable interest in the creation of synthetic ECM used to culture cells *in vitro*, (including decellularised ECM, or hydrogels displaying with ECM-sourced binding motifs) there has been limited research so far into hydrogels designed to capture and maintain native ECM components through the physical properties of the hydrogel itself. The work in this

Peptide amphiphile scaffolds and human induced pluripotent stem cells

Introduction

chapter introduces proof-of-concept studies designed to demonstrate the effect of engineering a minor physical difference into hydrogels and how this can alter the capture ECM components, such as GAGs within the hydrogel. The aim was to demonstrate if a relatively small change of charge of a hydrogel could then be used to change the native ECM within the stem cell microenvironment that could then affect the behaviour or response of the cells.

Peptide amphiphiles were used as they contain a range of residues that are expressed on the surface of the hydrogel nanofibres. These residues have a charge when at pH 7 and should therefore express a charge during culture. The PA hydrogels needed to be optimised for production in 96 wells plates to culture hiPSC clusters. These clusters would then be able to secrete native matrix components into the hydrogel, where it could be sequestered through the charged residues, see Figure 30. HA, CS/DS, KS, and HS will be secreted by hiPSCs and as they hold a negative charge, they will be a target for any capture of SNMCs via hydrogels with positive charges. Due to their ability to influence critical signalling pathways important in the retention of pluripotency as well as initiating and promoting differentiation there is the potential for bespoke control of cell behaviour if the general principle can be proven.

Peptide amphiphile scaffolds and human induced pluripotent stem cells

Introduction

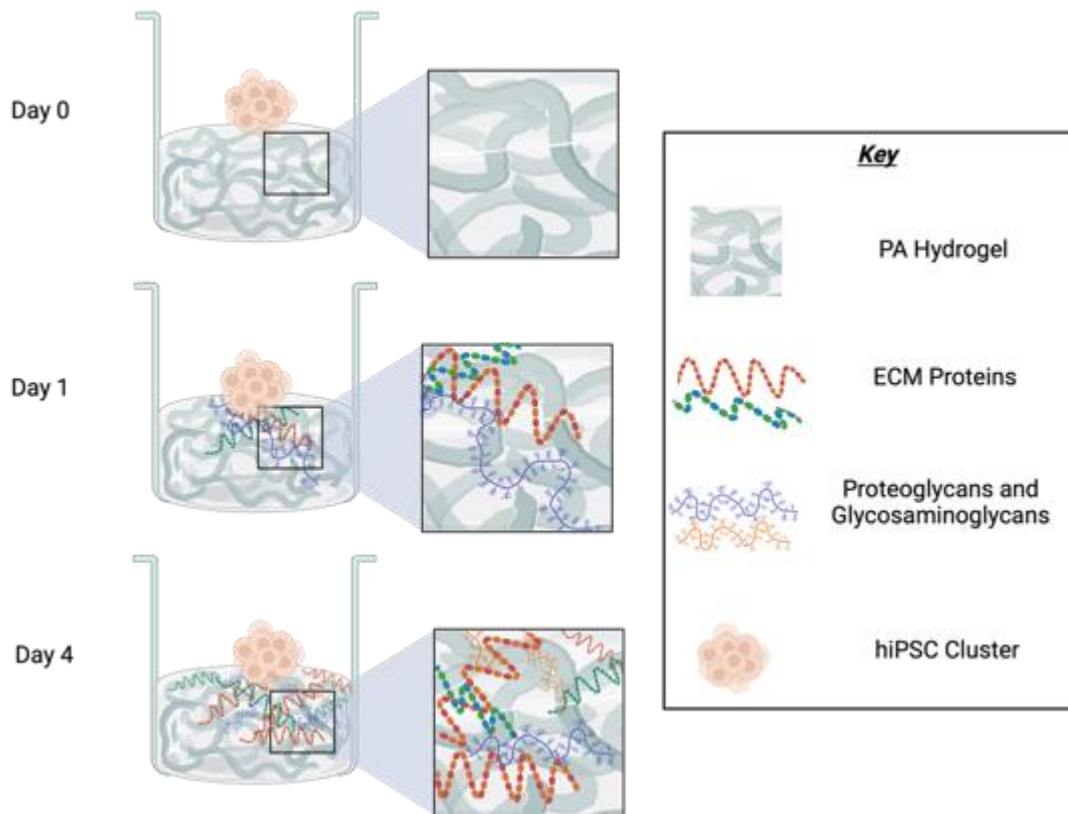


Figure 30. A diagrammatic representation showing the hypothesis that charged PAs can capture proteins and glycans secreted by hiPSC clusters.

The hypothesis suggests that the charges engineered into the PA hydrogels will allow for the capture of ECM components containing an opposite charge. These ECM components, such as structural proteins like collagen, glycosaminoglycans such as hyaluronic acid and proteoglycans such as perlecan would be secreted by the hiPSC clusters. The cartoon shows the potential increase in capture of these ECM components by PA gels over 4 days of culture. Figure made in Biorender.

Peptide amphiphile scaffolds and human induced pluripotent stem cells

Materials and methods

3.2 Materials and methods

3.2.1 Peptide amphiphiles

Peptide amphiphiles purchased from Biomatik (Canada). The PAs were stored at -20°C.

Table 7. The peptide amphiphiles used in this work. The PA used, with their the sequences are listed. All PAs were designed in house and then synthesised by biomatik.

PA	Sequence
K2	C ₁₆ -VVVAAA-KK
K3	C ₁₆ -VVVAAA-KKK
K4	C ₁₆ -VVVAAA-KKKK
E3	C ₁₆ -VVVAAA-EEE

3.2.2 E3 hydrogel for the encapsulation of hiPSC clusters

The glutamic acid containing PA E3 was dissolved in HEPES buffer (Gibco, USA) (10mM) to form a 1% w/v solution (Zhang et al., 2010). As the PA requires alkaline conditions to dissolve, NaOH (0.5M) (Thermo Fisher, USA) was added dropwise; the pH must be returned to 7 before adding the cells. The E3 was kept at room temperature or heated to 80°C and then cooled to 37°C, thereby aligning the E3 PAs (Zhang et al., 2010), 10µl droplets were plated on to a non-tissue coated 48 well plate. To set the E3 a range of CaCl₂ (Gibco, UK) concentrations were used (20mM, 15mM and 10mM) (Beniash et al., 2005).

Peptide amphiphile scaffolds and human induced pluripotent stem cells

Materials and methods

3.2.3 hiPSC culture on vitronectin with E8

Human induced Pluripotent stem cells (hiPSCs) (ReBL-PATs) (Mosqueira et al., 2018) were cultured on recombinant vitronectin (Gibco, USA) and maintained in E8 medium (Life Technologies, USA) during culture (Chen et al., 2011). The hiPSCs were passaged with TrypLE Express (Gibco, USA) and 10 μ M ROCK inhibitor Y-27632 (Stem Cell Technologies, UK). All cell culture was completed in antibiotic free conditions in humidity, at 37°C and 5% CO₂.

3.2.4 hiPSC cluster formation

The hiPSCs were formed into clusters using the hanging droplet method, as previously used (Lin, 2014., Ashworth et al., 2020a). The droplets containing the hiPSCs (100'000 cell/mL) in E8 medium were pipetted on to the lid of a petri dish (10cm) containing sterile PBS for hydration (Lin, 2014.). After 24 hours the hiPSC clusters were collected in E8 for up to 15 minutes, where they could be moved to the appropriate hydrogel.

3.2.5 Optimisation of hiPSC encapsulation in E3 hydrogel

The hiPSC clusters were added to the E3/HEPES solution, with 3 - 4 clusters per 10 μ l E3/HEPES droplet. Bright field images were taken immediately once the hydrogel was set. After incubation for an hour to ensure gelling, 250 μ l of E8 medium was added to each well for culture overnight at 37°C and 5% CO₂. Bright field images were again taken after 24 hours. Live / dead staining using Calcein AM and ethidium homodimer was carried out in the same concentrations as previously used (see section 2.2.5 , page 50). A laser scanning confocal microscope was used to collect the live/dead fluorescent images (Leica TCS SPE, UK).

Peptide amphiphile scaffolds and human induced pluripotent stem cells

Materials and methods

The bright field images were categorised as phenotype 1, 2, or 3. For each condition tested (aligned or non-aligned E3 and specific CaCl₂ concentration) the percentage of each phenotype was calculated $\left(\frac{\text{Number of clusters in specific condition categorised as phenotype } X}{\text{Number of clusters in specific condition}}\right) \times 100$.

This was used to assess the viability of the hiPSCs clusters between the range of CaCl₂ conditions and E3 alignment.

Table 8. Description of categories used to assess viability of hiPSC clusters. The viability assessment was based of bright field image analysis.

Phenotype 1:	flat, very pale with individual cells visible.
Phenotype 2	The inner core is still holding a cell cluster with smooth edges and dark colouring.
Phenotype 3	Paler than expected, individual cells visible or no visible inner core of normal looking cluster.

Afterwards, a repeat with additional conditions was conducted, to see if the reasons for cell death could be highlighted. One of the new conditions was 10µl of E8 medium containing hiPSC clusters adjusted with the CaCl₂ ranges, to assess any cytotoxic effects of CaCl₂. Another was the placement of hiPSC clusters in E3 that were not adulterated with CaCl₂, to assess any cytotoxic effect of E3 when in solution. Bright field images were taken and the hiPSC cluster were categorised. See Figure 31 and Figure 32 for graphical overviews of the protocol.

3.2.6 The creation of heatmaps

The data from the encapsulation of hiPSC clusters in E3 was displayed in heatmaps created by prism software version 7.0d. The percentages of clusters categorised as a phenotype were

Peptide amphiphile scaffolds and human induced pluripotent stem cells

Materials and methods

allocated a shade of blue, the darker the shade the closer to 100% of clusters categorised in the indicated phenotype.

3.2.7 Optimisation of PA hydrogels

All PA gels were formed at 37°C. K PAs were gelled by mixing with x10 PBS (Gibco, UK) (Redondo-Gómez et al., 2019) trials were conducted with varying ratios of K3 and PBS (x10) (Gibco, UK). E3 PA was gelled using 200mM CaCl₂ (Beniash et al., 2005). Volumes of PA/HEPES buffer and either PBS or CaCl₂ were altered till the hydrogel met the specifications. All hydrogels were set into the wells of 96 well plates, the E3 hydrogel required non coated plates (Thermo Fisher, USA). The order of mixing was also assessed, adding the gelator (PBS or CaCl₂) first was found to be best. The final PA: gelator ratios were, for K2, K3, K4 2.5:1 and for E3 4:1. These ratios were used for all further work.

The change in gelation time for the positively charged PAs was assessed depending upon the pH. The PA/HEPES solution was made to the selected formulation, and then the pH was measured, and the time taken till self-supporting was measured. All PA hydrogels were set at 37°C. The PA/HEPES solutions were altered with dropwise addition of either HCl (0.5M) (Gibco, UK) or NaOH (0.5M). The pH vales assessed for each PA/HEPES solution was pH 3 – 6. All pH measurements were checked on pH strips (31 508, VWR Chemical, UK).

3.2.8 Self-assembling peptide FEFEFKFK

The self-assembling peptide used was the octopeptide, FEFEFKFK (Pepceuticals, UK). The FEFEFKFK in dry powder form was used to make a 6mg/mL hydrogel using the previously published method (Ashworth et al., 2020a). The FEFEFKFK peptide (7.5g) was dissolved in sterile water (800µl), vortexed for 3 minutes and heated for 2 hours at 80°C. After which, NaOH

Peptide amphiphile scaffolds and human induced pluripotent stem cells

Materials and methods

(0.5M) was added incrementally till optically clear. After adding 100 μ l of PBS (x10), the FEFEFKFK was incubated at 80°C overnight. The precursor FEFEFKFK hydrogel was stored at 4°C. When needed the precursor FEFEFKFK gel was heated to 80°C for at least two hours, then cooled to 37°C in a water bath and then 250 μ l of E8 medium was added to the FEFEFKFK hydrogel by reverse pipetting. 50 μ l of the gel was then pipetted into the wells of 96 well plates, covered with 200 μ l of E8 and incubated overnight at 37°C and 5% CO₂. Previous work used the hydrogel at a depth of 100 μ l in a 96 well plate (Ashworth et al., 2020a) but it proved impossible to image hiPSCs on top of 100 μ l of FEFEFKFK hydrogel.

3.2.9 Size test of Cell Clusters

The most suitable size of hiPSC cluster to be cultured on top of the PA hydrogels was selected by culturing a range of cluster sizes on FEFEFKFK hydrogel (as detailed above). The clusters were created by the method previous mentioned, but the cell solution concentration varied, as shown in Table 9. 5-7 hiPSC clusters were placed on top of a FEFEFKFK coated well. Bright field images (Nikon Instruments Inc, USA) were taken the same day (day 0) they were placed on the wells and after 24 hours, until day 3. The cell concentration selected for further work was 2,000 cells per cluster. See Figure 31 and Figure 44 for a more detail of the protocol.

Peptide amphiphile scaffolds and human induced pluripotent stem cells

Materials and methods

Table 9. A table of the cell concentrations and droplet size to make a range of cell cluster sizes.

<i>Wanted cell number per cluster</i>	<i>Concentration (Cell/mL)</i>	<i>Droplet Volume (μl)</i>
750	50'000	15
1'000	50'000	20
1'500	100'000	15
2'000	100'000	20

3.2.10 Preparation of PA, FEFEFKFK, and Matrigel Hydrogels

The K2, K3, K4 PA hydrogels used the final trial ratio of 2.5:1 (PA: PBS) and E3 used the final ratio 2.3:1 (PA: CaCl₂). To maintain the sterilisation required for cell culture all PA powder was sterilised under UV light for an hour before being made into a hydrogel. For all culture on top of the gel there was a second hour of UV sterilisation once the gels were set. After which all PA gels were covered in E8 medium overnight at 37°C and 5% CO₂. Due to COVID and supervisor loss there were no measurement of the charges of the PAs and FEFEFKFK used to make the hydrogels.

Matrigel (Corning, UK) was used as the gold standard for hiPSC cluster culture. Ice cold Matrigel was used in a 1:1 mix with cold E8 medium due to limited supply of Matrigel (Ashworth et al., 2020b), only one batch of Matrigel was used for this study (356234, Corning). 100 μ l was then reverse pipetted into wells in a 96 well plate (Thermo Fisher, USA) and covered with 100 μ l of E8 medium overnight at 37°C and 5% CO₂. FEFEFKFK hydrogels were set as above.

Peptide amphiphile scaffolds and human induced pluripotent stem cells

Materials and methods

3.2.11 Culture of hiPSCs on top of PA, FEFEFKFK and Matrigel hydrogels

After hiPSC clusters had been made and all hydrogels had been cultured overnight at 37°C and 5% CO₂, the clusters were collected in E8 medium and 5-7 cluster were placed in each well on top of each gel. The E8 culture medium was replaced daily. On the final day of culture, live dead staining was completed, as previously described. The hiPSC clusters were imaged daily (bright field). See Figure 31 for a graphical overview of the protocol and Figure 47 for more detail.

3.2.12 Cross-sectional area of the hiPSC

To measure the cross-sectional area of the hiPSC clusters, the maximum and minimum radius was measured using Image J Fiji software (version 2.0.0-rc-69/1.52p) (Schindelin et al., 2012) and then entered into the formula for an oval area (Max Radius x Min Radius x Pi).

3.2.13 Distance from the hiPSC clusters to the furthest cell removed

For all hydrogels, the distance from the hiPSC clusters to the furthest cell removed from the cluster was measured. Three measurements were taken around each hiPSC cluster to measure the distance between the cluster and any cells that surrounded the cluster. These measurements were again taken on Image J Fiji (Schindelin et al., 2012).

3.2.14 Retention of clusters on hydrogel

The retention of the hiPSC clusters were calculated as a percentage for each hydrogel type and day of culture.

$$\left(\frac{\text{Number of clusters on day X}}{\text{number of clusters on day placed on hydrogel}} \right) \times 100.$$

Peptide amphiphile scaffolds and human induced pluripotent stem cells

Materials and methods

3.2.15 Immunostaining of PA gels

The wells selected for immunostaining were fixed with paraformaldehyde (polyscience, USA) at 4% w/v in PBS for 1 hour at room temperature (Ashworth et al., 2020b). The samples were then washed and stored in PBS at 4°C. Blocking buffer consisting of 0.1% Triton-X-100 (Gibco, USA), 0.5% bovine serum (Thermo Fisher, USA) and 10% goat serum (Thermo Fisher, USA) in PBS was added to samples for one hour. Primary antibodies/probes in blocking buffer were either anti-chondroitin sulphate (AB11570, Abcam, USA) (1:400), biotinylated hyaluronic acid binding protein (bHABP AMS.HKD-BC41 AMSBio, USA) (1:100) or anti-laminin (AB11575, Abcam, USA) (1:100). Both were incubated overnight at 4°C.

The samples were then washed with PBS three times and secondary antibody/labelled ligand in blocking buffer, was added. Either AF-488 goat anti-mouse IgG (A11029, Invitrogen) (1:100) and TRITC-Streptavidin (Stratech, UK) (1:100) with DAPI (D3571, Invitrogen, USA) (300nM) or AF-488 goat anti-mouse IgG and Phalloidin (F432/R415, Thermofisher, USA) (1:1000) with DAPI (300nM). The samples were then stored overnight at 4°C. Finally, the samples were washed in triplicate and then imaged using the laser scanning confocal microscope (Leica). Z-Stacks (~10µm) were taken of all imaged clusters though due to their size the confocal could not take a complete view of all clusters.

3.2.16 Statistics

The design of the experiment lends to a mixed ANOVA (a version of a repeated measure ANOVA) as there was two independent conditions, hydrogel type and day cultured, and the data was collected from the same samples (repeated). However, the poor retention of hiPSC clusters on some hydrogels meant there was missing data (cross-sectional area and measure

Peptide amphiphile scaffolds and human induced pluripotent stem cells

Materials and methods

of distance). If a mixed ANOVA was used, any hydrogels with missing data would have any previous measurements removed, this would have removed data from an already limited dataset.

Options to correct this could have been to replace the data with a multiple imputation. However, due to limited number of repeats and the fact that the missing data for some gels is considerable, multiple imputation would be inaccurate (Jakobsen et al., 2017, van Ginkel and Kroonenberg, 2014). The models used in multiple imputation can only predict what is known. There are several types of missing data: “Missing Completely At Random” data with no apparent cause due to the known data or unknown data, “Missing At Random” if the missing values depend upon known observed data and can be predicted or “Missing Not At Random” if the missing values due to data not measured, therefore the values cannot be replaced by a model. The observed data is the size of the cluster or a distance from a cluster. There is a bias within the data as K2 has a higher percentage of missing data, which may be due to growing on the K2 gel (observed value) but could be due to other factors listed above which were not seen within the observed data meaning the data is Missing Not At Random and cannot be taken through multiple imputation (van Ginkel and Kroonenberg, 2014, Jakobsen et al., 2017).

Another method to fill in the data would be to use an average (Jakobsen et al., 2017, van Ginkel and Kroonenberg, 2014). However, using an average was also unappealing as there were several extreme values found within the data and the limited repeats reduce any certainty that these extremes were true outliers, and the average was accurate.

Peptide amphiphile scaffolds and human induced pluripotent stem cells

Materials and methods

Considering this and with advice from a statistician, if the data was normal, MANOVAs were completed, and if there was a factor found to be significant the post hoc test Tukey HSD was used. If the data was not normal, then the non-parametric test Kruskal-Wallis test was used, if there was a significant factor the Bonferroni correction for multiple comparisons was used. Unlike a mixed ANOVA, both do not consider the compounded effect of both day and gel. Statistical significance was shown by * $p < 0.05$ and ** $p < 0.001$.

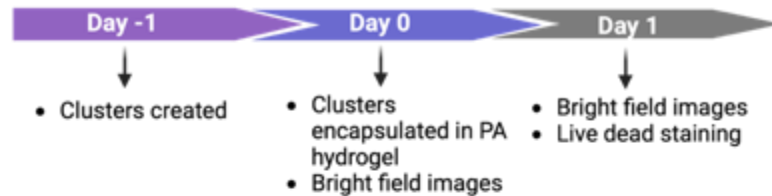
The number of repeats differed due to previously mentioned interruptions. When assessing the cytotoxicity of the PAs there was a variation in repeats. The nonaligned PA had $n = 3$ and the aligned $n = 1$. For each repeat there were up to 4 or 5 replicates each with 3 – 4 clusters in. Every cluster was imaged and categorised. The more complex assessment of cytotoxicity including additional controls (no CaCl_2 or medium) only had $n = 1$, with 5 replicates and 3 -4 clusters per replicate. All clusters were imaged and categorised. When assessing the optimum size of clusters for being placed on top of the hydrogel (FEFEFKFK) there was an $n = 3$, with 6 replicates per repeat and 5 – 7 clusters per replicate (on day 0). Every cluster on the hydrogel was imaged and measured.

The large experiment, comparing the size, retention and cell spread, the clusters on all hydrogels (K2, K3, K4, E3 and FEFEFKFK) had variable numbers of repeats. K2 had an $n = 3$ for day 0 - day 3 and an $n = 1$ for day 4. K3 and K4 had an $n = 4$ for day 0 – day 3 and $n = 2$ for day 4. FEFEFKFK had an $n = 3$ for day 0 - day 3 and an $n = 1$ for day 4. E3 and Matrigel had an $n = 2$. For each repeat there were three replicates and each replicate had 5 – 7 clusters (on day 0). All clusters remaining upon the hydrogel was imaged and assessed.

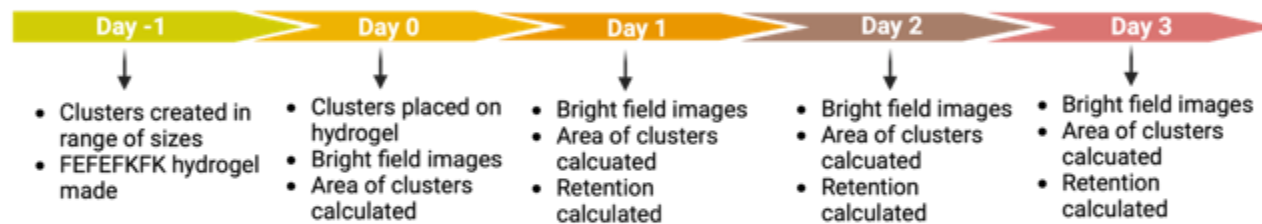
Peptide amphiphile scaffolds and human induced pluripotent stem cells

Materials and methods

Encapsulation of hiPSC clusters into PA hydrogel



Optimisation of hiPSC cluster size



HiPSC clusters cultured ontop of differently charged hydrogels

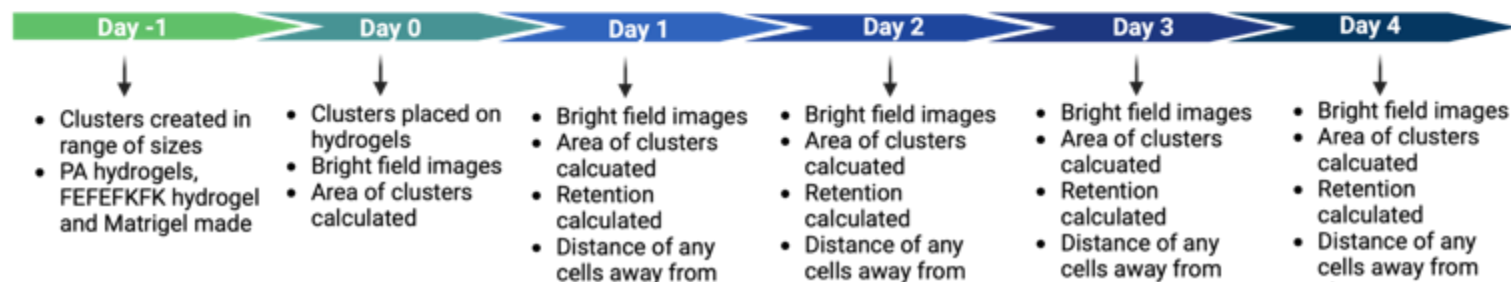


Figure 31. Overview of all protocols with hiPSC clusters.

A flow chart demonstrating the data collection of all experiments using hiPSC clusters. First is the encapsulation of the cluster in the E3 hydrogels. Second shows the optimisation of the hiPSC cluster size for culture above (2D culture) the FEFEFKFK hydrogel. Third, the clusters cultures upon the lysine PA hydrogels (K2, K3, K4), glutamic acid PA hydrogel (E3), FEFEFKFK hydrogel and Matrigel. Figure made in Biorender.

Peptide amphiphile scaffolds and human induced pluripotent stem cells

Hypothesis

3.3 Hypothesis

Peptide amphiphiles (PAs) are used to form hydrogels to provide culture environments for a variety of cell types (Hedegaard et al., 2020, Núria Marí-Buyé, 2013). PA hydrogels are applied in these settings as they replicate many of the properties of native ECM through their porosity, elasticity, and regulatable stiffness. Other benefits associated with the use of PA hydrogels for cell culture include their ability to form gels that incorporate ECM components such as fibronectin via ionic interactions formed between opposite charges engineered into the PAs and those of the ECM components (Hedegaard et al., 2018). The PAs themselves can be engineered to have a range of charges due to the specific residues from which they are made, and this work aimed to test the hypothesis that hydrogels with subtle differences in charge would interact with or 'capture' native ECM proteins and GAGs secreted by cells, thereby altering the cells' behaviour. If found to be the case, this system could be exploited to create a targeted selection of charged gels engineered to capture ECM proteins and GAGs tailored for specific cell culture applications. The captured proteins and GAGs will be a more complex mix than other systems where ECM components are exogenous (for example Chapter 2.). As the capture of ECM components proposed would capture a board range of the secreted proteins and GAGs and perhaps the capture of components that bind to already sequestered material, thereby creating a sequestered ECM.

The PAs used in this study included three PAs that would be positively charged when in solutions with a pH between 1 – 9 due to their increasing numbers of lysine (K) residues; (K2, K3, K4). One PA that would be negatively charged in solutions with a pH between 5 - 14, due to glutamic acid (E) residues, (E3). When at neutral pH or close to neutral pH the residues on both K and E3 PAs should be charged, previous work has found these PAs to have a positive charge (zeta potential) (Inostroza-Brito et al., 2015, Hedegaard et al., 2018) and E3 had a

Peptide amphiphile scaffolds and human induced pluripotent stem cells

Hypothesis

negative charge (Hedegaard et al., 2018). There was no assessment of these charges in this work.

The PAs used in this work are shown in Table 10 and Table 11. The PAs used all have the same basic structure; alkyl tail, β -sheet forming section and the hydrophilic head where the variation of charged residues are located (Table 10 and Table 11). These PA were selected as the positive charge upon the lysine PAs has been shown to ionically interact with negative charged ECM components when forming ECM containing hydrogels (Hedegaard et al., 2020, Hedegaard et al., 2018, Hartgerink et al., 2001). It was therefore expected that that positive charges would form electrostatic interactions with secreted native ECM components of negative charge, specifically GAGs. The increasing charge by the K PAs with increasing lysine residues provided an ability to assess whether the relative levels of charge impacts the capture of secreted native ECM components. The E3 PA with its negative charge was selected to assess if the opposite charge would capture different secreted native ECM, due to electrostatic repulsion.

To provide controls for the charged PAs, two hydrogels were used that were assumed to be neutral at physiological pH. One of these is an octapeptide hydrogel (FEFEFKFK) formed from alternating hydrophobic and hydrophilic residues, with both basic and acidic components that effectively balance each other out when close to pH 7. The peptide has been used extensively to support 3D *in vitro* culture of multiple cell types, including HCT116 colorectal cancer, MCF7 breast cancer cell lines, Patient-derived xenograft (PDX) cells from a triple negative breast cancer patient (BR8), mESCs and hiPSCs (Ashworth et al., 2020a, Ashworth et al., 2020b). In all these cell types cultured the FEFEFKFK hydrogel were able to grow and remain viable. The FEFEFKFK is a blank slate hydrogel that can be modified both with additional components (collagen) or stiffness alteration for a successful culture of a range of cell types. In addition,

Peptide amphiphile scaffolds and human induced pluripotent stem cells

Hypothesis

Matrigel was also used as it is widely used for many types of cell culture and is often described as the gold standard of a 3D *in vitro* matrix (Stock et al., 2016). An example of Matrigel usage is the long term culture (8 weeks) of hiPSCs differentiated into intestinal epithelial cells, the cells were able to proliferate, form organoids and maintained enzymatic activities to the same level as newly generated intestinal epithelial cells (Yoshida et al., 2020). Matrigel is comprised of many ECM proteins and glycans therefore can be used a condition with high levels of ECM components. These controls will provide a comparison been an assumed lack of ECM components in the neutrally charged hydrogel (FEFEFKFK) and high levels of ECM components in the Matrigel.

Peptide amphiphile scaffolds and human induced pluripotent stem cells

Hypothesis

Table 10. Description of peptides showing amino acid sequence, molecular formulae, and mass.

<i>Peptide</i>	<i>Sequence</i>	<i>Molecular Formula</i>	<i>Molecular Weight (g/mol)</i>
<i>K2</i>	C ₁₆ –VVVAAA-KK	C ₅₂ H ₉₉ N ₁₁ O ₉	1022.41
<i>K3</i>	C ₁₆ –VVVAAA-KKK	C ₅₈ H ₁₁₁ N ₁₃ O ₁₀	1150.58
<i>K4</i>	C ₁₆ –VVVAAA-KKKK	C ₆₄ H ₁₂₃ N ₁₅ O ₁₁	1278.75
<i>E3</i>	C ₁₆ –VVVAAA-EEE	C ₅₅ H ₉₆ N ₁₀ O ₁₆	1153.40
<i>FEFEFKFK</i>	FEFEFKFK	C ₅₈ H ₇₆ N ₁₀ O ₁₃	1121.28

Peptide amphiphile scaffolds and human induced pluripotent stem cells

Hypothesis

Table 11. Graphical representation of the peptides used, highlighting their structure and key features.

Denoted by the colour are defining features in the peptides. The carbon chain (yellow), β -sheet forming section (green), Lysine (K) residue basic (blue), Glutamic Acid (E) residues acidic (orange), Hydrophobic section (red), Hydrophilic section (purple).

Peptide	Structure
K2	
K3	
K4	
E3	
FEFEFKFK	

Results

3.4 Results

3.4.1 Optimisation of cell clusters encapsulated in E3 hydrogels

The K PAs have previously been used to create hydrogels when combined with other proteins, for example keratin (Hedegaard et al., 2018, Hedegaard et al., 2020, Capito et al., 2008). These have been used for cell encapsulation when mixed with another protein (Inostroza-Brito et al., 2015). Cells cannot be encapsulated directly in the K2, K3 and K4 PAs as the positive charge associated with the PAs is toxic to the cells (Newcomb et al., 2014). The presence of cationic residues in hydrogels has been used to form antibiotic scaffolds (Chang et al., 2017); the positive charge interacts with the bacterial cell membrane which is negatively charged due to the presence of peptidoglycans (Gupta et al., 2013, Åmand et al., 2012). Due to this well-known effect, the positively charged PAs used here were not applied to encapsulation of hiPSC clusters.

Experimental design

The E3 PA has previously been applied to the culture of MSCs where gelation of E3 hydrogels was triggered by the addition of CaCl_2 (Zhang et al., 2010). Therefore, an experiment was conducted to optimise the encapsulation of hiPSCs in E3 hydrogels to support maximum viability. The cell clusters were encapsulated in 1% E3 which was either kept at 37°C (non-aligned) or heated to 80°C then cooled to 37°C (aligned) before being introduced to the cells. In both cases, gelation was triggered using a range of CaCl_2 concentrations. The heat treatment changes the conformation of the E3 PA nanofibers, aligning them (Zhang et al., 2010). We anticipated that this could impact the behaviour of the encapsulated cells therefore, we tested both the aligned and non-aligned E3 hydrogel.

Peptide amphiphile scaffolds and human induced pluripotent stem cells

Results

The E3 hydrogels were created using 10 μ l droplets of E3, using CaCl₂ concentrations (one as used previously (10mM) (Beniash et al., 2005) and two other concentrations (15mM, 20mM), (Figure 32B, Table 12). Gelation was triggered in the E3 droplet hydrogels by addition of CaCl₂ swirled through the droplet, as demonstrated in Figure 32B. The CaCl₂ concentrations listed in Table 12 show the CaCl₂ concentration when added to the droplet and the concentration once medium was added for 24-hour culture. The flow chart in Figure 32A shows the experimental plan.

Peptide amphiphile scaffolds and human induced pluripotent stem cells

Results

A

Day -1	Day 0	Day 1
<ul style="list-style-type: none"> • Hanging droplets used to make hiPSC Clusters 	<ul style="list-style-type: none"> • E3 PA solution made <ul style="list-style-type: none"> • Non-aligned • Aligned • hiPSC clusters and E3 solution pipetted into 10ul droplets • Hydrogels set with one of the three concentrations of CaCl_2 and imaged • 30 minutes later 250ul medium was added to each well 	<ul style="list-style-type: none"> • Clusters cultured for 24 hours and imaged

B

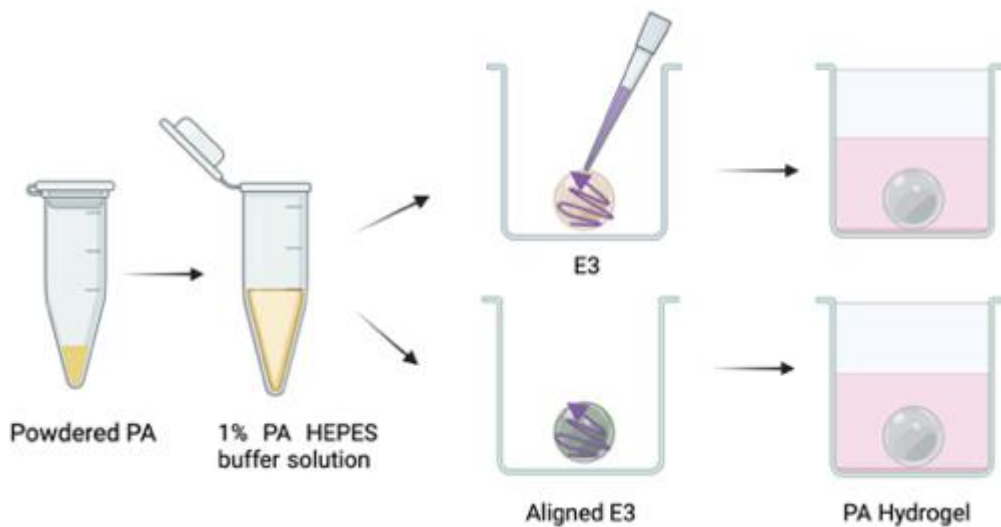


Figure 32. The experimental composition for the optimisation of hiPSC cluster viability when encapsulated in E3 droplet hydrogels.

A A Flow chart of the experimental plan. **B** A graphical representation of the procedure to make the E3 droplets. The E3 can be non-aligned (yellow) or aligned through heating to 80°C and cooled (green), gelled with CaCl_2 in a range of concentrations (purple). After 30 minutes the clusters were imaged and covered with medium (pink). After 24 hours the encapsulated clusters were imaged again. Figure made in Biorender.

Peptide amphiphile scaffolds and human induced pluripotent stem cells

Results

Table 12. The CaCl₂ concentrations in the 10 μ l droplets and once 250 μ l medium was added for overnight culture.

CaCl ₂ Concentration	
Droplets	Filled well
20mM	0.8mM
15mM	0.6mM
10mM	0.4mM

Phenotypic characterisation

The hiPSC clusters encapsulated were then categorised into one of three phenotypes on the day of encapsulation (day 0) and day 1. The representative images in

Figure 33B showed a clear difference between these phenotypes. Phenotype 1 displayed a flat cell cluster where the individual cells were visible and the cells within the cluster were more optically bright. Phenotype 2 displayed a well-defined raised central cluster surrounded by individual cells that were flat and optically bright. Phenotype 3 is a more intermediate phenotype, that showed optically bright cells on the periphery of the cultures, but without single cells being clearly visible. In these, there was no clear raised inner cluster, and the centre was optically dark (

Figure 33A and B).

To assess the viability of the hiPSCs, live dead staining was completed on day 1. Phenotype 1 clusters were found to be comprised of dead cells while phenotype 2 had a central core of living cells in the well-defined raised area while the edges were comprised of dead cells (Figure 34). It was impossible to determine the viability of phenotype 3 as there were almost no clusters of this type 3 on day 1.

Peptide amphiphile scaffolds and human induced pluripotent stem cells

Results

A

Phenotype	Categorisation Characteristics
1	<ul style="list-style-type: none"> • Single cells were visible • Cell cluster appeared to be flatter • The cells were optically bright
2	<ul style="list-style-type: none"> • Single cells within the centre of the clusters were not individually visible but it was a well-defined raised area • An area of disseminated cells surrounding the cluster • The outer cells were also flatter and optically bright
3	<ul style="list-style-type: none"> • Lighter and flatter cells on the edge of the cluster • Less optically bright in the centre • No well-defined raised central cluster

B

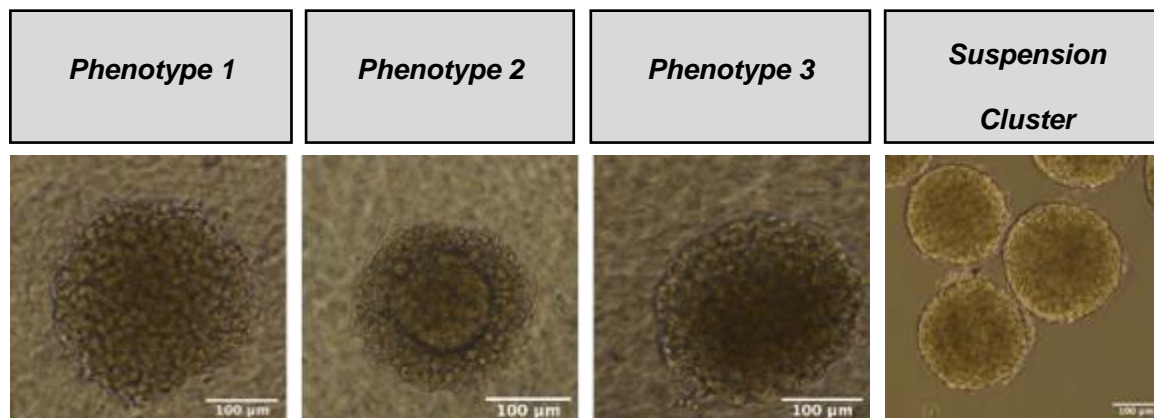


Figure 33. Categorisation of hiPSC Clusters.

A A table detailing the characteristics of each phenotype. **B** Representative images highlighting differences between phenotype 1, 2 and 3. Phenotype images taken in aligned E3 droplets with concentration 15mM over day 0 (30 minutes after encapsulation) and day 1. Cluster in suspension taken day 0. All scale bars = 100µm.

Results

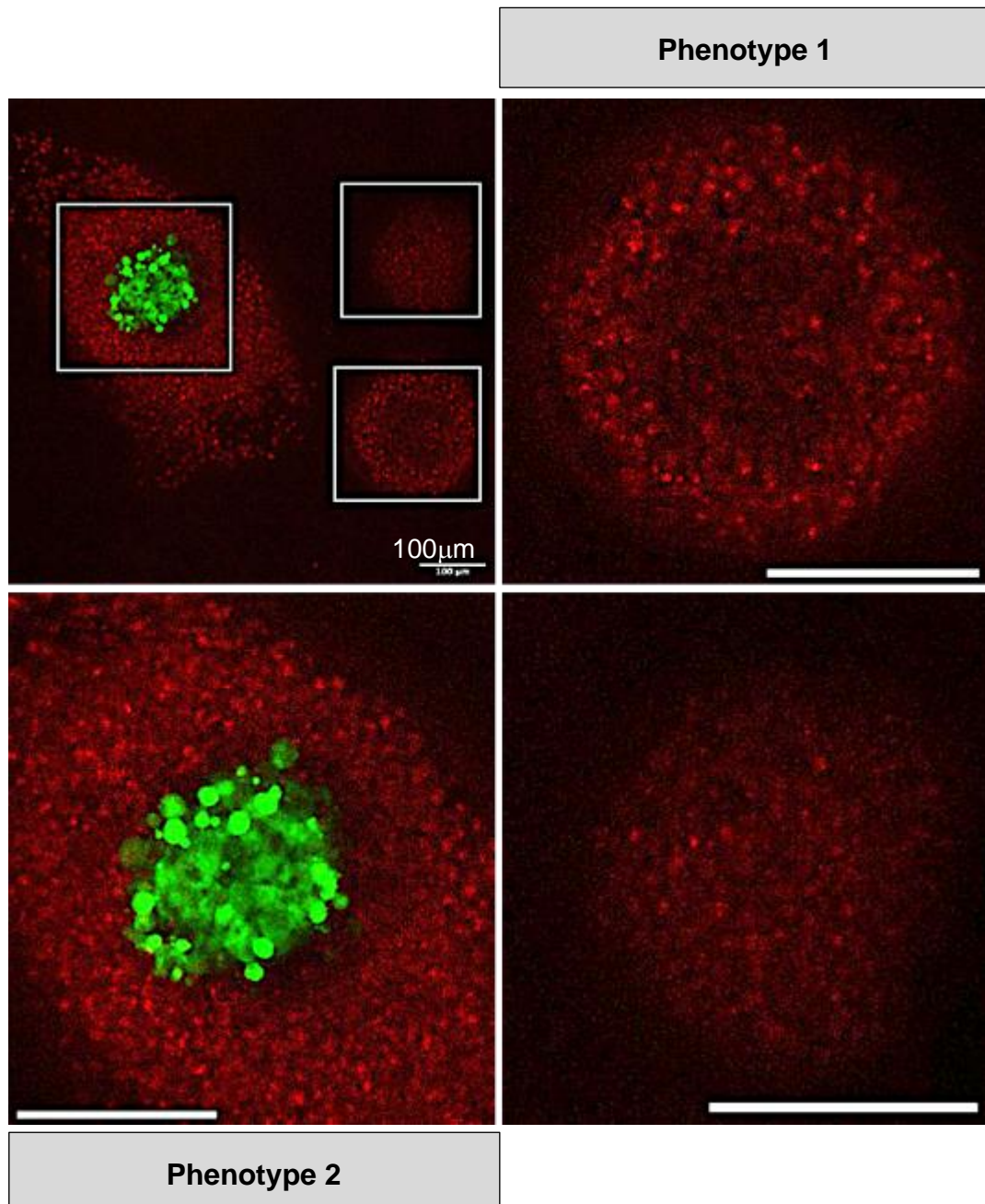


Figure 34. Cell viability in phenotype1 and 2 clusters. Viability (live/dead) staining of cell clusters in nonaligned E3 with CaCl_2 concentration 10mM on day 1. Clusters stained with Calcein AM and Ethidium Homodimer demonstrating the cell death in phenotype 1 and the outer dead cells and centre of live cells in phenotype 2. Scale bars 100µm.

Peptide amphiphile scaffolds and human induced pluripotent stem cells

Results

Phenotype prevalence per condition, day 0

The heatmaps shown in Figure 35 display the percentage of hiPSC clusters characterised as each phenotype per E3 type and CaCl₂ concentration. The number of hiPSC clusters imaged varied as more biological repeats were performed for the non-aligned E3 solution. There was also a decrease in the number of hiPSC clusters categorised on day 1 compared to day 0 as the hydrogel droplets could be damaged if the addition of medium was too aggressive (Figure 34). The CaCl₂ concentrations are shown in Table 12.

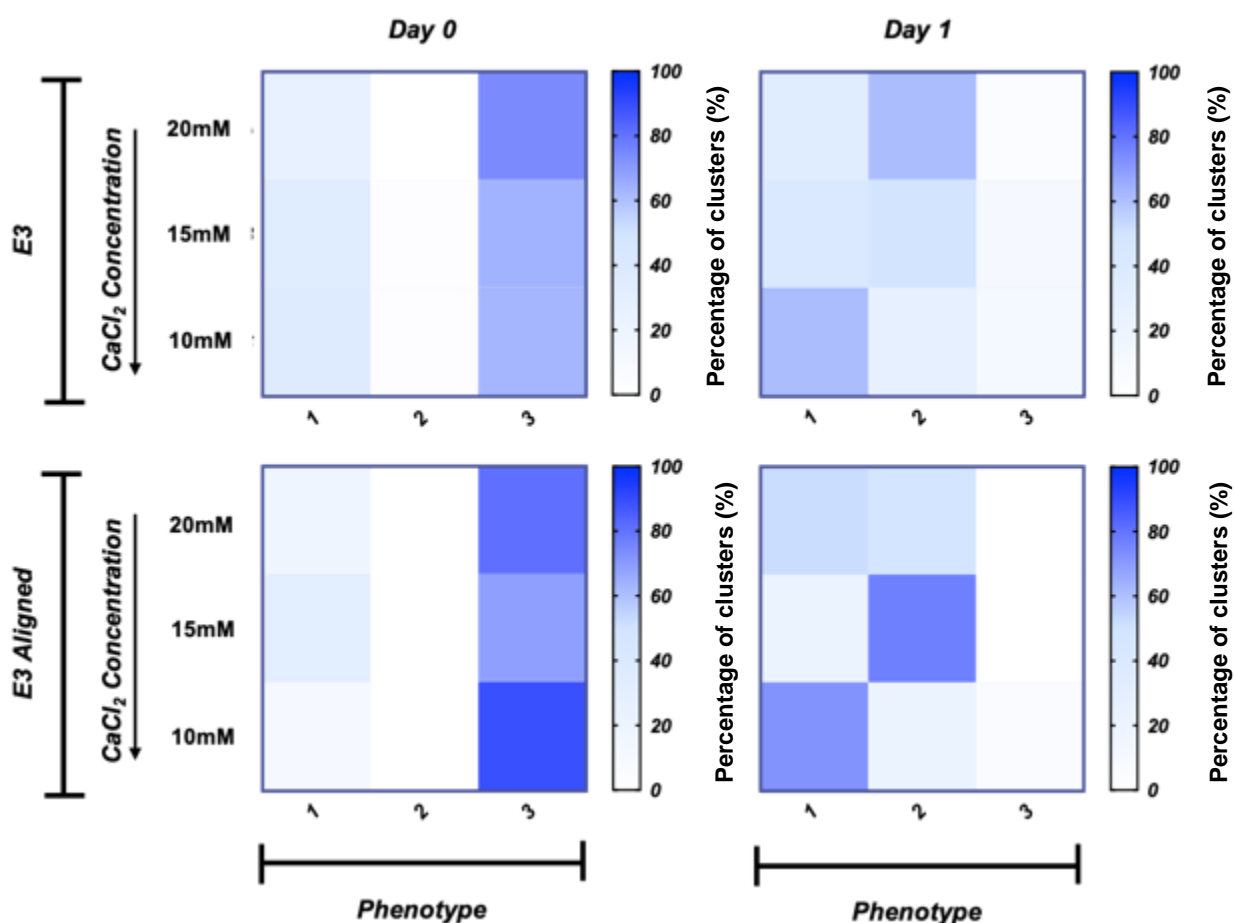
In both E3 solutions on day 0, there was a high percentage of hiPSC clusters categorised as phenotype 3, but almost none found on day 1, suggesting that phenotype 3 was transient (Figure 35). As mentioned, phenotype 3 shared characteristics with both other phenotypes (Figure 33); it could therefore be the intermediate between phenotype 2 with living cells and the dead cells found in phenotype 1. The clusters assigned phenotype 3 on day 0 may be the clusters that will go on to be categorised as phenotype 2 on day 1. This conclusion may also explain why there were no clusters categorised as phenotype 3 on day 1 (Figure 35).

The non-aligned E3 droplet hydrogels on day 0 had around 40% of clusters assigned as phenotype 1 (Figure 35), and therefore dead (Figure 34). There was only an extremely slight difference in the percentage of hiPSC clusters characterised as phenotype 1 between the concentrations of CaCl₂ in the non-aligned E3 droplets on day 0 (Figure 35). This suggested that at all tested concentrations of CaCl₂ (Table 12) the conditions were toxic to the cell clusters immediately (within 30 minutes) during gelation. This toxicity may not have been due to CaCl₂. There was also a higher percentage of hiPSC clusters categorised as phenotype 3 in the aligned E3 than non-aligned on day 0 (Figure 35), suggesting a less toxic environment in these gels immediately after gelation.

Peptide amphiphile scaffolds and human induced pluripotent stem cells

Results

A



B

		Non-aligned E3			Aligned E3		
		CaCl ₂ (mM)	20	15	10	20	15
Day	0	74	74	75	18	22	21
	1	62	53	46	18	13	10

Figure 35. Optimisation of hiPSCs viability when encapsulated in E3 hydrogels. The E3 PA was either non-aligned (n=3) or aligned E3 (n=1). **A** The heatmaps showing the percentages of each phenotype for each CaCl₂ concentration (20mM, 15mM and 10mM). The phenotype1 was shown in Figure 34 to be comprised of dead cells, while phenotype 2 showed live cells. The darker the shade of blue the higher the percentage of hiPSC clusters categorised as the indicated phenotype. In day 0 both non-aligned and aligned E3 were categorised as phenotype 3 independent of CaCl₂ concentration. On day 1, the 10mM concentration had more clusters identified as phenotype 1 and therefore dead. The CaCl₂ concentration with the highest percentage of clusters categorised as phenotype 2 (most viable phenotype) differed between aligned (15mM) and non-aligned E3 (20mM). Created in SPSS. **B** The number of clusters imaged and categorised.

Peptide amphiphile scaffolds and human induced pluripotent stem cells

Results

Phenotype prevalence per condition, day 1

The non-aligned E3 hydrogel droplets on day 1 showed a greater percentage of hiPSC clusters categorised as phenotype 2, with the highest CaCl_2 concentration (20mM). As phenotype 2 has the highest viability (Figure 34), this suggested that concentration 20mM in the non-aligned E3 hydrogels was the least toxic condition. The non-aligned E3 hydrogel had the lowest concentration of CaCl_2 was used for gelation (10mM) and was seen to have the greatest percentage of cell clusters within phenotype 1 (Figure 35). This indicated that an increased CaCl_2 concentration was required for reduced toxicity of the hydrogels.

The hiPSC clusters encapsulated in the aligned E3 hydrogel droplets also showed a reduction in viability when the CaCl_2 concentration was low (concentration 10mM), as ~70% of the hiPSC clusters were characterised as phenotype 1. However, the highest concentration of CaCl_2 did not produce the highest level of viability, with this observed for the intermediate concentration (15mM) (Figure 35). This therefore suggests that when using the aligned E3, there was some toxicity from the CaCl_2 . The data for the aligned E3 was gathered from only one experiment but may indicate a difference in optimum hydrogel conditions between the aligned and non-aligned E3 hydrogels. This experiment would need to be repeated multiple times to draw strong conclusions.

Peptide amphiphile scaffolds and human induced pluripotent stem cells

Results

Expanded experimental design

As the lower concentrations of CaCl_2 in both E3 and aligned E3 were associated with increased toxicity (Figure 35), there was a suggestion that the toxicity was from the PAs themselves, rather than the CaCl_2 . As E3 has been used to encapsulate other cell types without toxicity (Redondo-Gómez et al., 2019, Zhang et al., 2010), this required further investigation. Therefore, an expanded experiment was conducted, as shown in Figure 36. This allowed the assessment of both E3 groups independent of CaCl_2 . This would prevent the gelling of the E3 solution, but it would allow for an assessment of toxicity of E3 and aligned E3 in solution (Table 13). To assess the effect of CaCl_2 there was an additional group of hiPSC clusters were suspended in medium droplets to which specific CaCl_2 concentrations were added.

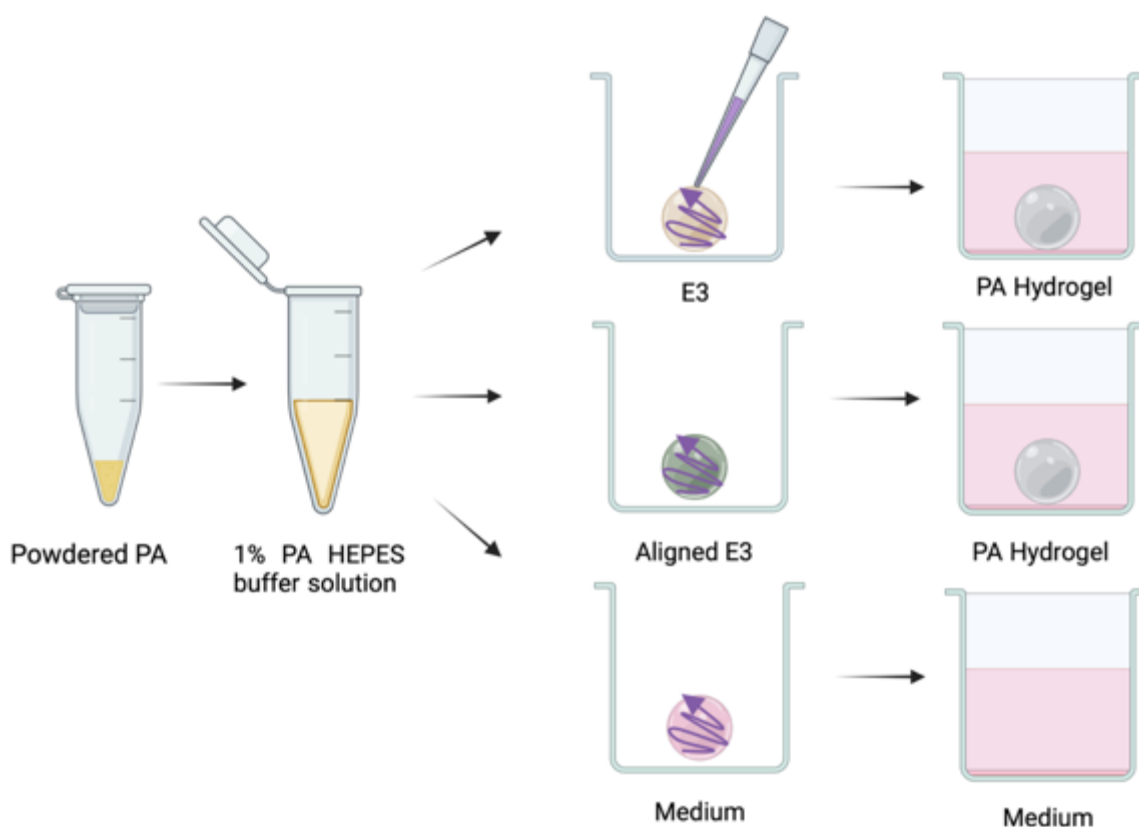


Figure 36. The protocol for further optimisation of E3 hiPSC cluster encapsulation. A daigramatic representation displaying the alterations to the experimental setup (n=1). The hiPSC clusters were in non-aligned E3 solutions (yellow), aligned E3 solution (green) and medium droplets (pink) to which a range of CaCl_2 concentrations (purple) were added. Figure made in Biorender.

Peptide amphiphile scaffolds and human induced pluripotent stem cells

Results

Table 13. The CaCl₂ concentrations used.

The concentration shown includes, first in the 10 μ l droplet of E3 PA solution and then when medium was added for overnight culture.

CaCl ₂ Concentrations	
Droplets	Filled well
20mM	0.8mM
15mM	0.6mM
10mM	0.4mM
0mM	0mM

Phenotype prevalence per condition

It became very clear that there was a toxic affect from the E3 (both aligned and non-aligned) when the cell clusters were in the E3 PA solution, as shown in Figure 37 (CaCl₂ concentration 0mM). When no CaCl₂ was added to the non-aligned E3 100% of imaged hiPSC clusters were categorised as phenotype 1 and therefore dead (Figure 37). Approximately ~80% of hiPSC clusters were categorised as phenotype 1 in the aligned E3 solution with no CaCl₂, suggesting that the change in alignment generated a solution that was still toxic, but to a lesser degree. The aligned E3 hydrogel droplets also differed to the non-aligned in that even without the addition of CaCl₂, the aligned E3 hydrogels were able to form a more self-supporting gel-like structure though it was more easily broken than the hydrogels formed by the addition of CaCl₂ (observation, no data supplied). This suggests that the toxicity may be due to the availability of the PA to the cell membrane as the aligned PAs form bundles while in solution not the micelles as found in the non-aligned (Zhang et al., 2010), therefore fewer individual PAs may have been able to interact with the cell membrane. This difference in pre-gelled structures may also cause the reduction in the time taken to gel.

Peptide amphiphile scaffolds and human induced pluripotent stem cells

Results

This expanded experiment (Figure 37) showed the same trend in the optimum CaCl_2 concentrations as previously (Figure 35); non-aligned E3 hydrogels had the optimal cell viability with the most concentrated CaCl_2 solution (concentration 20mM) and the aligned E3 hydrogels had the best cell viability with the intermediate concentration (concentration 15mM). This validates the previous results and increases the number of repeats for the aligned E3 (to an n of 2). The lowest concentration of CaCl_2 was found to be the most toxic, this could be due to the increase observed in the time taken for gelation, which allowed E3 to remain a solution in contact with the cells. Additionally, as the aligned E3 hydrogels underwent more rapid gelation, the intermediate concentration was sufficient for gelation without an excess of CaCl_2 that may be present when setting with concentration 20mM.

To test for the impact of increased CaCl_2 concentration alone, the hiPSC clusters were cultured in medium droplets to which were added a range of CaCl_2 concentrations for 30 minutes. After this, the dishes were filled with medium for overnight culture. As this was a suspension culture, the hiPSC clusters adhered together overnight, limiting the number of clusters that could be counted on day 1. The viability of the hiPSC clusters maintained in suspension culture, as measured by percentage categorised as phenotype 2, was higher than in any E3 hydrogels across all the concentrations of CaCl_2 tested on day 0, as shown in Figure 37. Therefore, there was no immediate negative effect of exposure to increased CaCl_2 . However, on day 1 there was a very slight decrease in the number hiPSC clusters categorised as phenotype 2 as the concentration of CaCl_2 increased. Therefore, the CaCl_2 concentration may have a slight toxic effect on the hiPSC clusters independent to any toxic effect from the E3 solution.

Peptide amphiphile scaffolds and human induced pluripotent stem cells

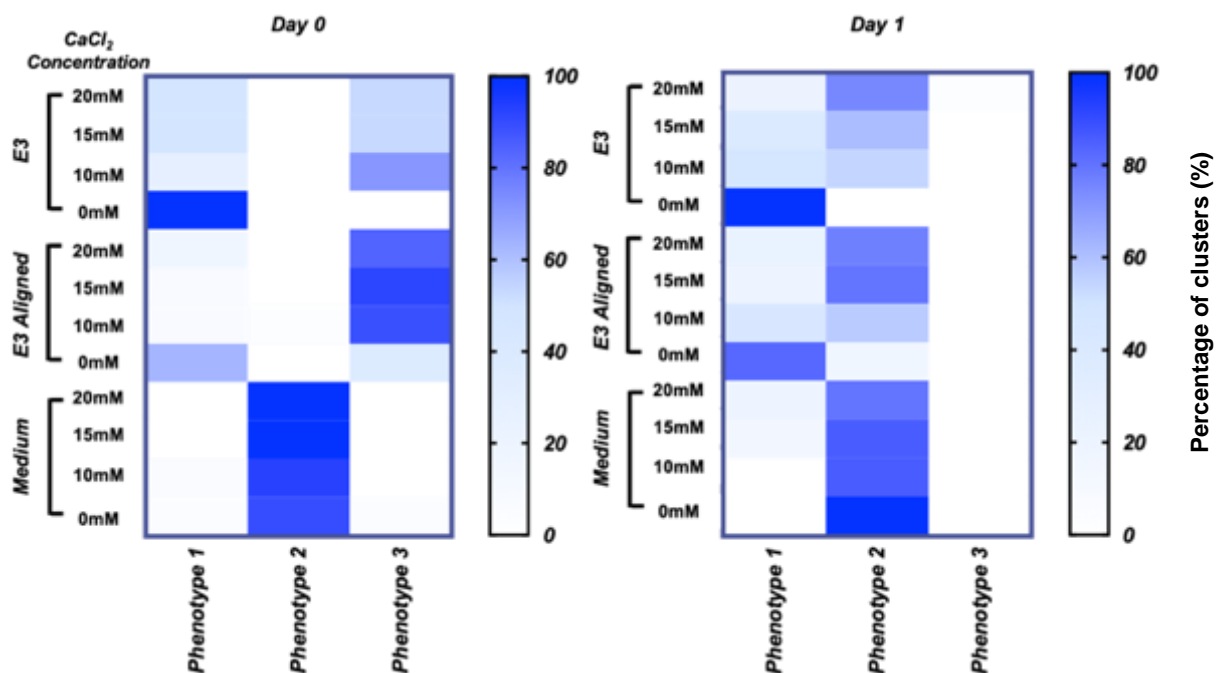
Results

However, it should be noted that the conditions tested in these limited experiments (Figure 35 and Figure 37) were not wide-ranging enough to find truly optimum conditions where the hiPSC clusters were able to be confidently cultured in E3 hydrogels. Even in the least toxic conditions, with the higher percentage of phenotype 2 hiPSC clusters, the clusters were still surrounded by dead cells. As the hiPSC clusters were already damaged, any conclusions based on the use of these should be approached with caution. It is possible that observed outcomes could be due to the degradation of the samples caused from the encapsulation method rather than by the experiments as designed. If time and access to labs during the pandemic had allowed, I would have continued optimisation to define an ideal encapsulation method, which would have been used to assess if encapsulation in E3 allowed for differential capture of ECM proteins and glycans, due to charge, rather than culturing the cell clusters on top of the E3 hydrogel. It was therefore clear that further experiments would not include the encapsulation of hiPSC clusters in E3.

Peptide amphiphile scaffolds and human induced pluripotent stem cells

Results

A



B

		Non-aligned E3				Aligned E3				Medium				
		CaCl ₂ (mM)	20	15	10	0	20	15	10	0	20	15	10	0
Day	0		30	17	24	20	19	24	30	12	36	10	14	25
	1		26	16	23	20	17	5	26	8	5	7	7	8

Figure 37. Further optimisation of hiPSCs viability.

A Heat maps displaying the percentage cell clusters found in each phenotype (as detailed in

Figure 33) per condition and CaCl₂ concentration. Phenotype 1 has been found to be dead cells, while phenotype 2 contain living cells (Figure 34). The darker the shade the higher the percentage of clusters categorised as a specific phenotype. On day 0 the only clusters in phenotype 2 are those in medium. On day 1 there was a slight reduction of clusters identified as phenotype 2 in medium when CaCl₂ concentrations were 20mM. When encapsulated in E3 without CaCl₂ there was a sharp increase in clusters identified as phenotype 1 (therefore dead). The optimum concentration for clusters to be categorised as phenotype 2 remained as those seen in Figure 35. Created by SPSS. **B** The number of clusters counted for each category. N = 1.

Peptide amphiphile scaffolds and human induced pluripotent stem cells

Results

3.4.2 Optimization of PA hydrogels for 2D culture

The K PAs were selected as their net charge should have been positive when in solutions with a pH range of 1 – 9. The net charge was assumed to be positive during all described work here as the pH was held close to 7. The charge upon the PAs could provide electrostatic interactions with secreted native ECM proteins and glycans that were negatively charged, thereby using the hydrogels' physical characteristics to capture ECM proteins. The series of K PAs have an increasing charge, provided hydrogels to assess the effect the strength of charge had upon the capture of native ECM components. The E3 PA was selected as it has a negative net charge between the pH values of 5 – 14. A hydrogel with a negative net charge provides an assessment of whether the capture of native ECM components was different.

Specifications for PA hydrogels

All experiments had to be conducted using the hydrogels as a coating for 2D hiPSC cluster culture, due to the toxic effect of both the K PAs (Newcomb et al., 2014) and E3 PA in 3D hiPSC culture (see section 3.4 , page 142). The specifications for the hydrogels included both physical characteristics and technical specifications for production, as seen (Figure 38). Due to the COVID-19 restrictions in place at the time these experiments were carried out, there were limited spaces and time within the laboratory to use the equipment, and therefore the maximum workable time for the PAs to form a hydrogel was an hour.

Other PA hydrogels have been formed into a range of shapes including noodles and spheres (Hedegaard et al., 2018, Zhang et al., 2010). We were keen to continue using hiPSC clusters rather than individual cells as previous work has demonstrated a clear benefit for cell viability in allowing the cells to remain as small clusters (Pakzad et al., 2010, Pijuan-Galitó et al., 2016). Due to the use of clusters, we coated the entire base of a well with hydrogel, enabling an

Peptide amphiphile scaffolds and human induced pluripotent stem cells

Results

average of 6 clusters to be placed in each well. In addition, we found that a depression in the surface on the well was optimal to keep the hiPSC clusters in a more central position in the well which removed any effect of the well walls on the hydrogel and improved imaging (Figure 38).

For culture over several days the hydrogel needs to endure the physical stresses of daily medium changes without disintegrating or undergoing severe deformation. If the hydrogel is unable to withstand this, then the hiPSC clusters will be lost during culture and this would not therefore be a reliable culture method.

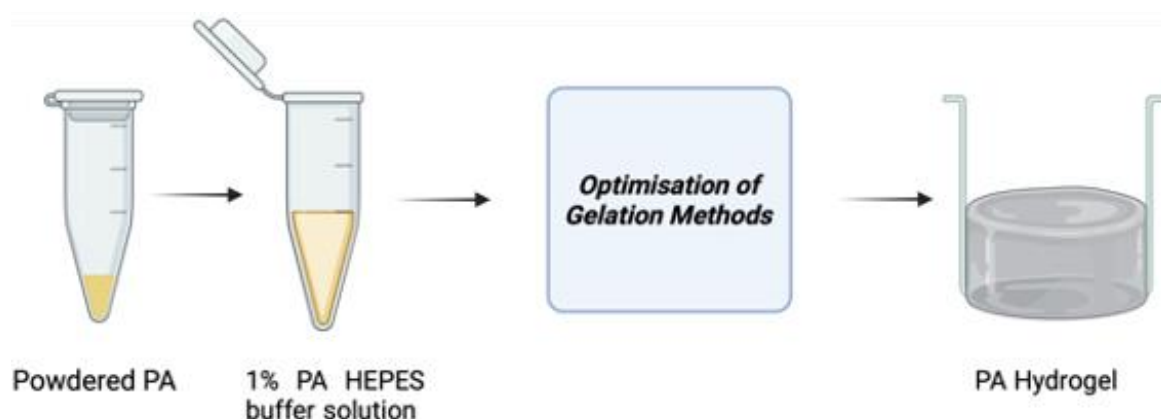
Peptide amphiphile scaffolds and human induced pluripotent stem cells

Results

A

Specifications for the hydrogels:

1. PA hydrogel formed within the hour
2. Self-supporting
3. Entire volume of PA gelled
4. Complete coverage of the well.
5. Slight dip within well to allow for cell cultures to keep to the centre of well.
6. Retains shape during medium changes.



B

Figure 38. Specifications for the creation of the PA hydrogels.

A List of the physical and technical specifications the hydrogels need to fill. **B** A graphical representation of the process used to produce the hydrogels. Powdered PAs are weighted and then made into a 1% solution with the addition of HEPES buffer. The optimisation of the gelation methods, through the trial of differing ratios of PA and gelator and the method of mixing these solutions. The gelator was dependent on the PA, with the K PAs being gelled by the addition of PBS and the E3 PA gelled through the addition of CaCl_2 . The gelled PA hydrogel (in grey) is a representation of the desired shape in a 96 well plate. The hydrogel completely fills the well and there is a slight depression at the centre of the hydrogel (darker grey) to allow for a more central placement of the cell clusters. Figure made in Biorender.

The K and E3 PAs differ in their method of gelation; the positively charged PAs are mixed with salts (PBS x10) and the negative PA was mixed with CaCl_2 . Optimisation of the formulation for each group of PAs was performed to make sure they had all the specifications mentioned. Optimisation of the K-series PAs was conducted upon K3 alone as stocks of the other PAs were critically limiting at the time.

Peptide amphiphile scaffolds and human induced pluripotent stem cells

Results

3.4.3 Optimisation K PAs

Formulations of K PA hydrogels

The first formulation tested was that where the PA charges of K3 were screened by the addition of sodium hydroxide thereby stimulating the formation of PA nanofibers (Xu et al., 2010a). However, as shown in Table 14, although a hydrogel was formed, there were several limitations, and it was unable to fit the specifications required. The point at which gelation occurred was extremely hard to identify and often resulted in the addition of excess sodium hydroxide and breakage of the hydrogel. Second, due to the small volumes of sodium hydroxide required it could not be dispersed throughout the entire volume of the PA solution, and gelation occurred non-homogenously. The gelled areas of the PA solution were then broken while more sodium hydroxide was added to try and achieve full gelation, as the dropwise method required repeated insertions into the hydrogel. A broken hydrogel is shown in Figure 39C, where the opaque sections are those where the hydrogel has been broken. Once broken these PA hydrogels do not reform.

The next formulation tested the current formulation used within the laboratory group to make small 10 μ l droplets. Instead of requiring the use of sodium hydroxide, gelation was triggered through the addition of x10 PBS. The salts screen the charges of the K3 PA and trigger formation of nanofibres. Gelation occurred in a 37 $^{\circ}$ C incubator, but this formulation did not meet the specifications as gelation took longer than an hour (Table 14). Next, the ratio of K3 solution to PBS was altered from 3:1 to 2:1 (formulation 2). This reduction allowed for a greater concentration of salts from the PBS to interact with the PAs, thereby allowing faster formation of nanofibres. Using this adaptation, gelation was complete in 25 minutes (Table 14). However, this formulation did not provide the depression required to keep the cell clusters localised, and this was suspected to be due to the total volume used to create the hydrogel. Therefore, this was tested (formulation 3), maintaining the ratio between PA and PBS at 2:1

Peptide amphiphile scaffolds and human induced pluripotent stem cells

Results

but reducing the total volume to 105 μ l. The formulation 3 hydrogel, showed gelation within the required time frame, completely filled the well, had no remaining PA in solution and had the required central depression. As a further test, the hydrogel was covered in medium (E8) that would be used for culturing the cell clusters. The hydrogel broke apart and deformed when the medium was changed. Therefore, the a final modification was tested (formulation 4) with a slight increase in the PA from a ratio of 2:1 (K3 solution: PBS) to 2.5:1, as previously the increase in salts has resulted in stronger hydrogels (Stendahl et al., 2006). This was selected as the final formulation that would be used for all the positively charged PAs (K2, K3 and K4), as it met the specific requirements list in Figure 38.

Mixing technique for producing the K PA hydrogels

The protocol used here was to swirl the solution being added from the bottom of the well to the top making sure to move through the centre of the well to prevent the formation of a hole. The swirl was the preferred method to mix the PA and PBS solutions as it better mixed the two solutions while not disturbing any of the nanofibres that had begun to form. When insufficiently mixed, small PA droplets can form, surrounded by remaining PA solution. In addition, any attempt to manually mix both solutions by pipetting fragments any of the nanofibres formed. The order of addition of the PA solution and PBS to the well to create the hydrogels determined the physical characteristics of the hydrogels (Figure 39A).

As listed in Figure 39 when the PA solution is swirled into the PBS solution, the hydrogel fragments as there is less capacity to swirl the PA solution into the PBS without the pipette tip moving through forming nanofibres. The small volume of PBS resulted in spheres of hydrogel forming surrounded by PA solution (Figure 39), which does not comply with the specification (Figure 38). When the PBS was added to the PA solution it was much easier to successfully

Peptide amphiphile scaffolds and human induced pluripotent stem cells

Results

swirl the PBS without fragmenting the hydrogel (Figure 39). Therefore, going forward all the positively charged PA hydrogels were formed by adding the PBS to the PA solution (Figure 42).

Peptide amphiphile scaffolds and human induced pluripotent stem cells

Results

Table 14. Observations of K3 formulations.

Conditions tested and observations made during optimisation. All tested on K3 1% gel, n = 3.

	<i>Mixture (μl)</i>			<i>Ratio</i>	<i>Observations</i>
	<i>PA-K3</i>	<i>PBS (x10)</i>	<i>NaOH (0.5M)</i>		
Standard protocol	100	-	Drop wise (~4)	-	<ul style="list-style-type: none"> • Self-supporting hydrogel forms but hard to clearly see the hydrogel/liquid interface • Small volume of NaOH added and therefore not dispersed evenly throughout the gel • Method produced gels that were broken due to pipetting action
Formulation 1	90	30	-	3:1	<ul style="list-style-type: none"> • Method based on that used for creating small gel droplets • Gelation occurred gradually, over 1 hour + • Failed to achieve the required characteristic of gelation in 1 hour
Formulation 2	100	50	-	2:1	<ul style="list-style-type: none"> • Self-supporting hydrogel formed in 25 minutes at 37°C • Volume required meant that the central depression required to hold the cell clusters in place was lost • Reduced volume attempted in Formulation 3
Formulation 3	75	30	-	2:1	<ul style="list-style-type: none"> • Self-supporting hydrogel formed with the required central depression • Gel was very weak and easily damaged during medium changes
Formulation 4	70	35	-	2.5:1	<ul style="list-style-type: none"> • Self-supporting gel with a central depression formed within 25 minutes • Gel stable during medium changes • Formulation selected for further work on all PA gels containing lysine (K2, K3, K4)

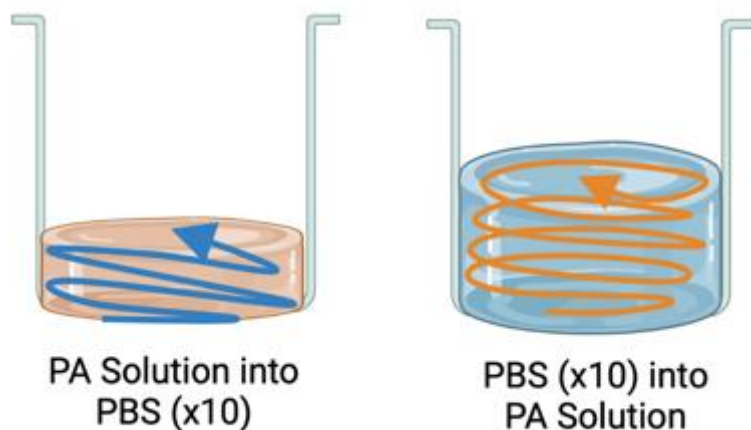
Peptide amphiphile scaffolds and human induced pluripotent stem cells

Results

A

<i>Order of additions</i>	<i>Observations</i>
PA Solution into PBS (x10)	<ul style="list-style-type: none"> • For all ratios, tended to form a broken, disrupted hydrogel • Small volume of PBS caused the pipette tip to break the hydrogel • Hard to create a level gel, if a constant swirl of PA not achieved this tended to create a spherical gel
PSB (x10) into PA Solution	<ul style="list-style-type: none"> • Much easier to swirl the PBS (x10) into the larger volume of PA solution allowing for greater control of the pipette tip and the formation of a full well gel without breaking

B



C

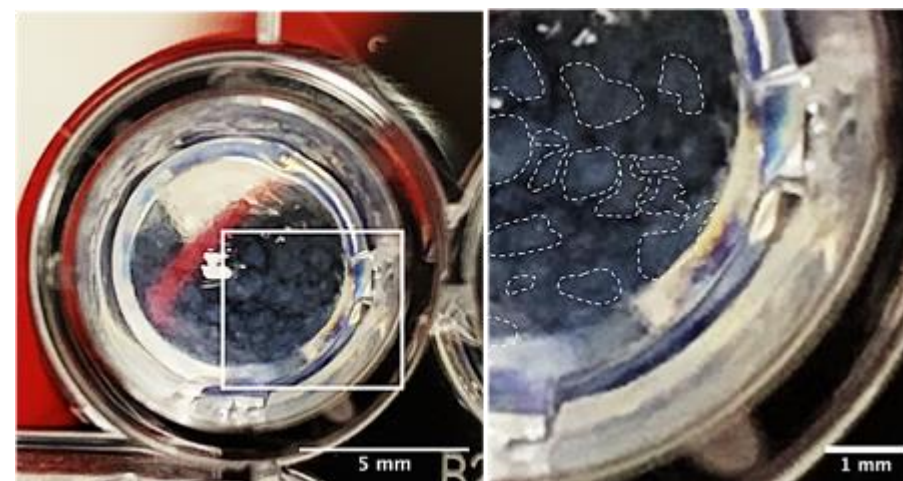


Figure 39. Optimisation of method of mixing PBS and PA solutions.

A A table with the observations for both methods to mix the positively charged hydrogels, $n = 3$. Figure made in Biorender. **B** A diagrammatical representation demonstrating the methods used to mix reagents. Two wells shown with the arrows displaying the direction of pipetting, PBS (orange) and PA solution (blue). **C** Representative image of a broken K3 gel (formulation 4) made by swirling PA into PBS, magnified section with dotted lines showing the fragments of hydrogel. Scale bars 5mm and 1 mm respectively.

Peptide amphiphile scaffolds and human induced pluripotent stem cells

Results

Optimisation of K PA hydrogels

The pH differed between the different positively charged PAs when they were in solution (without adulteration); K2 was ~pH 6, K3 was ~pH5 and K4 was ~pH 4 (bold value in Table 15). To assess whether there was an optimum pH for the creation of the hydrogels, each positive PA was gelled at a range of pH values and the time required for this recorded. The alteration of the pH influences the net charge of the amino acids present. The positive charge is present as the amino groups on the side chain of lysine residues are protonated. When the pH is high there is an excess of hydrogen ions (H^+), which raises the number of protonated amino groups in the equilibrium. This optimisation was necessary to account for the known batch to batch variation in supplied PAs. For example, the incomplete removal of trifluoroacetic acid (TFA) present during PA production (Section 3.2.1 p126) (Mata et al., 2012), results in more acidic PA solutions. The pH of the PAs in solution was altered by addition of sodium hydroxide or hydrochloric acid (0.5M). A maximum of 60 minutes was allowed for gelation according to the specification (Figure 38).

While K2 gelled and became self-supporting quickly across all tested pHs; for both K3 and K4 gelation was achieved fastest at pH 4 or 5, (the pH of the K3 and K4 respectively when dissolved in HEPES buffer). Gelation of K3 and K4 was delayed when the PA solution was more acidic, which is likely to be a result of increased charge repulsion requiring screening for the fibres to form.

Independent of the differing pH levels, the tested PAs had a distinct pattern in the time required for gelation, with $K2 < K3 < K4$ (Table 15). This suggests that, as the number of lysine residues and charge increases (Table 10) the time required for gelation also increases. The increased charge associated with the PAs ($K2 < K3 < K4$) increases the repulsion between PA fibres. As

Peptide amphiphile scaffolds and human induced pluripotent stem cells

Results

K2 has fewer protonated amino groups, the PBS was likely to contain more salt than charged amino groups. Thereby, the electrostatic repulsion was overcome quickly. As the number of lysine residues increases the number of protonated amino groups increases but there is no additional PBS or salt.

In addition, while in solution the PAs form transient micelles (spherical aggregates) that form due to the hydrophobic collapse that draws PAs together. When the force of the hydrophobic collapse was stronger than the charge repulsion between the hydrophilic heads of the PAs. Therefore, the K2 PA with a smaller charge may have had a larger number of micelles or larger micelles, with K3 and K4 having reducing number and size of micelles. If there was a substantial number or size of micelles in the K2 PA/HEPES solution, then the PAs were already close to each other allowing for a quick reorganisation into a self-supporting hydrogel. However, as the charge repulsion increases through K3 and K4, the PAs themselves were more disrupted throughout the HEPES solution, and the longer it would take to reorganise the individual PAs into the nanofibres, once the gelator (PBS) was added.

Physical differences between positively charged hydrogels.

In addition, the speed of gelation impacts the physical characteristics of the hydrogels. As seen in Figure 40, the K2 hydrogel was the least homogenous and the K4 hydrogel was the most uniform with fewest defects. There were larger deformities (areas that appear to be less dense surrounded by denser areas) in the K2 and K3 hydrogels, (highlighted with * in Figure 40). The deformities in the K2 hydrogels could be as large (Figure 40). As K2 gels more rapidly (Table 15) it was likely that there was reduced diffusion of the PBS into the PA solution before some of the hydrogel set. This could have produced areas of the hydrogel that set rapidly and are more resistant to deformities and other areas of the hydrogel with less access to the PBS

Peptide amphiphile scaffolds and human induced pluripotent stem cells

Results

that are more prone to deformities. The K4 PA produced the hydrogel that best fit the specification as it had least deformities when combined with cells and applied for *in vitro* cell culture and was the most homogenous.

Table 15. Optimisation of pH for K2, K3 and K4 gelation. Optimisation of pH for each positivity charged PA, assessed using time to achieve gelation. The **bold pH** is the original pH of the PA HEPES solutions (n=3).

		K2				K3				K4			
pH		3	4	5	6	3	4	5	6	3	4	5	6
Time Taken for gelation at 37°C (Minutes)	10	X	X	X	X								
	20						X	X					
	30								X		X	X	
	40												X
	50					X							
	60									X			
	Not Set												

Peptide amphiphile scaffolds and human induced pluripotent stem cells

Results

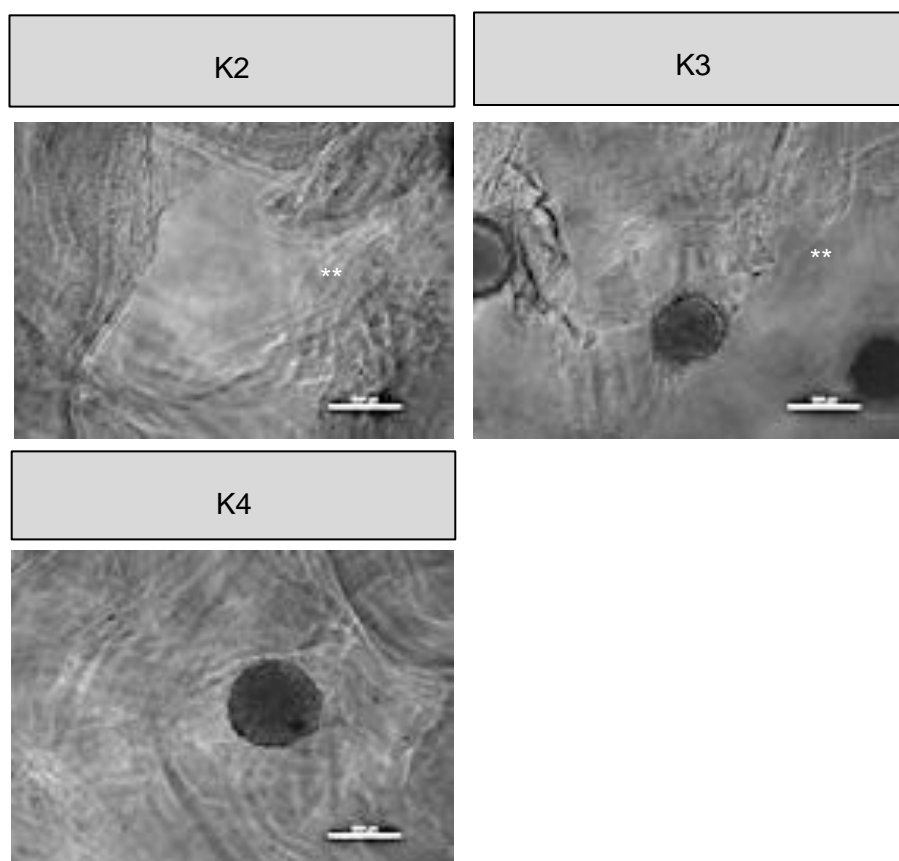


Figure 40. Representative bright field images, showing the physical differences in the PA hydrogels.

Images taken 48 hours after gelation, in culture conditions. ** showing a deep deformity in the hydrogel because they appear to be less dense than the hydrogel surrounding it. hiPSC clusters placed on the hydrogels, during culture the deformities may have adversely affected the retention of clusters on the hydrogels. Scale bar = 200mm.

3.4.4 Optimisation E3 PA hydrogel

Hydrogels formed using the E3 PA are typically created via the formation of interactions with proteins (Osuna de la Peña et al., 2021) or are alternatively triggered via the addition of bivalent cations (i.e., as CaCl_2 or NaCl) (Zhang et al., 2010, Osuna de la Peña et al., 2021). For this project, the E3 hydrogels were required to fit the same specified requirements as the positively charged hydrogels (Figure 38).

Peptide amphiphile scaffolds and human induced pluripotent stem cells

Results

The E3 PA used from this point on was non-aligned, as aligning the E3 nanofibres added significant time to the process, preventing the hydrogel setting in an hour and therefore falling outside of the required specification.

Formulations for the E3 hydrogel

The previously established protocol (used in sections 3.4 and 3.4.2) was assessed against the specification in Figure 38. To completely cover the well and maintain a similar volume to the positively charged PA hydrogels, the protocol was scaled up to create a 105µl hydrogel (Table 16). The scaled-up formulation was fully self-supporting within 25 minutes, however pipetting 5µl of CaCl₂ through 100µl of E3 solution rarely produced an even distribution of CaCl₂. It was very difficult to swirl the much smaller volume of CaCl₂ through the E3, making sure to evenly distribute the CaCl₂ from the bottom to the top of the well as demonstrated in Figure 41A. This uneven distribution of CaCl₂ increased the possibility of inhomogeneity within the E3 solution, with regions not gelling completely, every time the hydrogel was made. Therefore, the ratio of PA:CaCl₂ was altered, as seen in Table 16, this allowed for the disruption of CaCl₂ dispersed more throughout the PA solution.

Formulation 1 achieved a self-supporting gel within 10 minutes, completely covered the well with a depression in the centre. However, while the distribution of CaCl₂ into the PA solution was much more successful than the scaled-up formulation, it remained difficult to pipette the CaCl₂ in the required, optimal, 'swirl' pattern. When the formulation 1 hydrogels were placed in routine culture conditions including medium (E8), the hydrogel deformed after three days (Figure 41). This suggested that, either the CaCl₂ had not diffused sufficiently through the PA solution, or that the hydrogel was not robust enough to maintain its integrity when challenged by medium changes. In an attempt to counteract this, an additional formulation was tested

Peptide amphiphile scaffolds and human induced pluripotent stem cells

Results

with an increased volume of CaCl_2 may increase the hydrogel stiffness (Stendahl et al., 2006), the ratio changed from 9:1 to 4:1 in formulation 2 (Table 16).

Formulation 2 achieved a self-supporting gel within 5 minutes and, importantly, the volume of CaCl_2 could be swirled reliably throughout the entire E3 solution (Table 16). The hydrogels made using this formulation were able to meet all the required specifications (Figure 38), including maintaining a self-supporting hydrogel in culture conditions (Figure 41). Therefore, formulation 2 was selected for all further E3 hydrogels.

The erosion of the formulation 1 hydrogels observed when exposed to cell culture, and the contrasting lack of erosion observed in the formulation 2 hydrogels suggested that the increased PA: Ca^{2+} ratio in formulation 2 resulted in stiffer hydrogels. However, the E3 gel and the positivity charged hydrogels were insufficiently robust to be tested using a standard plate rheometer, preventing an assessment of this.

For all the formulations tested, any attempts to reverse the mode of addition, to pipette the E3 solution into the much smaller volumes of CaCl_2 , resulted in the same fragmented hydrogels previously seen with the positivity charged PA hydrogels when K PA solution was added to the smaller PBS solution (Figure 39). Therefore, to create a hydrogel that meet the specifications, all the E3 hydrogels were made by adding the CaCl_2 to the E3 solution in the 96 well plate. Figure 42 provides an overview to the differing gelation methods for the K hydrogels and the E3 hydrogel.

Peptide amphiphile scaffolds and human induced pluripotent stem cells

Results

Table 16. Optimisation of the formulation for the E3 hydrogels.
All E3 solutions were 1%. N = 3.

	<i>Mixture (ul)</i>		<i>Ratio</i>	<i>Time to gel (Mins) at 37C</i>	<i>Observations</i>
	<i>E3</i>	<i>CaCl₂ (200mM)</i>			
Standard protocol	10	0.5	20: 1	30	<ul style="list-style-type: none"> • Small volumes allow for gelation of entire droplet over time
Scaled up	100	5	20: 1	25	<ul style="list-style-type: none"> • The small volume of CaCl₂ makes it difficult to ensure equal distribution throughout the PA solution • Increased possibility of some of the PA solution not gelling
Formulation 1 (F1)	90	10	9: 1	10	<ul style="list-style-type: none"> • Increased volume of CaCl₂ allows for better distribution of CaCl₂ throughout the PA solution • Not enough CaCl₂ to swirl from the base of well to the top • Often results in the hydrogel eroding in the centre after a few days in culture (see below)
Formulation 2 (F2)	80	20	4: 1	5	<ul style="list-style-type: none"> • Increase in CaCl₂ volume allows for a complete swirl of CaCl₂ to be pipetted throughout the PA solution (as shown below) • Self-supporting gel then stable over multiple days

Peptide amphiphile scaffolds and human induced pluripotent stem cells

Results

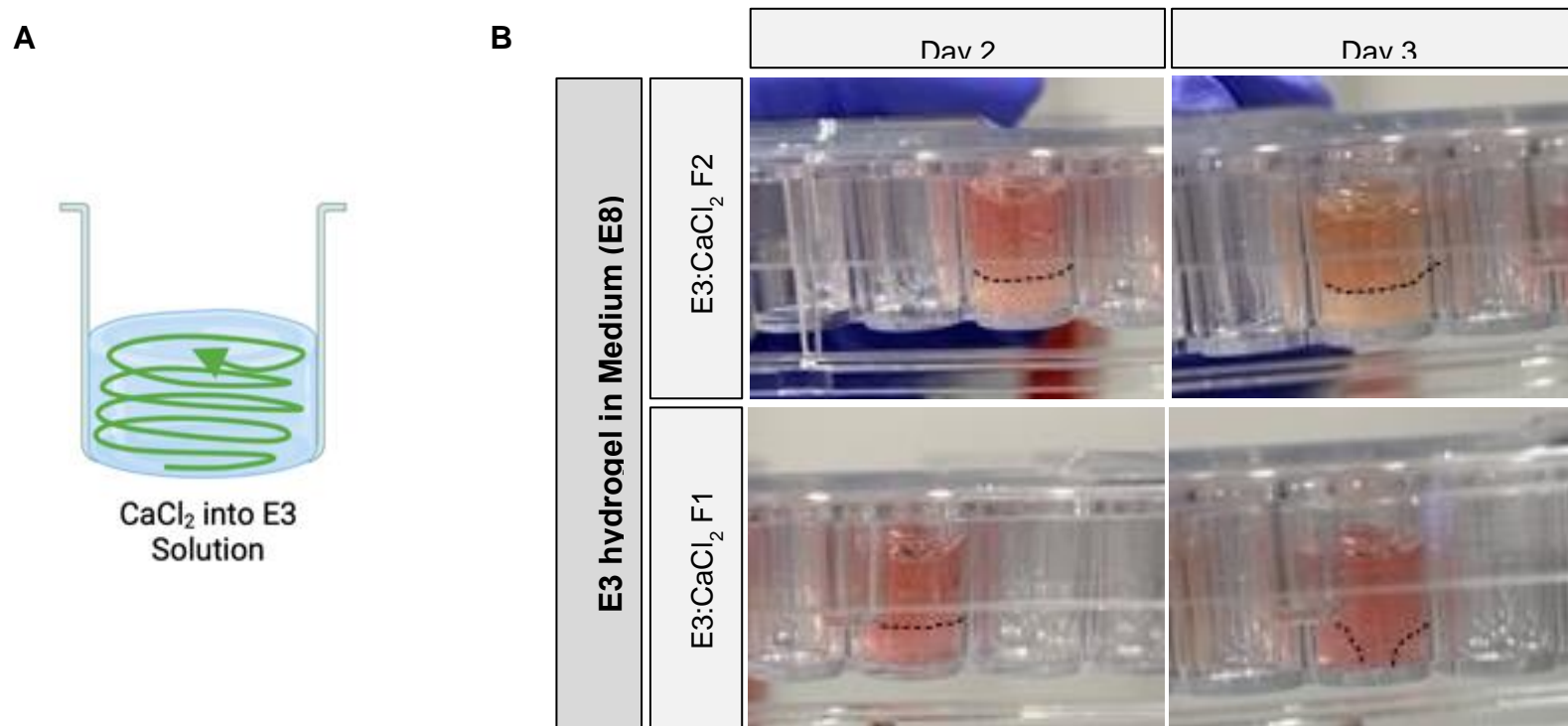


Figure 41. Optimisation of method for E3 hydrogels.

A A diagrammatical representation, demonstrating the method used to make gels from E3 PA, for optimum production. The CaCl₂ solution in green was pipetted into the E3 PA solution (blue) (PA in HEPES buffer), The CaCl₂ is dispersed through the entire PA solution from the base of the well to the top. This makes sure that all of the CaCl₂ was dispersed to facilitate the diffusion of CaCl₂ into the E3 PA solution. Figure made in Biorender. **B** Representative images highlighting the erosion of the E3 hydrogels formulation 1 after three days of culture. Here, hydrogels were exposed to routine culture conditions (medium changes) without cells in 96 well plate with E8 medium. Formulation 1 (F1) was found to erode after three days of culture. Formulation 2 (F2) was found to be optimum as there was no erosion.

Peptide amphiphile scaffolds and human induced pluripotent stem cells

Results

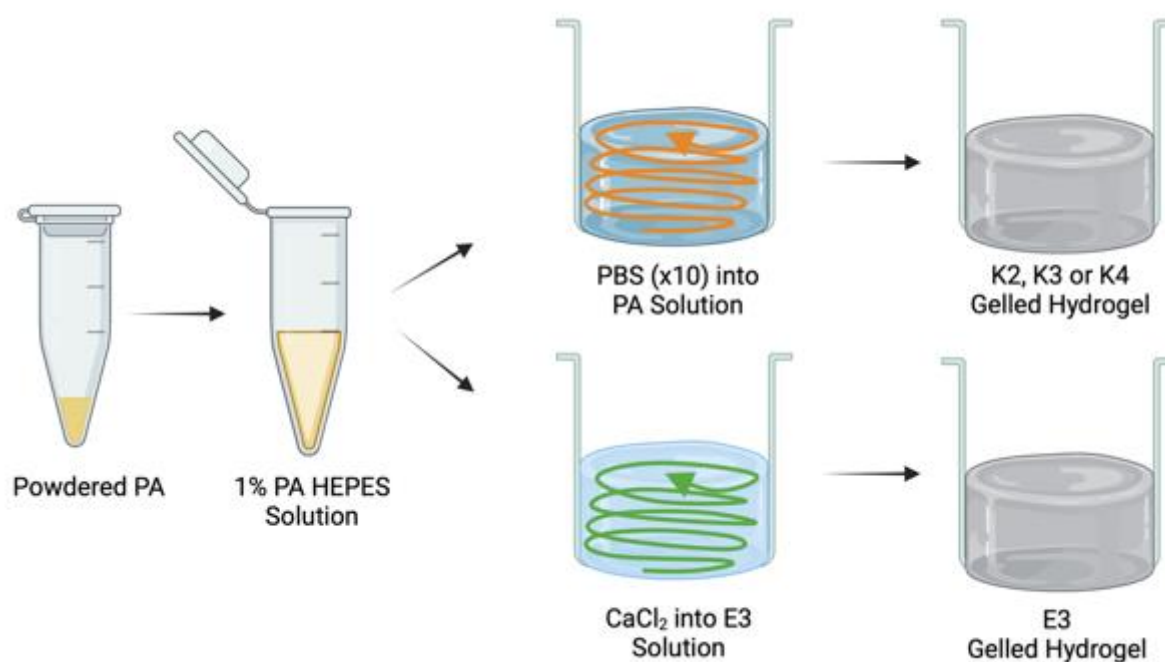


Figure 42. Graphical representation of the process to make the various hydrogels after optimisation.

First the PA are weighed into an Eppendorf tube (gold), then adjusted to generate a 1% solution with the addition of HEPES buffer (yellow). For the K PAs this solution is added to a well and x10 PBS (orange) is swirled through the PA solution (blue) to form a self-supporting hydrogel. The optimum formulation was a ratio PA:PBS 2.5:1. For the E3 PA, CaCl₂ (green) is swirled through the E3 solution (light blue) thereby forming a self-supporting gelled hydrogel. The optimum formulation ratio was PA:CaCl₂ 4:1. Figure made in Biorender.

Peptide amphiphile scaffolds and human induced pluripotent stem cells

Results

3.4.5 PA hydrogels their pH values

The net charge of the different PAs was of vital importance as this is the physical characteristic that was hypothesised to be able to interact with and then capture secreted native ECM components. As mentioned at a range of pH values the K PAs (pH 1 – 9) had a net positive charge and the E3 PA had a negative charge (pH 5 – 14). At or around neutral both PAs will be charged. The pH has have a controlling effect upon the charge. The positive charge is a result of the amino groups on the K residues which are protonated. The negative charge is the result of the deprotonation of the E residues carboxyl group. Both are part of an equilibrium, while the charge is maintained there is still a constant rate of pronation and deprotonation. When the pH is altered the presence of protons (H^+) is altered and the equilibrium is changed to compensate. For example, for the K PAs the more acidic the pH (increased protons) there is more protonation of the amino groups.

As the various PA hydrogels were tested for their ability to withstand cell medium changes, it was noted that the phenol red indicator in the medium was highlighting different pH environments between the hydrogels. Phenol red transitions from yellow to a fuchsia colour over the pH range 6.8 to 8.2. Therefore, to assess pH of the different PA hydrogels when exposed to cell culture medium (a buffered environment), the hydrogels were imaged after 24 hours of culture (in phenol red containing medium). As shown in Figure 43, there was an observable difference in pH between the set hydrogels, in addition to the expected difference seen in the PA solutions. This suggests that the addition of PBS has not completely neutralised the charge on the PAs in the K series gels. Subtle differences were observed between the positively charged K series PA hydrogels with the K4 hydrogel appearing most acidic followed by K3 and K2 (Figure 43).

Peptide amphiphile scaffolds and human induced pluripotent stem cells

Results

To observe differences more clearly between the PAs, the preparations were scaled down to 10 μ l hydrogel droplets, to which 2% phenol red was added. As can be seen in Figure 43, the positively charged PAs, and particularly K3 and K4 remained acidic and after gelation.

Clearly, phenol red can only report over a relatively limited pH range and is not an accurate measure, although it is appropriate for use in the cell culture settings used here. However, the differences observed suggest that while the E3 hydrogel appears to be close to pH7, the K series gels remain acidic.

The overall aim of this work was to prepare a range of hydrogels providing differently charged environments allowing us to assess the ability of these to capture ECM components secreted by cells in culture. The data shown in Figure 43 demonstrated that the PA hydrogels present differing pHs which may be due to the increase in K residues and increased protonation. This could suggest that the PA hydrogels have charges and suggests that these PAs were appropriate hydrogels with which to test our hypothesis.

Peptide amphiphile scaffolds and human induced pluripotent stem cells

Results

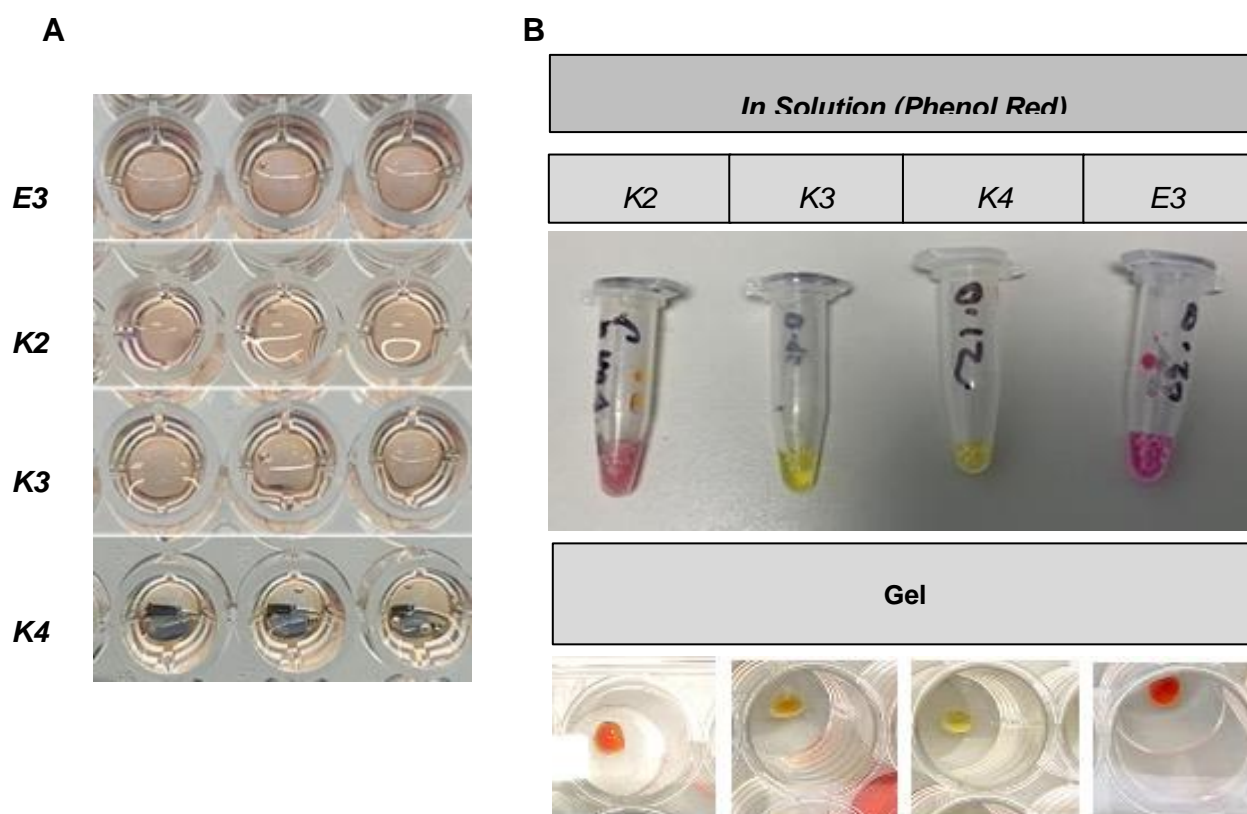


Figure 43. The K PAs showed a decreasing pH that was still present after gelation.

A Observation of pH of gels after 24 hours of culture in medium containing phenol red. The change in colour (with no cells present) suggests that the K4 and K3 gels are more acidic (yellow) than the K2. **B** The PA solutions with the addition of 2% phenol red, showing that the K3 and K4 PA solutions are more acidic than K2 and that this is maintained after gelation. The E3 is alkaline (fuchsia) before gelation but appears neutral (red) once a gelled.

3.4.6 Optimisation of cell cluster size

Once optimisation of the formulations of the hydrogels was complete and there was sufficient evidence to show that the PA hydrogels should express a range of charges, the size of the hiPSC clusters was optimised. For these experiments, clusters were placed on top of the hydrogels instead of being encapsulated within them. As highlighted previously, the hiPSC clusters were held within the depression formed on the surface of the hydrogels in a 96 well plate. The hiPSC clusters are formed by the hanging droplet method where droplets of cell containing medium are placed on to a Petri dish lid that is inverted overnight. This method has been previously used to produce the clusters encapsulated by the E3 hydrogels (in sections

Peptide amphiphile scaffolds and human induced pluripotent stem cells

Results

3.4 and 3.4.2) and in synthetic hydrogels including the FEFEFKFK octapeptide (Ashworth et al., 2020b).

To assess the optimum size for the clusters, we used the FEFEFKFK hydrogel, which is neutrally charged when set. This hydrogel was selected as the handling properties of this gel were well established, they complied with the needed specifications set for the PA hydrogels and there were no COVID-related supply issues associated with the peptide used, unlike the PAs (Figure 38). The hiPSC clusters were made using a range of cell numbers within the droplets (750, 1000, 1500, 2000) of note, when previously encapsulated in the FEFEFKFK hydrogel the clusters were formed from 2000 cells (Ashworth et al., 2020b).

The optimisation focused upon assessing if smaller clusters could be used due to concerns about the ability to retain larger clusters in 2D culture on PA hydrogels over several days. This needed to be assessed against the benefits of smaller clusters as these are preferable for downstream processing e.g., for confocal imaging, which is technically more challenging with larger clusters, as the confocal is unable to image the entirety of a cluster.

The experimental design is outlined in Figure 44. The clusters were created on day -1 and the FEFEFKFK hydrogel was cast into the 96 well plate. On day 0 the clusters were placed on the hydrogels via manual pipetting, to maintain the number of clusters per well. Images were taken on day one to record the size of the clusters, dependent upon the starting cell number. Images were taken every day (before medium changes) for three days.

Peptide amphiphile scaffolds and human induced pluripotent stem cells

Results

Specifications for hiPSC clusters

For the size of cluster be considered optimal for use in larger scale experiments, the clusters needed to have met the specifications listed in Figure 44. First, all clusters needed to be formed with the expected appearance. Previous work as well as the appearance of the clusters in suspension culture (as seen in

Figure 33B) suggests that clusters should be spherical with cells forming a tight colony with no clear cell:cell boundaries and cells with a high nucleus to cytoplasm ratio as seen in hiPSC colonies (Totonchi et al., 2010, rezaei larijani et al., 2011). Secondly, it was critical for future experiments that formation of the hiPSC clusters on the gels was uniform both in number and size. The third, was the clusters needed to be visible during handling, to allow collecting and placing upon the hydrogels. Similarly, the fourth requirement was that the clusters were not damaged by the repeated pipetting needed to place the clusters on top of the hydrogel and that this plating could be completed within an hour to maintain viability (Figure 44). The fifth requirement was that the hiPSC clusters needed to be retained over several days of culture, including throughout the required daily medium changes. As the focus of interest was the GAG or protein ECM components trapped by the hydrogel, the clusters needed time to secrete this material. Finally, as the clusters were to be cultured over several days, they must be able to at the very least maintain their initial size, or ideally to grow. This would indicate good viability (Figure 44).

Peptide amphiphile scaffolds and human induced pluripotent stem cells

Results

A

Specification for hiPSC Clusters	
1. Clusters must have been able to form (no individual cells, tightly packed spheroid shape and cells with high nucleus to cytoplasm ratio)	3. Clusters were visible during handling
2. Reliably made by hanging droplet method	4. Clusters could be placed in position on top of hydrogel within an hour and not damaged
	5. Clusters need to be retained over several days of culture
	6. Clusters increase in cross sectional area over culture

B

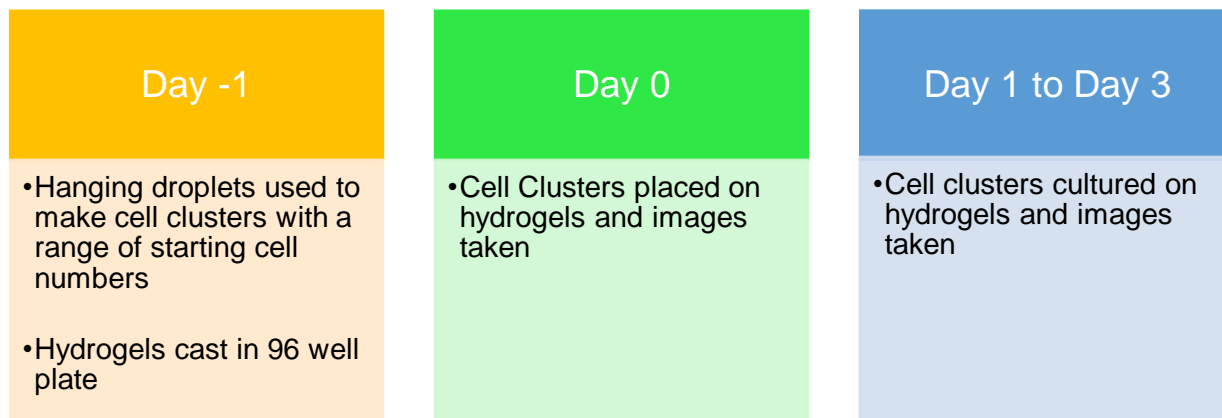


Figure 44. The specifications for the optimisation of the cell clusters.

A The requirements for the cell clusters, including technical and physical specifications. **B** A flow chart detailing the experimental set-up and data collection per day for a clearer understanding of the following figures. Day -1 was the production of the hiPSC clusters and FEFEFKFK hydrogel. Day 0 was the beginning of culture on the hydrogel. Culture was ended on day 3.

Peptide amphiphile scaffolds and human induced pluripotent stem cells

Results

Optimisation of cell number for hiPSC clusters used with PA hydrogels

The hiPSC clusters created using lower starting numbers of cells (750, 1000) appeared to include some abnormal clusters that were not spherical, with individual cells apparent on the surface of the clusters (Table 17). While these abnormal clusters could be removed prior to assessing the clusters on the hydrogels, this process was time consuming, wasteful of resources and demonstrated a potential problem for longer term experiments. These abnormal clusters were rarely seen when larger numbers of cells (1500 and 2000) were used (Table 17).

In addition, when using smaller starting cell numbers (750 and 1000), there were fewer clusters produced from the same number of hanging droplets. This was likely due to the reduced concentration of cells in the hanging droplets. Therefore, when starting with 750 and 1000 cells per droplet, more time and effort was required to achieve the required number of clusters. Working with larger starting numbers of hiPSCs to generate clusters was considerably more efficient (Table 17). The larger starting cell numbers were therefore optimal for efficient and reliable cluster formation.

As the number of hiPSCs used to create the clusters increased, it was easier to handle them, with clusters formed from more cells visible by eye during handling. Clusters made from 2000 cells were the easiest to see. Clusters from fewer cells (750) were the hardest to see, increasing handling time. The handling difficulties additionally made it much harder to place the required number of clusters in the depression on the surface of the hydrogel. This meant that either there was a need to remove clusters carefully without damaging the hydrogel or times when medium was added without clusters. For ease of handling and plating the optimal cluster was made from cells at from 2000 cells per droplet.

Peptide amphiphile scaffolds and human induced pluripotent stem cells

Results

Table 17. Comparison of the different size of cluster (starting cell number clusters during production and handling).

Clusters starting cell number	Observations during production and handling
750	<ul style="list-style-type: none"> • Abnormal clusters, not spherical with individual cells on surface • Fewer clusters formed per hanging droplets • Most difficult to see during handling • Difficult to place on the hydrogel, taking extended time
1000	<ul style="list-style-type: none"> • Abnormal clusters, not spherical with individual cells on surface • Fewer clusters formed per hanging droplets • Difficult to see during handling • Difficult to place upon the hydrogel
1500	<ul style="list-style-type: none"> • Clusters spherical and consistent in colour and appearance • Hanging droplets reliably made clusters • Visible during handling • Could be placed with ease upon the hydrogel
2000	<ul style="list-style-type: none"> • Clusters spherical and consistent in colour and appearance • Hanging droplets reliably made clusters • Easily visible during handling • The easiest and the quickest to place upon the hydrogel

Comparison of differently sized clusters during culture

As a preliminary measure, the cross-sectional area (μm^2) was used as a simple measure of viability on the basis that a non-viable cluster would decrease in area whereas a viable cluster would maintain or increase cross-sectional area. The cross-sectional area was calculated from

Peptide amphiphile scaffolds and human induced pluripotent stem cells

Results

measurements of cluster radius from a single bright field image. A Kruskal Wallis H test was used to analyse two effects: differences in cross-sectional area between clusters from different number of starting cells per droplet and then the difference over several days. As a mixed ANOVA could not be used (as mentioned previously (section 3.2.16 p133)), the two effects were analysed separately. To make this clear the same cross-sectional area data was displayed in two graphs in Figure 45. The median value for each starting value was selected is shown in Table 18. The identified outliers by SPSS were removed from the median calculations. The outliers were shown as dots or for the extreme outliers as stars in Figure 45.

On day one there were significant differences between clusters formed from different starting cell numbers, demonstrating a positive correlation between number of cells used to generate the cluster and cross-sectional area (Figure 45) suggesting these tests were valid in assessing the specifications mentioned above (Figure 44). There are outliers, suggesting that the hanging drop method can produce clusters that are not uniform in size (Figure 45). From careful observation, it is likely that these outliers have resulted from droplets merging while the clusters were forming, as supported as the outliers were the larger clusters outside of each group of starting cell numbers not smaller clusters (Figure 45). For this reason, the statistical analysis was completed on the data with the identified outliers removed. The outliers were thought to be due to the hanging droplet method, where droplets could merge (increasing in size).

Starting with the smallest number of starting cells used to generate clusters (750 cells per droplet) a decreasing trend in cluster cross-sectional area was seen over days 0 - 3 suggesting a loss of cell adhesion and/or viability (Figure 45 and Table 18). Figure 15 displays the data as proportion of clusters retained under each condition. Viewing the data in this way demonstrates that, for all conditions, clusters were progressively lost over the course of the

Peptide amphiphile scaffolds and human induced pluripotent stem cells

Results

experiment. This is likely due to detachment of clusters during daily medium change or, alternatively, to clusters disintegrating. In addition to the overall negative trend in cluster cross-sectional area, the smallest clusters had the lowest retention on all days 1 and 2 till no clusters were found by day 3. The clusters of this size therefore do not meet the speciation/requirements listed in Figure 44.

The cross-sectional area of clusters formed from 1000 cells per droplet was also found to significantly decrease between day 0 and day 1, but then stabilised to be similar to that on day 0 at days 2 and 3 (Figure 45 and Table 18). This suggests that there was an initial loss of viability with some recovery, but not expansion. The retention of clusters formed from 1000 cells on the gels was good (> 40% at day 1) but again quickly fell on day 2 and 3 (Figure 46). The decrease in cross-sectional area and low retention rate made this method unsuitable for larger scale experiments, particularly in light of the above-mentioned difficulties in handling.

Similarly, clusters formed from 1500 cells per droplet also demonstrated an initial loss of viability as demonstrated by the significant decrease in size between day 0 and day 1 (although it's worth noting that there is considerable heterogeneity in the day 1 readings) (Figure 45). Interestingly, the clusters did increase in cross-sectional area by day 3 suggesting that these conditions may be suitable for the support of proliferation (Table 18). However, while clusters formed using 1500 cells per droplet were retained on the hydrogel very well (~80%) on day 1, by day 3, the percentage of retained clusters was low. The relatively good retention of clusters between day 0 and day 1 for clusters formed from 750, 1000 and 1500 cells per droplet (and the positive trend across this series) could potentially be due to their smaller size (Table 18). The early benefit seen from higher retention was, however, not strong enough to overcome the apparent challenge for cell viability (Figure 45). Due to this and the

Peptide amphiphile scaffolds and human induced pluripotent stem cells

Results

less-than-ideal handling conditions the 1500 cells per droplet condition was also not considered further.

The largest clusters, formed from 2000 cells per droplet, were the most efficient to make and the easiest to handle and plate. This therefore met several of the specifications required for a suitable protocol (Table 17 and Figure 44). These clusters were significantly larger than those generated from fewer cells (perhaps not surprisingly) and here, we observed no significant differences in cross-sectional area over days 0 - 3 (Figure 45). However, the median cross-sectional area did increase during culture (Table 18). Since there was no significant difference in area of cluster over the days studied, we propose that cell viability is maintained.

Interestingly, using more cells (2000) per droplet clusters appeared to negatively impact retention at day 1, potentially because these larger clusters are more easily dislodged from or adhere more poorly to the gel surface. However, this appeared to stabilise between days 2-3, with a similar number of clusters at day 3 to that seen for clusters formed from 1500 cells/droplet. Therefore, this condition was selected to make the clusters for culture on top of the hydrogels.

Peptide amphiphile scaffolds and human induced pluripotent stem cells

Results

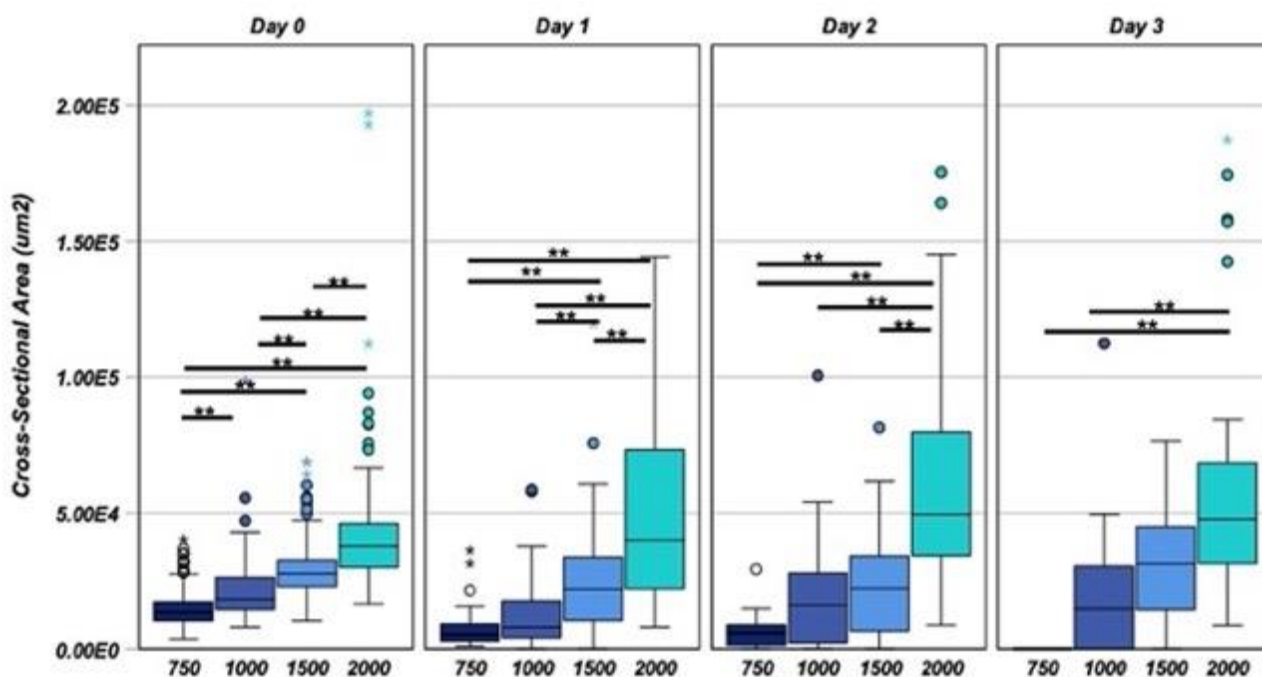
Table 18. The median cross-sectional area of the hiPSC clusters across all days of culture (μm^2). The only clusters that did not decrease in cross-sectional area was those made from 2000 cells per droplet. N = 3.

<i>Day of Culture</i>	<i>Cell Number per Droplet</i>			
	<i>750</i>	<i>1000</i>	<i>1500</i>	<i>2000</i>
<i>0</i>	1.34×10^4	1.83×10^4	2.77×10^4	3.78×10^4
<i>1</i>	5.32×10^3	7.93×10^3	2.21×10^4	4.00×10^4
<i>2</i>	5.79×10^3	1.62×10^4	2.23×10^4	4.94×10^4
<i>3</i>	0.00	1.48×10^4	3.15×10^4	4.77×10^4

Peptide amphiphile scaffolds and human induced pluripotent stem cells

Results

A



B

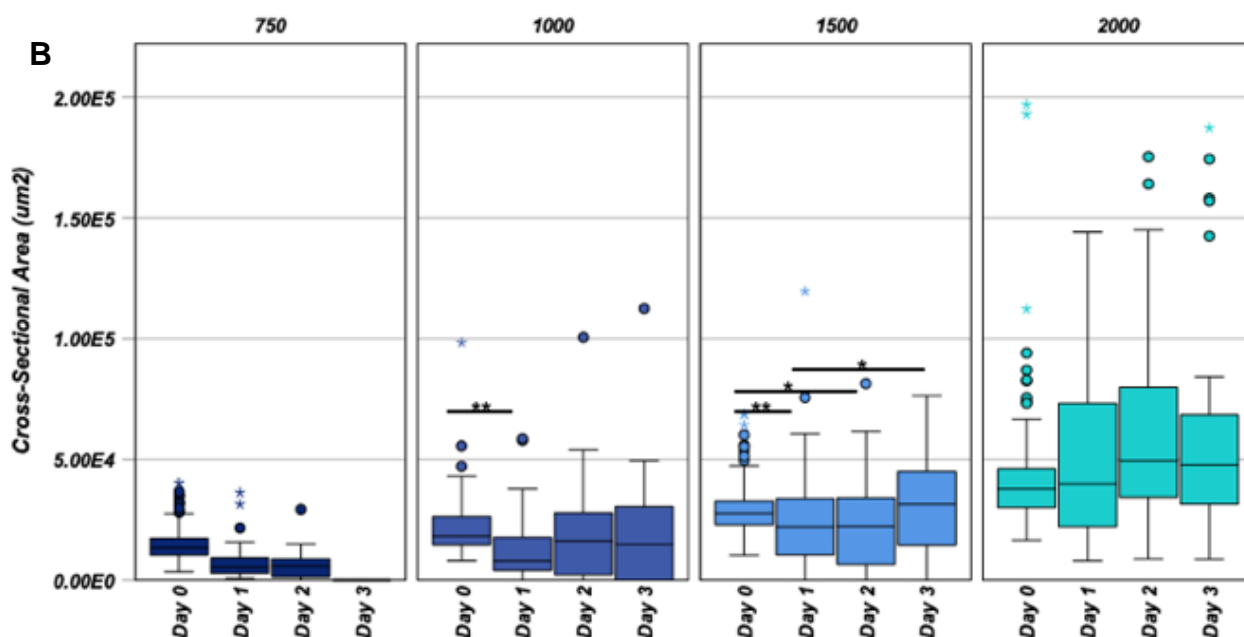


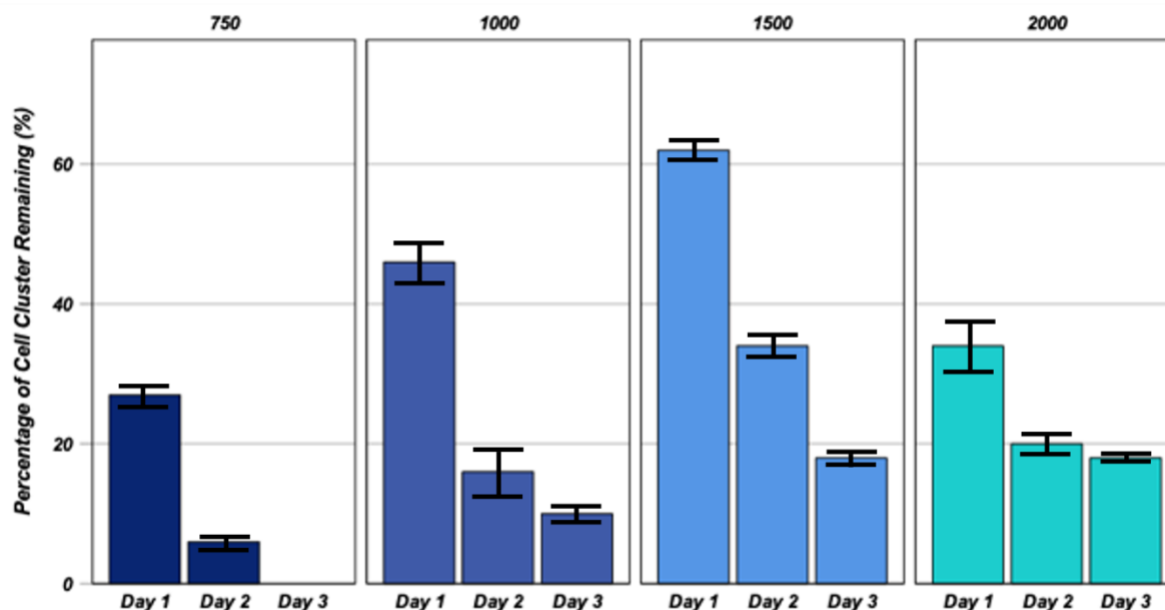
Figure 45. Optimisation of cell cluster size.

A The cross-sectional area (µm²) of clusters formed from hiPSCs (750, 1000, 1500 or 2000 cells per drop using the hanging drop method) was measured over 3 days on FEFEFKFK hydrogel. The different cell numbers per droplet produced clusters of increasing size. There was no statistical difference in size between 1500 and 2000 by day 3. Clusters made from 750 were not retained on the hydrogel. **B** The same data displayed to show the change in cross-sectional area per cell starting number per day. There area of the clusters reduced in all clusters bar those made from 2000 cell per droplet. Both box and whisker plot show the median and quantile ranges. Outliers shown as dots, extreme outliers shown as stars. * = p<0.05 and ** = p<0.001. N = 3 with three replicates per repeat.

Peptide amphiphile scaffolds and human induced pluripotent stem cells

Results

A



B

Day	Number of clusters imaged			
	750	1000	1500	2000
0	156	123	158	157
1	42	56	101	60
2	9	20	55	35
3	0	12	30	31

Figure 46. The retained cultures across all cultured day.

A The percentage, normalised to day 0 with standard errors, of cell clusters remaining on the FEFEFKFK hydrogel over the 3 days. Clusters made from 750 or 1000 cells per droplet were retained the worst. Despite an initial high retention on day 1, the retention of both 1500 and 2000 cells per droplet clusters was the same. **B** A table showing the number of clusters imaged and counted for the retention graph and measured for Figure 45 area calculation, $n = 3$.

Peptide amphiphile scaffolds and human induced pluripotent stem cells

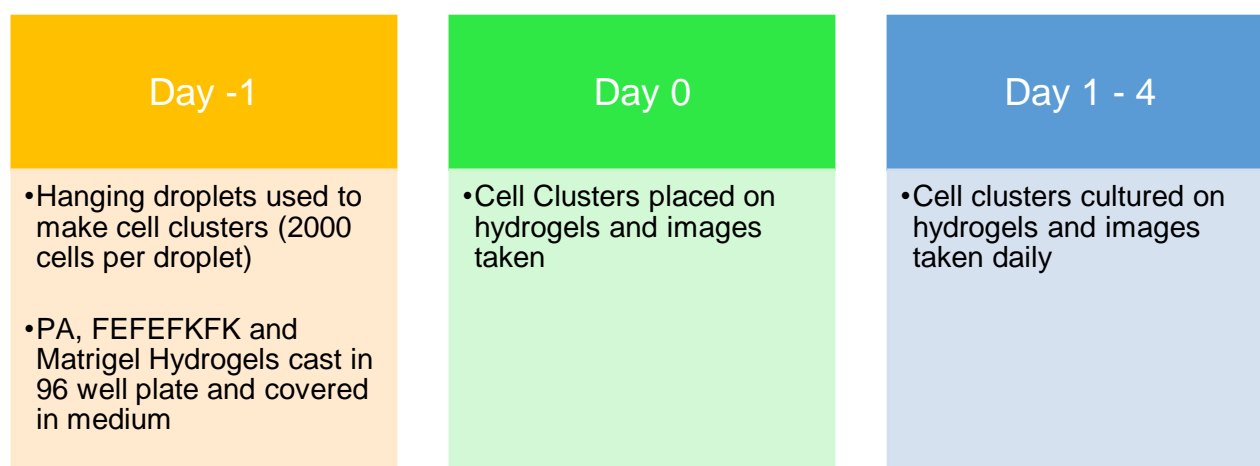
Results

3.4.7 Observations of the clusters cultured upon differently charged hydrogels

To compare the effects of differently charged hydrogels on the hiPSC clusters, all of the PA hydrogel formulations, as previously optimised were cast within wells of 96 well plate. As controls for the PA gels, we also included the FEFEFKFK peptide gels (assumed to be neutral at pH 7) and the current 'gold standard' *in vitro* hydrogel, Matrigel. The inclusion of Matrigel allows us to demonstrate impact of the presence of ECM components whereas the simple octapeptide FEFEFKFK hydrogel was theorised non-specifically trap matrix components secreted by the cells. Figure 47 shows the experimental set-up per day, for clarity when the data was separated by day. The day 0 images show the clusters prior to any impact from the hydrogels and show the initial morphology of the clusters.

Figure 47. Flow chart detailing the experimental set-up.

As with the optimisation of hiPSC cluster size protocol, day -1 was the production of clusters and hydrogels, day 0 was the start of culture and day 4 the end of culture.



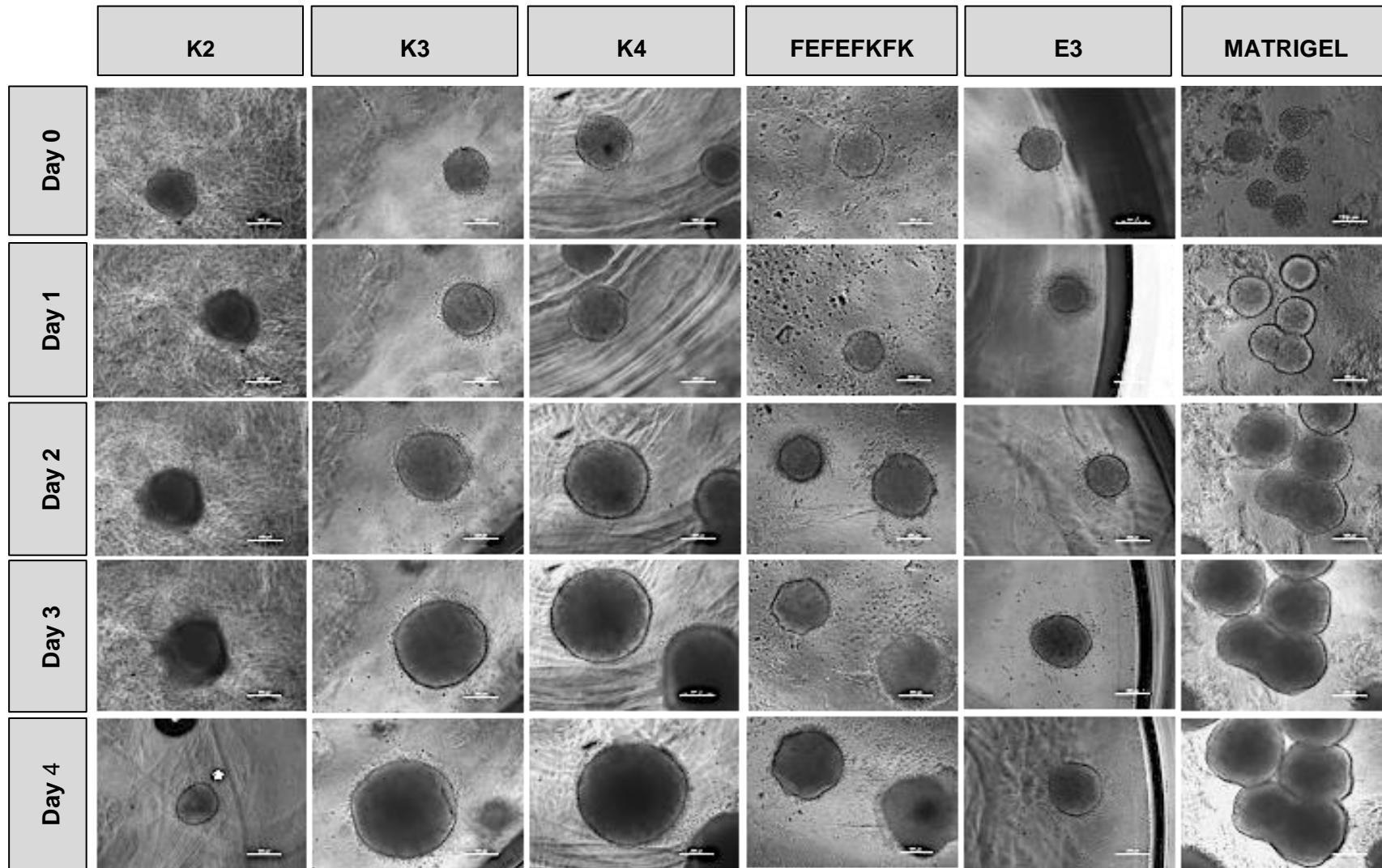


Figure 48. Observed impact of culture on hiPSC clusters grown on hydrogels. The hydrogels supported survival of hiPSC clusters in all conditions. All clusters met specifications. The Matrigel, K4 and K3 clusters were seen to proliferate the most. The same cluster is imaged over all culture days except for K2 where * denotes the image of different cell cluster than previous images. Bright field images taken at x20 magnification. Scale bar 200 μ m.

Peptide amphiphile scaffolds and human induced pluripotent stem cells

Results

Observations of the hiPSC clusters on all hydrogels

All the hydrogels were able to support viable clusters over 4 days in pluripotency maintaining medium (E8) (Figure 48) The clusters were all well-defined with a smooth appearance (no single cells were visible separate from the clusters). Figure 48, showed the morphology of clusters on the hydrogels over 4 days in maintenance medium, the images were of one cluster over the culture days except for the PA K2 hydrogel where there it was not possible to locate the same cluster. This was due to the inability of the clusters to be retained upon the K2 hydrogel (discussed in further detail below). For all hydrogels the hiPSC clusters appeared to proliferate, as they increased in size (Figure 48). The clusters were viable on all the hydrogels including the PA hydrogels assumed to express a charge (see section 3.4.5 , page 173). Interestingly, this confirms that the PA E3 was toxic to the cells when in solution (also shown in section 3.4 , page 142) but is tolerated when presented to the cells as a pre-cast gel.

One major difference between the PA hydrogels, FEFEFKFK hydrogel and Matrigel was that the clusters remained separate on the Matrigel, whereas the clusters on the PA hydrogels and FEFEFKFK hydrogel were able to merge shown in Figure 49. There could be several reasons for the difference, but it is likely that, as Matrigel is comprised from ECM components, the clusters would be immediately exposed to these and would have the opportunity to interact with them from day 0. This may make it harder for the cell-to-cell interactions needed for the clusters to merge. However, this was not investigated further due to lack of time.

Peptide amphiphile scaffolds and human induced pluripotent stem cells

Results

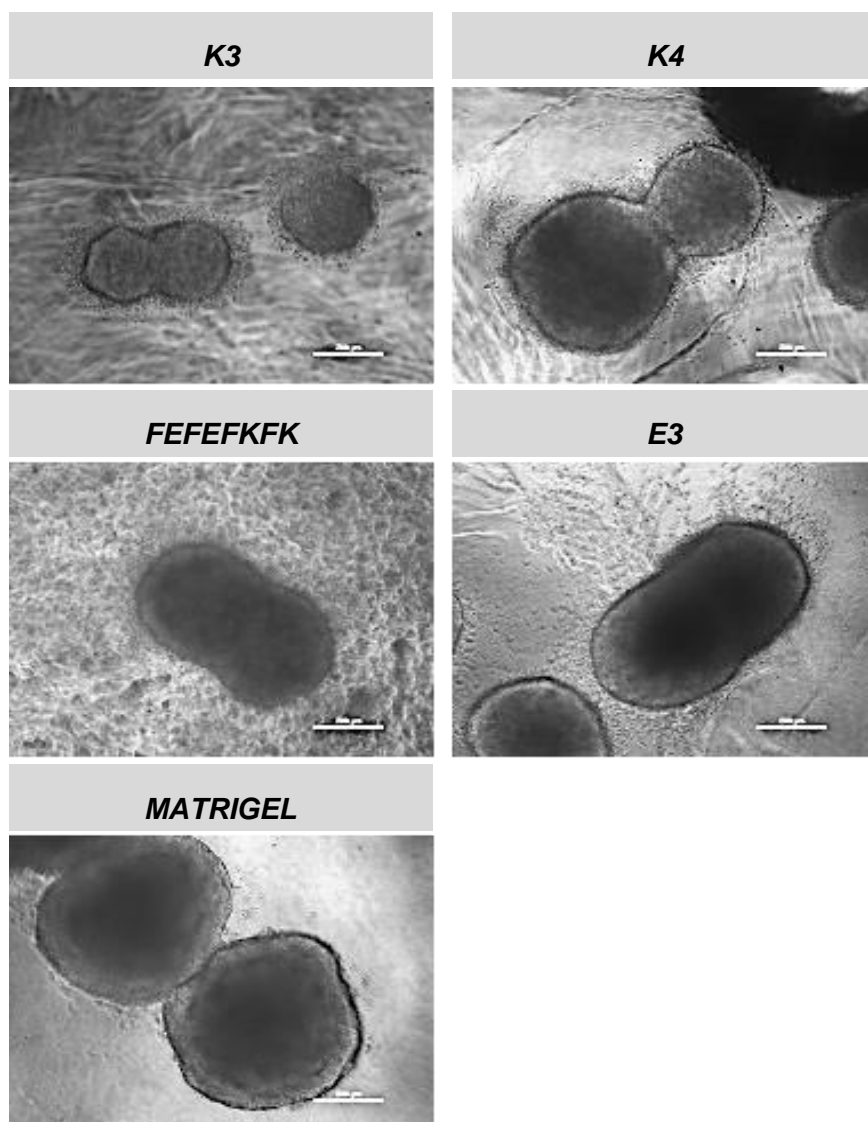


Figure 49. Observation of hiPSC clusters merging. Examples of cell clusters merging in several of the hydrogels, images from day 4 except for K3 which was from day 2. There was no image for from K2 hydrogel due to the limited retention of the clusters (Figure 52). Scale bars 200 μ m. Bright field images taken at x20 magnification.

Changes in hiPSC clusters on charged hydrogels analysed by time and hydrogel

To analyse the viability of the clusters on the hydrogels, their cross-sectional area was measured. For clarity, the data shown in Figure 50 displays the behaviour of clusters on each hydrogel over several days and Figure 51 then displays the same data but here looking at the

Peptide amphiphile scaffolds and human induced pluripotent stem cells

Results

differences between the clusters cultured on different hydrogels at each day stage. To compare the cross-sectional area between the differently charged hydrogels, there needed to be an understanding of any difference in size due to the hanging drop process of cluster formation. This is a particular concern as, due to supply chain shortages and other practical limitations, it was not possible to always carry out the tests on the same batch of hiPSC clusters. I was able to carry out one repeat with all conditions, but the other repeats were carried out only on sub-sets of the hydrogels. Indeed, the complete experiment itself may have added to these significant differences between the area of the clusters, as it took a considerable time (2+ hours) to plate the hanging drops for all the hydrogels which may have impacted on viability. On day 0 there was no significant difference in cross-sectional area between clusters on K2, K3 and K4 gels, therefore their cluster sizes can be compared without concern. However, there were significant differences between cluster sizes on several hydrogels (Figure 51 and Table 19). Unfortunately, time pressures and severe limits on available materials prevented additional repeats.

Table 19. The significant differences found between cluster cross-sectional areas on day 0. The significant differences are present in Figure 51 and are highlighted here for clarity. These differences in area were due to the inability to culture clusters on all hydrogels simultaneously and a lack of repeats.

Hydrogel	Significantly different from hydrogel in left column		
K2	E3	FEFEFKFK	Matrigel
K3	E3	FEFEFKFK	Matrigel
K4	E3	Matrigel	
E3	FEFEFKFK		

Peptide amphiphile scaffolds and human induced pluripotent stem cells

Results

In addition to the assessment of cross-sectional area, Figure 52 showed that there was a difference in the ability of the clusters to be retained during culture between the different hydrogels. The percentage of clusters remaining each day after medium change for each hydrogel. Each percentage was calculated by comparing the number of clusters per day against day 0. The area and retention data were collated from several batches of hiPSC clusters upon subsets of the hydrogels, as such there is variation in the number of repeats per hydrogel. Due to limited product, there were only two repeats upon the E3 and Matrigel hydrogels. For the K2 and FEFEFKFK hydrogels there were fewer repeats due to infection.

Table 20. The median cross-sectional areas (μm^2) for the hiPSC clusters on all hydrogels for 4 days of culture.

Matrigel and K4 produced the clusters that proliferated the most. The number of repeats varied; K2 n = 3 (day 0 - day 3) and n = 1 (day 4), K3 and K4 n = 4 (day 0 – day 3) and n = 2 (day 4), FEFEFKFK n = 3 (day 0 - day 3) and n = 1 (day 4), E3 and Matrigel n = 2. The \$\$ denotes there was only a n = 1 and a large number of cell clusters were not retained.

	Day 0	Day 1	Day 2	Day 3	Day 4
K2	3.45×10^4	2.92×10^4	3.26×10^4	5.78×10^4	1.78×10^5 \$\$
K3	3.19×10^4	3.15×10^4	5.96×10^4	9.45×10^4	1.16×10^5
K4	3.50×10^4	4.11×10^4	7.62×10^4	1.17×10^5	1.59×10^5
FEFEFKFK	4.05×10^4	5.62×10^4	8.15×10^4	8.35×10^4	1.29×10^5 \$\$
E3	4.48×10^4	4.74×10^4	6.67×10^4	7.23×10^4	9.47×10^4
MATRIGEL	4.09×10^4	6.09×10^4	1.22×10^5	1.92×10^5	2.77×10^5

Peptide amphiphile scaffolds and human induced pluripotent stem cells

Results

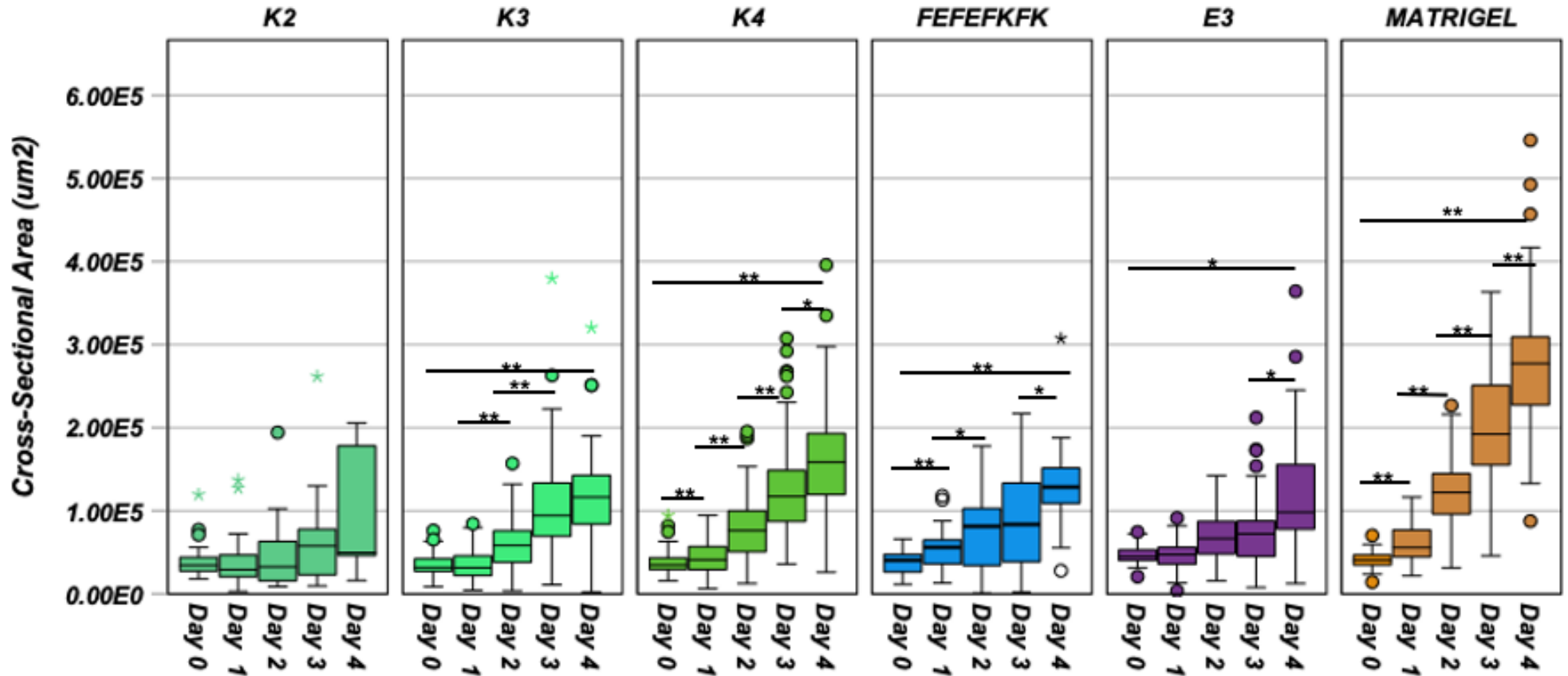


Figure 50. The difference in cross-sectional area per hydrogel.

Box and whisker plots showing the cross-sectional area of cell clusters (µm²) by hydrogel over all days. The clusters on Matrigel and K4 hydrogels proliferated consistently over all culture days. The clusters upon K3, FEFEFKFK and E3 proliferated over the time in culture. Only K2 was found to have no significant change in area size. The statistics were completed by MANOVA using SPSS Statistics * p < 0.05 ** p < 0.001. The number of repeats varied; K2 n = 3 (day 0 - day 3) and n = 1 (day 4), K3 and K4 n = 4 (day 0 - day 3) and n = 2 (day 4), FEFEFKFK n = 3 (day 0 - day 3) and n = 1 (day 4), E3 and Matrigel n = 2. Three replicated were present per condition and all clusters (5 - 7 per replicate on day 0) were imaged and measured per day. Outliers shown as dots, extreme outliers shown as stars. The same data is shown in Figure 51.

Peptide amphiphile scaffolds and human induced pluripotent stem cells

Results

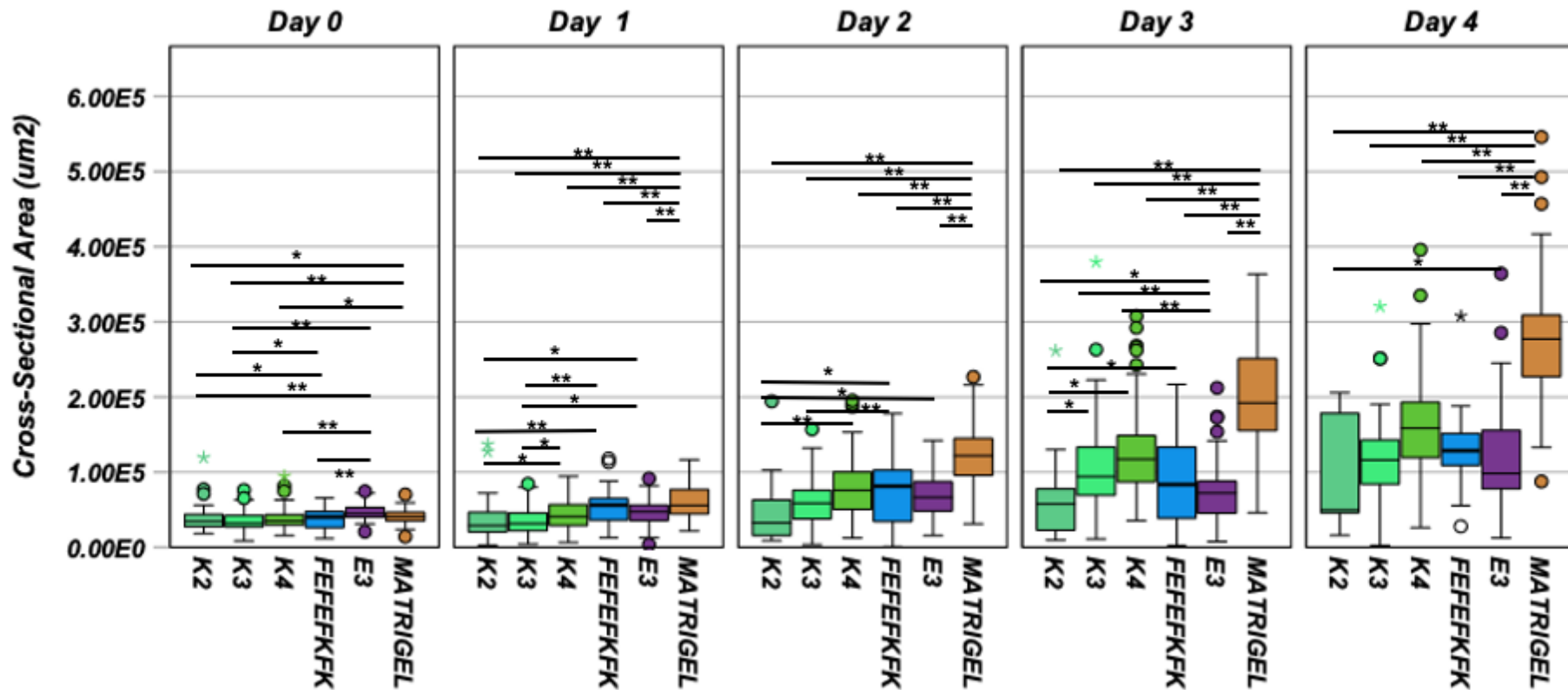


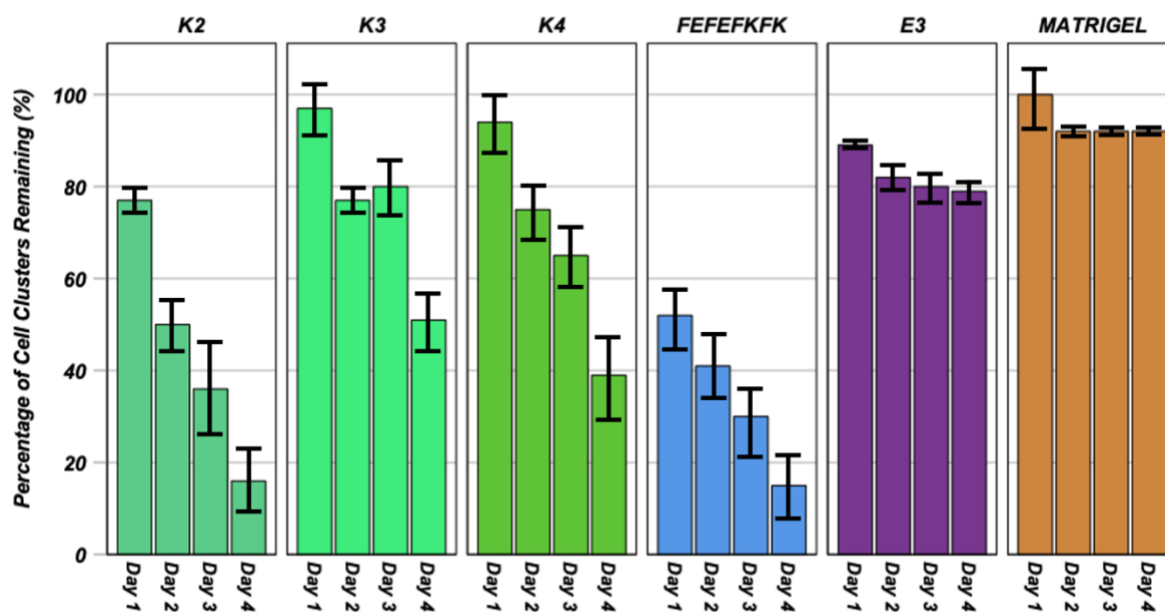
Figure 51. The difference in cross-sectional area per day.

Box and whisker plots showing the data per day to highlight the differences in cross-sectional area (μm^2) between the hydrogels. There were differences in area between clusters when placed upon the hydrogel on day 0. The clusters on Material proliferated (as shown by the increase in area) more than those on the other hydrogels. For the K hydrogels the proliferation increased as the charge increased, with the most proliferation from clusters on the K4 hydrogel. The area of the clusters on K3, FEFEFKFK and E3 hydrogels were not significantly different by the end of culture. Statistics completed by MANOVA using SPSS Statistics * $p < 0.05$ ** $P < 0.001$. The number of repeats varied; K2 $n = 3$ (day 0 – day 3) and $n = 1$ (day 4), K3 and K4 $n = 4$ (day 0 – day 3) and $n = 2$ (day 4), FEFEFKFK $n = 3$ (day 0 – day 3) and $n = 1$ (day 4), E3 and Matrigel $n = 2$. The number of repeats varied; K2 $n = 3$ (day 0 – day 3) and $n = 1$ (day 4), K3 and K4 $n = 4$ (day 0 – day 3) and $n = 2$ (day 4), FEFEFKFK $n = 3$ (day 0 – day 3) and $n = 1$ (day 4), E3 and Matrigel $n = 2$. Three replicates were present per condition and all clusters (5 - 7 per replicate on day 0) were imaged and measured per day. The same data is shown in Figure 50. Outliers shown as dots, extreme outliers shown as stars.

Peptide amphiphile scaffolds and human induced pluripotent stem cells

Results

A



B

Day	K2	K3	K4	FEFEFKFK	E3	MATRIGEL
0	44	98	124	118	66	66
1	34	95	116	61	59	61
2	22	75	93	48	54	61
3	16	78	80	35	53	61
4	7	50	48	18	52	61

Figure 52. The percentage loss of cell clusters over the culture time.

A The percentage loss is calculated by dividing the number of imaged clusters per day and hydrogel by the number of clusters imaged on day 0. Matrigel and E3 retained the clusters the best. K2 and FEFEFKFK retained the clusters the worst. Standard errors shown. **B** The number of clusters imaged per day and hydrogel. The number of repeats varied; K2 n = 3 (day 0 - day 3) and n=1 (day 4), K3 and K4 n=4 (day 0 – day 3) and n=2 (day 4), FEFEFKFK n=3 (day 0 - day 3) and n=1 (day 4), E3 and Matrigel n = 2.

Peptide amphiphile scaffolds and human induced pluripotent stem cells

Results

The median cross-sectional area of clusters on the K2 hydrogel initially lagged but then increased on day 3 and 4 (Figure 50 and Table 20). However, the considerable heterogeneity in area of clusters at later day stages meant that, despite this trend, there was no significant difference between days. This highlights a key issue as the area for the K2 clusters on day 4 was calculated from one batch of clusters due to the lack of delays in PA production, and as many of the clusters were dislodged from the gel over each day, with only 16% of the day 0 clusters left by day 4 there were few data points (Figure 52). The poor retention may highlight the detrimental effect of the deformities present in K2 hydrogel (see section 3.4.3 , page 159). More repeats would be needed to obtain reliable data, although the loss of clusters does suggest this is not an optimal growth environment. In summary, the K2 hydrogel was able to maintain viable clusters over 4 days with a suggestion that, despite loss of the clusters, possibly due to a lack of adhesion, clusters which did attach could proliferate.

A similar trend was seen for the K3 and K4 hydrogels (Table 20). Here, the K3 hydrogels, the cross-sectional area showed a significant increase from day 1 to day 2 and day 2 to 3, as well as a significant increase from day 0 to day 4 (Figure 50). There was improved retention of the clusters on the K3 gel (~ 50% of clusters remaining at day 4) compared to K2. Therefore, the clusters on the K3 hydrogel were able to both maintain cluster adhesion and proliferate and increase in size.

For the K4 gels, there was a significant increase in cross-sectional area between day 0 and day 4 (Figure 50 and Table 20). Adhesion of clusters to the K4 hydrogel was not as good as for the K3 gels (< 40 % of clusters still attached at day 4) but better than for K2. As the K2 hydrogel is the least charged of the positive hydrogels and K4 the most charged. As K4 has larger clusters this may have a factor in the strength of a cluster to adhere to the hydrogel.

Peptide amphiphile scaffolds and human induced pluripotent stem cells

Results

The clusters cultured on the K2 hydrogels were significantly smaller in cross-sectional area than the clusters on K4 hydrogels and smaller than K3 clusters on all days with more than one repeat (Figure 51). A comparison of the median values for the cross-sectional areas showed that the K3 clusters were consistently smaller than the K4 values (Table 20). Therefore, for the K PAs hydrogels clusters proliferated the least upon the K2 hydrogel, then the K3 clusters, and the most proliferation was seen on the K4. This was in line with the hydrogels' increase in charge. There was no difference in cluster area on day 0, therefore this conclusion was not influenced by the production of the clusters (Table 19). Taken together, this may indicate that the increase in charge increases the ability of the gel to support hiPSC cluster proliferation.

In the current experiment, there was rapid loss of clusters from The FEFEFKFK (neutral) hydrogel (<20% of clusters remaining by day 4), The FEFEFKFK hydrogel day 4 also only has one batch repeat due to the lack of retention, as other repeats did not have any clusters remaining. As the neutral hydrogel and the weakest positively charged hydrogel were the least able to retain clusters there may be a role for increased charge in retention of hiPSC clusters. There was, however, a significant increase in cross-sectional area of clusters on the FEFEFKFK hydrogel between each day (except between day 2 and 3), and as well as a significant increase from day 0 to day 4 (Figure 50 and Table 20). Therefore, the clusters on the neutral hydrogel do appear to be able to proliferate. It could be that either the charge is less important than the lack of proliferation by clusters on K2 (compared to K3 and K4) would suggest, or that there are different physical characteristics that differ between the PA hydrogels and the FEFEFKFK hydrogel that allowed for proliferation.

Peptide amphiphile scaffolds and human induced pluripotent stem cells

Results

The clusters upon K2 and K3 hydrogels were significantly smaller in cross-sectional area than the neutrally charged FEFEFKFK hydrogel (Figure 51). As the FEFEFKFK clusters were significantly bigger on day 0, that may be a reason for the larger size (Figure 51 and Table 20). Therefore, the K3 clusters may be proliferating more but they take more time to “catch up” to the size of the clusters on FEFEFKFK hydrogel, as they started larger. The cross-sectional area of clusters cultured upon the K4 hydrogel’ was not significantly different to those cultured on the FEFEFKFK hydrogel (Figure 51). It could be that either the charge is less important than the lack of proliferation by clusters on K2 (compared to K3 and K4) would suggest, or that there are different physical characteristics that differ between the PA hydrogels and the FEFEFKFK hydrogel that allowed for proliferation.

hiPSC clusters cultured on the negatively charged hydrogel E3 demonstrated an increasing median cross-sectional area, with a significant increase in area between day 3 and day 4 and an overall significant increase from day 0 to day 4 (Table 20 and Figure 50). Retention of clusters on the gels was also excellent, with ~80% remaining by day 4. The clusters were able to be maintained and they appear to have proliferated. However, due to time pressures, only two repeats of this experiment were carried out and it is clear that the suggested proliferation would have to be validated (or refuted) by additional work.

E3 clusters proliferated more than the clusters on K2 hydrogels (Figure 51 and Table 20). There was no visible trend that the E3 clusters differed in area compared to the K3 (Table 20 and Figure 51). The larger cross-sectional area of the E3 clusters may be a remainder from being significantly larger on day 0. Due to lack of further data, it was hard to conclude that there was a distinct difference between the clusters cultured on K3 and E3 hydrogels, despite their differing charges.

Peptide amphiphile scaffolds and human induced pluripotent stem cells

Results

The K4 clusters were significantly larger than the E3 clusters on day 3 and the median cross-section areas were consistently larger (Figure 51 and Table 20). The data therefore suggests that the K4 clusters had a similar distribution of cross-sectional areas over the culture days, but they may have been larger than the E3 clusters. The E3 hydrogel produced clusters that proliferated more than the clusters on K2, close to K3 and less than K4 hydrogels.

The E3 hydrogel clusters start significantly smaller than FEFEFKFK clusters on day 0 but are not significantly different on the remaining days (Figure 51). The E3 median cross-sectional areas are constantly lower than the FEFEFKFK clusters, suggesting similar or slightly less proliferation than the FEFEFKFK clusters (Table 20).

Finally, the hiPSC clusters cultured on Matrigel demonstrated significantly increased cross-sectional area every day, as expected. This likely demonstrates an increased ability to proliferate (Figure 51 and Table 20). Retention of clusters was also by far the best of the conditions tested at ~90% by day 4. The increase in the cross-sectional area was dramatic and the cross-sectional area was significantly larger than all other hydrogels, including the FEFEFKFK, and E3 clusters, which were larger on day 0 (Figure 51 and Table 19). As such the increase in Matrigel clusters was not due to the size of clusters on day 0. The increase in size was therefore likely due to the supportive environment provided by the Matrigel, suggesting a role for increased ECM components in the increased proliferation of hiPSC clusters.

To summarise, the cross-sectional area is used here as a proxy for a measure of hiPSC proliferation and, as expected the Matrigel hydrogel provided the optimal proliferative environment. The K PA hydrogels showed a trend, with the least charged showing the least

Peptide amphiphile scaffolds and human induced pluripotent stem cells

Results

amount of proliferation and the hydrogel with the highest positive charge, K4, showed the most proliferation. This may indicate that proliferation can be controlled through alteration in hydrogel positive charges.

The clusters on the E3 hydrogel (expected to be negatively charged) had a similar cross-sectional area and proliferation as the clusters on the K3 hydrogel despite the opposite charge. The neutral hydrogel FEFEFKFK had clusters that may be smaller than K3 and K4 by the end of the culture but were larger than the E3 clusters. This may suggest that the strength of the charge was more important for proliferation control than the type of charge (positive or negative). This demonstrated that there was an ability to control proliferation of hiPSC cluster through the control of hydrogel charge. The immunostaining below will attempt to illuminate the possible basis of this, by assessing if there was a difference in the GAGs sequestered.

There was a similar trend in the ability of the clusters to be maintained upon the hydrogels, Matrigel was the optimum again. There was a reduction in retention when the charge of the K PA hydrogel was at its lowest (K2), which was found to be similar to the neutrally charged FEFEFKFK hydrogel. The increasing positive charge altered the ability of the clusters to be retained. The E3 hydrogel provided the second-best retention ability. This indicates that the difference in type of charge (positive or negative) could select for differing properties either attachment or proliferation ability. This difference could be the result of differing GAGs or ECM proteins sequestered dependent upon charge.

Results

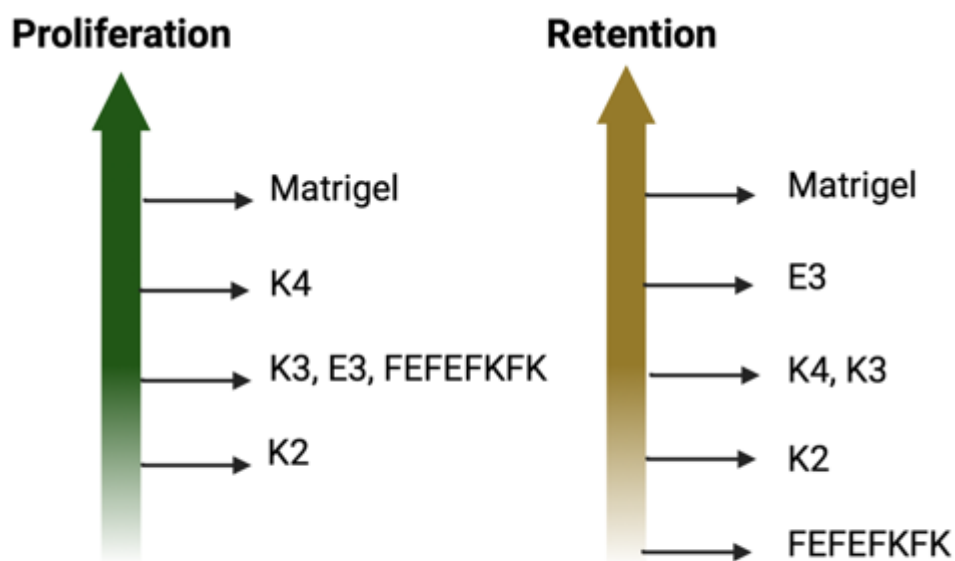


Figure 53. A summary of the cross-sectional area and retention data.

The clusters upon a range of differently charged hydrogels can display different behaviours. The clusters on Matrigel displayed the most proliferation (cross-sectional area) and attachment (through retention of clusters). The increased strength of positive charge increased both proliferation and attachment. The clusters attachment behaviour was changed through the type of charge.

3.4.8 Observed differences in cells escaping from the clusters between hydrogels.

To validate our approach, using cross-sectional area as a proxy for cell viability and proliferation, we additionally completed a live dead stain. Figure 54 showed that the clusters were viable on day 4 or day 3 (K2 only) which reinforces the images and cross-sectional area (Figure 48 and Figure 50). This was only performed once due to limitations on materials. Matrigel produced the most compact clusters where there were almost no cells “escaping” the cluster (single cells no longer within the clusters but migrating upon the hydrogel surface). However, several of the clusters on other hydrogels were surrounded by escaping cells (Figure 54). These plumes of escaping cells were seen in bright field images shown in Figure 55.

Peptide amphiphile scaffolds and human induced pluripotent stem cells

Results

The viability of the cells escaping the cluster and their distance from the cluster.

The clusters on hydrogel K2 (enlarged images in Figure 55) showed that there were plumes of cells surrounding the main clusters, but that the cells were small and dead cells (Figure 54).

To quantify the number of cells in these plumes, for each cluster three measurements were taken from the cluster to the edge of a plume equidistant around the cluster.

Table 21. The median values for the furthest cell distance from the cluster (μm).

The clusters on material and K4 had the least cells outside the clusters. K2, FEFEFKFK and E3 had cells the furthest from the clusters. The \$\$ denotes there was only a $n = 1$ and many cell clusters were not retained. The number of repeats varied; K2 $n = 3$ (day 0 - day 3) and $n = 1$ (day 4), K3 and K4 $n = 4$ (day 0 - day 3) and $n = 2$ (day 4), FEFEFKFK $n = 3$ (day 0 - day 3) and $n = 1$ (day 4), E3 and Matrigel $n = 2$.

	Day 1	Day 2	Day 3	Day 4
K2	53.33	67.206	63.28	73.05\$\$
K3	52.15	43.133	41.04	30.90
K4	20.54	21.87	25.35	26.82
FEFEFKFK	44.82	53.37	46.21	42.69\$\$
E3	72.09	53.07	32.25	66.78
MATRIGEL	0	0	0	0

Peptide amphiphile scaffolds and human induced pluripotent stem cells

Results

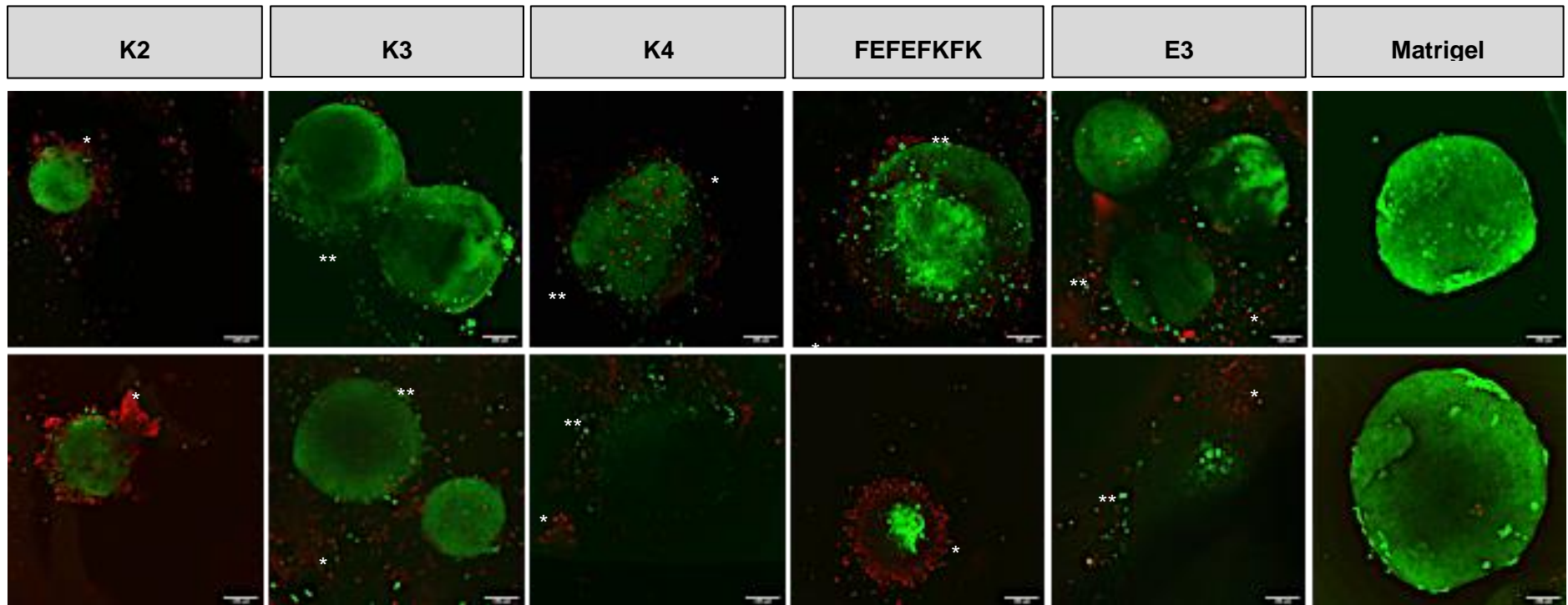


Figure 54. Live/dead staining of all the clusters on hydrogels.

Calcian AM and ethidium Homodimer stained clusters. The clusters upon Matrigel and K4 had the lowest presence of dead cells. The cells that had escaped the clusters on the other hydrogels were a mixture of live and dead cells. No clusters were seen to be dead on any hydrogel, as such images were selected for the best view of the escaping cells. K2 is imaged on day 3 and the remaining imaged on day 4. N = 1, Scale bar = 100 μ m. * dead cells and ** live cells.

Peptide amphiphile scaffolds and human induced pluripotent stem cells

Results

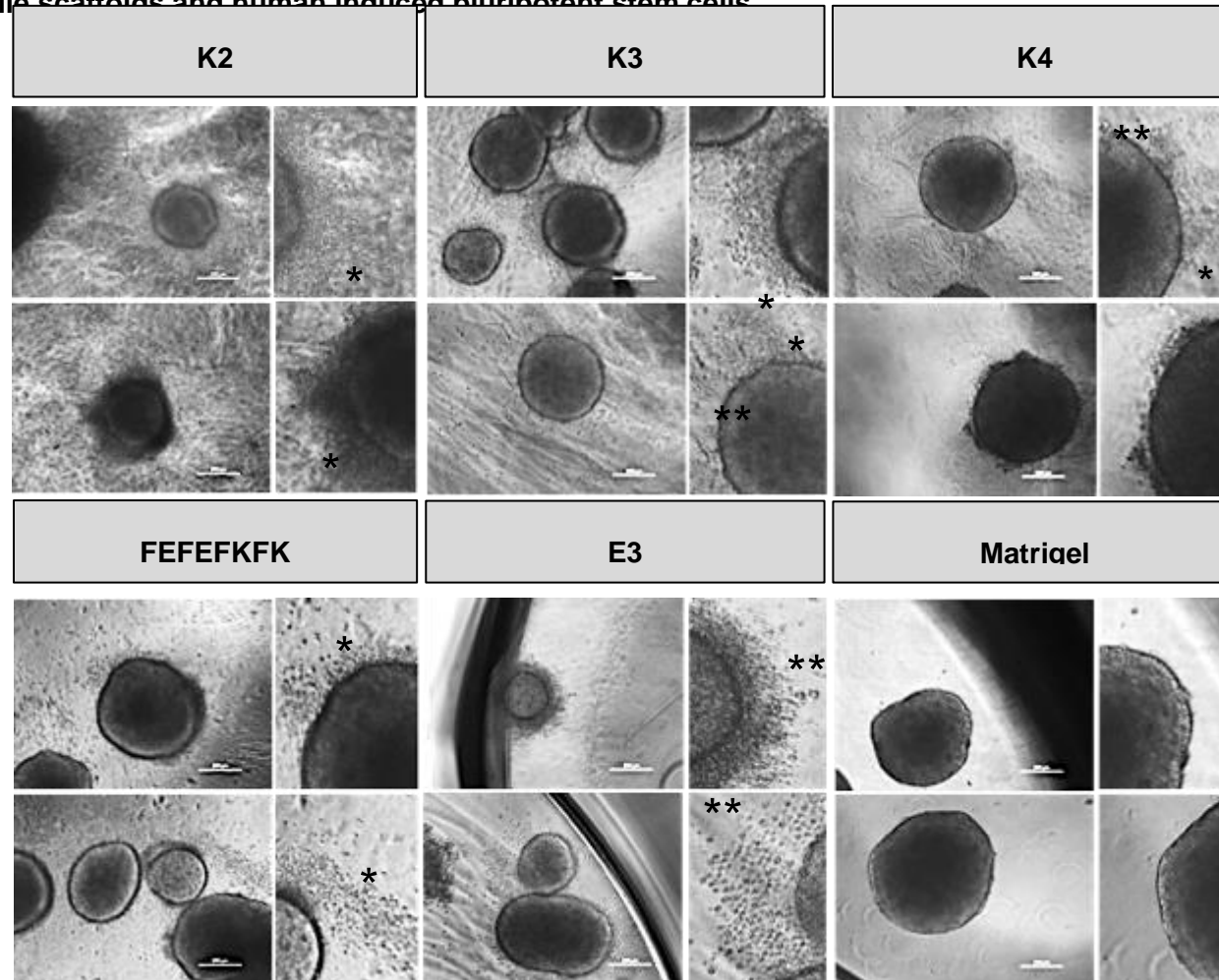


Figure 55. Observations of the cells extending from the surface of the cluster.

Bright field images showing the morphology of the cells surrounding the cell cluster day 4. * May be dead cells and ** cells that may be alive, they are larger and more defined. There is a mixture of both live and dead cells surrounding the cell clusters. K2, K3 and FEFEFKFK hydrogels had escaping cells that looked to be predominantly dead cells. E3 showed predominantly live cells but a great number of cells had escaped the clusters. K4 hydrogels showed clusters the most similar to Matrigel, with few cells escaping. The number of repeats varied; K2 n = 3 (day 0 - day 3) and n = 1 (day 4), K3 and K4 n = 4 (day 0 – day 3) and n = 2 (day 4), FEFEFKFK n = 3 (day 0 - day 3) and n = 1 (day 4), E3 and Matrigel n = 2. Three replicates were present per condition and all clusters (6-8 per replicate) were imaged and measured per day. Scale bar 500µm.

Peptide amphiphile scaffolds and human induced pluripotent stem cells

Results

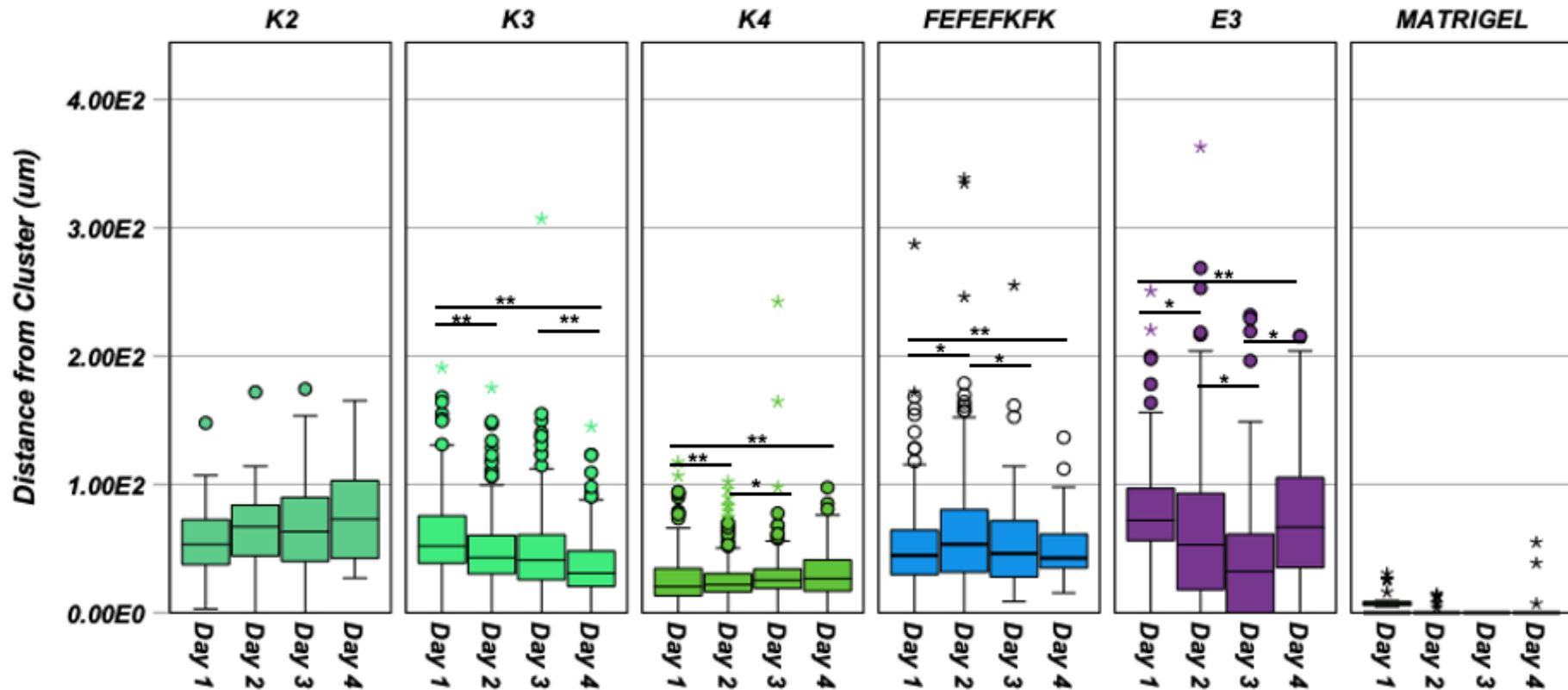


Figure 56. The distance of cells surrounding the clusters per day.

Box and whisker plots showing the difference in the distance (μm) of cells extending from the cluster per day. The cells on Matrigel rarely left the clusters. The distances of cells escaping the clusters on K4 and FEFEFKFK varied slightly. The distance on the E3 hydrogel varied a great deal whereas the distance on the K2 hydrogel remained constituent. There was a reduction on the distance on the K3 hydrogel. Statistics completed MANOVA using SPSS Statistics * $p < 0.05$ ** $P < 0.001$. The number of repeats varied; K2 $n = 3$ (day 0 – day 3) and $n = 1$ (day 4), K3 and K4 $n = 4$ (day 0 – day 3) and $n = 2$ (day 4), FEFEFKFK $n = 3$ (day 0 – day 3) and $n = 1$ (day 4), E3 and Matrigel $n = 2$. Three replicates were present per condition and all clusters (6–8 per replicate) were imaged and measured per day. Outliers shown as dots, extreme outliers shown as stars. The same data as Figure 57.

Peptide amphiphile scaffolds and human induced pluripotent stem cells

Results

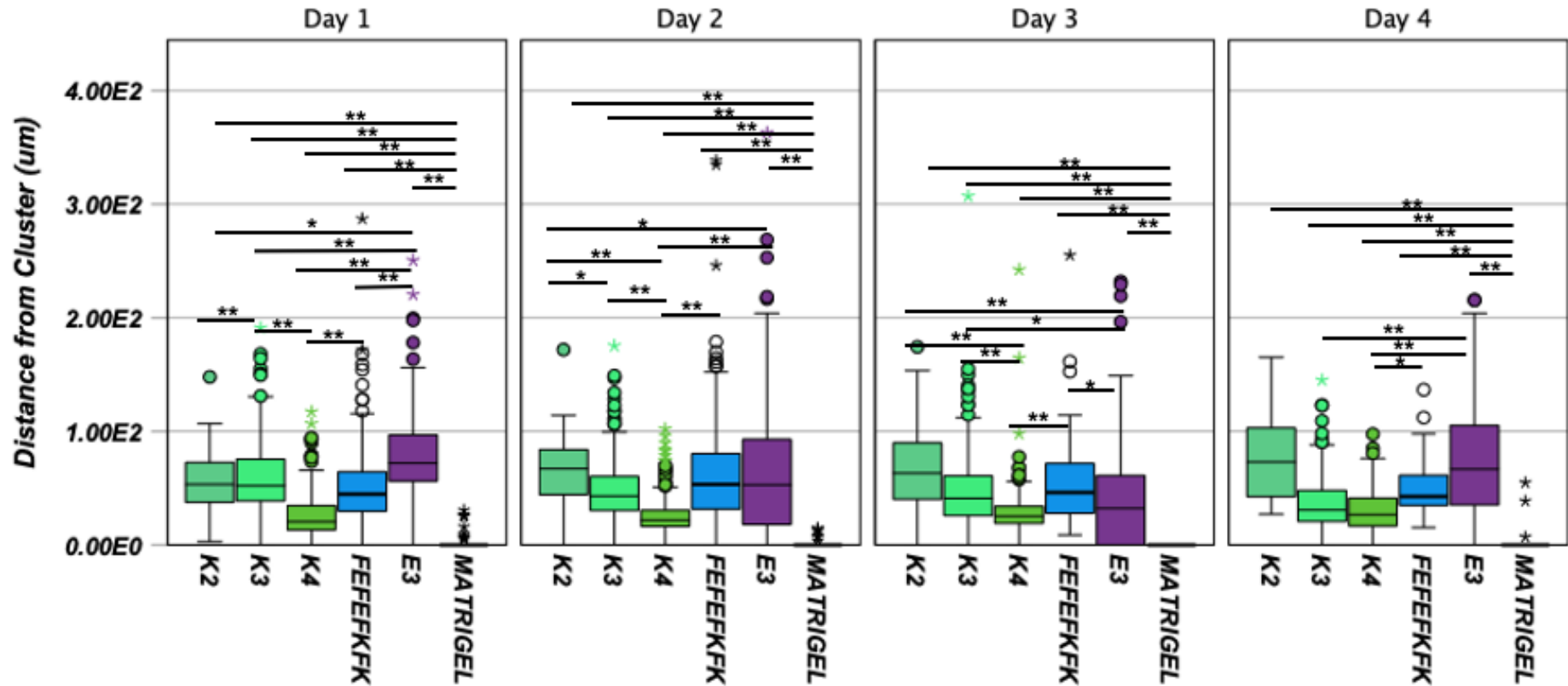


Figure 57. The distance of cells surrounding the clusters per hydrogel.

Box and whisker plots showing the difference in the distance (μm) of cells extending from the cluster per hydrogel. The Matrigel had the lowest distance of cells from the clusters. K4 had was the most similar to Matrigel. There was a decrease in distance of cells from the cluster as the charge increased of the K hydrogels (K2 to K4). Overall, the K2, FEFEFKFK and E3 hydrogels showed similar distances. Statistics completed by MANOVA using SPSS Statistics * $p < 0.05$ ** $P < 0.001$. The number of repeats varied; K2 $n = 3$ (day 0 - day 3) and $n = 1$ (day 4), K3 and K4 $n = 4$ (day 0 - day 3) and $n = 2$ (day 4), FEFEFKFK $n = 3$ (day 0 - day 3) and $n = 1$ (day 4), E3 and Matrigel $n = 2$. Three replicated were present per contition and all clusters (6-8 per replicate) were imaged and measured per day. Outliers shown as dots, extreme outliers shown as stars. The same data as Figure 56.

Peptide amphiphile scaffolds and human induced pluripotent stem cells

Results

There was no significant change in the distance from the cluster to the edge of the plumes of escaping cells, over day 0 - 4 for the clusters on K2 hydrogels (Figure 56). The large interquartile ranges suggest that the plumes around the cluster were not of equal size (Figure 56). The data from K2 clusters on day 4 was compiled from one experiment only and would need repeating to be valid. The clusters on the K2 hydrogel had the largest median spread of all hydrogels and this was significantly larger than the clusters on the K4 hydrogels (Table 21 and Figure 57). The distance travelled by the individual cells on the K2 hydrogels were significantly larger than those on K3 hydrogels until day 1, though the median size of K2 distance was larger than K3 over all days (Table 21 and Figure 57). The hiPSC clusters on K2 produced the largest distance of cell plumes compared to the other positively charged hydrogels, and these cells were mainly dead (Figure 57 and Figure 54).

The distance between cluster and the edge of a plume of cells on the K3 hydrogel decreased over the experiment (Figure 56) as the clusters get bigger (Figure 50). These plumes of cells were mainly dead cells as shown in Figure 54. This could be reinforced by the enlarged images in Figure 55 as the cells surrounding the cluster are dark and flat as seen on the K2 hydrogel where the cells are dead (Figure 54) Therefore, less cells move away from the cluster and die as the culture proceeds. The cells reached a greater distance from the cluster than K4, although the difference was not significant by day 4 (Table 21 and Figure 56). The cells surrounding the clusters on the K4 hydrogel appeared to be a mix of both live and dead cells (Figure 54). In the enlarged image the cells thought to be live were more spherical and raised (Figure 55). This differs from the other positively charged hydrogels. In addition, the clusters on K4 had a much shorter distance between the clusters and the edge of the “escaped” cells, than K2 and K3 (Figure 57). The data also showed a reduction in the interquartile ranges compared to the K2 and K3 data, suggesting that the plumes stretched out from the cluster surface were more uniform in addition to being smaller (Figure 56). There does appear to be

Peptide amphiphile scaffolds and human induced pluripotent stem cells

Results

a trend in the positively charged hydrogels where increasing positive charge (K2<K3<K4) is associated with increased retention of hiPSCs in the cluster.

The distance between cluster and plume edge on neutrally charged hydrogel FEFEFKFK decreased over time (Figure 56), perhaps due to the increased size of the clusters (Figure 50). The cells surrounding the clusters on the FEFEFKFK cluster were both live and dead (Figure 54). The distance between the clusters and the edge of the escaping cells was similar to K2 and not significantly different from K3 (Table 21 and Figure 57). The distance was larger than the distance measured on the K4 hydrogels as shown in Figure 57.

When the distance between the E3 clusters and the edge of cells that had plumed out was measured it decreased from day 1 until day 3, when there was a sudden increase on day 4 (Figure 56). The cells on surface were a mix of live and dead cells (Figure 54 and Figure 55). The distance measured on the E3 hydrogel in Figure 56 showed large interquartile ranges across all days of culture, thereby suggesting that the plumes of cells were not constant and equal around the cluster. The median distances on the E3 hydrogel were similar to those of K2 and FEFEFKFK (Table 21) and except for day 3, was found to be significantly different to the distance on K4 (Figure 57). The extreme reduction in distance on day 3, may have been a true value but there is also a chance it is due to medium changes removing the cells surrounding the cluster.

The clusters grown on Matrigel had no cells extending from their surface and this data was therefore significantly different from all other hydrogels used (Figure 56 and Figure 57). The increased ECM components that were present in the Matrigel have provided an environment

Peptide amphiphile scaffolds and human induced pluripotent stem cells

Results

that encouraged hiPSCs to remain within clusters during culture. The next hydrogel with smallest extensions of cells was K4 (Figure 57).

To conclude, the cells surrounding the K2 and K3 hydrogels were mostly dead, whereas in the other hydrogels there was a mix of live and dead cells. The reduction of dead cells upon the K4 hydrogel when compared to K2 and K3 clusters, despite the assumed increase in charge may have been simply due to the reduced presence of cells leaving the clusters. The cells escaping from clusters on the E3 hydrogel are believed to be more live than dead, though the live/dead staining (with $n = 1$) would need to be repeated to validate this. The cells may remain viable when upon the E3 hydrogel unlike those encapsulated in E3 as the clusters were placed upon set hydrogels not the more cytotoxic E3 solution.

The cells upon the K2, FEFKFK and E3 hydrogels had the largest distance of cells from the cluster. K4 had the shortest distance of all the PA hydrogels and was most similar to Matrigel, which may suggest an increase in ECM components in the K4 hydrogel that maintained the cells within the clusters. The higher distances of the escaped cells upon the K2 and FEFKFK could indicate a reduction in GAGs or ECM proteins, required to keep the cells within the clusters. To assess this, preliminary immunostaining for GAGs was completed. The migration of escaping cells upon the E3 hydrogels could be the result of reduced sequestration of proteins or due to a potential difference in sequestered proteins. It was also possible that other factors may be at the cause of these observations; including the stiffness of the hydrogel, and these were not able to be assessed.

Peptide amphiphile scaffolds and human induced pluripotent stem cells

Results

3.4.9 Identification of ECM components secreted by hiPSCs cultured on hydrogels

Preliminary immunostaining was completed to test the hypothesis that the different charges expressed on the hydrogels were able to capture different ECM components or to do so with differing efficiency. These changes in native ECM detection could then be considered when reviewing the differences in size, retention, and cell extension from the clusters. The immunostaining was preliminary, as due to several factors there were very few repeats completed. In addition, these preliminary samples were challenging to image due to the large size of the clusters when using the confocal microscope. When imaged, not every plane of the cluster could be captured, which resulted in the images having a darker centre. To counteract this, plans were made to section, paraffin embed and then section the hydrogels.

Due to the practical limitations discussed above, it was impossible to include many of the required control images. It was ensured that the antibodies used had been tested by other lab members and had been found to be specific, but these experiments would need to be repeated in my specific settings before publication. While the FEFEFKFK hydrogel was stained, clusters were rapidly lost from the hydrogel during processing (seen by eye and in agreement with the lack of adhesion noted earlier (Figure 52)) meaning that there were no clusters remaining after the immunostaining. A similar lack of retention also meant there was only one cluster on the K2 hydrogel to be stained and successfully imaged. This reinforced the need for paraffin embedding and sectioning. The images were created from a maximum intensity image across z-stacks.

The preliminary immunostaining aimed to assess the presence of HA (hyaluronic acid) and CS (chondroitin sulfate), both GAG components found in the ECM (sections 1.3 and 3.1 intro). HA binding protein detected HA in the clusters cultured on K3 and K4 hydrogels (Figure 58).

Peptide amphiphile scaffolds and human induced pluripotent stem cells

Results

The staining is weak, whether due to limited HA or abnormal immunostaining was unknown, as it was not present in all repeats. There was no evidence that there was a difference in the amount of HA in either K3 or K4 (Figure 58).

CS is present on the more positively charged hydrogels K3 and K4 but not K2 (Figure 58). CS showed two distinct distribution patterns (Figure 58 and Figure 59). The K3 clusters retained CS on individual cells on the surface of the cluster but does not present on every cell. The clusters cultured on K4 showed an increased amount of CS compared to K3 (Figure 58 and Figure 59). CS was observed on single cells (Figure 58, shown by *) but was also found in plumes extending from the cluster (Figure 59). This data suggests that there was trend along the K hydrogels, where an increase in charge resulted in an increase in retention of the CS GAG present around the cluster. However, the lack of CS in the K2 hydrogel may be due to abnormal data or the limited sample size (n=1).

The data shown in Figure 58 and Figure 59 provides preliminary evidence that the charged PA hydrogels were able to capture and maintain at least one GAG, and that this may be charge strength specific. The increase in CS demonstrated the principle. More immunostaining would be needed to get a full picture of the retention of GAGs and other ECM components that could be affected by charged hydrogels. K4 was the most positively charged gel tested (Figure 51), the second most proliferative and demonstrated lowest extension of cells from the cluster (Figure 57) it was therefore the most similar to Matrigel cultured clusters. The increased retention of CS, another GAGs or protein could be responsible for the behaviour of the K4 clusters.

Peptide amphiphile scaffolds and human induced pluripotent stem cells

Results

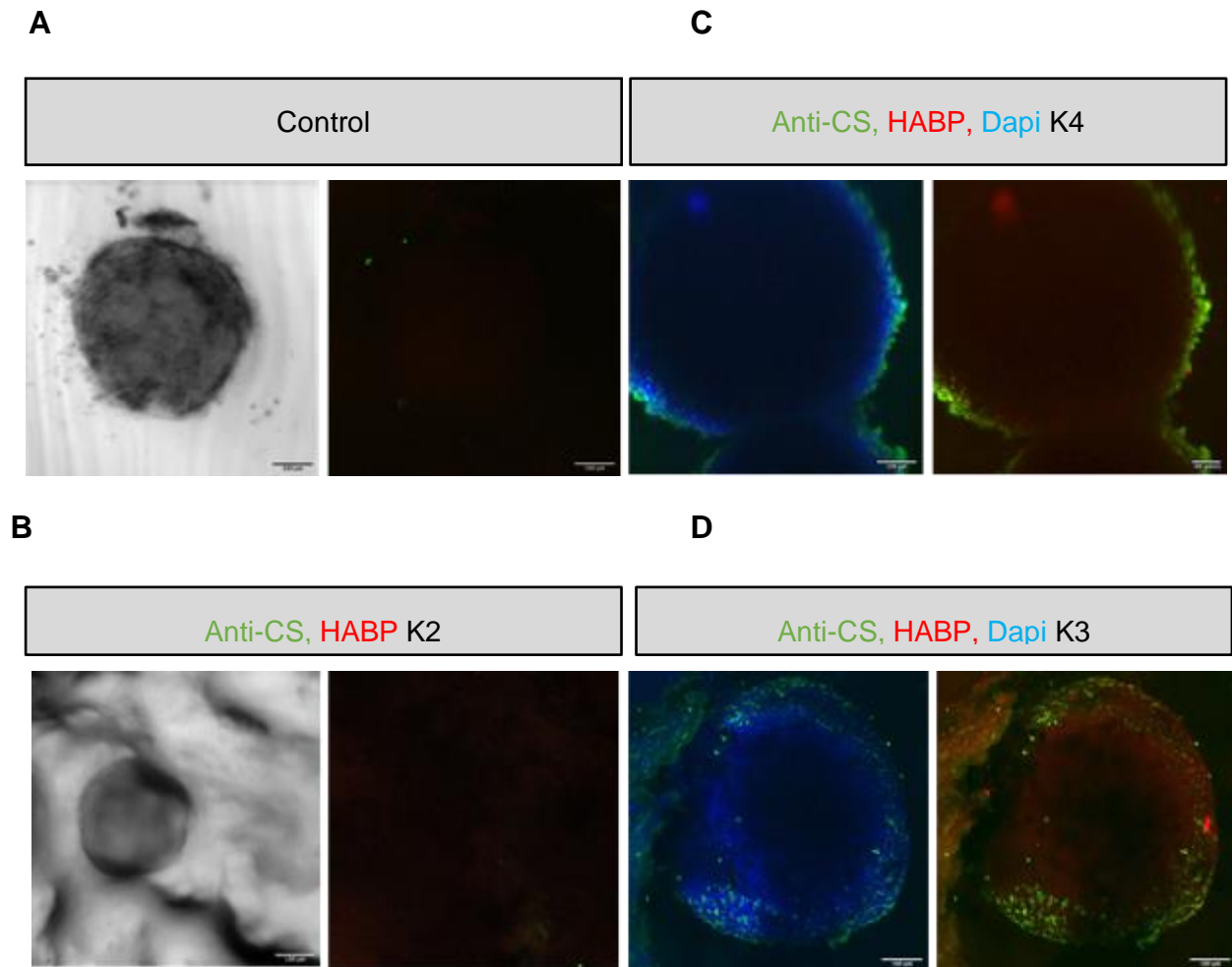


Figure 58. Representative images of Chondroitin Sulphate and HA binding protein immunostaining on day 4.

The ECM proteins HA and CS were identified within clusters on K PA hydrogels. **A** Control immunostaining without primary antibody, showing no non specific staining of the secondary antibody. **B** Cluster cultured on K2 hydrogel, no HA and CS were identified. **C** Cluster cultured on K4 hydrogel, there was identification of HA and CS. **D** Cluster cultured on K3 hydrogel, HA and CS were identified. Scale bars 100µm n=3.

Results

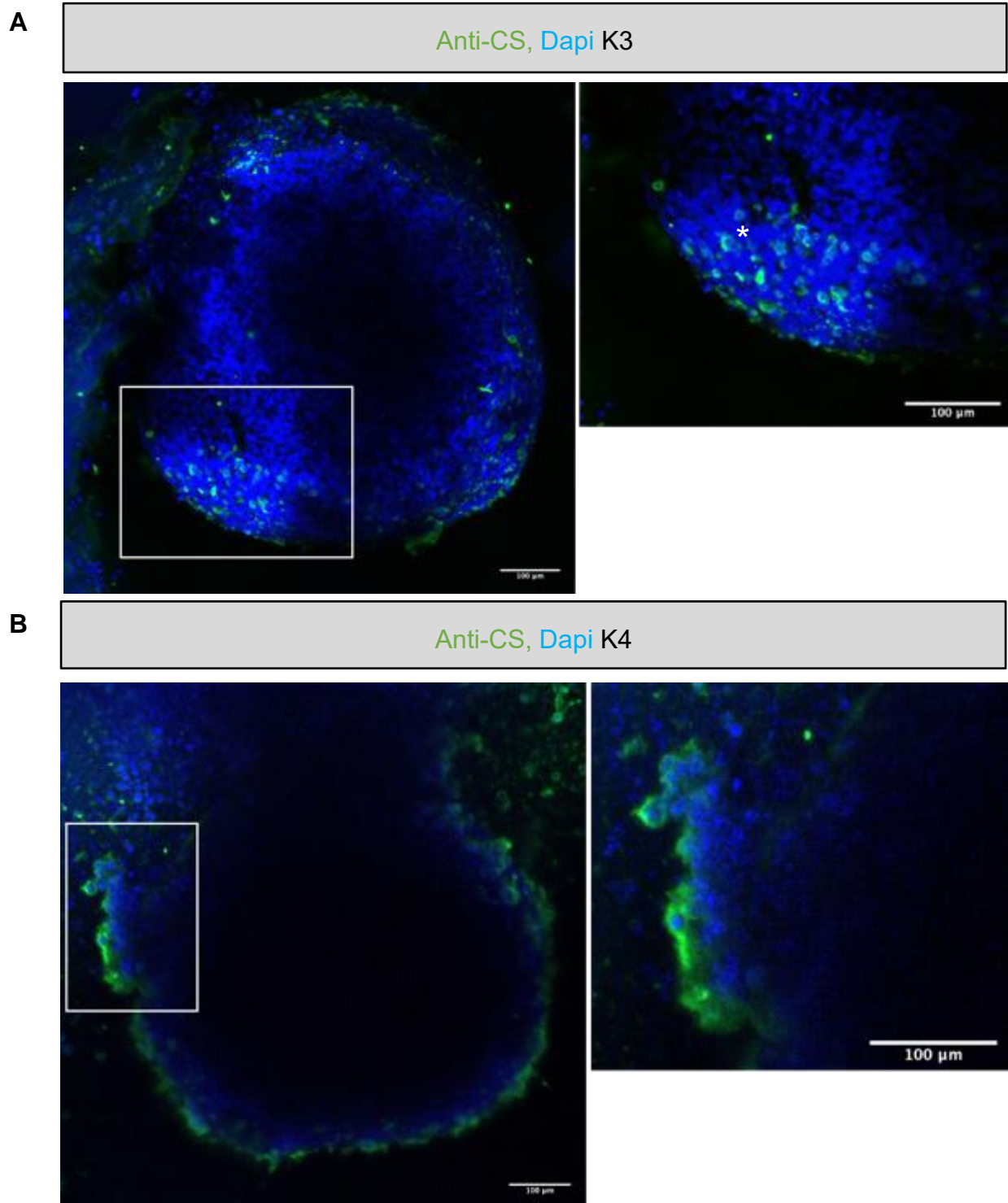


Figure 59. Enlarged representative images of CS immunostaining in K3 and K4 on day 4. **A** K3 cluster close-up of anti-chondroitin sulphate antibody and dapi. The CS was located around single cells of the clusters, this was denoted by * single cell presence of anti-chondroitin sulfate highlighting the difference in expression pattern. The K3 hydrogel had reduced and more localised CS than K4. **B** K4 cluster close-up of anti-chondroitin sulphate antibody and dapi. The CS staining located in plumes extending from the cluster. N=3. All scale bars =100mm.

Discussion

3.5 Discussion

3.5.1 The encapsulation of hiPSC clusters in E3 PA

When encapsulated using the E3 PA, toxicity to the hiPSC clusters was observed. This was found to be associated with exposure of the cells to PA when in solution, whether nonaligned or aligned (E3). The cells categorised as dead were flat and optically clear which may indicate a puncture of the phospholipid bilayer by the PA. The CaCl₂ concentrations (10mM, 15mM and 20mM) had a slight toxic effect but it was found that there was an optimum concentration, dependent upon the alignment of the E3. The nonaligned E3 had the least cell death when the highest CaCl₂ concentration was used (20mM) and the aligned E3 had the optimum retention of cell viability when the CaCl₂ concentration was intermediate (15mM). An explanation for this could be that the PA is toxic when in solution but was not toxic, or at least less so, once formed into a hydrogel. As the aligned E3 gelled quicker, a lower concentration of CaCl₂ was needed to achieve gelation. There was, however, a limited number of repeats for the optimisation of encapsulation of clusters in E3 and further work would need to be conducted to clarify this observation.

3.5.2 Toxicity of E3 to the hiPSCs

E3 PA interactions with the hiPSC cell membranes

The toxicity of the E3 PA was demonstrated by the change in morphology from condensed smooth cell clusters to visible flat, lighter cells, and the subsequent live dead staining. Clusters cultured in not set E3 (no CaCl₂) had the highest percentage of dead clusters (category 1). This toxicity was unexpected, as the cell membrane has a negative charge due to the presence of negatively charged glycans, including GAGs (Yamada et al., 2012, Nishino et al., 2020) and there was an expectation that a negatively charged PA would not interact with the cell membrane due to charge repulsion (Bakhti et al., 2013, Li et al., 2022b). To reinforce this

Peptide amphiphile scaffolds and human induced pluripotent stem cells

Discussion

conclusion, E3 has been used to encapsulate viable cells (Webber et al., 2010c, Zhang et al., 2010).

Most cell penetrating peptides (CPP) are cationic (Derakhshankhah and Jafari, 2018) and as such, there will be an interaction between the positively charged peptide and the negative cell membrane. CPPs, as mentioned above, are molecules that are able to penetrate the cell membrane and are often positively charged, reviewed (Derakhshankhah and Jafari, 2018). CPPs have been researched for their usage as carriers for macromolecules (Bolhassani et al., 2017) and in cancer treatment (due to an increased positive charge upon cancer cells, preferentially attaching CPPs) (Song et al., 2015). CPPs are 5 – 30 residues long (Derakhshankhah and Jafari, 2018). CPP's have several methods of entering cells, but the most relevant here is direct penetration through the cell membrane (Derakhshankhah and Jafari, 2018).

The pericellular ECM or glycocalyx differs between cell types, for example the human dermal cells have a consistent glycocalyx with a thickness of 10 - 22nm, and the undifferentiated murine cardiac cells had a heterogeneous glycocalyx of 2 – 200nm, the differentiated murine cardiac cells had a smooth thin glycocalyx with a thickness of 12 – 25nm (Janczyk et al., 2010, Junior et al., 2016). It may be the case that the glycocalyx on different cell types also differs in the strength of the negative charge, for example the human bladder cancer cell line T24 is more negatively charged than the benign immortalised urothelial UROtsa cell line (von Palubitzki et al., 2020). Therefore potentially allowing the negative PA to interact with the cell membrane, despite the negative repulsion. It may be that the concentration of the individual PAs was so high that interactions between the PAs and cell membranes was inevitable. There has been interaction between negative penetrating peptides with the negative cell membrane

Peptide amphiphile scaffolds and human induced pluripotent stem cells

Discussion

(though rare) (Oehlke et al., 2002, Kim et al., 2021). The negatively charged CPPs were needed to have higher concentrations (Oehlke et al., 2002, Kim et al., 2021).

When comparing the current study with previous work, it is possible that there is some impact of the specific concentration of PAs to which cells are exposed. In the experiments carried out by *Webber et al.* the concentration of the PAs within the hydrogels was 0.01%w/v (*Webber et al.*, 2010d). In the work described here, we used PAs at 1% w/v (~ 8.67mM). This, therefore, increased the concentration of PA molecules that could interact with the encapsulated cells and may have increased toxicity. One possibility is that there is a minimum number of PA interactions that can be tolerated by the cells. A second possibility was that differing cell types are more sensitive to the PA interactions with the cell membrane.

Previously the interactions of positive CPPs with HS upon the cell membrane were shown to be the result of electrostatic interactions, hydrogen bonding and hydrophobic interaction (*Åmand et al.*, 2012). Therefore, hydrogen bonding or hydrophobic interactions with GAGs or ECM proteins, expressed on the hiPSCs may be enough to result in interactions with E3 molecules PA molecules despite the electrostatic repulsion.

Cytotoxicity of the PA solution

While most CPPs in use are not cytotoxic, some have been found to be so when at high concentrations, for example the amphipathic peptide FLUOS-KLALKLALKALKKAALKLA-NH₂ was found to be toxic to aortic endothelial cells at concentrations above 2µM (*Scheller et al.*, 1999). The cationic peptides are known to cause cell death through membrane disruption, and that may also be the cause of the cell death here (*Lv et al.*, 2006, *Åmand et al.*, 2012). For example, MAP (a CCP) can kill microbial cells by disturbing their cell membranes (*Saar*

Peptide amphiphile scaffolds and human induced pluripotent stem cells

Discussion

et al., 2005) due to its amphipathic nature (Zorko and Langel, 2005). Amphipathic CPPs can form pores within the cell membrane due to their hydrophobic regions (Moutal et al., 2015). MAP can then cause cell death as the contents of the cells can leak out and finally result in cell membrane collapse (Saar et al., 2005).

Newcomb et al. demonstrated that the cytotoxic segment of positive PAs was the hydrophobic alkyl tail, when the alkyl tail was not present the positive PAs were not cytotoxic (Newcomb et al., 2014). E3 contains the same alkyl tail. Specifically, the positive PA molecules were seen to intergrade into the cell membrane followed by rapid cell death (Newcomb et al., 2014). The addition of the individual PAs into the cell membrane has been theorised to increase the membrane fluidity resulting in increased curvature and rupture (Newcomb et al., 2014, Heerklotz, 2008). Cell rupture resulting in membrane leakage may also explain the appearance of the dead cells, where they were flat and optically clear as if the internal structures are no longer present.

The beta-sheet forming residues have been seen to be a critical factor in defining the outcome of PA interactions with cell membranes. Typically, the stronger the hydrogen bonds formed between PA units, the more viable the cells (Helen Zha et al., 2016). This is because the PAs in solution form micelles due to the beta-sheet residues (Helen Zha et al., 2016) thereby preventing the PAs from interacting with the cell membrane (Schreier et al., 2000). The weaker the micelle the greater the chance of PAs interacting with (and disrupting) the cell membrane (Newcomb et al., 2014, Monteiro et al., 2014). To extend this, PAs are toxic when “free” to interact with the cell membrane, but when captured into structures, as such when formed into nanofibers, the PAs are less toxic. This is reinforced by the death of all the hiPSC clusters while in presence of E3 monomers in solution.

Peptide amphiphile scaffolds and human induced pluripotent stem cells

Discussion

The non-aligned E3 preserved the highest proportion of live cells with the highest concentration (20mM). This could be due to a potentially more rapid formation of nanofibres, compared when gelled with the lower concentrations (10mM 15mM). This is likely due to there being more Ca^{2+} ions to screen the charges upon the individual PAs and trigger the cytotoxic PAs into nanofibres where their ability to interact with the cell membrane was reduced. Once gelled the PAs cannot then interact with the cell membrane. The aligned E3 gelled much quicker (Zhang et al., 2010) than the non-aligned and therefore required less CaCl_2 to achieve nanofibres. The increased speed of gelation in aligned E3 was the result of heating which caused alignment of individual PAs. After alignment, the PAs form a structure described by *Zhang et al* as fused bundles, where the PAs were already in close contact with one another, thereby reducing the time taken to achieve gelation (Zhang et al., 2010). The reduced toxicity observed for the aligned E3 could also be due to a reduced ability of individual PAs to interact with the cell membrane as they are already within a fused bundle structure (Zhang et al., 2010) not micelles.

A fluorescently labelled E3 PA, membrane impermeable dye (propidium iodide) (Dengler et al., 1995) or cell membrane marker (MemGlow probes) (Collot et al., 2019) could allow for a deeper understating of the method through which the E3 PA was cytotoxic by live imaging in the time immediately following the clusters being placed within the E3 solution. Quantification of any cell membrane damage could be completed by the lactate dehydrogenase (LDH) leakage assay. LDH is an enzyme that is released upon damage to the cell membrane, the number of lysed cells can then be assessed through a colour change reaction (Saar et al., 2005). Another common method to study peptide-membrane interactions is the creation of large unilamellar vesicles (LUV) with an encapsulated fluorophore. Once the LUV are damaged the fluorophore is released and a fluorescence signal is released (Madani and Gräslund, 2022).

Peptide amphiphile scaffolds and human induced pluripotent stem cells

Discussion

3.5.3 Gelation by CaCl₂

The presence of Ca²⁺ ions are a major component in the maintenance of eukaryotic cells as it is involved in many different pathways within the cells (Ahamad et al., 2021, Murgia et al., 2009). However, it has been linked to cell death (Quarato et al., 2022) as reviewed in (Orrenius et al., 2003). Previously in preliminary work for an alginate hydrogel with Schwann cell line (RSCs 96, CRL 2765) were treated with concentrations of CaCl₂ (100mM, 500mM and 1M), all resulted in the cell death for 50% of cells (Cao et al., 2012) and as such any use of CaCl₂ should be monitored for cytotoxic effects..

CaCl₂ is a common method used to trigger PA gelation. In a previous study, differing cell types encapsulated with 10mM CaCl₂ were shown to be viable (Beniash et al., 2005). This suggests that any toxic effect from CaCl₂ would only be minimal at this concentration. However, in the method applied in the current study, CaCl₂ was used at higher concentrations (20mM and 15mM) for 30 minutes before the addition of culture medium.

The gelling solution used into gel E3 in the present study was a CaCl₂ solution in varying concentrations, was different from those used previously. *Zhang et al* used 160mM NaCl and 7mM CaCl₂ to create instantaneous threads/noodles by dragging the PA solution through the gelling solution, an extremely quick gelation occurred when using this mixture of salts (Zhang et al., 2010). As Ca²⁺ ions form more robust PA hydrogels than Na⁺ (Beniash et al., 2005), it is suspected that the high concentration of NaCl of 160mM caused the increase in speed of gelation. As a quicker gelation of the E3 hydrogel may reduce cell death in the clusters investigating the concentration and range of ions used to trigger gelation, could offer an additional factor for further analysis.

Peptide amphiphile scaffolds and human induced pluripotent stem cells

Discussion

3.5.4 Formulations of PA hydrogels

The optimisation of PA hydrogels for the culture of hiPSCs on their surface. The toxicity of the PAs was believed present when in solution not when gelled. Due to the inability of the individual PA molecules to interact with and penetrate the cell membrane as, once set, the PAs have formed nanofibres, keeping the hydrophobic alkyl chains in the centre of the fibre. Therefore, further work on the cultures was conducted upon gelled hydrogels.

The specifications for the PA hydrogels were influenced by the physical limitations in place during the re-opening of the labs post-pandemic, as well as technical specifications. The final optimised method used a 100µl PA hydrogel which was strong enough to withstand medium changes during culture, with a central depression. This fulfilled the specification of forming a self-supporting gel within one hour. This is the first time PA hydrogels, without co-assembly of ECM components, have been formed in 96 well plates. In the previous studies, the PA hydrogels were gelled through other means or with different specifications required. For example, hydrogels gelled on coverslips (Storrie et al., 2007), droplets in a well (Osuna de la Peña et al., 2021) or were much larger for implantation (Mata et al., 2010). These methods were not suitable for creating PA hydrogels in wells as it was necessary to fill the entire well to make sure all clusters were in contact with the PA hydrogel. To gel the PA hydrogel the optimum method was to swirl the salt solution (PBS or CaCl₂) through the PA solution (E3 or K) to create a gel that filled the well.

As discussed above, gelation of the E3 PA hydrogel was achieved using CaCl₂. Although the concentrations used in the present study were different from those used previously (for E3) the incubation of the set hydrogels with medium overnight prior to addition of hiPSC clusters was predicted to reduce the risk of any negative effect from the increased concentration of

Peptide amphiphile scaffolds and human induced pluripotent stem cells

Discussion

Ca²⁺. In addition, the use of CaCl₂ as a gelator has been shown to produce a stronger hydrogel than those made through pH alteration (Greenfield et al., 2010, Stendahl et al., 2006). Therefore, the use of Ca²⁺ allowed for a hydrogel that did not deform during culture.

Gelation of the K PA hydrogels was achieved using a salt solution (PBS) as had been used previously (Beniash et al., 2005, Hartgerink et al., 2002). The pH of the K PA solutions for K3 and K4, altered the time it took for them to gel, as the pH was more acidic, the charges on the lysine more positive which may result in reduce micelle formation in solution due to increased charge repulsion. Thereby increasing the time to gel the K3 and K4 hydrogels when the pH was 3. As the unaltered pH was the quickest to gel for both K3 (pH 5) and K4 (pH 4), that pH was selected for further gel production, as time was an important specification.

The hydrogels in this work were specific to the desired specifications for this application and, while not applicable to all research within the area of PA hydrogels, it demonstrated how adjusting the parameters for creating PA gels changed the outcome. The application of PA hydrogels allows for the design of shapes with desired characteristics and a complete control of any hydrogels produced (Capito et al., 2008, Mata et al., 2009, Redondo-Gómez et al., 2019).

The K2 hydrogel was quick to form under all tested pHs which may suggest an application in 3D printing. As the material is printed, any non-gelled material can deform due to gravity and liquid like nature of the printed material, the quicker a material gels the better the printed shape is retained (Shiwarski et al., 2021, Sakai et al., 2021). This prevents the layer-by-layer building of the required shape. When the printed material is quick to gel and rigid enough, it is possible to build complex structures.

Peptide amphiphile scaffolds and human induced pluripotent stem cells

Discussion

3.5.5 pH of PA hydrogels

This work was the first to provide evidence that PA hydrogels have distinct pH values dependent upon the individual PA, not just while in solution but when gelled. K4 was shown to be the most acidic PA assessed with the lowest pH while in solution and even following gelation. The differences in pH were seen to be small as phenol red demonstrates a limited pH range. The assumed charges associated with the PAs were not sufficient to cause toxicity to hiPSC clusters, the medium will be involved in buffering the pH to levels safe for the cells. The differences in pH were however, enough to suggest that there was a difference in charge upon the hydrogels as it demonstrated the difference in H⁺ ions present in the PA hydrogels. The K4 hydrogel has the most K residues and should have the most protonation thereby potentially having a higher H⁺ presence. The PA hydrogels and their perceived charge could capture different levels of GAGs, providing support for the selection of these PAs to test the hypothesis. Ideally, there would be a measurement of the PA hydrogel charge after gelation, repeated daily to assess changes in charge during culture by surface zeta potential (Goto and Teramoto, 2020). This assessment of charge would demonstrate if the charge of the hydrogels is buffered by the addition of medium over the culture days.

In the future, alterations in PA concentrations could be used to increase the charge of the PA hydrogels. A further analysis of whether there will be an increase in sequestration due to this change in charge and if there is a difference in composition of sequestered matrix proteins. This may allow an assessment of additional characteristics for tuneable hydrogels for a desired purpose.

Peptide amphiphile scaffolds and human induced pluripotent stem cells

Discussion

3.5.6 Size for hiPSC clusters

Once the PA hydrogels were optimised the hiPSCs cluster size was assessed both for the ability to be physically manipulated and the viability of the clusters on top of the hydrogels. The cell density within embryoid bodies (cell clusters able to differentiate into all three embryonic lineages) influences viability and larger aggregates can suffer from necrotic cores (Valamehr et al., 2008, Van Winkle et al., 2012). Embryoid bodies have been formed from cell numbers as low as 150-200 (hESCs and hiPSCs) (Bogacheva et al., 2021, Mohr et al., 2010). The ability to physically manipulate the hiPSC clusters demonstrated that the larger sized clusters (1500 and 2000) were most suitable for further experiments due to the easier visibility, reliability of cluster production and their robustness. This is in line with other research when embryoid bodies made from 1000 cells were difficult to see (Sharma, 2016).

In previous studies, cross-sectional area has been used as a measure of hiPSC health (Mohr et al., 2010). In the present study, all the cell densities tested produced clusters of differing size with some variation as expected. Further to this, small sized clusters were found to decrease in size over the culture days, perhaps due to an inability to proliferate. Small aggregates of hESCs have been found to proliferate less than larger aggregates, using the proliferation marker Ki-67 (Nath et al., 2017). The decrease was suspected to be due to reduced cell-cell interaction (Xu et al., 2010b) and a reduction in growth factor expression (Nath et al., 2017), though it is unknown if this is the case in the current study. The cross-sectional area of the clusters created using 1000 cells did increase over the culture time, demonstrating that there was no overt toxic effect from the hydrogel and that the reduction in size observed with the smaller aggregates was likely due to the starting cell number. In addition, this could explain why some of the clusters began to decrease in size in the early days of culture but grew on later days. It likely took time for the cell number to reach a sufficient level to promote proliferation, and the clusters that could not reach this number decreased in

Peptide amphiphile scaffolds and human induced pluripotent stem cells

Discussion

size. The largest hiPSC clusters had a greater variation of cross-sectional area due to the greater risk of clusters touching and thereby merging, this increased the number of outliers.

The smaller hiPSC clusters were also found to have the poorest retention on top of the PA hydrogels. hiPSC clusters made by *Bogacheva et al* using 50 to 100 cells were seen to dissociate over the first two days of culture (Bogacheva et al., 2021), which could explain the lack of retention. The clusters made using 200 – 1000 cells were able to be maintained in suspension culture and encapsulated in a hydrogel (Bogacheva et al., 2021). In the present study, clusters formed from 750 cells were no longer present by day 3. The process of encapsulation and suspension culture may have protected the clusters in the *Bogacheva* study from stress during culture, in a way that culture on top of the PA hydrogels could not (Bogacheva et al., 2021). The lack of retention may also have been due to the inability of the hiPSC clusters to maintain their attachment to the PA hydrogel, particularly as the limited number of cells present would reduce the total amount of SNMC released to interact with the hydrogel which, in turn, could reduce potential attachment sites to the PA hydrogel. The clusters formed from 1500 cells were the most able to be retained on the PA hydrogels. This was likely due to their attachment being stronger than for the smaller clusters and that these clusters may express more SNMCs resulting in a stronger connection to the PA hydrogel.

However, by the end of the culture period (4 days) no difference was observed between the clusters formed from 1500 and 2000 cells, suggesting that there was a size at which the clusters could not be maintained, most likely due to the physical stress involved in medium changes. The effect of the forces present during medium changes was stronger than the connection the clusters had to the hydrogel, perhaps through the SNMC captured.

Peptide amphiphile scaffolds and human induced pluripotent stem cells

Discussion

3.5.7 Viability of hiPSC clusters on the hydrogels

The clusters were then cultured on top of the hydrogels (Matrigel, K PAs hydrogels, FEFEFKFK and E3). The hiPSCs clusters were viable on all the hydrogels, in contrast to the cell death that was observed when they were encapsulated in E3 PA in solution. However, the individual cells (migrated away from the cluster) on the K2, K3, K4 and E3 hydrogels were found to be both live and dead cells. There has been research to suggest that the hiPSC being in single cells is detrimental (Pakzad et al., 2010, Pijuan-Galitó et al., 2016) but as the cell death was perceived to be greater on the K2 and K3, the K PAs may play a role in the cell death. The individual PAs in the K hydrogels were in the nanofibre structure as the hydrogel was formed prior to exposure to the cells, and therefore the individual PAs should have been unable to interact with the cell membrane. However, there were areas of the K2 and K3 hydrogel that showed deformities or holes during culture. It may therefore have been possible for cell death to occur due to broken nanofibres on the surface interacting with single cells, leading to cell death, similar to that seen in the PA solution.

3.5.8 The sequestration of GAGs and ECM proteins and differences in behaviour

Clusters upon Matrigel

Matrigel and the FEFEFKFK hydrogels have been used previously to culture hiPSC clusters (Ashworth et al., 2020b). Matrigel was a control to demonstrate the effect of having exogenous ECM components present upon the hiPSC clusters. Matrigel provided excellent attachment between the clusters and hydrogel. The presence and absorption of exogenous ECM proteins (i.e., fibronectin, have been found control the ability of cells to adhere to scaffolds (Calonder et al., 2005). The ECM components (including fibronectin and laminin) abundant within Matrigel (Kleinman and Martin, 2005) could have allowed for interactions with integrins and other cell receptors and as such there were strong enough connections between the Matrigel

Peptide amphiphile scaffolds and human induced pluripotent stem cells

Discussion

and the hiPSC clusters that few clusters were lost. The presence of ECM components within Matrigel may also enhance sequestration of matrix components secreted by the cells due to the extensive binding capacity of ECM components.

The measurement of cluster cross-sectional area demonstrated that there was a difference in proliferation between clusters clustered on different hydrogels. As expected, using Matrigel had the greatest proliferation in the clusters. The enriched ECM environment provided an optimised environment for proliferation, whether through maintenance of focal adhesions allowing retention of cell clusters on the scaffold or sequestration of growth factors (Gérard and Goldbeter, 2014).

Matrigel showed negligible numbers of cells separate from the clusters suggesting that the high levels of ECM components in Matrigel provided an environment that supported the cells to form strong cell-cell connections and did not encourage migration away from the cluster. From careful observation it appeared that the clusters were sufficiently discrete that, even if clusters were close enough to touch and make contact, the cells remained discretely within their distinct clusters, unlike those on the other hydrogels.

While the work presented here has been completed on a 2D hydrogel there have been previous studies investigating the effect of matrix density on non-directional cell migration. Typically, the denser matrices were associated with a reduction in cell migration (Plou et al., 2018, Gonçalves and Garcia-Aznar, 2021). The more ECM components in the matrix and the smaller the pore size, the less migration observed (Wolf et al., 2013, Sabeh et al., 2009). In the current study, it may be that the Matrigel has provided an environment with sufficiently dense ECM components that the hiPSCs cannot easily migrate away from the clusters.

Peptide amphiphile scaffolds and human induced pluripotent stem cells

Discussion

Transmission electron microscopy imaging to assess the pore size of the hydrogels before and after culture would be useful to investigate if the density of sequestered ECM components was playing a role in preventing hiPSC migration.

Clusters upon K hydrogels

The K hydrogels showed that the charged hydrogels do sequester GAGs, specifically, chondroitin sulfate (CS) and that the hydrogel with the greatest charge (K4) sequestered the most CS. This conclusion was drawn from a limited set of immunostaining data, however there was good consistency between images. The HA staining was less consistent and could not be used to draw conclusions. However, the CS sequestration shown provides good initial data to encourage further confirmatory work to investigate the ability of physical characteristics of hydrogels, in this case charge, to control the sequestration of GAGs from cells in culture.

While the current project is novel in that my focus is on the sequestration of native secreted matrix and GAGs, this work is in line with previous studies that have demonstrated how charged (both positive and negative) synthetic hydrogels can capture exogenous proteins (Nagy-Smith et al., 2016). Proteins contain regions of both positive and negative charge (Hartvig et al., 2011) and therefore would be potential targets for sequestration by the charges displayed on the hydrogels whether positive (K hydrogels) or negative (E3 hydrogels) (Nagy-Smith et al., 2016, Schulz et al., 2018).

The present study indicated that there was a correlation between the level of assumed charge on the PA and the amount of sequestration. Previous work on charged hydrogels has additionally identified a link between the charge density and the amount of protein absorbed (Tan et al., 2017, Schillemans et al., 2011). This again is reinforced by the work here, as the

Peptide amphiphile scaffolds and human induced pluripotent stem cells

Discussion

K PAs contains an increasing number of lysine residues with charged side chains (at a pH 7) from K2 to K4 and there was more CS sequestered on K4. The K hydrogels are believed to attract oppositely charged proteins and GAGs. In the case of GAGs, binding sites within GAG ligands typically include basic residues (lysine or arginine) (Xu et al., 2022) and it is therefore not surprising that the K PAs could sequester the CS as observed using immunostaining. Previously, synthetic positively charged hydrogels have been found to absorb proteins, specifically fibronectin and vitronectin (Tanahashi and Mikos, 2003, Schulz et al., 2018). While both molecules are negatively charged at physiological conditions, vitronectin (Whateley and Knox, 1980) was more so (fibronectin 5.6–6.1 and vitronectin 4.8–5.0) (Boughton and Simpson, 1984, Whateley and Knox, 1980) and may therefore have been better retained in charged hydrogels. The K hydrogels were likely to have sequestered ECM proteins and GAGs.

The K PA hydrogels showed an increase in cells attachment from K2 to K3/K4. Careful observation suggests that this may be the result of the manufacturing process, as the K2 hydrogel was found to have physical deformities (holes) in the hydrogel. While K3 was also found to have deformities, they did not prevent attachment of the clusters when compared to those on the K4 hydrogel. This may therefore be due to an increase in sequestered ECM material on K3 and K4 hydrogels. The change in retention may also be due to the sequestered native matrix components (SNMCs). The ability of cells to adhere to a biomaterial can be the result of several different interactions between integrins, other attachment receptors and the ECM components they can bind (Cohen et al., 2004). Previously, positively charged synthetic scaffolds have been found to support adhesion of neural stem cells (Sallouh et al., 2017) and endothelial cells, with evidence of adsorbed fibronectin and vitronectin (Kikuchi et al., 1992). In agreement, hydrogels with increasing positive charge were found to show increased protein

Peptide amphiphile scaffolds and human induced pluripotent stem cells

Discussion

absorption, cellular adhesion to the scaffold (Human mesenchymal stem cells), and an increase in the expression of the $\alpha 5$ integrin subunit (Schulz et al., 2018).

The CS seen on the clusters in K3 and K4 hydrogels may be the from CS on cell membrane PG i.e., syndecans (Iozzo and Schaefer, 2015b). The increased CS content could then form electrostatic interactions with the positive charge on the K hydrogels or with other sequestered ECM proteins, for example fibronectin or collagen (Oldberg and Ruoslahti, 1982, Barkalow and Schwarzbauer, 1994). Alternatively, the increase in CS may be the result of extracellular PGs sequestered into the hydrogel where they could form interactions with integrins (Shida et al., 2019) and CD44 receptors (Hurt-Camejo et al., 1999) on the cells, thereby increasing retention.

In a similar fashion, if there is an increase in HS retained by the K PAs on membrane bound HSPGs will have a further increase in interactions with any ECM components sequestered they can interact with (i.e. collagen, laminin fibronectin, vitronectin (Ori et al., 2011). HA interacts with the CD44 transmembrane protein (Zimmerman et al., 2002, Lee et al., 1993) and has additionally been suggested to promote integrin adhesion (Cohen et al., 2006). The addition of HA to 2D culture systems has been found to increase cellular adhesion (Li et al., 2015, Niepel et al., 2019).

In addition to the sequestration of adhesion proteins and potential electrostatic interaction with integrins, studies have suggested that charge can drive an alteration in the binding between fibronectin and the $\alpha 5\beta 1$ integrin. The positive charges upon the hydrogel were observed to have altered the conformation of fibronectin to allow improved access to binding sites, thereby increasing adhesion (Tang et al., 2018). Further work would need to be completed to identify

Peptide amphiphile scaffolds and human induced pluripotent stem cells

Discussion

the relative influence of retained ECM components and direct cell: scaffold electrostatic interactions on cell attachment in these hydrogels.

Positively and negatively charged hydrogels have demonstrated increased proliferation when compared to non-charged equivalents, and several demonstrated that the positively charged hydrogels showed greater proliferation than the negatively charged (Lesný et al., 2006, Naganuma and Traversa, 2014). This was in line with the proliferation seen in this work. The increase in charge upon the hydrogel has been found to drive greater proliferation (Tan et al., 2017) as seen here in the K hydrogels (K2 < K3 < K4). Previously fibronectin has been able to increase proliferation (Arredondo et al., 2021, Song et al., 2008), as has laminin (Le Bellego et al., 2005) and vitronectin (Heydarkhan-Hagvall et al., 2012), all other possible sequestered matrix proteins. CS (Hsu et al., 2022, Xiong et al., 2021), HS (Öztürk et al., 2016, Dombrowski et al., 2009) and HA (Ehlers et al., 2001, Liu et al., 2016, Hanagiri et al., 2012) have been responsible for increased proliferation.

K4 PA had reduced cell migration away from the clusters than all other PA hydrogels (K2, K3 and E3) and FEFELFK. This may indicate that a greater sequestration of ECM components and a greater retention of cells within the cluster. As with Matrigel, the increased presence of SNMC may produce a dense ECM surrounding the cluster and reducing migration. As the actions of GAG are spatiotemporally controlled by the distinct proteoglycans they are attached to and the sulfation location and amount, further work would be needed to determine if CS or other GAGs play a role in cell retention in clusters on K4 PA and Matrigel, apart from physically interacting with the other SNMC to form a matrix around the cluster.

Peptide amphiphile scaffolds and human induced pluripotent stem cells

Discussion

Taken together it may be that the GAG CS and sequestered matrix components may drive an increase in proliferation, retention on hydrogel and cell retention in cluster, though it is currently impossible to say which the signalling pathway drives this behaviour. As there was differing cellular behaviour on between the K hydrogels and the E3 hydrogels it could also suggest that there is a difference in SNMC due to the presence of opposite charges. As the positively charged hydrogels have the potential to bind to GAGs as well as other ECM components it also poses the question of how much material can be sequestered before there is preferential binding, with selection for the strongest opposite charge.

Difference in sequestration between K and E3 hydrogels

Similarly fibronectin, laminin and collagen I have been found to be adsorbed into negatively charged hydrogels (in the presence of serum containing medium) (Liu et al., 2011). Therefore, it is possible that these ECM components could be adsorbed onto both the K hydrogels and E3 hydrogel.

Although logical to propose that there is reduced GAG accumulation in the E3 PA gels due to the hydrogel and the GAGs having the same charge, this would obviously need experimental validation. Looking at previous studies in this area, platelet adhesion (to HUVECs) when grown on negatively charged hydrogels (substrate) was better than to cells grown on non-charged hydrogel, the authors of the study theorised this was due to a reduced HS content (Chen et al., 2007b). It is impossible to conclude that the E3 hydrogel has no GAGs without further work. As, in specific circumstances, for example during chondrogenesis, GAGs have been observed to increase on negatively charged hydrogels (Calabrese et al., 2017). The interaction of molecules of the same charge was assessed by *Abraham et al.* using charged hydrogels, there was no suggestion that electrostatic repulsion contributed to the release of

Peptide amphiphile scaffolds and human induced pluripotent stem cells

Discussion

like charged cargo (Abraham et al., 2020). It is, therefore, impossible to rule out sequestration of GAGs due to interaction with the nanofibre network of the hydrogel. In an alternative point, the negatively charged GAGs bind to other factors (growth factors etc) or proteins through an electrostatic interaction (Xu et al., 2022), as the E3 hydrogel may be negatively charged it may be able to interact with same proteins that GAGs usually do, allowing retention of the GAGs through secondary sequestration (matrix components binding matrix components already sequestered).

The negatively charged hydrogel may have fewer possible binding options (due to potential charge repulsion of GAGs) and as such a more controlled/specific sequestration. This control in the sequestration will then alter the of range of additional SNMCs sequestered, as these matrix components will bind to one another to form a matrix around the cluster. The closer to the cluster the higher the competition for the positive charges upon the K hydrogels, as new SNMC is continuously being secreted. Therefore, the SNMC with the greater negative charge will remain longer than those with weaker. Keeping the fibronectin example, fibronectin has a smaller charge than vitronectin (Boughton and Simpson, 1984, Whateley and Knox, 1980) and the vitronectin would have a stronger interaction with the K hydrogel charge than fibronectin and may replace fibronectin closer to the cluster. On the E3 hydrogel the ECM proteins with the most positive residues and the those with a less negative charge may be preferentially located near the cluster (Figure 60). As the culture days increase the number sequestration of the SNMC was theorised to increase, if this is the case more SNMC will interact with the already sequestered components. This will result in increased SNMC interacting with previously sequestered SNMC to form a matrix around the clusters. As there may be a preference to binding SNMC due to their charge the surrounding matrix built by interacting with them will differ between differently charged hydrogels.

Peptide amphiphile scaffolds and human induced pluripotent stem cells

Discussion

The PA hydrogels will only have a finite number of accessible charges displayed in the proximity to the cluster, considering; the large variety in ECM components that may be sequestered (with preferential sequestration based on charge), the physical and electrostatic interactions of this sequestered components to each other. The K hydrogels will have GAGs and ECM proteins competing for sequestration against the salts (within the medium and those used to trigger gelation). In addition, the SNMC will have to balance the electrostatic attraction to the K hydrogel positive charge, the electrostatic repulsion between the SNMC themselves and getting close enough to a PA charge to interact. Some SNMC will be unable to interact with the positive hydrogel charges (K hydrogel) if several SNMC are already in close juxtaposition with negative charges (electrostatic repulsion between SNMC and physical space).

While the E3 hydrogels will have to cope with electrostatic repulsion (negative residues on the proteins and between the proteins themselves) the reduction in SNMC attempting to bind to the hydrogel may allow for more ECM proteins to be sequestered proximal to the cluster than the K hydrogels. This assumes that the difference in charge of the PA hydrogels does not alter the amount of composition of SNMC being secreted.

Peptide amphiphile scaffolds and human induced pluripotent stem cells

Discussion

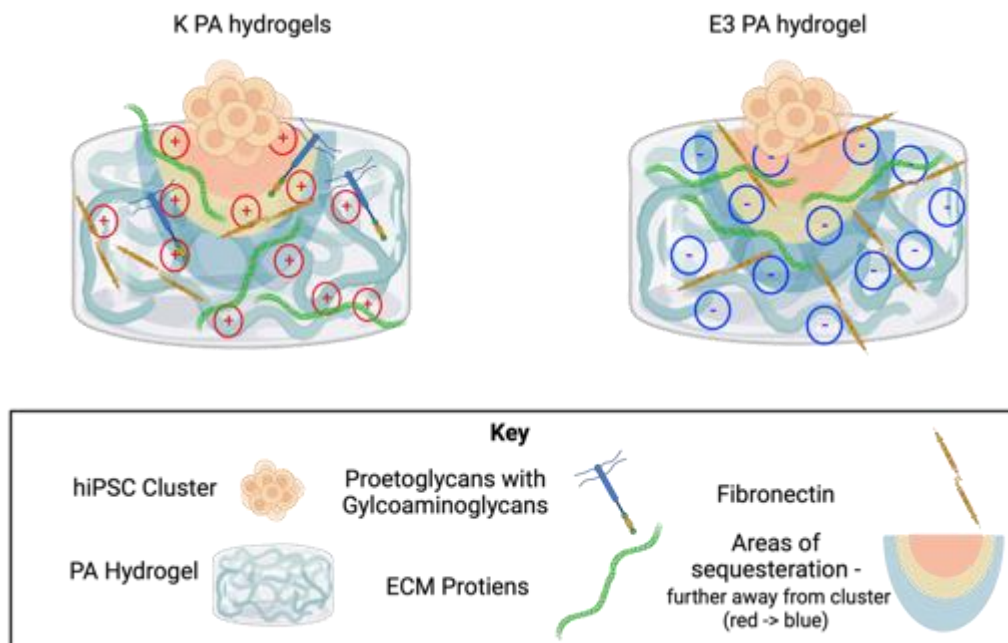


Figure 60. Potential differences in SNMC sequestration between K and E3 hydrogels. K hydrogels are believed to be able to sequester GAGs and ECM proteins, while the E3 hydrogel may only sequester ECM proteins. The areas of sequestration show the key zones for the SNMC to be sequestered in, those closest to the cluster will have a larger affect upon the cells. As the more negatively charged GAGs with bind with greater affinity to the positive charges upon K hydrogels. It may be that due to the GAGs binding less ECM proteins are able to bind to the K hydrogel, particularly the less negative ECM proteins (e.g., Fibronectin).

Clusters upon E3 hydrogel

While previous work using mouse pre-osteoclasts (mouse MC3T3-E1 Subclone 4) (substrate) showed no difference in the retention of cells between negatively and positively charged hydrogels (Tan et al., 2017), here the retention of clusters was greater (~80%) on the E3 hydrogel suggesting a possible difference in ECM proteins sequestered, not considering GAGs. However further work would need to be done to fully assess the extent of this. It is possible that the reduced retention cell clusters on K4 PAs compared to E3 may be due to the larger size of the clusters on the K4 hydrogel. The larger the cluster the greater the forces it

Peptide amphiphile scaffolds and human induced pluripotent stem cells

Discussion

could experience in the medium changes (Brindley et al., 2011) as the clusters are on top the hydrogel.

On negative hydrogels bovine foetal aorta endothelial cells (BFAECs) (Chen et al., 2009b), human umbilical endothelial cells (HUVECs) (Chen et al., 2005), and rabbit synovial tissue-derived fibroblast cells (RSTFCs) were found to proliferate, (Chen et al., 2009a). The clusters on the E3 hydrogel were smaller than the K4 clusters but larger than K2, and K3 hydrogels. This may be due to reduction in charge, 4 lysine residues present upon K4 PAs and only 3 glutamic acid residues on E3 PAs, sequestering less SNMC.

The clusters grown on the E3 hydrogels were associated with individual cells that were distributed further from the clusters than seen on the other hydrogels used. It is possible that this could have been the result of less sequestered material on the E3 gel resulting in less physical impedance (less dense ECM) to cell migration. However, as there was a high retention and increased proliferation (than FEFEFKFK and K2) it seems likely there more were SNMC sequestered than K2 and FEFEFKFK hydrogels. As discussed above, the E3 hydrogel may have less sequestered GAGs than the K series PA hydrogels. Therefore, it's possible that retained ECM proteins, specifically fibronectin could be the basis of retention of clusters on the E3 hydrogel. This increase in adhesion may also lead to an increase in migratory cells as adhesion is one requirement for migration (Pascalis and Etienne-Manneville, 2017). Fibronectin is a major matrix component that can result in cell migration reviewed by (Thiery, 1984, Hynes and Naba, 2012).

Peptide amphiphile scaffolds and human induced pluripotent stem cells

Discussion

FEFEFKFK

Due to their neutral charge at physiological pH, the FEFEFKFK hydrogel was suggested to be the least able to sequester ECM proteins and GAGs. Without these ECM components, the cells would be less able to attach, compared to the charged hydrogels, and this was indeed the case.

In our study, the FEFEFKFK hydrogel was more successful than the K2 PA at supporting cell proliferation, which may suggest that sequestration of matrix materials might not be the critical factor, assuming that the neutral gel was less able to retain matrix factors than K2 PA. A major factor impacting on cell: scaffold interactions is the relative stiffness of the scaffold. This was not specifically addressed in the current study; we need to consider that stiffness influences many aspects of cell behaviour including proliferation (Hadjipanayi et al., 2009). A stiffer hydrogel has been demonstrated to support increased mESC proliferation (Evans et al., 2009), reviewed by (Chan et al., 2020).

Practical limitations meant that I was unable to compare the rheological properties of the PA hydrogels. However, the FEFEFKFK hydrogel has been analysed (500 Pa) (Ashworth et al., 2020b, Ashworth et al., 2020a), suggesting it was a stiff/stronger hydrogel than the PA hydrogels, and this may have supported increased proliferation despite the neutral FEFEFKFK gel having less sequestration of ECM components compared to the PA gels or Matrigel. The effect of stiffness by the PA hydrogels (K or E3) is currently unknown.

Clusters grown on the neutral FEFEFKFK hydrogel showed poor attachment and a high proportion of single cells were also observed, compared to the K4 PA gels and Matrigel. This

Peptide amphiphile scaffolds and human induced pluripotent stem cells

Further work

could be associated with a lack of retention of ECM components (as discussed in detail above) which could then lead to a reduced physical barrier to cell migration.

3.6 Further work

3.6.1 Broader investigation into the sequestered matrix components

The most immediate need is to further investigate the range and relative proportions of matrix components sequestered by the different synthetic environments. This would allow us to address the major remaining questions more directly: Does the increase in charge truly increase the sequestration of matrix components? Is there a distinct difference between matrix sequestration in the positive (K) and negative (E3) hydrogels?

One option would be to undertake metabolic labelling of the secreted matrix proteins, through the incorporation of non-canonical amino acids analogues which are then incorporated into the proteins synthesised by the cells (Loebel et al., 2022). This will give an overview of the amount of selected material without having to identify individual proteins. It will however not label GAGs like HA but will label the PGs some GAGs are bound to. Previous work have used fluorescent beads within the hydrogel to visualise if secreted native matrix proteins physically deformed the hydrogel (Loebel et al., 2022). Pulse labelling using this method would allow for view across culture time, to visualise how the secreted matrix proteins alter their local environment (Loebel et al., 2022).

For a more detailed approach including GAGs without PGs other methods would need to be used. Relatively simple methodologies to do so, would be western blotting or to section the clusters prior to immunostaining. This would allow improved access to the cell: hydrogel

Peptide amphiphile scaffolds and human induced pluripotent stem cells

Further work

interface and, potentially, quantification of staining to directly compare samples. This was attempted, but unfortunately not completed as part of the current study (Ashworth et al., 2020b). Sectioning the hydrogels would provide an increased number of samples to allow for multiple stains (and controls) over serial sections while limiting the number of PA gels required. The work presented here suggests that there may be a difference in the level of CS sequestered in the gel, likely due to charge with the increased lysine residues (positive residue) located on the K4 PA associated with the greatest amount of CS detected. If this is the case, a similar trend may be found to occur with other GAGs including HS, DS and KS. Important targets to include for immunostaining would be heparan sulfate, HA, fibronectin, laminin, and several form of collagens (IV).

A more informative approach may be to an conduct to spatial proteomics, thereby identifying the SNMC quantifiably. One protocol for such relies upon laser-capture microdissection and orbitrap mass spectrometry (Li et al., 2022a). While such a method will provide a general location based proteomic analysis there is a technology that can now be used to analyse proteomics with location targeting to a cellular level through a fluorescent *in situ* hybridisation (He et al., 2022). This would allow for a detailed understanding of the captured SMNC upon each hydrogel in 3D close to and away from the clusters.

Spatial transcriptomics using either tomoseq (van den Brink et al., 2020) or the previously mentioned *in situ* hybridisation (He et al., 2022) potentially linked to spatial proteomics (above) (Yerly et al., 2022) could demonstrate if there is a difference in cellular RNA expression and thereby cell behaviour (e.g., individual cell migration away from the cluster) and what the accompanying SNMC sequestration was. This would allow researchers to select the charged hydrogel that produced the desired behaviour. The spatial transcriptome could also assess if

Peptide amphiphile scaffolds and human induced pluripotent stem cells

Further work

the cells in the centre of the cluster were transcriptionally the same as those on the surface that will be closer to the sequestered SNMC.

The quantification of these proteins will allow for an analysis of whether the increasing amplitude of charge (K2 < K3 < K4) truly results in increased sequestration and whether there are differing matrix components sequestered between K and E3 hydrogels. In addition, it would be useful to study the proteoglycan core proteins the sequestered GAGs are linked to and whether those sequestered were those with the most GAG chains. The number of GAGs linked to a PG can be anywhere from 2 to 100 (Iozzo and Schaefer, 2015b) and influence the behaviour of the cells (Gandhi and Mancera, 2008).

3.6.2 Rheology

Another critical factor to study further is the relative stiffness and elasticity of the gels. The proliferation and migration of cells are cellular behaviours that are influenced by the stiffness and elasticity of biomaterials (Zhong et al., 2020). As changes in these cellular behaviours were observed in the current study it is particularly important to assess the effect of any difference in stiffness. For example, the current theory that associates the cell migration observed on the E3 hydrogel as being due to the sequestration of fibronectin may also be due to a change in stiffness due to the electrostatic repulsion of the charges as seen in work by Gu et al. (2022).

Alternative methods to assess the rheological properties of the PA gels could be tested e.g., atomic force microscopy (AFM). AFM is comprised of a tip mounted to a cantilever, which can then be scanned across a surface. The deformation in the AFM tip can then be computed into a measurement of mechanical properties including Young's modulus through force-distance

Peptide amphiphile scaffolds and human induced pluripotent stem cells

Further work

graphs (Cebull et al., 2017, Ben Bouali et al., 2020). If differences in stiffness were identified between the hydrogels and these were associated with the difference in charge, then it may be possible to alter the stiffness of the PA hydrogels to specific, targeted levels of stiffness, by adjusting the concentration of PA or by alteration of CaCl₂ concentration used. Different PAs have been seen to increase with concentration (Koch et al., 2018) and CaCl₂ concentration (Stendahl et al., 2006). Removing any difference in stiffness will allow a more confident conclusion that the differences seen in cellular behaviour (i.e., proliferation and migration) were due to a difference in SNMC sequestration related to charge. In addition, if the different hydrogels have the same stiffness before any SNMC are captured, then it will be possible to assess if the different sequestration has also resulted in a change in hydrogel stiffness over culture.

3.6.3 Spontaneous differentiation

The ability of the hiPSC clusters to retain their pluripotency was not assessed in the current study and could be addressed with quantification of expressed pluripotency markers (i.e., Nanog and Oct4 using PCR). There is no evidence to suggest that the clusters had differentiated, and the cells were cultured in medium that retains pluripotency. E8, with the presence of TGF- β and FGF2 was expected to maintain pluripotency (Lippmann et al., 2014, Chen et al., 2011). As the clusters were kept in an assumed pluripotent state there was no ability to assess if the differently charged hydrogels could alter the differentiation of the clusters. The charge of hydrogels has been seen to influence the differentiation of hMSCs, into osteogenic, and chondrogenic lineages when on negatively charged hydrogels (Calabrese et al., 2017). As the composition of the ECM, including GAGs, can influence differentiation, as mentioned by the requirement of GAGs to be present for stem cells to differentiate, reviewed by (Wang et al., 2017), it is possible that the sequestration of differing matrix components could result in differing outcomes.

Peptide amphiphile scaffolds and human induced pluripotent stem cells

Further work

Spontaneous differentiation using a reduced medium (E6), has the potential to allow for differentiation into multiple lineages (hiPSCs) (Ashworth et al., 2020b). Spontaneous differentiation in different hydrogels generated in this study would demonstrate if the sequestered matrix components were enough to result in changes to differentiation outcome and whether the different hydrogels could stimulate different differentiations. The ECM is known to be able to control differentiation through stiffness, sequestration of growth factors and direct interaction with ECM components (Schoonjans et al., 1995, Padhi and Nain, 2020). The CS on the K3 and K4 hydrogels may be beneficial for the differentiation into chondrocytes (Varghese et al., 2008, Huang et al., 2015) or a neural differentiation, as CS has been seen to increase differentiations these lineages (Gu et al., 2009, Mencio et al., 2021). The ability of these hydrogels to stimulate spontaneous differentiation may lead to a culture method that uses the secreted matrix to drive directed differentiation.

RNA sequencing (RNAseq) of the clusters on the hydrogels would allow for a complete comparison of the transcriptome (Kim et al., 2022). RNAseq would allow for understanding of the differences across the hydrogels, in multiple areas of cell behaviour (e.g., differentiation, metabolism and ECM deposition). This would provide a complete view of the changes in the cells cultured upon the different hydrogels. Analysis of the transcriptome on a single cell level would allow for an assessment of the differing areas of the clusters, not just the internal vs the surface cells but the cells in contact with the SNMC or the cells with no contact (top of culture). Does the SNMC exert control over the cells in contact with it and do these cells then direct those neighbouring to them?

Peptide amphiphile scaffolds and human induced pluripotent stem cells

Further work

Previous spontaneous differentiation was completed over a longer time frame of 22 days, here the longest cultured was 4 days. This was due to a lack of retention of the clusters on the hydrogels. It may be that further alterations to the method may be needed to allow sufficient time to demonstrate evidence of differentiation.

If a hydrogel was found to show an ability to stimulate differentiation, it may then be worth completing a directed differentiation to see if the hydrogel and the FEFKFK control had similar differentiation.

3.6.4 Additional complexity to the PA hydrogel

To increase the complexity of the hydrogel, motifs be added to the PAs to direct a wanted cellular behaviour. For example, to prevent the low retention of the clusters on the K2 and K3 hydrogels the bioactive epitope, RGDS, could be added to the PAs. The charged residues on the PA containing RGDS (PA-RGDS) were still present in previous PA hydrogels with these epitopes and the PAs had no problems gelling following the addition of oppositely charged proteins (Derkus et al., 2020). The PA with the bioactive epitope could then be mixed with the PA, so make sure that the lowest percentage of PA-RGDS was present while increasing the attachment of the clusters without adversely affecting the behaviour of the cells. There would need to be care, to make sure that any further conclusions are not due to the bioactive epitope. This could be taken further, if a particular PA was found to direct differentiation to a specific lineage but which did not sequester an ECM component that was known to support differentiation, an epitope to allow binding of that ECM component could be added to the selected PA. This would allow for further tuneability for a hydrogel system.

Peptide amphiphile scaffolds and human induced pluripotent stem cells

Conclusion

3.6.5 Encapsulation of hiPSC clusters in PA hydrogels

Despite the use of hydrogels within this chapter, the hydrogels were used as a 2D base for spheroid culture. This results in the spheroids not being able to interact with SNMC in 360° and as such only a small section of the culture is exposed to the SNMC. In addition, as the top of the clusters are not exposed to the hydrogel these cells are not exposed to mechanical stimulation. An improved model would completely encapsulate the clusters.

As shown the encapsulation of the clusters in E3 was not successful and the current optimum concentration of CaCl₂ and the aligned E3 were not suitable for the culture of clusters without significant cell death. It would therefore need further optimisation including alterations to the gelator solution to include NaCl (Zhang et al., 2010) and changes in concentration of PA, which may reduce the interactions of individual PAs and the cell membranes. The use of the aligned E3, would be more likely to allow successful encapsulation as it was less cytotoxic than non-aligned E3. If encapsulation in E3 hydrogel was found to be non-toxic due to these or other alterations, it could allow for the sequestration of secreted matrix proteins around the entire cluster not just under the cluster as shown here.

3.7 Conclusion

To conclude, this is a novel use of a synthetic hydrogel to selectively capture secreted native matrix components through a range of differing charges upon the hydrogels. This work opens the door to a culture system that could capture a range of matrix components in a controllable manner to direct cell behaviour through the cells' own ECM. The cell-controlled secretion of native matrix components will allow for the creation of a complex environment with the optimal ECM and potentially optimal stiffness for the cells to complete a desired behaviour. The use

Peptide amphiphile scaffolds and human induced pluripotent stem cells

Conclusion

of charge will allow for the sequestration of a large range of ECM components that will more accurately represent the tissue or cell niche being modelled.

This pilot study assessed the ability of E3 to encapsulate hiPSC clusters. When the clusters were not found to survive when encapsulated, optimisation was completed to culture hiPSCs on a range of PA hydrogels with an assumed difference in charge. All the hydrogels provided a 2D environment for viable hiPSCs clusters. There was an increase in retained GAGs (CS) associated with an increase in lysine residues upon PAs. Importantly there a difference in proliferation, cluster attachment to the hydrogel and the migration of individual cells away from the clusters, when the clusters were placed on different PA hydrogels. These cellular behaviours were altered in the same pattern as the amount of GAG CS captured. The capture of secreted native matrix components, specifically GAGs can alter the behaviour of cells cultured.

References

CHAPTER 4. REFERENCES

- ABDOLAH, S., GHAZVINIAN, Z., MUHAMMADNEJAD, S., SALEH, M., ASADZADEH AGHDAEI, H. & BAGHAEI, K. 2022. Patient-derived xenograft (PDX) models, applications and challenges in cancer research. *J Transl Med*, 20, 206.
- ABRAHAM, B. L., TORIKI, E. S., TUCKER, N. J. & NILSSON, B. L. 2020. Electrostatic interactions regulate the release of small molecules from supramolecular hydrogels. *J Mater Chem B*, 8, 6366-6377.
- ABUHATTUM, S., KOTZBECK, P., SCHLÜSSLE, R., HARGER, A., ARIZA DE SCHELLENBERGER, A., KIM, K., ESCOLANO, J.-C., MÜLLER, T., BRAUN, J., WABITSCH, M., TSCHÖP, M., SACK, I., BRANKATSCHK, M., GUCK, J., STEMMER, K. & TAUBENBERGER, A. V. 2022. Adipose cells and tissues soften with lipid accumulation while in diabetes adipose tissue stiffens. *Scientific Reports*, 12, 10325.
- ABUNE, L., LEE, K. & WANG, Y. 2022. Development of a Biomimetic Extracellular Matrix with Functions of Protein Sequestration and Cell Attachment Using Dual Aptamer-Functionalized Hydrogels. *ACS Biomaterials Science & Engineering*, 8, 1279-1289.
- AHAMAD, N., SUN, Y., NASCIMENTO DA CONCEICAO, V., XAVIER PAUL EZHILAN, C. R. D., NATARAJAN, M. & SINGH, B. B. 2021. Differential activation of Ca²⁺ influx channels modulate stem cell potency, their proliferation/viability and tissue regeneration. *npj Regenerative Medicine*, 6, 67.
- AHFELDT, T., SCHINZEL, R. T., LEE, Y. K., HENDRICKSON, D., KAPLAN, A., LUM, D. H., CAMAHORT, R., XIA, F., SHAY, J., RHEE, E. P., CLISH, C. B., DEO, R. C., SHEN, T., LAU, F. H., COWLEY, A., MOWRER, G., AL-SIDDIQI, H., NAHRENDORF, M., MUSUNURU, K., GERSZTEN, R. E., RINN, J. L. & COWAN, C. A. 2012. Programming human pluripotent stem cells into white and brown adipocytes. *Nat Cell Biol*, 14, 209-19.
- AHMAD, A., STROHBUECKER, S., TUFARELLI, C. & SOTTILE, V. 2017. Expression of a SOX1 overlapping transcript in neural differentiation and cancer models. *Cellular and molecular life sciences : CMLS*, 74, 4245-4258.
- AHMAD, Z., SALMAN, S., KHAN, S. A., AMIN, A., RAHMAN, Z. U., AL-GHAMDI, Y. O., AKHTAR, K., BAKHSH, E. M. & KHAN, S. B. 2022. Versatility of Hydrogels: From Synthetic Strategies, Classification, and Properties to Biomedical Applications. *Gels*, 8.
- AKHIR, H. M. & TEOH, P. L. 2020. Collagen type I promotes osteogenic differentiation of amniotic membrane-derived mesenchymal stromal cells in basal and induction media. *Bioscience Reports*, 40.
- AKKAYA, E. & GÜNGÖR, H. R. 2022. The dark side of the animal experiments. *Jt Dis Relat Surg*, 33, 479-483.
- AL-GOBLAN, A. S., AL-ALFI, M. A. & KHAN, M. Z. 2014. Mechanism linking diabetes mellitus and obesity. *Diabetes Metab Syndr Obes*, 7, 587-91.
- ALBRECHT, F. B., DOLDERER, V., NELLINGER, S., SCHMIDT, F. F. & KLUGER, P. J. 2022. Gellan Gum Is a Suitable Biomaterial for Manual and Bioprinted Setup of Long-Term Stable, Functional 3D-Adipose Tissue Models. *Gels*, 8.
- ALI, M. Y., CHUANG, C. Y. & SAIF, M. T. 2014. Reprogramming cellular phenotype by soft collagen gels. *Soft Matter*, 10, 8829-37.

References

- ALSBERG, E., ANDERSON, K. W., ALBEIRUTI, A., FRANCESCHI, R. T. & MOONEY, D. J. 2001. Cell-interactive alginate hydrogels for bone tissue engineering. *J Dent Res*, 80, 2025-9.
- ÅMAND, H. L., RYDBERG, H. A., FORNANDER, L. H., LINCOLN, P., NORDÉN, B. & ESBJÖRNER, E. K. 2012. Cell surface binding and uptake of arginine- and lysine-rich penetratin peptides in absence and presence of proteoglycans. *Biochimica et Biophysica Acta (BBA) - Biomembranes*, 1818, 2669-2678.
- ANDERSEN, T., AUK-EMBLEM, P. & DORNISH, M. 2015. 3D Cell Culture in Alginate Hydrogels. *Microarrays (Basel)*, 4, 133-61.
- ANDERSON, J. M., ANDUKURI, A., LIM, D. J. & JUN, H. W. 2009. Modulating the gelation properties of self-assembling peptide amphiphiles. *ACS Nano*, 3, 3447-54.
- ANG, X. M., LEE, M. H. C., BLOCKI, A., CHEN, C., ONG, L. L. S., ASADA, H. H., SHEPPARD, A. & RAGHUNATH, M. 2014. Macromolecular crowding amplifies adipogenesis of human bone marrow-derived mesenchymal stem cells by enhancing the pro-adipogenic microenvironment. *Tissue engineering. Part A*, 20, 966-981.
- ANNABI, N., NICHOL, J. W., ZHONG, X., JI, C., KOSHY, S., KHADEMOSSEINI, A. & DEGHANI, F. 2010. Controlling the porosity and microarchitecture of hydrogels for tissue engineering. *Tissue Eng Part B Rev*, 16, 371-83.
- ANTONIOU, N., PRODROMIDOU, K., KOUROUPI, G., BOUMPOUREKA, I., SAMIOTAKI, M., PANAYOTOU, G., XILOURI, M., KLOUKINA, I., STEFANIS, L., GRAILHE, R., TAOUFIK, E. & MATSAS, R. 2022. High content screening and proteomic analysis identify a kinase inhibitor that rescues pathological phenotypes in a patient-derived model of Parkinson's disease. *npj Parkinson's Disease*, 8, 15.
- ANTRAS, J., HILLIOU, F., REDZINIAK, G. & PAIRAULT, J. 1989. Decreased biosynthesis of actin and cellular fibronectin during adipose conversion of 3T3-F442A cells. Reorganization of the cytoarchitecture and extracellular matrix fibronectin. *Biol Cell*, 66, 247-54.
- ANTTINEN, H., OIKARINEN, A. & KIVIRIKKO, K. I. 1977. Age-related changes in human skin collagen galactosyltransferase and collagen glucosyltransferase activities. *Clinica Chimica Acta*, 76, 95-101.
- ARREDONDO, R., POGGIOLI, F., MARTÍNEZ-DÍAZ, S., PIERA-TRILLA, M., TORRES-CLARAMUNT, R., TÍO, L. & MONLLAU, J. C. 2021. Fibronectin-coating enhances attachment and proliferation of mesenchymal stem cells on a polyurethane meniscal scaffold. *Regen Ther*, 18, 480-486.
- ARUFFO, A., STAMENKOVIC, I., MELNICK, M., UNDERHILL, C. B. & SEED, B. 1990. CD44 is the principal cell surface receptor for hyaluronate. *Cell*, 61, 1303-13.
- ASHWORTH, J. C., MORGAN, R. L., LIS-SLIMAK, K., MEADE, K. A., JONES, S., SPENCE, K., SLATER, C. E., THOMPSON, J. L., GRABOWSKA, A. M., CLARKE, R. B., FARNIE, G. & MERRY, C. L. R. 2020a. Preparation of a User-Defined Peptide Gel for Controlled 3D Culture Models of Cancer and Disease. *J Vis Exp*.
- ASHWORTH, J. C., THOMPSON, J. L., JAMES, J. R., SLATER, C. E., PIJUAN-GALITÓ, S., LIS-SLIMAK, K., HOLLEY, R. J., MEADE, K. A., THOMPSON, A., ARKILL, K. P., TASSIERI, M., WRIGHT, A. J., FARNIE, G. & MERRY, C. L. R. 2020b. Peptide gels of fully-defined composition and mechanics for probing cell-cell and cell-matrix interactions in vitro. *Matrix Biol*, 85-86, 15-33.
- ASSMANN, V., JENKINSON, D., MARSHALL, J. F. & HART, I. R. 1999. The intracellular hyaluronan receptor RHAMM/IHABP interacts with microtubules and actin filaments. *Journal of Cell Science*, 112, 3943-3954.

References

- ASSUMPCÃO, J. A. F., PASQUARELLI-DO-NASCIMENTO, G., DUARTE, M. S. V., BONAMINO, M. H. & MAGALHÃES, K. G. 2022. The ambiguous role of obesity in oncology by promoting cancer but boosting antitumor immunotherapy. *Journal of Biomedical Science*, 29, 12.
- AUMAILLEY, M., BRUCKNER-TUDERMAN, L., CARTER, W. G., DEUTZMANN, R., EDGAR, D., EKBLOM, P., ENGEL, J., ENGVALL, E., HOHENESTER, E., JONES, J. C. R., KLEINMAN, H. K., MARINKOVICH, M. P., MARTIN, G. R., MAYER, U., MENEGUZZI, G., MINER, J. H., MIYAZAKI, K., PATARROYO, M., PAULSSON, M., QUARANTA, V., SANES, J. R., SASAKI, T., SEKIGUCHI, K., SOROKIN, L. M., TALTS, J. F., TRYGGVASON, K., UITTO, J., VIRTANEN, I., VON DER MARK, K., WEWER, U. M., YAMADA, Y. & YURCHENCO, P. D. 2005. A simplified laminin nomenclature. *Matrix Biology*, 24, 326-332.
- AUMAILLEY, M., EL KHAL, A., KNÖSS, N. & TUNGGAL, L. 2003. Laminin 5 processing and its integration into the ECM. *Matrix biology*, 22, 49-54.
- AZARNIA, R. & RUSSELL, T. R. 1985. Cyclic AMP effects on cell-to-cell junctional membrane permeability during adipocyte differentiation of 3T3-L1 fibroblasts. *The Journal of Cell Biology*, 100, 265.
- BABA, S., JACENE, H. A., ENGLER, J. M., HONDA, H. & WAHL, R. L. 2010. CT Hounsfield Units of Brown Adipose Tissue Increase with Activation: Preclinical and Clinical Studies. *Journal of Nuclear Medicine*, 51, 246-250.
- BADYLAK, S. F., TULLIUS, R., KOKINI, K., SHELBORNE, K. D., KLOOTWYK, T., VOYTIK, S. L., KRAINE, M. R. & SIMMONS, C. 1995. The use of xenogeneic small intestinal submucosa as a biomaterial for Achille's tendon repair in a dog model. *Journal of Biomedical Materials Research*, 29, 977-985.
- BAJPAI, S. K. & SHARMA, S. 2004. Investigation of swelling/degradation behaviour of alginate beads crosslinked with Ca²⁺ and Ba²⁺ ions. *Reactive and Functional Polymers*, 59, 129-140.
- BAKHTI, M., SNAIDERO, N., SCHNEIDER, D., AGGARWAL, S., MÖBIUS, W., JANSHOFF, A., ECKHARDT, M., NAVE, K. A. & SIMONS, M. 2013. Loss of electrostatic cell-surface repulsion mediates myelin membrane adhesion and compaction in the central nervous system. *Proc Natl Acad Sci U S A*, 110, 3143-8.
- BALASUBRAMANIAN, R. & ZHANG, X. 2016. Mechanisms of FGF gradient formation during embryogenesis. *Semin Cell Dev Biol*, 53, 94-100.
- BALDWIN, R. J., TEN DAM, G. B., VAN KUPPEVELT, T. H., LACAUD, G., GALLAGHER, J. T., KOUSKOFF, V. & MERRY, C. L. R. 2008. A Developmentally Regulated Heparan Sulfate Epitope Defines a Subpopulation with Increased Blood Potential During Mesodermal Differentiation. *STEM CELLS*, 26, 3108-3118.
- BARBU, A., NEAMTU, B., ZĂHAN, M., IANCU, G. M., BACILA, C. & MIREȘAN, V. 2021. Current Trends in Advanced Alginate-Based Wound Dressings for Chronic Wounds. *J Pers Med*, 11.
- BARCZYK, M., CARRACEDO, S. & GULLBERG, D. 2010. Integrins. *Cell Tissue Res*, 339, 269-80.
- BARKALOW, F. J. & SCHWARZBAUER, J. E. 1994. Interactions between fibronectin and chondroitin sulfate are modulated by molecular context. *J Biol Chem*, 269, 3957-62.
- BARRESI, R. & CAMPBELL, K. P. 2006. Dystroglycan: from biosynthesis to pathogenesis of human disease. *J Cell Sci*, 119, 199-207.
- BECK, K., HUNTER, I. & ENGEL, J. 1990. Structure and function of laminin: anatomy of a multidomain glycoprotein. *Faseb j*, 4, 148-60.

References

- BEN BOUALI, A., MONTEBAULT, A., DAVID, L., VON BOXBERG, Y., VIALON, M., HAMDI, B., NOTHIAS, F., FODIL, R. & FÉRÉOL, S. 2020. Nanoscale mechanical properties of chitosan hydrogels as revealed by AFM. *Progress in Biomaterials*, 9, 187-201.
- BENIASH, E., HARTGERINK, J. D., STORRIE, H., STENDAHL, J. C. & STUPP, S. I. 2005. Self-assembling peptide amphiphile nanofiber matrices for cell entrapment. *Acta Biomaterialia*, 1, 387-397.
- BERG, R. A. & PROCKOP, D. J. 1973. The thermal transition of a non-hydroxylated form of collagen. Evidence for a role for hydroxyproline in stabilizing the triple-helix of collagen. *Biochem Biophys Res Commun*, 52, 115-20.
- BHAVSAR, M. B., CATO, G., HAUSCHILD, A., LEPPIK, L., COSTA OLIVEIRA, K. M., EISCHEN-LOGES, M. J. & BARKER, J. H. 2019. Membrane potential (V_{mem}) measurements during mesenchymal stem cell (MSC) proliferation and osteogenic differentiation. *PeerJ*, 7, e6341.
- BIANCO, P. 2014. "Mesenchymal" Stem Cells. *Annual Review of Cell and Developmental Biology*, 30, 677-704.
- BILTZ, N. K. & MEYER, G. A. 2017. A novel method for the quantification of fatty infiltration in skeletal muscle. *Skeletal Muscle*, 7, 1.
- BIRCH, H. L. 2018. Extracellular Matrix and Ageing. In: HARRIS, J. R. & KOROLCHUK, V. I. (eds.) *Biochemistry and Cell Biology of Ageing: Part I Biomedical Science*. Singapore: Springer Singapore.
- BISSELL, M. J., HALL, H. G. & PARRY, G. 1982. How does the extracellular matrix direct gene expression? *J Theor Biol*, 99, 31-68.
- BLACHE, U., VALLMAJO-MARTIN, Q., HORTON, E. R., GUERRERO, J., DJONOV, V., SCHERBERICH, A., ERLER, J. T., MARTIN, I., SNEDEKER, J. G., MILLERET, V. & EHRBAR, M. 2018. Notch-inducing hydrogels reveal a perivascular switch of mesenchymal stem cell fate. *EMBO Rep*, 19.
- BLASZCZAK, A. M., JALILVAND, A. & HSUEH, W. A. 2021. Adipocytes, Innate Immunity and Obesity: A Mini-Review. *Frontiers in Immunology*, 12.
- BOGACHEVA, M. S., HARJUMÄKI, R., FLANDER, E., TAALAS, A., BYSTRIAKOVA, M. A., YLIPERTTULA, M., XIANG, X., LEUNG, A. W. & LOU, Y. R. 2021. Differentiation of Human Pluripotent Stem Cells Into Definitive Endoderm Cells in Various Flexible Three-Dimensional Cell Culture Systems: Possibilities and Limitations. *Front Cell Dev Biol*, 9, 726499.
- BOLHASSANI, A., JAFARZADE, B. S. & MARDANI, G. 2017. In vitro and in vivo delivery of therapeutic proteins using cell penetrating peptides. *Peptides*, 87, 50-63.
- BONNANS, C., CHOU, J. & WERB, Z. 2014. Remodelling the extracellular matrix in development and disease. *Nature Reviews Molecular Cell Biology*, 15, 786.
- BOUGHTON, B. J. & SIMPSON, A. W. 1984. The biochemical and functional heterogeneity of circulating human plasma fibronectin. *Biochemical and Biophysical Research Communications*, 119, 1174-1180.
- BOUHLEL, W., KUI, J., BIBETTE, J. & BREMOND, N. 2022. Encapsulation of Cells in a Collagen Matrix Surrounded by an Alginate Hydrogel Shell for 3D Cell Culture. *ACS Biomater Sci Eng*, 8, 2700-2708.
- BOURGUIGNON, L. Y. W. 2012. Hyaluronan-CD44 interaction promotes microRNA signaling and RhoGTPase activation leading to tumor progression. *Small GTPases*, 3, 53-59.

References

- BRACHVOGEL, P. E. S.-S. U. & MAYER, B. S. K. N. Y. 2004. U: Collagen IV is essential for basement membrane stability but dispensable for initiation of its assembly during early development. *Development*, 131, 1619-1628.
- BRADLEY, J. M., VRANKA, J., COLVIS, C. M., CONGER, D. M., ALEXANDER, J. P., FISK, A. S., SAMPLES, J. R. & ACOTT, T. S. 1998. Effect of matrix metalloproteinases activity on outflow in perfused human organ culture. *Investigative Ophthalmology & Visual Science*, 39, 2649-2658.
- BREEDVELD, V., NOWAK, A. P., SATO, J., DEMING, T. J. & PINE, D. J. 2004. Rheology of Block Copolyptide Solutions: Hydrogels with Tunable Properties. *Macromolecules*, 37, 3943-3953.
- BRINCKMANN, J., TRONNIER, M., SCHMELLER, W., NOTBOHM, H., AÇIL, Y., FIETZEK, P. P., MÜLLER, P. K. & BÄTGE, B. 1999. Overhydroxylation of lysyl residues is the initial step for altered collagen cross-links and fibril architecture in fibrotic skin. *Journal of investigative dermatology*, 113, 617-621.
- BRINDLEY, D., MOORTHY, K., LEE, J. H., MASON, C., KIM, H. W. & WALL, I. 2011. Bioprocess forces and their impact on cell behavior: implications for bone regeneration therapy. *J Tissue Eng*, 2011, 620247.
- BROWN, B. N., FREUND, J. M., HAN, L., RUBIN, J. P., REING, J. E., JEFFRIES, E. M., WOLF, M. T., TOTTEY, S., BARNES, C. A., RATNER, B. D. & BADYLAK, S. F. 2011. Comparison of three methods for the derivation of a biologic scaffold composed of adipose tissue extracellular matrix. *Tissue Eng Part C Methods*, 17, 411-21.
- BRYANT, S. J. & ANSETH, K. S. 2002. Hydrogel properties influence ECM production by chondrocytes photoencapsulated in poly(ethylene glycol) hydrogels. *J Biomed Mater Res*, 59, 63-72.
- BRYANT, S. J. & ANSETH, K. S. 2003. Controlling the spatial distribution of ECM components in degradable PEG hydrogels for tissue engineering cartilage. *J Biomed Mater Res A*, 64, 70-9.
- BRYCHTA, R. J. & CHEN, K. Y. 2017. Cold-induced thermogenesis in humans. *European Journal of Clinical Nutrition*, 71, 345-352.
- BURDICK, J. A. & PRESTWICH, G. D. 2011. Hyaluronic Acid Hydrogels for Biomedical Applications. *Advanced Materials*, 23, H41-H56.
- BURRAGE, P. S., MIX, K. S. & BRINCKERHOFF, C. E. 2006. Matrix metalloproteinases: role in arthritis. *Front Biosci*, 11, 529-43.
- BUTCHER, D. T., ALLISTON, T. & WEAVER, V. M. 2009. A tense situation: forcing tumour progression. *Nat Rev Cancer*, 9, 108-22.
- BUXBOIM, A., RAJAGOPAL, K., BROWN, A. E. & DISCHER, D. E. 2010. How deeply cells feel: methods for thin gels. *J Phys Condens Matter*, 22, 194116.
- CAI, R., NAKAMOTO, T., HOSHIBA, T., KAWAZOE, N. & CHEN, G. 2016. Matrices secreted during simultaneous osteogenesis and adipogenesis of mesenchymal stem cells affect stem cells differentiation. *Acta Biomaterialia*, 35, 185-193.
- CALABRESE, R., RAI, N., HUANG, W., GHEZZI, C. E., SIMON, M., STALL, C., WEISS, A. S. & KAPLAN, D. L. 2017. Silk-ionomer and silk-tropoelastin hydrogels as charged three-dimensional culture platforms for the regulation of hMSC response. *Journal of Tissue Engineering and Regenerative Medicine*, 11, 2549-2564.
- CALIARI, S. R. & BURDICK, J. A. 2016. A practical guide to hydrogels for cell culture. *Nature Methods*, 13, 405-414.

References

- CALIARI, S. R., PEREPELYUK, M., COSGROVE, B. D., TSAI, S. J., LEE, G. Y., MAUCK, R. L., WELLS, R. G. & BURDICK, J. A. 2016. Stiffening hydrogels for investigating the dynamics of hepatic stellate cell mechanotransduction during myofibroblast activation. *Scientific Reports*, 6, 21387.
- CALONDER, C., MATTHEW, H. W. T. & VAN TASSEL, P. R. 2005. Adsorbed layers of oriented fibronectin: A strategy to control cell–surface interactions. *Journal of Biomedical Materials Research Part A*, 75A, 316-323.
- CAMPIGLIO, E. C., CERIANI, F. & DRAGHI, L. 2019. 3D Encapsulation Made Easy: A Coaxial-Flow Circuit for the Fabrication of Hydrogel Microfibers Patches. *Bioengineering*, 6.
- CANDIELLO, J., GRANDHI, T. S. P., GOH, S. K., VAIDYA, V., LEMMON-KISHI, M., ELIATO, K. R., ROS, R., KUMTA, P. N., REGE, K. & BANERJEE, I. 2018. 3D heterogeneous islet organoid generation from human embryonic stem cells using a novel engineered hydrogel platform. *Biomaterials*, 177, 27-39.
- CAO, H., DUAN, L., ZHANG, Y., CAO, J. & ZHANG, K. 2021. Current hydrogel advances in physicochemical and biological response-driven biomedical application diversity. *Signal Transduction and Targeted Therapy*, 6, 426.
- CAO, N., CHEN, X. B. & SCHREYER, D. J. 2012. Influence of Calcium Ions on Cell Survival and Proliferation in the Context of an Alginate Hydrogel. *ISRN Chemical Engineering*, 2012, 516461.
- CAPITO, R. M., AZEVEDO, H. S., VELICHKO, Y. S., MATA, A. & STUPP, S. I. 2008. Self-Assembly of Large and Small Molecules into Hierarchically Ordered Sacs and Membranes. *Science*, 319, 1812-1816.
- CASALE, J. & CRANE, J. S. 2022. *Biochemistry, Glycosaminoglycans*, Treasure Island (FL), StatPearls Publishing.
- CASEY, J., YUE, X., NGUYEN, T. D., ACUN, A., ZELLMER, V. R., ZHANG, S. & ZORLUTUNA, P. 2017. 3D hydrogel-based microwell arrays as a tumor microenvironment model to study breast cancer growth. *Biomed Mater*, 12, 025009.
- CEBULL, H. L., STUKEL, J. M. & WILLITS, R. Developing AFM Techniques for Testing PEG Hydrogels. 2017.
- CHAMPLIAUD, M.-F., LUNSTRUM, G. P., ROUSSELLE, P., NISHIYAMA, T., KEENE, D. R. & BURGESSON, R. E. 1996. Human amnion contains a novel laminin variant, laminin 7, which like laminin 6, covalently associates with laminin 5 to promote stable epithelial-stromal attachment. *The Journal of cell biology*, 132, 1189-1198.
- CHAMPLIAUD, M.-F., VIRTANEN, I., TIGER, C.-F., KORHONEN, M., BURGESSON, R. & GULLBERG, D. 2000. Posttranslational modifications and β/γ chain associations of human laminin $\alpha 1$ and laminin $\alpha 5$ chains: purification of laminin-3 from placenta. *Experimental Cell Research*, 259, 326-335.
- CHAN, S. W., RIZWAN, M. & YIM, E. K. F. 2020. Emerging Methods for Enhancing Pluripotent Stem Cell Expansion. *Frontiers in Cell and Developmental Biology*, 8.
- CHANG, R., SUBRAMANIAN, K., WANG, M. & WEBSTER, T. J. 2017. Enhanced Antibacterial Properties of Self-Assembling Peptide Amphiphiles Functionalized with Heparin-Binding Cardin-Motifs. *ACS Applied Materials & Interfaces*, 9, 22350-22360.
- CHEN, G., GULBRANSON, D. R., HOU, Z., BOLIN, J. M., RUOTTI, V., PROBASCIO, M. D., SMUGA-OTTO, K., HOWDEN, S. E., DIOL, N. R., PROPSON, N. E., WAGNER, R., LEE, G. O., ANTOSIEWICZ-BOURGET, J., TENG, J. M. C. & THOMSON, J. A. 2011. Chemically defined conditions for human iPSC derivation and culture. *Nature Methods*, 8, 424-429.

References

- CHEN, J., SUN, T., YOU, Y., WU, B., WANG, X. & WU, J. 2021. Proteoglycans and Glycosaminoglycans in Stem Cell Homeostasis and Bone Tissue Regeneration. *Front Cell Dev Biol*, 9, 760532.
- CHEN, P. Y., HUANG, L. L. & HSIEH, H. J. 2007a. Hyaluronan preserves the proliferation and differentiation potentials of long-term cultured murine adipose-derived stromal cells. *Biochem Biophys Res Commun*, 360, 1-6.
- CHEN, Y., LEE, K., CHEN, Y., YANG, Y., KAWAZOE, N. & CHEN, G. 2019. Preparation of Stepwise Adipogenesis-Mimicking ECM-Deposited PLGA–Collagen Hybrid Meshes and Their Influence on Adipogenic Differentiation of hMSCs. *ACS Biomaterials Science & Engineering*, 5, 6099-6108.
- CHEN, Y.-S., CHEN, Y.-Y., HSUEH, Y.-S., TAI, H.-C. & LIN, F.-H. 2016. Modifying alginate with early embryonic extracellular matrix, laminin, and hyaluronic acid for adipose tissue engineering. *Journal of Biomedical Materials Research Part A*, 104, 669-677.
- CHEN, Y.-T., RAMALINGAM, L., GARCIA, C. R., DING, Z., WU, J., MOUSTAID-MOUSSA, N. & LI, W. 2022. Engineering and Characterization of a Biomimetic Microchip for Differentiating Mouse Adipocytes in a 3D Microenvironment. *Pharmaceutical Research*, 39, 329-340.
- CHEN, Y. M., GONG, J. P., TANAKA, M., YASUDA, K., YAMAMOTO, S., SHIMOMURA, M. & OSADA, Y. 2009a. Tuning of cell proliferation on tough gels by critical charge effect. *Journal of Biomedical Materials Research Part A*, 88A, 74-83.
- CHEN, Y. M., OGAWA, R., KAKUGO, A., OSADA, Y. & GONG, J. P. 2009b. Dynamic cell behavior on synthetic hydrogels with different charge densities. *Soft Matter*, 5, 1804-1811.
- CHEN, Y. M., SHIRAIISHI, N., SATOKAWA, H., KAKUGO, A., NARITA, T., GONG, J. P., OSADA, Y., YAMAMOTO, K. & ANDO, J. 2005. Cultivation of endothelial cells on adhesive protein-free synthetic polymer gels. *Biomaterials*, 26, 4588-4596.
- CHEN, Y. M., TANAKA, M., GONG, J. P., YASUDA, K., YAMAMOTO, S., SHIMOMURA, M. & OSADA, Y. 2007b. Platelet adhesion to human umbilical vein endothelial cells cultured on anionic hydrogel scaffolds. *Biomaterials*, 28, 1752-1760.
- CHENG, Y.-S., CHAMPLAUD, M.-F., BURGESSON, R. E., MARINKOVICH, M. P. & YURCHENCO, P. D. 1997. Self-assembly of laminin isoforms. *Journal of Biological Chemistry*, 272, 31525-31532.
- CHIN, M. H., MASON, M. J., XIE, W., VOLINIA, S., SINGER, M., PETERSON, C., AMBARTSUMYAN, G., AIMIUWU, O., RICHTER, L., ZHANG, J., KHVOROSTOV, I., OTT, V., GRUNSTEIN, M., LAVON, N., BENVENISTY, N., CROCE, C. M., CLARK, A. T., BAXTER, T., PYLE, A. D., TEITELL, M. A., PELEGRINI, M., PLATH, K. & LOWRY, W. E. 2009. Induced pluripotent stem cells and embryonic stem cells are distinguished by gene expression signatures. *Cell Stem Cell*, 5, 111-23.
- CHO, S. Y., PARK, P. J., SHIN, H. J., KIM, Y.-K., SHIN, D. W., SHIN, E. S., LEE, H. H., LEE, B. G., BAIK, J.-H. & LEE, T. R. 2007. (-)-Catechin suppresses expression of Kruppel-like factor 7 and increases expression and secretion of adiponectin protein in 3T3-L1 cells. *American Journal of Physiology-Endocrinology and Metabolism*, 292, E1166-E1172.
- CHRISTIANE HOEFNER, CHRISTIAN MUHR, HANNES HORDER, MIRIAM WIESNER, KATHARINA WITTMANN, DANIEL LUKASZYK, KATRIN RADELOFF, MARC WINNEFELD, MATTHIAS BECKER, TORSTEN BLUNK & BAUER-KREISEL, P. 2020. Human Adipose-Derived Mesenchymal Stromal/Stem Cell Spheroids Possess High Adipogenic Capacity and Acquire an Adipose Tissue-like Extracellular Matrix Pattern. *Tissue Engineering Part A*, 26, 915-926.

References

- CHUAH, Y. J., PECK, Y., LAU, J. E. J., HEE, H. T. & WANG, D.-A. 2017. Hydrogel based cartilaginous tissue regeneration: recent insights and technologies. *Biomaterials Science*, 5, 613-631.
- CHUN, S. Y., LIM, J. O., LEE, E. H., HAN, M.-H., HA, Y.-S., LEE, J. N., KIM, B. S., PARK, M. J., YEO, M., JUNG, B. & KWON, T. G. 2019. Preparation and Characterization of Human Adipose Tissue-Derived Extracellular Matrix, Growth Factors, and Stem Cells: A Concise Review. *Tissue engineering and regenerative medicine*, 16, 385-393.
- CHUN, Y. S., BYUN, K. & LEE, B. 2011. Induced pluripotent stem cells and personalized medicine: current progress and future perspectives. *Anat Cell Biol*, 44, 245-55.
- COHEN, M., JOESTER, D., GEIGER, B. & ADDADI, L. 2004. Spatial and Temporal Sequence of Events in Cell Adhesion: From Molecular Recognition to Focal Adhesion Assembly. *ChemBioChem*, 5, 1393-1399.
- COHEN, M., KAM, Z., ADDADI, L. & GEIGER, B. 2006. Dynamic study of the transition from hyaluronan- to integrin-mediated adhesion in chondrocytes. *Embo j*, 25, 302-11.
- COLLOT, M., ASHOKKUMAR, P., ANTON, H., BOUTANT, E., FAKLARIS, O., GALLI, T., MÉLY, Y., DANGLLOT, L. & KLYMCHENKO, A. S. 2019. MemBright: A Family of Fluorescent Membrane Probes for Advanced Cellular Imaging and Neuroscience. *Cell Chemical Biology*, 26, 600-614.e7.
- COLOGNATO, H. & YURCHENCO, P. D. 2000. Form and function: the laminin family of heterotrimers. *Developmental dynamics: an official publication of the American Association of Anatomists*, 218, 213-234.
- COMPERA, N., ATWELL, S., WIRTH, J., VON TÖRNE, C., HAUCK, S. M. & MEIER, M. 2022. Adipose microtissue-on-chip: a 3D cell culture platform for differentiation, stimulation, and proteomic analysis of human adipocytes. *Lab on a Chip*.
- COOPER, A. R., KURKINEN, M., TAYLOR, A. & HOGAN, B. L. M. 1981. Studies on the Biosynthesis of Laminin by Murine Parietal Endoderm Cells. *European Journal of Biochemistry*, 119, 189-197.
- COOPER, A. R. & MACQUEEN, H. A. 1983. Subunits of laminin are differentially synthesized in mouse eggs and early embryos. *Dev Biol*, 96, 467-71.
- CORNING. 2022. *Corning Matrigel Matrix* [Online]. [Accessed 03.03.22 2022].
- CORTINI, F., VILLA, C., MARINELLI, B., COMBI, R., PESATORI, A. C. & BASSOTTI, A. 2019. Understanding the basis of Ehlers-Danlos syndrome in the era of the next-generation sequencing. *Arch Dermatol Res*, 311, 265-275.
- CRUZ-ACUÑA, R., QUIRÓS, M., FARKAS, A. E., DEDHIA, P. H., HUANG, S., SIUDA, D., GARCÍA-HERNÁNDEZ, V., MILLER, A. J., SPENCE, J. R., NUSRAT, A. & GARCÍA, A. J. 2017. Synthetic hydrogels for human intestinal organoid generation and colonic wound repair. *Nat Cell Biol*, 19, 1326-1335.
- CSIGE, I., UJVÁROSY, D., SZABÓ, Z., LŐRINCZ, I., PARAGH, G., HARANGI, M. & SOMODI, S. 2018. The Impact of Obesity on the Cardiovascular System. *J Diabetes Res*, 2018, 3407306.
- CUI, H., MURAOKA, T., CHEETHAM, A. G. & STUPP, S. I. 2009. Self-assembly of giant peptide nanobelts. *Nano Lett*, 9, 945-51.
- CUI, H., WEBBER, M. J. & STUPP, S. I. 2010. Self-assembly of peptide amphiphiles: from molecules to nanostructures to biomaterials. *Biopolymers*, 94, 1-18.
- CURRAN, M. E., ATKINSON, D. L., EWART, A. K., MORRIS, C. A., LEPPERT, M. F. & KEATING, M. T. 1993. The elastin gene is disrupted by a translocation associated with supravalvular aortic stenosis. *Cell*, 73, 159-168.

References

- CYPESS, A. M., WEINER, L. S., ROBERTS-TOLER, C., FRANQUET ELÍA, E., KESSLER, S. H., KAHN, P. A., ENGLISH, J., CHATMAN, K., TRAUGER, S. A., DORIA, A. & KOLODNY, G. M. 2015. Activation of human brown adipose tissue by a β 3-adrenergic receptor agonist. *Cell Metab*, 21, 33-8.
- D'ANDREA, L. D., IACCARINO, G., FATTORUSSO, R., SORRIENTO, D., CARANNANTE, C., CAPASSO, D., TRIMARCO, B. & PEDONE, C. 2005. Targeting angiogenesis: structural characterization and biological properties of a de novo engineered VEGF mimicking peptide. *Proc Natl Acad Sci U S A*, 102, 14215-20.
- DALHEIM, M. Ø., OMTVEDT, L. A., BJØRGE, I. M., AKBARZADEH, A., MANO, J. F., AACHMANN, F. L. & STRAND, B. L. 2019. Mechanical Properties of Ca-Saturated Hydrogels with Functionalized Alginate. *Gels*, 5, 23.
- DALTON, C. J. & LEMMON, C. A. 2021. Fibronectin: Molecular Structure, Fibrillar Structure and Mechanochemical Signaling. *Cells*, 10.
- DAQUINAG, A. C., SOUZA, G. R. & KOLONIN, M. G. 2012. Adipose Tissue Engineering in Three-Dimensional Levitation Tissue Culture System Based on Magnetic Nanoparticles. *Tissue Engineering Part C: Methods*, 19, 336-344.
- DARLING, E. M., TOPEL, M., ZAUSCHER, S., VAIL, T. P. & GUILAK, F. 2008. Viscoelastic properties of human mesenchymally-derived stem cells and primary osteoblasts, chondrocytes, and adipocytes. *Journal of biomechanics*, 41, 454-464.
- DARNELL, M., GU, L. & MOONEY, D. 2018. RNA-seq reveals diverse effects of substrate stiffness on mesenchymal stem cells. *Biomaterials*, 181, 182-188.
- DAVIDENKO, N., SCHUSTER, C. F., BAX, D. V., FARNDAL, R. W., HAMAIA, S., BEST, S. M. & CAMERON, R. E. 2016. Evaluation of cell binding to collagen and gelatin: a study of the effect of 2D and 3D architecture and surface chemistry. *J Mater Sci Mater Med*, 27, 148.
- DE MELO, N., MCGINLAY, S., MARKUS, R., MACRI-PELLIZZERI, L., SYMONDS, M. E., AHMED, I. & SOTTILE, V. 2019. Live Simultaneous Monitoring of Mineral Deposition and Lipid Accumulation in Differentiating Stem Cells. *Biomimetics (Basel)*, 4.
- DEBARI, M. K., NG, W. H., GRIFFIN, M. D., KOKAI, L. E., MARRA, K. G., RUBIN, J. P., REN, X. & ABBOTT, R. D. 2021. Engineering a 3D Vascularized Adipose Tissue Construct Using a Decellularized Lung Matrix. *Biomimetics (Basel)*, 6.
- DELLA SALA, F., BIONDI, M., GUARNIERI, D., BORZACCHIELLO, A., AMBROSIO, L. & MAYOL, L. 2020. Mechanical behavior of bioactive poly(ethylene glycol) diacrylate matrices for biomedical application. *J Mech Behav Biomed Mater*, 110, 103885.
- DENAYER, T., STÖHR, T. & VAN ROY, M. 2014. Animal models in translational medicine: Validation and prediction. *New Horizons in Translational Medicine*, 2, 5-11.
- DENGLER, W. A., SCHULTE, J., BERGER, D. P., MERTELSMANN, R. & FIEBIG, H. H. 1995. Development of a propidium iodide fluorescence assay for proliferation and cytotoxicity assays. *Anticancer Drugs*, 6, 522-32.
- DERAKHSHANKHAH, H. & JAFARI, S. 2018. Cell penetrating peptides: A concise review with emphasis on biomedical applications. *Biomedicine & Pharmacotherapy*, 108, 1090-1096.
- DERKUS, B., OKESOLA, B. O., BARRETT, D. W., D'ESTE, M., CHOWDHURY, T. T., EGLIN, D. & MATA, A. 2020. Multicomponent hydrogels for the formation of vascularized bone-like constructs in vitro. *Acta Biomaterialia*, 109, 82-94.
- DEY, T. K., KARMAKAR, B. C., SARKAR, A., PAUL, S. & MUKHOPADHYAY, A. K. 2021. A Mouse Model of Helicobacter pylori Infection. In: SMITH, S. M. (ed.) *Helicobacter Pylori*. New York, NY: Springer US.

References

- DI GREGORIO, G. B., YAO-BORENGASSER, A., RASOULI, N., VARMA, V., LU, T., MILES, L. M., RANGANATHAN, G., PETERSON, C. A., MCGEHEE, R. E. & KERN, P. A. 2005. Expression of CD68 and macrophage chemoattractant protein-1 genes in human adipose and muscle tissues: association with cytokine expression, insulin resistance, and reduction by pioglitazone. *Diabetes*, 54, 2305-13.
- DIDANGELOS, A., YIN, X., MANDAL, K., SAJE, A., SMITH, A., XU, Q., JAHANGIRI, M. & MAYR, M. 2011. Extracellular matrix composition and remodeling in human abdominal aortic aneurysms: a proteomics approach. *Mol Cell Proteomics*, 10, M111.008128.
- DING, X., GAO, J., YU, X., SHI, J., CHEN, J., YU, L., CHEN, S. & DING, J. 2022. 3D-Printed Porous Scaffolds of Hydrogels Modified with TGF- β 1 Binding Peptides to Promote In Vivo Cartilage Regeneration and Animal Gait Restoration. *ACS Applied Materials & Interfaces*, 14, 15982-15995.
- DOHMEN, R. G. J., HUBALEK, S., MELKE, J., MESSMER, T., CANTONI, F., MEI, A., HUEBER, R., MITIC, R., REMMERS, D., MOUTSATSOU, P., POST, M. J., JACKISCH, L. & FLACK, J. E. 2022. Muscle-derived fibro-adipogenic progenitor cells for production of cultured bovine adipose tissue. *npj Science of Food*, 6, 6.
- DOI, A., PARK, I. H., WEN, B., MURAKAMI, P., ARYEE, M. J., IRIZARRY, R., HERB, B., LADD-ACOSTA, C., RHO, J., LOEWER, S., MILLER, J., SCHLAEGER, T., DALEY, G. Q. & FEINBERG, A. P. 2009. Differential methylation of tissue- and cancer-specific CpG island shores distinguishes human induced pluripotent stem cells, embryonic stem cells and fibroblasts. *Nat Genet*, 41, 1350-3.
- DOLIANA, R., BELLINA, I., BUCCIOTTI, F., MONGIAT, M., PERRIS, R. & COLOMBATTI, A. 1997. The human α 3b is a full-sized laminin chain variant with a more widespread tissue expression than the truncated α 3a. *FEBS letters*, 417, 65-70.
- DOMBROWSKI, C., SONG, S. J., CHUAN, P., LIM, X., SUSANTO, E., SAWYER, A. A., WOODRUFF, M. A., HUTMACHER, D. W., NURCOMBE, V. & COOL, S. M. 2009. Heparan sulfate mediates the proliferation and differentiation of rat mesenchymal stem cells. *Stem Cells Dev*, 18, 661-70.
- DOMINICI, M., LE BLANC, K., MUELLER, I., SLAPER-CORTENBACH, I., MARINI, F., KRAUSE, D., DEANS, R., KEATING, A., PROCKOP, D. & HORWITZ, E. 2006. Minimal criteria for defining multipotent mesenchymal stromal cells. The International Society for Cellular Therapy position statement. *Cytotherapy*, 8, 315-7.
- DUARTE CAMPOS, D., BLAESER, A., KORSTEN, A., NEUSS-STEIN, S., JÄKEL, J., VOGT, M. & FISCHER, H. 2014. The Stiffness and Structure of Three-Dimensional Printed Hydrogels Direct the Differentiation of Mesenchymal Stromal Cells Toward Adipogenic and Osteogenic Lineages. *Tissue engineering. Part A*, 21.
- DURBEEJ, M. 2010. Laminins. *Cell Tissue Res*, 339, 259-68.
- DZIADEK, M., FUJIWARA, S., PAULSSON, M. & TIMPL, R. 1985. Immunological characterization of basement membrane types of heparan sulfate proteoglycan. *The EMBO Journal*, 4, 905-912.
- ECKES, B., NISCHT, R. & KRIEG, T. 2010. Cell-matrix interactions in dermal repair and scarring. *Fibrogenesis & tissue repair*, 3, 1-11.
- EGEBLAD, M., RASCH, M. G. & WEAVER, V. M. 2010. Dynamic interplay between the collagen scaffold and tumor evolution. *Current opinion in cell biology*, 22, 697-706.
- EGLES, C., CLAUDEPIERRE, T., MANG LAPUS, M. K., CHAMPLAUD, M.-F., BRUNKEN, W. J. & HUNTER, D. D. 2007. Laminins containing the β 2 chain modulate the precise organization of CNS synapses. *Molecular and Cellular Neuroscience*, 34, 288-298.

References

- EHLERS, E. M., BEHRENS, P., WÜNSCH, L., KÜHNEL, W. & RUSSLIES, M. 2001. Effects of hyaluronic acid on the morphology and proliferation of human chondrocytes in primary cell culture. *Ann Anat*, 183, 13-7.
- EMONT, M. P., YU, H., JUN, H., HONG, X., MAGANTI, N., STEGEMANN, J. P. & WU, J. 2015. Using a 3D Culture System to Differentiate Visceral Adipocytes In Vitro. *Endocrinology*, 156, 4761-4768.
- EVANS, M. J. & KAUFMAN, M. H. 1981. Establishment in culture of pluripotential cells from mouse embryos. *Nature*, 292, 154-6.
- EVANS, N. D., MINELLI, C., GENTLEMAN, E., LAPOINTE, V., PATANKAR, S. N., KALLIVRETAKI, M., CHEN, X., ROBERTS, C. J. & STEVENS, M. M. 2009. Substrate Stiffness Affects Early Differentiation Events in Embryonic Stem Cells. *Journal of European Cells and Materials*, 18, 1-14.
- EWART, A. K., MORRIS, C. A., ATKINSON, D., JIN, W., STERNES, K., SPALLONE, P., STOCK, A. D., LEPPERT, M. & KEATING, M. T. 1993. Hemizygoty at the elastin locus in a developmental disorder, Williams syndrome. *Nature genetics*, 5, 11-16.
- EYRE, D. R., WEIS, M., HUDSON, D. M., WU, J. J. & KIM, L. 2011. A novel 3-hydroxyproline (3Hyp)-rich motif marks the triple-helical C terminus of tendon type I collagen. *J Biol Chem*, 286, 7732-7736.
- FANG, Z., LYU, J., LI, J., LI, C., ZHANG, Y., GUO, Y., WANG, Y., ZHANG, Y. & CHEN, K. 2022. Application of bioreactor technology for cell culture-based viral vaccine production: Present status and future prospects. *Front Bioeng Biotechnol*, 10, 921755.
- FAZIO, M., OLSEN, D., KUIVANIEMI, H., CHU, M., DAVIDSON, J., ROSENBLOOM, J. & UITTO, J. 1988. Isolation and characterization of human elastin cDNAs, and age-associated variation in elastin gene expression in cultured skin fibroblasts. *Laboratory investigation; a journal of technical methods and pathology*, 58, 270-277.
- FEKETE, N., BÉLAND, A. V., CAMPBELL, K., CLARK, S. L. & HOESLI, C. A. 2018. Bags versus flasks: a comparison of cell culture systems for the production of dendritic cell-based immunotherapies. *Transfusion*, 58, 1800-1813.
- FERNANDES, H., MENTINK, A., BANK, R., STOOP, R., VAN BLITTERSWIJK, C. & DE BOER, J. 2010. Endogenous collagen influences differentiation of human multipotent mesenchymal stromal cells. *Tissue Eng Part A*, 16, 1693-702.
- FERREIRA, D. S., MARQUES, A. P., REIS, R. L. & AZEVEDO, H. S. 2013a. Hyaluronan and self-assembling peptides as building blocks to reconstruct the extracellular environment in skin tissue. *Biomaterials Science*, 1, 952-964.
- FERREIRA, D. S., MARQUES, A. P., REIS, R. L. & AZEVEDO, H. S. 2013b. Hyaluronan and self-assembling peptides as building blocks to reconstruct the extracellular environment in skin tissue. *Biomater Sci*, 1, 952-964.
- FERREIRA, S. A., MOTWANI, M. S., FAULL, P. A., SEYMOUR, A. J., YU, T. T. L., ENAYATI, M., TAHEEM, D. K., SALZLECHNER, C., HAGHIGHI, T., KANIA, E. M., OOMMEN, O. P., AHMED, T., LOAIZA, S., PARZYCH, K., DAZZI, F., VARGHESE, O. P., FESTY, F., GRIGORIADIS, A. E., AUNER, H. W., SNIJDERS, A. P., BOZEC, L. & GENTLEMAN, E. 2018. Bi-directional cell-pericellular matrix interactions direct stem cell fate. *Nat Commun*, 9, 4049.
- FERRIGNO, O., VIROLLE, T., GALLIANO, M. F., CHAUVIN, N., ORTONNE, J. P., MENEGUZZI, G. & ABERDAM, D. 1997. Murine laminin alpha3A and alpha3B isoform chains are generated by usage of two promoters and alternative splicing. *J Biol Chem*, 272, 20502-7.

References

- FFRENCH-CONSTANT, C. 1995. Alternative Splicing of Fibronectin—Many Different Proteins but Few Different Functions. *Experimental Cell Research*, 221, 261-271.
- FLAUMENHAFT, R. & RIFKIN, D. B. 1991. Extracellular matrix regulation of growth factor and protease activity. *Current Opinion in Cell Biology*, 3, 817-823.
- FONG, D., DUCEPPE, N. & HOEMANN, C. D. 2017. Mesenchymal stem cell detachment with trace trypsin is superior to EDTA for in vitro chemotaxis and adhesion assays. *Biochem Biophys Res Commun*, 484, 656-661.
- FRANCE, L. A., SCOTCHFORD, C. A., GRANT, D. M., RASHIDI, H., POPOV, A. A. & SOTTILE, V. 2014. Transient serum exposure regimes to support dual differentiation of human mesenchymal stem cells. *Journal of Tissue Engineering and Regenerative Medicine*, 8, 652-663.
- FRANK, D. E. & CARTER, W. G. 2004. Laminin 5 deposition regulates keratinocyte polarization and persistent migration. *Journal of cell science*, 117, 1351-1363.
- FRANTZ, C., STEWART, K. M. & WEAVER, V. M. 2010. The extracellular matrix at a glance. *Journal of Cell Science*, 123, 4195-4200.
- FREEMAN, F. E. & KELLY, D. J. 2017. Tuning Alginate Bioink Stiffness and Composition for Controlled Growth Factor Delivery and to Spatially Direct MSC Fate within Bioprinted Tissues. *Scientific Reports*, 7, 17042.
- FRONTIER, E. 2022. ESTIMATING THE FULL COSTS OF OBESITY.
- FUCHS, E., TUMBAR, T. & GUASCH, G. 2004. Socializing with the neighbors: stem cells and their niche. *Cell*, 116, 769-78.
- FUJII, Y., KOIZUMI, W. C., IMAI, T., YOKOBORI, M., MATSUO, T., OKA, K., HOTTA, K. & OKAJIMA, T. 2021. Spatiotemporal dynamics of single cell stiffness in the early developing ascidian chordate embryo. *Communications Biology*, 4, 341.
- FUJITANI, N., FURUKAWA, J., ARAKI, K., FUJIOKA, T., TAKEGAWA, Y., PIAO, J., NISHIOKA, T., TAMURA, T., NIKAIDO, T., ITO, M., NAKAMURA, Y. & SHINOHARA, Y. 2013. Total cellular glycomics allows characterizing cells and streamlining the discovery process for cellular biomarkers. *Proc Natl Acad Sci U S A*, 110, 2105-10.
- FUJIWARA, S., SHINKAI, H., DEUTZMANN, R., PAULSSON, M. & TIMPL, R. 1988. Structure and distribution of N-linked oligosaccharide chains on various domains of mouse tumour laminin. *Biochemical Journal*, 252, 453-461.
- GABRIEL, E., ALBANNA, W., PASQUINI, G., RAMANI, A., JOSIPOVIC, N., MARIAPPAN, A., SCHINZEL, F., KARCH, C. M., BAO, G., GOTTARDO, M., SUREN, A. A., HESCHELER, J., NAGEL-WOLFRUM, K., PERSICO, V., RIZZOLI, S. O., ALTMÜLLER, J., RIPARBELLI, M. G., CALLAINI, G., GOUREAU, O., PAPANTONIS, A., BUSSKAMP, V., SCHNEIDER, T. & GOPALAKRISHNAN, J. 2021. Human brain organoids assemble functionally integrated bilateral optic vesicles. *Cell Stem Cell*, 28, 1740-1757.e8.
- GANDHI, N. S. & MANCERA, R. L. 2008. The Structure of Glycosaminoglycans and their Interactions with Proteins. *Chemical Biology & Drug Design*, 72, 455-482.
- GAO, Y., MA, K., KANG, Y., LIU, W., LIU, X., LONG, X., HAYASHI, T., HATTORI, S., MIZUNO, K., FUJISAKI, H. & IKEJIMA, T. 2022. Type I collagen reduces lipid accumulation during adipogenesis of preadipocytes 3T3-L1 via the YAP-mTOR-autophagy axis. *Biochimica et Biophysica Acta (BBA) - Molecular and Cell Biology of Lipids*, 1867, 159181.
- GARCIA ABREU, J., COFFINIER, C., LARRAÍN, J., OELGESCHLÄGER, M. & DE ROBERTIS, E. M. 2002. Chordin-like CR domains and the regulation of evolutionarily conserved extracellular signaling systems. *Gene*, 287, 39-47.

References

- GARCIA, R. A., ROEMMICH, J. N. & CLAYCOMBE, K. J. 2016. Evaluation of markers of beige adipocytes in white adipose tissue of the mouse. *Nutrition & Metabolism*, 13, 24.
- GASIMLI, L., HICKEY, A. M., YANG, B., LI, G., DELA ROSA, M., NAIRN, A. V., KULIK, M., DORDICK, J. S., MOREMEN, K. W., DALTON, S. & LINHARDT, R. J. 2014. Changes in glycosaminoglycan structure on differentiation of human embryonic stem cells towards mesoderm and endoderm lineages. *Biochimica et biophysica acta*, 1840 6, 1993-2003.
- GATTAZZO, F., URCIUOLO, A. & BONALDO, P. 2014. Extracellular matrix: a dynamic microenvironment for stem cell niche. *Biochim Biophys Acta*, 1840, 2506-19.
- GEHRIS, A. L., OBERLENDER, S. A., SHEPLEY, K. J., TUAN, R. S. & BENNETT, V. D. 1996. Fibronectin mRNA alternative splicing is temporally and spatially regulated during chondrogenesis in vivo and in vitro. *Dev Dyn*, 206, 219-30.
- GEORGE, E. L., GEORGES-LABOUESSE, E. N., PATEL-KING, R. S., RAYBURN, H. & HYNES, R. O. 1993. Defects in mesoderm, neural tube and vascular development in mouse embryos lacking fibronectin. *Development*, 119, 1079-1091.
- GÉRARD, C. & GOLDBETER, A. 2014. The balance between cell cycle arrest and cell proliferation: control by the extracellular matrix and by contact inhibition. *Interface Focus*, 4, 20130075.
- GHALI, O., BROUX, O., FALGAYRAC, G., HAREN, N., VAN LEEUWEN, J. P., PENEL, G., HARDOUIN, P. & CHAUVEAU, C. 2015. Dexamethasone in osteogenic medium strongly induces adipocyte differentiation of mouse bone marrow stromal cells and increases osteoblast differentiation. *BMC cell biology*, 16, 1-15.
- GHARIB, S. A., MANICONE, A. M. & PARKS, W. C. 2018. Matrix metalloproteinases in emphysema. *Matrix Biology*, 73, 34-51.
- GHORBANI, M., CLAUS, T. H. & HIMMS-HAGEN, J. 1997. Hypertrophy of brown adipocytes in brown and white adipose tissues and reversal of diet-induced obesity in rats treated with a beta3-adrenoceptor agonist. *Biochem Pharmacol*, 54, 121-31.
- GHORBANIAN, S., QASAIMAH, M. A., AKBARI, M., TAMAYOL, A. & JUNCKER, D. 2014. Microfluidic direct writer with integrated declogging mechanism for fabricating cell-laden hydrogel constructs. *Biomedical Microdevices*, 16, 387-395.
- GILLETTE, B. M., JENSEN, J. A., WANG, M., TCHAO, J. & SIA, S. K. 2010. Dynamic Hydrogels: Switching of 3D Microenvironments Using Two-Component Naturally Derived Extracellular Matrices. *Advanced Materials*, 22, 686-691.
- GIUSEPPE, M. D., LAW, N., WEBB, B., A. MACRAE, R., LIEW, L. J., SERCOMBE, T. B., DILLEY, R. J. & DOYLE, B. J. 2018. Mechanical behaviour of alginate-gelatin hydrogels for 3D bioprinting. *Journal of the Mechanical Behavior of Biomedical Materials*, 79, 150-157.
- GJALTEMA, R. A. F. & BANK, R. A. 2017. Molecular insights into prolyl and lysyl hydroxylation of fibrillar collagens in health and disease. *Critical Reviews in Biochemistry and Molecular Biology*, 52, 74-95.
- GLAGOV, S., VITO, R., GIDDENS, D. P. & ZARINS, C. K. 1992. Micro-architecture and composition of artery walls: relationship to location, diameter and the distribution of mechanical stress. *J Hypertens Suppl*, 10, S101-4.
- GOCZE, P. M. & FREEMAN, D. A. 1994. Factors underlying the variability of lipid droplet fluorescence in MA-10 leydig tumor cells. *Cytometry*, 17, 151-158.
- GOLAY, A. & YBARRA, J. 2005. Link between obesity and type 2 diabetes. *Best Pract Res Clin Endocrinol Metab*, 19, 649-63.

References

- GONÇALVES, I. G. & GARCIA-AZNAR, J. M. 2021. Extracellular matrix density regulates the formation of tumour spheroids through cell migration. *PLoS Comput Biol*, 17, e1008764.
- GONZALEZ PORRAS, M. A., STOJKOVA, K., VAICIK, M. K., PELOWE, A., GODDI, A., CARMONA, A., LONG, B., QUTUB, A. A., GONZALEZ, A., COHEN, R. N. & BREY, E. M. 2021. Integrins and extracellular matrix proteins modulate adipocyte thermogenic capacity. *Scientific Reports*, 11, 5442.
- GOODARZI, K. & RAO, S. S. 2021. Hyaluronic acid-based hydrogels to study cancer cell behaviors. *Journal of Materials Chemistry B*, 9, 6103-6115.
- GOTO, K. & TERAMOTO, Y. 2020. Development of chitinous nanofiber-based flexible composite hydrogels capable of cell adhesion and detachment. *Polymer Journal*, 52, 959-967.
- GREENFIELD, M. A., HOFFMAN, J. R., OLVERA DE LA CRUZ, M. & STUPP, S. I. 2010. Tunable Mechanics of Peptide Nanofiber Gels. *Langmuir*, 26, 3641-3647.
- GS, A. K., RAJ, B., SANTHOSH, K. S., SANJAY, G. & KARTHA, C. C. 2014. Ascending aortic constriction in rats for creation of pressure overload cardiac hypertrophy model. *J Vis Exp*, e50983.
- GU, J., GUO, Y., LI, Y., WANG, J., WANG, W., CAO, Y. & XUE, B. 2022. Tuning Strain Stiffening of Protein Hydrogels by Charge Modification. *Int J Mol Sci*, 23.
- GU, W. L., FU, S. L., WANG, Y. X., LI, Y., LÜ, H. Z., XU, X. M. & LU, P. H. 2009. Chondroitin sulfate proteoglycans regulate the growth, differentiation and migration of multipotent neural precursor cells through the integrin signaling pathway. *BMC Neurosci*, 10, 128.
- GUÉNANTIN, A.-C., BRIAND, N., CAPEL, E., DUMONT, F., MORICHON, R., PROVOST, C., STILLITANO, F., JEZIOROWSKA, D., SIFFROI, J.-P., HAJJAR, R. J., FÈVE, B., HULOT, J.-S., COLLAS, P., CAPEAU, J. & VIGOUROUX, C. 2017. Functional Human Beige Adipocytes From Induced Pluripotent Stem Cells. *Diabetes*, 66, 1470-1478.
- GUENTHER, M. G., FRAMPTON, G. M., SOLDNER, F., HOCKEMEYER, D., MITALIPOVA, M., JAENISCH, R. & YOUNG, R. A. 2010. Chromatin structure and gene expression programs of human embryonic and induced pluripotent stem cells. *Cell Stem Cell*, 7, 249-57.
- GUIMOND, S. E., TURNBULL, J. E. & YATES, E. A. 2006. Engineered Bio-Active Polysaccharides from Heparin. *Macromolecular Bioscience*, 6, 681-686.
- GULER, M. O., SOUKASENE, S., HULVAT, J. F. & STUPP, S. I. 2005. Presentation and Recognition of Biotin on Nanofibers Formed by Branched Peptide Amphiphiles. *Nano Letters*, 5, 249-252.
- GUPTA, S., KAPOOR, P., CHAUDHARY, K., GAUTAM, A., KUMAR, R. & RAGHAVA, G. P. 2013. In silico approach for predicting toxicity of peptides and proteins. *PLoS One*, 8, e73957.
- HACKAM, D. G. & REDELMEIER, D. A. 2006. Translation of research evidence from animals to humans. *Jama*, 296, 1727-1732.
- HADJIPANAYI, E., MUDERA, V. & BROWN, R. A. 2009. Close dependence of fibroblast proliferation on collagen scaffold matrix stiffness. *Journal of Tissue Engineering and Regenerative Medicine*, 3, 77-84.
- HALL, C. L., WANG, C., LANGE, L. A. & TURLEY, E. A. 1994. Hyaluronan and the hyaluronan receptor RHAMM promote focal adhesion turnover and transient tyrosine kinase activity. *Journal of Cell Biology*, 126, 575-588.

References

- HANAGIRI, T., SHINOHARA, S., TAKENAKA, M., SHIGEMATSU, Y., YASUDA, M., SHIMOKAWA, H., NAGATA, Y., NAKAGAWA, M., URAMOTO, H., SO, T. & TANAKA, F. 2012. Effects of hyaluronic acid and CD44 interaction on the proliferation and invasiveness of malignant pleural mesothelioma. *Tumor Biology*, 33, 2135-2141.
- HANDORF, A. M., ZHOU, Y., HALANSKI, M. A. & LI, W. J. 2015. Tissue stiffness dictates development, homeostasis, and disease progression. *Organogenesis*, 11, 1-15.
- HARMS, M. & SEALE, P. 2013. Brown and beige fat: development, function and therapeutic potential. *Nat Med*, 19, 1252-63.
- HARMS, M. J., ISHIBASHI, J., WANG, W., LIM, H. W., GOYAMA, S., SATO, T., KUROKAWA, M., WON, K. J. & SEALE, P. 2014. Prdm16 is required for the maintenance of brown adipocyte identity and function in adult mice. *Cell Metab*, 19, 593-604.
- HARTGERINK, J. D., BENIASH, E. & STUPP, S. I. 2001. Self-assembly and mineralization of peptide-amphiphile nanofibers. *Science*, 294, 1684-8.
- HARTGERINK, J. D., BENIASH, E. & STUPP, S. I. 2002. Peptide-amphiphile nanofibers: a versatile scaffold for the preparation of self-assembling materials. *Proc Natl Acad Sci U S A*, 99, 5133-8.
- HARTVIG, R. A., VAN DE WEERT, M., ØSTERGAARD, J., JORGENSEN, L. & JENSEN, H. 2011. Protein adsorption at charged surfaces: the role of electrostatic interactions and interfacial charge regulation. *Langmuir*, 27, 2634-2643.
- HASCALL, V. C., MAJORS, A. K., DE LA MOTTE, C. A., EVANKO, S. P., WANG, A., DRAZBA, J. A., STRONG, S. A. & WIGHT, T. N. 2004. Intracellular hyaluronan: a new frontier for inflammation? *Biochim Biophys Acta*, 1673, 3-12.
- HATANO, H., SHIGEISHI, H., KUDO, Y., HIGASHIKAWA, K., TOBIUME, K., TAKATA, T. & KAMATA, N. 2011. RHAMM/ERK interaction induces proliferative activities of cementifying fibroma cells through a mechanism based on the CD44–EGFR. *Laboratory Investigation*, 91, 379-391.
- HAUG, A. 1964. *Composition And Properties Of Alginates*. Ph.D. Thesis., University Of Trondheim.
- HAUG, A., SMIDSRØD, O. A., HˆGDAHL, B., ˆYVE, H. A., RASMUSSEN, S. E., SUNDE, E. & SˆRENSEN, N. A. 1970. Selectivity of Some Anionic Polymers for Divalent Metal Ions. *Acta Chemica Scandinavica*, 24, 843-854.
- HE, S., BHATT, R., BROWN, C., BROWN, E. A., BUHR, D. L., CHANTRANUVATANA, K., DANAHER, P., DUNAWAY, D., GARRISON, R. G., GEISS, G., GREGORY, M. T., HOANG, M. L., KHAFIZOV, R., KILLINGBECK, E. E., KIM, D., KIM, T. K., KIM, Y., KLOCK, A., KORUKONDA, M., KUTCHMA, A., LEWIS, Z. R., LIANG, Y., NELSON, J. S., ONG, G. T., PERILLO, E. P., PHAN, J. C., PHAN-EVERSON, T., PIAZZA, E., RANE, T., REITZ, Z., RHODES, M., ROSENBLUM, A., ROSS, D., SATO, H., WARDHANI, A. W., WILLIAMS-WIETZIKOSKI, C. A., WU, L. & BEECHEM, J. M. 2022. High-plex Multiomic Analysis in FFPE at Subcellular Level by Spatial Molecular Imaging. *bioRxiv*, 2021.11.03.467020.
- HEDEGAARD, C. L., COLLIN, E. C., REDONDO-GÓMEZ, C., NGUYEN, L. T. H., NG, K. W., CASTREJÓN-PITA, A. A., CASTREJÓN-PITA, J. R. & MATA, A. 2018. Hydrodynamically Guided Hierarchical Self-Assembly of Peptide–Protein Bioinks. *Advanced Functional Materials*, 28, 1703716.
- HEDEGAARD, C. L., REDONDO-GÓMEZ, C., TAN, B. Y., NG, K. W., LOESSNER, D. & MATA, A. 2020. Peptide-protein coassembling matrices as a biomimetic 3D model of ovarian cancer. *Science Advances*, 6, eabb3298.

References

- HEER, N. C. & MARTIN, A. C. 2017. Tension, contraction and tissue morphogenesis. *Development*, 144, 4249-4260.
- HEERKLOTZ, H. 2008. Interactions of surfactants with lipid membranes. *Quarterly Reviews of Biophysics*, 41, 205-264.
- HELDIN, P. & PERTOFT, H. 1993. Synthesis and assembly of the hyaluronan-containing coats around normal human mesothelial cells. *Exp Cell Res*, 208, 422-9.
- HELEN ZHA, R., VELICHKO, Y. S., BITTON, R. & STUPP, S. I. 2016. Molecular design for growth of supramolecular membranes with hierarchical structure. *Soft Matter*, 12, 1401-1410.
- HELGERUD, T., GÅSERØD, O., FJÆREIDE, T., ANDERSEN, P. O. & LARSEN, C. K. 2009. Alginates. *Food Stabilisers, Thickeners and Gelling Agents*, 50-72.
- HEYDARKHAN-HAGVALL, S., GLUCK, J. M., DELMAN, C., JUNG, M., EHSANI, N., FULL, S. & SHEMIN, R. J. 2012. The effect of vitronectin on the differentiation of embryonic stem cells in a 3D culture system. *Biomaterials*, 33, 2032-2040.
- HIEW, V. V. & TEOH, P. L. 2022. Collagen Modulates the Biological Characteristics of WJ-MSCs in Basal and Osteoinduced Conditions. *Stem Cells International*, 2022, 2116367.
- HINEK, A., KEELEY, F. W. & CALLAHANS, J. 1995. Recycling of the 67-kDa elastin binding protein in arterial myocytes is imperative for secretion of tropoelastin. *Experimental cell research*, 220, 312-324.
- HINTERMANN, E., YANG, N., O'SULLIVAN, D., HIGGINS, J. M. & QUARANTA, V. 2005. Integrin $\alpha 6\beta 4$ -erbB2 complex inhibits haptotaxis by up-regulating E-cadherin cell-cell junctions in keratinocytes. *Journal of Biological Chemistry*, 280, 8004-8015.
- HINZ, B. 2016. The role of myofibroblasts in wound healing. *Curr Res Transl Med*, 64, 171-177.
- HIRANO, K., SASAKI, N., ICHIMIYA, T., MIURA, T., VAN KUPPEVELT, T. H. & NISHIHARA, S. 2012. 3-O-Sulfated Heparan Sulfate Recognized by the Antibody HS4C3 Contribute to the Differentiation of Mouse Embryonic Stem Cells via Fas Signaling. *PLOS ONE*, 7, e43440.
- HIRAYAMA, K., OKITSU, T., TERAMAE, H., KIRIYA, D., ONOE, H. & TAKEUCHI, S. 2013. Cellular building unit integrated with microstrand-shaped bacterial cellulose. *Biomaterials*, 34, 2421-2427.
- HO, T. C., CHANG, C. C., CHAN, H. P., CHUNG, T. W., SHU, C. W., CHUANG, K. P., DUH, T. H., YANG, M. H. & TYAN, Y. C. 2022. Hydrogels: Properties and Applications in Biomedicine. *Molecules*, 27.
- HOGREBE, N. J., REINHARDT, J. W., TRAM, N. K., DEBSKI, A. C., AGARWAL, G., REILLY, M. A. & GOOCH, K. J. 2018. Independent control of matrix adhesiveness and stiffness within a 3D self-assembling peptide hydrogel. *Acta Biomaterialia*, 70, 110-119.
- HOHENESTER, E. 2019. Structural biology of laminins. *Essays in Biochemistry*, 63, 285-295.
- HOLLEY, R. J., PICKFORD, C. E., RUSHTON, G., LACAUD, G., GALLAGHER, J. T., KOUSKOFF, V. & MERRY, C. L. 2011. Influencing hematopoietic differentiation of mouse embryonic stem cells using soluble heparin and heparan sulfate saccharides. *J Biol Chem*, 286, 6241-52.
- HONDARES, E., ROSELL, M., DÍAZ-DELFIN, J., OLMOS, Y., MONSALVE, M., IGLESIAS, R., VILLARROYA, F. & GIRALT, M. 2011. Peroxisome proliferator-activated receptor α (PPAR α) induces PPAR γ coactivator 1 α (PGC-1 α) gene expression and contributes

References

- to thermogenic activation of brown fat: involvement of PRDM16. *J Biol Chem*, 286, 43112-22.
- HOPFER, U., FUKAI, N., HOPFER, H., WOLF, G., JOYCE, N., LI, E. & OLSEN, B. R. 2005. Targeted disruption of Col8a1 and Col8a2 genes in mice leads to anterior segment abnormalities in the eye. *The FASEB Journal*, 19, 1232-1244.
- HOSHIBA, T., KAWAZOE, N., TATEISHI, T. & CHEN, G. 2010. Development of extracellular matrices mimicking stepwise adipogenesis of mesenchymal stem cells. *Adv Mater*, 22, 3042-7.
- HSIAO, A. Y., OKASHI, T. & TAKEUCHI, S. 2015a. Human Adipose-Derived stem cell fiber for breast reconstruction. *2015 28th IEEE International Conference on Micro Electro Mechanical Systems (MEMS)*. Portugal: IEEE.
- HSIAO, A. Y., OKITSU, T. & TAKEUCHI, S. Human adipose-derived stem cell fiber for breast reconstruction. *2015 28th IEEE International Conference on Micro Electro Mechanical Systems (MEMS)*, 18-22 Jan. 2015 2015b. 643-645.
- HSIAO, A. Y., OKITSU, T., TERAMAE, H. & TAKEUCHI, S. 2016. 3D Tissue Formation of Unilocular Adipocytes in Hydrogel Microfibers. *Advanced Healthcare Materials*, 5, 548-556.
- HSU, H. C., KE, Y. L., LAI, Y. H., HSIEH, W. C., LIN, C. H., HUANG, S. S., PENG, J. Y. & CHEN, C. H. 2022. Chondroitin Sulfate Enhances Proliferation and Migration via Inducing β -Catenin and Intracellular ROS as Well as Suppressing Metalloproteinases through Akt/NF- κ B Pathway Inhibition in Human Chondrocytes. *J Nutr Health Aging*, 26, 307-313.
- HU, B.-Y., WEICK, J. P., YU, J., MA, L.-X., ZHANG, X.-Q., THOMSON, J. A. & ZHANG, S.-C. 2010a. Neural differentiation of human induced pluripotent stem cells follows developmental principles but with variable potency. *Proceedings of the National Academy of Sciences of the United States of America*, 107, 4335-4340.
- HU, M., DENG, R., SCHUMACHER, K. M., KURISAWA, M., YE, H., PURNAMAWATI, K. & YING, J. Y. 2010b. Hydrodynamic spinning of hydrogel fibers. *Biomaterials*, 31, 863-869.
- HUANG, Z., NOOEAD, P., KOHL, B., ROETHER, J. A., SCHUBERT, D. W., MEIER, C., BOCCACCINI, A. R., GODKIN, O., ERTEL, W., ARENS, S. & SCHULZE-TANZIL, G. 2015. Chondrogenesis of human bone marrow mesenchymal stromal cells in highly porous alginate-foams supplemented with chondroitin sulfate. *Materials Science and Engineering: C*, 50, 160-172.
- HUDSON, D. M., WEIS, M. & EYRE, D. R. 2011. Insights on the evolution of prolyl 3-hydroxylation sites from comparative analysis of chicken and *Xenopus* fibrillar collagens. *PLoS One*, 6, e19336.
- HUGHES, C. S., POSTOVIT, L. M. & LAJOIE, G. A. 2010. Matrigel: a complex protein mixture required for optimal growth of cell culture. *Proteomics*, 10, 1886-90.
- HUMPHREY, J. D., DUFRESNE, E. R. & SCHWARTZ, M. A. 2014. Mechanotransduction and extracellular matrix homeostasis. *Nat Rev Mol Cell Biol*, 15, 802-12.
- HUNG, A. & SMIDSRØD, O. 1970. Selectivity of Some Anionic Polymers for Divalent Metal Ions. *ACTA Chemica Scandinavica*, 24, 843-854.
- HURT-CAMEJO, E., ROSENGREN, B., SARTIPY, P., ELFSBERG, K., CAMEJO, G. & SVENSSON, L. 1999. CD44, a Cell Surface Chondroitin Sulfate Proteoglycan, Mediates Binding of Interferon- γ and Some of Its Biological Effects on Human Vascular Smooth Muscle Cells*. *Journal of Biological Chemistry*, 274, 18957-18964.
- HYNES, R. O. 2002. Integrins: bidirectional, allosteric signaling machines. *cell*, 110, 673-687.

References

- HYNES, R. O. 2009. The extracellular matrix: not just pretty fibrils. *Science*, 326, 1216-1219.
- HYNES, R. O. & NABA, A. 2012. Overview of the matrisome--an inventory of extracellular matrix constituents and functions. *Cold Spring Harb Perspect Biol*, 4, a004903.
- IKEDA, K., NAGATA, S., OKITSU, T. & TAKEUCHI, S. 2017. Cell fiber-based three-dimensional culture system for highly efficient expansion of human induced pluripotent stem cells. *Scientific Reports*, 7, 2850.
- INOSTROZA-BRITO, K. E., COLLIN, E., SITON-MENDELSON, O., SMITH, K. H., MONGE-MARCET, A., FERREIRA, D. S., RODRIGUEZ, R. P., ALONSO, M., RODRIGUEZ-CABELLO, J. C., REIS, R. L., SAGUES, F., BOTTO, L., BITTON, R., AZEVEDO, H. S. & MATA, A. 2015. Co-assembly, spatiotemporal control and morphogenesis of a hybrid protein-peptide system. *Nat Chem*, 7, 897-904.
- IOANNIDOU, A., ALATAR, S., SCHIPPER, R., BAGANHA, F., ÅHLANDER, M., HORNELL, A., FISHER, R. M. & HAGBERG, C. E. 2022. Hypertrophied human adipocyte spheroids as in vitro model of weight gain and adipose tissue dysfunction. *The Journal of Physiology*, 600, 869-883.
- IOZZO, R. V. & SCHAEFER, L. 2015a. Proteoglycan form and function: A comprehensive nomenclature of proteoglycans. *Matrix Biol*, 42, 11-55.
- IOZZO, R. V. & SCHAEFER, L. 2015b. Proteoglycan form and function: A comprehensive nomenclature of proteoglycans. *Matrix Biology*, 42, 11-55.
- ISHIDA, A., OSHIKAWA, M., AJIOKA, I. & MURAOKA, T. 2020. Sequence-Dependent Bioactivity and Self-Assembling Properties of RGD-Containing Amphiphilic Peptides as Extracellular Scaffolds. *ACS Applied Bio Materials*, 3, 3605-3611.
- IZUMIKAWA, T., SATO, B. & KITAGAWA, H. 2014. Chondroitin sulfate is indispensable for pluripotency and differentiation of mouse embryonic stem cells. *Sci Rep*, 4, 3701.
- JABŁOŃSKA-TRYPUĆ, A., MATEJCZYK, M. & ROSOCHACKI, S. 2016. Matrix metalloproteinases (MMPs), the main extracellular matrix (ECM) enzymes in collagen degradation, as a target for anticancer drugs. *Journal of Enzyme Inhibition and Medicinal Chemistry*, 31, 177-183.
- JACOB, M. & HORNEBECK, W. 1985. Isolation and characterization of insoluble and kappa-elastins. *Frontiers of matrix biology*, 10, 92-129.
- JAKOBSEN, J. C., GLUUD, C., WETTERSLEV, J. & WINKEL, P. 2017. When and how should multiple imputation be used for handling missing data in randomised clinical trials - a practical guide with flowcharts. *BMC Med Res Methodol*, 17, 162.
- JANCZYK, P., HANSEN, S., BAHRAMSOLTANI, M. & PLENDL, J. 2010. The glycocalyx of human, bovine and murine microvascular endothelial cells cultured in vitro. *Journal of Electron Microscopy*, 9, 291-298.
- JANSEN, K. A., ATHERTON, P. & BALLESTREM, C. 2017. Mechanotransduction at the cell-matrix interface. *Seminars in Cell & Developmental Biology*, 28, 75-83.
- JASTRZEBSKI, Z. D. 1959. *Nature and properties of engineering materials*, New York, Wiley.
- JHA, A. K., XU, X., DUNCAN, R. L. & JIA, X. 2011. Controlling the adhesion and differentiation of mesenchymal stem cells using hyaluronic acid-based, doubly crosslinked networks. *Biomaterials*, 32, 2466-2478.
- JIANG, H., GULER, M. O. & STUPP, S. I. 2007. The internal structure of self-assembled peptide amphiphiles nanofibers. *Soft Matter*, 3, 454-462.
- JIN, T. R. N. S. R. C. M. R. N. L. L. R. N. L. K.-K. Collagen matrix stiffness influencing on fibroblast contraction force. *Frontiers in Bioengineering and Biotechnology*.

References

- JOHNSON, C. E., CRAWFORD, B. E., STAVRIDIS, M., TEN DAM, G., WAT, A. L., RUSHTON, G., WARD, C. M., WILSON, V., VAN KUPPEVELT, T. H., ESKO, J. D., SMITH, A., GALLAGHER, J. T. & MERRY, C. L. 2007. Essential alterations of heparan sulfate during the differentiation of embryonic stem cells to Sox1-enhanced green fluorescent protein-expressing neural progenitor cells. *Stem Cells*, 25, 1913-23.
- JOSAN, C., KAKAR, S. & RAHA, S. 2021. Matrigel® enhances 3T3-L1 cell differentiation. *Adipocyte*, 10, 361-377.
- JUNIOR, I., CASTRO, M., SILVA, D. & CORTEZ, C. 2016. Relevance of Hydrodynamic Effects for the Calculation of Outer Surface Potential of Biological Membrane Using Electrophoretic Data. *Anais da Academia Brasileira de Ciências*, 88.
- KADLER, K. E., BALDOCK, C., BELLA, J. & BOOT-HANDFORD, R. P. 2007. Collagens at a glance. *Journal of cell science*, 120, 1955-1958.
- KADLER, K. E., HOLMES, D. F., TROTTER, J. A. & CHAPMAN, J. A. 1996. Collagen fibril formation. *Biochem J*, 316 (Pt 1), 1-11.
- KAJIMURA, S., SEALE, P., KUBOTA, K., LUNSFORD, E., FRANGIONI, J. V., GYGI, S. P. & SPIEGELMAN, B. M. 2009. Initiation of myoblast to brown fat switch by a PRDM16-C/EBP-beta transcriptional complex. *Nature*, 460, 1154-8.
- KAJITA, K., MUNE, T., IKEDA, T., MATSUMOTO, M., UNO, Y., SUGIYAMA, C., MATSUBARA, K., MORITA, H., TAKEMURA, M., SEISHIMA, M., TAKEDA, J. & ISHIZUKA, T. 2008. Effect of fasting on PPARgamma and AMPK activity in adipocytes. *Diabetes research and clinical practice*, 81 2, 144-9.
- KANG, E., CHOI, Y. Y., CHAE, S.-K., MOON, J.-H., CHANG, J.-Y. & LEE, S.-H. 2012. Microfluidic Spinning of Flat Alginate Fibers with Grooves for Cell-Aligning Scaffolds. *Advanced Materials*, 24, 4271-4277.
- KANG, S.-M., LEE, J.-H., HUH, Y. S. & TAKAYAMA, S. 2021. Alginate Microencapsulation for Three-Dimensional In Vitro Cell Culture. *ACS Biomaterials Science & Engineering*, 7, 2864-2879.
- KAPALCZYŃSKA, M., KOLENDA, T., PRZYBYŁA, W., ZAJĄCZKOWSKA, M., TERESIAK, A., FILAS, V., IBBS, M., BLIŹNIAK, R., ŁUCZEWSKI, Ł. & LAMPERSKA, K. 2018. 2D and 3D cell cultures - a comparison of different types of cancer cell cultures. *Arch Med Sci*, 14, 910-919.
- KARAMANOS, N. K., PIPERIGKOU, Z., THEOCHARIS, A. D., WATANABE, H., FRANCHI, M., BAUD, S., BRÉZILLON, S., GÖTTE, M., PASSI, A., VIGETTI, D., RICARD-BLUM, S., SANDERSON, R. D., NEILL, T. & IOZZO, R. V. 2018. Proteoglycan Chemical Diversity Drives Multifunctional Cell Regulation and Therapeutics. *Chem Rev*, 118, 9152-9232.
- KAWABE, K., TATEYAMA, D., TOYODA, H., KAWASAKI, N., HASHII, N., NAKAO, H., MATSUMOTO, S., NONAKA, M., MATSUMURA, H., HIROSE, Y., MORITA, A., KATAYAMA, M., SAKUMA, M., KAWASAKI, N., FURUE, M. K. & KAWASAKI, T. 2013. A novel antibody for human induced pluripotent stem cells and embryonic stem cells recognizes a type of keratan sulfate lacking oversulfated structures. *Glycobiology*, 23, 322-36.
- KIKUCHI, A., KATAOKA, K. & TSURUTA, T. 1992. Adhesion and proliferation of bovine aortic endothelial cells on monoamine- and diamine-containing polystyrene derivatives. *Journal of Biomaterials Science, Polymer Edition*, 3, 253-260.
- KIM, G. C., CHEON, D. H. & LEE, Y. 2021. Challenge to overcome current limitations of cell-penetrating peptides. *Biochimica et Biophysica Acta (BBA) - Proteins and Proteomics*, 1869, 140604.

References

- KIM, H. J., PARK, Y. J., JIN, S., YOON, S., KWAK, J.-Y. & JEONG, H. Y. 2019. A Microfluidic Chip Embracing a Nanofiber Scaffold for 3D Cell Culture and Real-Time Monitoring. *Nanomaterials*, 9.
- KIM, S., MIN, S., CHOI, Y. S., JO, S.-H., JUNG, J. H., HAN, K., KIM, J., AN, S., JI, Y. W., KIM, Y.-G. & CHO, S.-W. 2022. Tissue extracellular matrix hydrogels as alternatives to Matrigel for culturing gastrointestinal organoids. *Nature Communications*, 13, 1692.
- KIRIYA, D., KAWANO, R., ONOE, H. & TAKEUCHI, S. 2012. Microfluidic Control of the Internal Morphology in Nanofiber-Based Macroscopic Cables. *Angewandte Chemie International Edition*, 51, 7942-7947.
- KIRKPATRICK, C. A., DIMITROFF, B. D., RAWSON, J. M. & SELLECK, S. B. 2004. Spatial Regulation of Wingless Morphogen Distribution and Signaling by Dally-like Protein. *Developmental Cell*, 7, 513-523.
- KISLER, K., SAGARE, A. P., LAZIC, D., BAZZI, S., LAWSON, E., HSU, C. J., WANG, Y., RAMANATHAN, A., NELSON, A. R., ZHAO, Z. & ZLOKOVIC, B. V. 2023. Anti-malaria drug artesunate prevents development of amyloid- β pathology in mice by upregulating PICALM at the blood-brain barrier. *Mol Neurodegener*, 18, 7.
- KLEINMAN, H. K. & MARTIN, G. R. 2005. Matrigel: Basement membrane matrix with biological activity. *Seminars in Cancer Biology*, 15, 378-386.
- KLEINMAN, H. K., MCGARVEY, M. L., LIOTTA, L. A., ROBEY, P. G., TRYGGVASON, K. & MARTIN, G. R. 1982. Isolation and characterization of type IV procollagen, laminin, and heparan sulfate proteoglycan from the EHS sarcoma. *Biochemistry*, 21, 6188-93.
- KLEINMAN, H. K., WEEKS, B. S., CANNON, F. B., SWEENEY, T. M., SEPHEL, G. C., CLEMENT, B., ZAIN, M., OLSON, M. O. J., JUCKER, M. & BURROUS, B. A. 1991. Identification of a 110-kDa nonintegrin cell surface laminin-binding protein which recognizes an a chain neurite-promoting peptide. *Archives of Biochemistry and Biophysics*, 290, 320-325.
- KLINGELHUTZ, A. J., GOURRONC, F. A., CHALY, A., WADKINS, D. A., BURAND, A. J., MARKAN, K. R., IDIGA, S. O., WU, M., POTTHOFF, M. J. & ANKRUM, J. A. 2018. Scaffold-free generation of uniform adipose spheroids for metabolism research and drug discovery. *Scientific Reports*, 8, 523.
- KLOTZ, B. J., GAWLITTA, D., ROSENBERG, A., MALDA, J. & MELCHELS, F. P. W. 2016. Gelatin-Methacryloyl Hydrogels: Towards Biofabrication-Based Tissue Repair. *Trends Biotechnol*, 34, 394-407.
- KOCH, F., MÜLLER, M., KÖNIG, F., MEYER, N., GATTLEN, J., PIELES, U., PETERS, K., KREIKEMEYER, B., MATHES, S. & SAXER, S. 2018. Mechanical characteristics of beta sheet-forming peptide hydrogels are dependent on peptide sequence, concentration and buffer composition. *R Soc Open Sci*, 5, 171562.
- KOMATSU, N., KAJIYA, M., MOTOIKE, S., TAKEWAKI, M., HORIKOSHI, S., IWATA, T., OUHARA, K., TAKEDA, K., MATSUDA, S., FUJITA, T. & KURIHARA, H. 2018. Type I collagen deposition via osteoinduction ameliorates YAP/TAZ activity in 3D floating culture clumps of mesenchymal stem cell/extracellular matrix complexes. *Stem Cell Research & Therapy*, 9, 342.
- KOVANEN, V. 2002. Intramuscular extracellular matrix: complex environment of muscle cells. *Exercise and sport sciences reviews*, 30, 20-25.
- KOZEL, B. A., MECHAM, R. P. & ROSENBLOOM, J. 2011. Elastin. In: MECHAM, R. P. (ed.) *The Extracellular Matrix: an Overview*. Berlin, Heidelberg: Springer Berlin Heidelberg.
- KOZLOWSKI, M. T., CROOK, C. J. & KU, H. T. 2021. Towards organoid culture without Matrigel. *Communications Biology*, 4, 1387.

References

- KRISTENSEN, J. H. & KARSDAL, M. A. 2016. Chapter 30 - Elastin. *In: KARSDAL, M. A. (ed.) Biochemistry of Collagens, Laminins and Elastin*. Academic Press.
- KUBO, Y., KAIJZU, S., NAKAJIMA, I., TAKENOUCI, K. & NAKAMURA, F. 2000. Organization of extracellular matrix components during differentiation of adipocytes in long-term culture. *In Vitro Cellular & Developmental Biology - Animal*, 36, 38-44.
- KUO, C. K. & MA, P. X. 2001. Ionically crosslinked alginate hydrogels as scaffolds for tissue engineering: Part 1. Structure, gelation rate and mechanical properties. *Biomaterials*, 22, 511-521.
- KUO, C. K. & TUAN, R. S. 2008. Mechanoactive tenogenic differentiation of human mesenchymal stem cells. *Tissue Eng Part A*, 14, 1615-27.
- KURODA, M., WADA, H., KIMURA, Y., UEDA, K. & KIOKA, N. 2017. Vinculin promotes nuclear localization of TAZ to inhibit ECM stiffness-dependent differentiation into adipocytes. *Journal of cell science*, 130, 989-1002.
- KWAN, H. Y., WU, J., SU, T., CHAO, X. J., LIU, B., FU, X., CHAN, C. L., LAU, R. H. Y., TSE, A. K. W., HAN, Q. B., FONG, W. F. & YU, Z. L. 2017. Cinnamon induces browning in subcutaneous adipocytes. *Sci Rep*, 7, 2447.
- LAM, M. T. & LONGAKER, M. T. 2012. Comparison of several attachment methods for human iPS, embryonic and adipose-derived stem cells for tissue engineering. *Journal of tissue engineering and regenerative medicine*, 6 Suppl 3, s80-s86.
- LAPERLE, A., HSIAO, C., LAMPE, M., MORTIER, J., SAHA, K., PALECEK, S. P. & MASTERS, K. S. 2015. α -5 Laminin Synthesized by Human Pluripotent Stem Cells Promotes Self-Renewal. *Stem Cell Reports*, 5, 195-206.
- LAU, W. K., NORUDDIN, N. A. A., ARIFFIN, A. H., MAHMUD, M. Z., NOOR, M. H. M., AMANAH, A., HAMZAH, M. F. & ZAFARINA, Z. 2019. Novel discovery of Averrhoa bilimbi ethanolic leaf extract in the stimulation of brown fat differentiation program in combating diet-induced obesity. *BMC Complementary and Alternative Medicine*, 19, 243.
- LAURENT, T. C. & FRASER, J. R. 1992. Hyaluronan. *Faseb j*, 6, 2397-404.
- LAWLER, H. M., UNDERKOFER, C. M., KERN, P. A., ERICKSON, C., BREDBECK, B. & RASOULI, N. 2016. Adipose Tissue Hypoxia, Inflammation, and Fibrosis in Obese Insulin-Sensitive and Obese Insulin-Resistant Subjects. *J Clin Endocrinol Metab*, 101, 1422-8.
- LE BELLEGO, F., FABRE, S., PISSELET, C. & MONNIAUX, D. 2005. Cytoskeleton reorganization mediates α 6 β 1 integrin-associated actions of laminin on proliferation and survival, but not on steroidogenesis of ovine granulosa cells. *Reproductive biology and endocrinology : RB&E* [Online], 3. Available: <http://europepmc.org/abstract/MED/15892896>
- <https://doi.org/10.1186/1477-7827-3-19>
- <https://europepmc.org/articles/PMC1156948>
- <https://europepmc.org/articles/PMC1156948?pdf=render> [Accessed 2005/05/].
- LEBERFINGER, A., RAVNIC, D., DHAWAN, A. & OZBOLAT, I. 2017. Concise Review: Bioprinting of Stem Cells for Transplantable Tissue Fabrication. *STEM CELLS Translational Medicine*, 6.
- LEE, G., HYNES, R. & KIRSCHNER, M. 1984. Temporal and spatial regulation of fibronectin in early *Xenopus* development. *Cell*, 36, 729-40.
- LEE, G., PAPAPETROU, E. P., KIM, H., CHAMBERS, S. M., TOMISHIMA, M. J., FASANO, C. A., GANAT, Y. M., MENON, J., SHIMIZU, F., VIALE, A., TABAR, V., SADELAIN,

References

- M. & STUDER, L. 2009a. Modelling pathogenesis and treatment of familial dysautonomia using patient-specific iPSCs. *Nature*, 461, 402-6.
- LEE, G. M., JOHNSTONE, B., JACOBSON, K. & CATERSON, B. 1993. The dynamic structure of the pericellular matrix on living cells. *J Cell Biol*, 123, 1899-907.
- LEE, H., HONG, H. J., AHN, S., KIM, D., KANG, S. H., CHO, K. & KOH, W. G. 2023. One-Pot Synthesis of Double-Network PEG/Collagen Hydrogel for Enhanced Adipogenic Differentiation and Retrieval of Adipose-Derived Stem Cells. *Polymers (Basel)*, 15.
- LEE, J. S., SHIN, J., PARK, H.-M., KIM, Y.-G., KIM, B.-G., OH, J.-W. & CHO, S.-W. 2014. Liver Extracellular Matrix Providing Dual Functions of Two-Dimensional Substrate Coating and Three-Dimensional Injectable Hydrogel Platform for Liver Tissue Engineering. *Biomacromolecules*, 15, 206-218.
- LEE, K. H., SHIN, S. J., KIM, C.-B., KIM, J. K., CHO, Y. W., CHUNG, B. G. & LEE, S.-H. 2010. Microfluidic synthesis of pure chitosan microfibers for bio-artificial liver chip. *Lab on a Chip*, 10, 1328-1334.
- LEE, K. H., SHIN, S. J., PARK, Y. & LEE, S.-H. 2009b. Synthesis of Cell-Laden Alginate Hollow Fibers Using Microfluidic Chips and Microvascularized Tissue-Engineering Applications. *Small*, 5, 1264-1268.
- LEE, M.-J. & FRIED, S. K. 2014. Optimal protocol for the differentiation and metabolic analysis of human adipose stromal cells. *Methods in enzymology*, 538, 49-65.
- LEFTEROVA, M. I., ZHANG, Y., STEGER, D. J., SCHUPP, M., SCHUG, J., CRISTANCHO, A., FENG, D., ZHUO, D., STOECKERT, C. J., JR., LIU, X. S. & LAZAR, M. A. 2008. PPARgamma and C/EBP factors orchestrate adipocyte biology via adjacent binding on a genome-wide scale. *Genes Dev*, 22, 2941-52.
- LEIKINA, E., MERTTS, M., KUZNETSOVA, N. & LEIKIN, S. 2002. Type I collagen is thermally unstable at body temperature. *Proceedings of the National Academy of Sciences*, 99, 1314-1318.
- LEIVO, I., VAHERI, A., TIMPL, R. & WARTIOVAARA, J. 1980. Appearance and distribution of collagens and laminin in the early mouse embryo. *Dev Biol*, 76, 100-14.
- LESNÝ, P., PŘÁDNÝ, M., JENDELOVA, P., MICHALEK, J., VACIK, J. & SYKOVÁ, E. 2006. Macroporous hydrogels based on 2-hydroxyethyl methacrylate. Part 4: growth of rat bone marrow stromal cells in three-dimensional hydrogels with positive and negative surface charges and in polyelectrolyte complexes. *Journal of Materials Science: Materials in Medicine*, 17, 829-833.
- LI, H., GHAZANFARI, R., ZACHARAKI, D., LIM, H. C. & SCHEDING, S. 2016. Isolation and characterization of primary bone marrow mesenchymal stromal cells. *Ann N Y Acad Sci*, 1370, 109-18.
- LI, H., QI, Z., ZHENG, S., CHANG, Y., KONG, W., FU, C., YU, Z., YANG, X. & PAN, S. 2019. The Application of Hyaluronic Acid-Based Hydrogels in Bone and Cartilage Tissue Engineering. *Advances in Materials Science and Engineering*, 2019, 3027303.
- LI, J., CHEN, J. & KIRSNER, R. 2007. Pathophysiology of acute wound healing. *Clin Dermatol*, 25, 9-18.
- LI, J., MA, J., ZHANG, Q., GONG, H., GAO, D., WANG, Y., LI, B., LI, X., ZHENG, H., WU, Z., ZHU, Y. & LENG, L. 2022a. Spatially resolved proteomic map shows that extracellular matrix regulates epidermal growth. *Nature Communications*, 13, 4012.
- LI, J., ZHANG, K., WU, J., ZHANG, L., YANG, P., TU, Q. & HUANG, N. 2015. Tailoring of the titanium surface by preparing cardiovascular endothelial extracellular matrix layer on the hyaluronic acid micro-pattern for improving biocompatibility. *Colloids and Surfaces B: Biointerfaces*, 128, 201-210.

References

- LI, L. & XIE, T. 2005. STEM CELL NICHE: Structure and Function. *Annual Review of Cell and Developmental Biology*, 21, 605-631.
- LI, M., CHU, X., WANG, D., JIAN, L., LIU, L., YAO, M., ZHANG, D., ZHENG, Y., LIU, X., ZHANG, Y. & PENG, F. 2022b. Tuning the surface potential to reprogram immune microenvironment for bone regeneration. *Biomaterials*, 282, 121408.
- LI, R. H., ALTREUTER, D. H. & GENTILE, F. T. 1996. Transport characterization of hydrogel matrices for cell encapsulation. *Biotechnology and Bioengineering*, 50, 365-373.
- LI, Z. 2019. 5.40 - In Vitro Micro Tissue and Organ Models for Toxicity Testing☆. In: MOO-YOUNG, M. (ed.) *Comprehensive Biotechnology (Third Edition)*. Oxford: Pergamon.
- LIBBY, R. T., CHAMPLIAUD, M.-F., CLAUDEPIERRE, T., XU, Y., GIBBONS, E. P., KOCH, M., BURGESSON, R. E., HUNTER, D. D. & BRUNKEN, W. J. 2000. Laminin expression in adult and developing retinae: evidence of two novel CNS laminins. *Journal of Neuroscience*, 20, 6517-6528.
- LIDELL, M. E. 2019. Brown Adipose Tissue in Human Infants. *Handb Exp Pharmacol*, 251, 107-123.
- LIN, C.-C. & ANSETH, K. S. 2009. PEG hydrogels for the controlled release of biomolecules in regenerative medicine. *Pharmaceutical research*, 26, 631-643.
- LIN, J. Z. & FARMER, S. R. 2016. Morphogenetics in brown, beige and white fat development. *Adipocyte*, 5, 130-5.
- LIN, Y. A. C., G., 2014. Embryoid body formation from human pluripotent stem cells in chemically defined E8 media The Stem Cell Research Community, StemBook.
- LIPPMANN, E. S., ESTEVEZ-SILVA, M. C. & ASHTON, R. S. 2014. Defined Human Pluripotent Stem Cell Culture Enables Highly Efficient Neuroepithelium Derivation Without Small Molecule Inhibitors. *Stem Cells*, 32, 1032-1042.
- LISIGNOLI, G., CRISTINO, S., PIACENTINI, A., CAVALLO, C., CAPLAN, A. I. & FACCHINI, A. 2006. Hyaluronan-based polymer scaffold modulates the expression of inflammatory and degradative factors in mesenchymal stem cells: Involvement of Cd44 and Cd54. *Journal of Cellular Physiology*, 207, 364-373.
- LISSITZKY, J. C., KOPP, F., CHARPIN, C., CHIAROTTI, Y., BIGNON, C. & MARTIN, P. M. 1986. [Laminin: biosynthesis, structure and functions]. *Pathol Biol (Paris)*, 34, 955-63.
- LIU, C., HUANG, K., LI, G., WANG, P., LIU, C., GUO, C., SUN, Z. & PAN, J. 2017a. Ascorbic acid promotes 3T3-L1 cells adipogenesis by attenuating ERK signaling to upregulate the collagen VI. *Nutrition & Metabolism*, 14, 79.
- LIU, D., WANG, S., ZHANG, J., XIAO, W., MIAO, C. H., KONKLE, B. A., WAN, X.-F. & LI, L. 2021. Site-Specific N- and O-Glycosylation Analysis of Human Plasma Fibronectin. *Frontiers in chemistry* [Online], 9. Available: <http://europepmc.org/abstract/MED/34211961>
- <https://doi.org/10.3389/fchem.2021.691217>
- <https://europepmc.org/articles/PMC8239226>
- <https://europepmc.org/articles/PMC8239226?pdf=render> [Accessed 2021].
- LIU, H., YANG, L., ZHANG, E., ZHANG, R., CAI, D., ZHU, S., RAN, J., BUNPETCH, V., CAI, Y., HENG, B. C., HU, Y., DAI, X., CHEN, X. & OUYANG, H. 2017b. Biomimetic tendon extracellular matrix composite gradient scaffold enhances ligament-to-bone junction reconstruction. *Acta Biomater*, 56, 129-140.
- LIU, J. F., CHEN, Y. M., YANG, J. J., KUROKAWA, T., KAKUGO, A., YAMAMOTO, K. & GONG, J. P. 2011. Dynamic behavior and spontaneous differentiation of mouse

References

- embryoid bodies on hydrogel substrates of different surface charge and chemical structures. *Tissue Eng Part A*, 17, 2343-57.
- LIU, M., ZHOU, Z., CHAI, Y., ZHANG, S., WU, X., HUANG, S., SU, J. & JIANG, J. 2017c. Synthesis of cell composite alginate microfibers by microfluidics with the application potential of small diameter vascular grafts. *Biofabrication*, 9, 025030.
- LIU, R.-M., SUN, R.-G., ZHANG, L.-T., ZHANG, Q.-F., CHEN, D.-X., ZHONG, J.-J. & XIAO, J.-H. 2016. Hyaluronic acid enhances proliferation of human amniotic mesenchymal stem cells through activation of Wnt/ β -catenin signaling pathway. *Experimental Cell Research*, 345, 218-229.
- LIU, X., LONG, X., GAO, Y., LIU, W., HAYASHI, T., MIZUNO, K., HATTORI, S., FUJISAKI, H., OGURA, T., ONODERA, S., WANG, D. O. & IKEJIMA, T. 2020a. Type I collagen inhibits adipogenic differentiation via YAP activation in vitro. *Journal of Cellular Physiology*, 235, 1821-1837.
- LIU, X., WU, H., BYRNE, M., JEFFREY, J., KRANE, S. & JAENISCH, R. 1995. A targeted mutation at the known collagenase cleavage site in mouse type I collagen impairs tissue remodeling. *The Journal of cell biology*, 130, 227-237.
- LIU, Y., LI, Z., LI, J., YANG, S., ZHANG, Y., YAO, B., SONG, W., FU, X. & HUANG, S. 2020b. Stiffness-mediated mesenchymal stem cell fate decision in 3D-bioprinted hydrogels. *Burns Trauma*, 8, tkaa029.
- LIYANAGE, S., DASSANAYAKE, R. S., BOUYANFIF, A., RAJAKARUNA, E., RAMALINGAM, L., MOUSTAID-MOUSSA, N. & ABIDI, N. 2017. Optimization and validation of cryostat temperature conditions for trans-reflectance mode FTIR microspectroscopic imaging of biological tissues. *MethodsX*, 4, 118-127.
- LOEBEL, C., MAUCK, R. L. & BURDICK, J. A. 2019. Local nascent protein deposition and remodelling guide mesenchymal stromal cell mechanosensing and fate in three-dimensional hydrogels. *Nat Mater*, 18, 883-891.
- LOEBEL, C., SALEH, A. M., JACOBSON, K. R., DANIELS, R., MAUCK, R. L., CALVE, S. & BURDICK, J. A. 2022. Metabolic labeling of secreted matrix to investigate cell-material interactions in tissue engineering and mechanobiology. *Nature Protocols*, 17, 618-648.
- LOGAN, CLARE V., COSSINS, J., RODRÍGUEZ CRUZ, PEDRO M., PARRY, DAVID A., MAXWELL, S., MARTÍNEZ-MARTÍNEZ, P., RIEPSAAME, J., ABDELHAMED, ZAKIA A., LAKE, ALICE V. R., MORAN, M., ROBB, S., CHOW, G., SEWRY, C., HOPKINS, PHILIP M., SHERIDAN, E., JAYAWANT, S., PALACE, J., JOHNSON, COLIN A. & BEESON, D. 2015. Congenital Myasthenic Syndrome Type 19 Is Caused by Mutations in COL13A1, Encoding the Atypical Non-fibrillar Collagen Type XIII α 1 Chain. *The American Journal of Human Genetics*, 97, 878-885.
- LOU, J., STOWERS, R., NAM, S., XIA, Y. & CHAUDHURI, O. 2018. Stress relaxing hyaluronic acid-collagen hydrogels promote cell spreading, fiber remodeling, and focal adhesion formation in 3D cell culture. *Biomaterials*, 154, 213-222.
- LOUIS, F., KITANO, S., MANO, J. F. & MATSUSAKI, M. 2019. 3D collagen microfibers stimulate the functionality of preadipocytes and maintain the phenotype of mature adipocytes for long term cultures. *Acta Biomaterialia*, 84, 194-207.
- LOUIS, F., PANNETIER, P., SOUGUIR, Z., LE CERF, D., VALET, P., VANNIER, J.-P., VIDAL, G. & DEMANGE, E. 2017. A biomimetic hydrogel functionalized with adipose ECM components as a microenvironment for the 3D culture of human and murine adipocytes. *Biotechnology and Bioengineering*, 114, 1813-1824.
- LOUIS, F., SOWA, Y., KITANO, S. & MATSUSAKI, M. 2022. High-throughput drug screening models of mature adipose tissues which replicate the physiology of patients' Body Mass Index (BMI). *Bioact Mater*, 7, 227-241.

References

- LU, H. F., CHAI, C., LIM, T. C., LEONG, M. F., LIM, J. K., GAO, S., LIM, K. L. & WAN, A. C. 2014. A defined xeno-free and feeder-free culture system for the derivation, expansion and direct differentiation of transgene-free patient-specific induced pluripotent stem cells. *Biomaterials*, 35, 2816-26.
- LU, P., TAKAI, K., WEAVER, V. M. & WERB, Z. 2011. Extracellular matrix degradation and remodeling in development and disease. *Cold Spring Harb Perspect Biol*, 3.
- LUTOLF, M. P. & HUBBELL, J. A. 2005. Synthetic biomaterials as instructive extracellular microenvironments for morphogenesis in tissue engineering. *Nat Biotechnol*, 23, 47-55.
- LUTOLF, M. P., LAUER-FIELDS, J. L., SCHMOEKEL, H. G., METTERS, A. T., WEBER, F. E., FIELDS, G. B. & HUBBELL, J. A. 2003. Synthetic matrix metalloproteinase-sensitive hydrogels for the conduction of tissue regeneration: engineering cell-invasion characteristics. *Proceedings of the National Academy of Sciences of the United States of America*, 100, 5413-5418.
- LV, H., ZHANG, S., WANG, B., CUI, S. & YAN, J. 2006. Toxicity of cationic lipids and cationic polymers in gene delivery. *J Control Release*, 114, 100-9.
- MACHIDA-SANO, I., OGAWA, S., UEDA, H., KIMURA, Y., SATOH, N. & NAMIKI, H. 2012. Effects of Composition of Iron-Cross-Linked Alginate Hydrogels for Cultivation of Human Dermal Fibroblasts. *International Journal of Biomaterials*, 2012, 8.
- MADANI, F. & GRÄSLUND, A. 2022. Membrane Molecular Interactions and Induced Structures of CPPs. *In: LANGEL, Ü. (ed.) Cell Penetrating Peptides: Methods and Protocols*. New York, NY: Springer US.
- MAHERALI, N., SRIDHARAN, R., XIE, W., UTIKAL, J., EMINLI, S., ARNOLD, K., STADTFELD, M., YACHECHKO, R., TCHIEU, J., JAENISCH, R., PLATH, K. & HOCHEDLINGER, K. 2007. Directly reprogrammed fibroblasts show global epigenetic remodeling and widespread tissue contribution. *Cell Stem Cell*, 1, 55-70.
- MANDL, M., VIERTLER, H. P., HATZMANN, F. M., BRUCKER, C., GROSSMAN, S., WALDEGGER, P., RAUCHENWALD, T., MATTESICH, M., ZWIERZINA, M., PIERER, G. & ZWERSCHKE, W. 2022. An organoid model derived from human adipose stem/progenitor cells to study adipose tissue physiology. *Adipocyte*, 11, 164-174.
- MARTIN, G. R. 1981. Isolation of a pluripotent cell line from early mouse embryos cultured in medium conditioned by teratocarcinoma stem cells. *Proc Natl Acad Sci U S A*, 78, 7634-8.
- MARTINO, M. M., MOCHIZUKI, M., ROTHENFLUH, D. A., REMPEL, S. A., HUBBELL, J. A. & BARKER, T. H. 2009. Controlling integrin specificity and stem cell differentiation in 2D and 3D environments through regulation of fibronectin domain stability. *Biomaterials*, 30, 1089-1097.
- MATA, A., GENG, Y., HENRIKSON, K. J., APARICIO, C., STOCK, S. R., SATCHER, R. L. & STUPP, S. I. 2010. Bone regeneration mediated by biomimetic mineralization of a nanofiber matrix. *Biomaterials*, 31, 6004-12.
- MATA, A., HSU, L., CAPITO, R., APARICIO, C., HENRIKSON, K. & STUPP, S. I. 2009. Micropatterning of bioactive self-assembling gels. *Soft Matter*, 5, 1228-1236.
- MATA, A., PALMER, L., TEJEDA-MONTES, E. & STUPP, S. I. 2012. Design of Biomolecules for Nanoengineered Biomaterials for Regenerative Medicine. *In: NAVARRO, M. & PLANELL, J. A. (eds.) Nanotechnology in Regenerative Medicine: Methods and Protocols*. Totowa, NJ: Humana Press.
- MATACCHIONE, G., PERUGINI, J., DI MERCURIO, E., SABBATINELLI, J., PRATTICIZZO, F., SENZACQUA, M., STORCI, G., DANI, C., LEZOCHÉ, G., GUERRIERI, M.,

References

- GIORDANO, A., BONAFÈ, M. & OLIVIERI, F. 2022. Senescent macrophages in the human adipose tissue as a source of inflammaging. *GeroScience*.
- MATSON, J. B. & STUPP, S. I. 2012. Self-assembling peptide scaffolds for regenerative medicine. *Chemical Communications*, 48, 26-33.
- MAU, K. H. T., KARIMLOU, D., BARNEDA, D., BROCHARD, V., ROYER, C., LEEKE, B., DE SOUZA, R. A., PAILLES, M., PERCHARDE, M., SRINIVAS, S., JOUNEAU, A., CHRISTIAN, M. & AZUARA, V. 2022. Dynamic enlargement and mobilization of lipid droplets in pluripotent cells coordinate morphogenesis during mouse peri-implantation development. *Nature Communications*, 13, 3861.
- MAZARI-ARRIGHI, E., OKITSU, T., TERAMAE, H., AOYAGI, H., KIYOSAWA, M., YANO, M., CHATELAIN, F., FUCHS, A. & TAKEUCHI, S. 2022. In vitro proliferation and long-term preservation of functional primary rat hepatocytes in cell fibers. *Scientific Reports*, 12, 8813.
- MCCLOY, R. A., ROGERS, S., CALDON, C. E., LORCA, T., CASTRO, A. & BURGESS, A. 2014. Partial inhibition of Cdk1 in G2 phase overrides the SAC and decouples mitotic events. *Cell Cycle*, 13, 1400-1412.
- MCCONNELL, B. B. & YANG, V. W. 2010. Mammalian Krüppel-like factors in health and diseases. *Physiol Rev*, 90, 1337-81.
- MCELREAVEY, K. D., IRVINE, A. I., ENNIS, K. T. & MCLEAN, W. H. 1991. Isolation, culture and characterisation of fibroblast-like cells derived from the Wharton's jelly portion of human umbilical cord. *Biochem Soc Trans*, 19, 29s.
- MECHAM, R. P. 1998. Overview of Extracellular Matrix. *Current Protocols in Cell Biology*, 00, 10.1.1-10.1.14.
- MEHTA, F., THEUNISSEN, R. & POST, M. J. 2019. Adipogenesis from Bovine Precursors. In: RØNNING, S. B. (ed.) *Myogenesis: Methods and Protocols*. New York, NY: Springer New York.
- MENCIO, C. P., HUSSEIN, R. K., YU, P. & GELLER, H. M. 2021. The Role of Chondroitin Sulfate Proteoglycans in Nervous System Development. *J Histochem Cytochem*, 69, 61-80.
- MERRY, C. L., LINDAHL, U., COUCHMAN, J. & ESKO, J. D. 2022. Proteoglycans and Sulfated Glycosaminoglycans. In: VARKI A, C. R. & ESKO JD (eds.) *Essentials of Glycobiology*. NY: Cold Spring Harbor Laboratory Press.
- MESCHER, A. 2016. *Junqueira's Basic Histology Text & Atlas (14th ed.)*.
- MINER, J. H. & YURCHENCO, P. D. 2004. Laminin functions in tissue morphogenesis. *Annu. Rev. Cell Dev. Biol.*, 20, 255-284.
- MIRABEDINI, A. 2018. *Developing novel spinning methods to fabricate continuous multifunctional fibres for bioapplications*, Springer.
- MOFFAT, D., YE, K. & JIN, S. 2022. Decellularization for the retention of tissue niches. *Journal of Tissue Engineering*, 13, 20417314221101151.
- MOHR, J. C., ZHANG, J., AZARIN, S. M., SOERENS, A. G., DE PABLO, J. J., THOMSON, J. A., LYONS, G. E., PALECEK, S. P. & KAMP, T. J. 2010. The microwell control of embryoid body size in order to regulate cardiac differentiation of human embryonic stem cells. *Biomaterials*, 31, 1885-93.
- MOHSEN-KANSON, T., HAFNER, A.-L., WDZIEKONSKI, B., TAKASHIMA, Y., VILLAGEOIS, P., CARRIÈRE, A., SVENSSON, M., BAGNIS, C., CHIGNON-SICARD, B., SVENSSON, P.-A., CASTEILLA, L., SMITH, A. & DANI, C. 2014. Differentiation of

References

- Human Induced Pluripotent Stem Cells into Brown and White Adipocytes: Role of Pax3. *Stem Cells*, 32, 1459-1467.
- MONK, J. M., LIDDLE, D. M., HUTCHINSON, A. L. & ROBINSON, L. E. 2020. Studying Adipocyte and Immune Cell Cross Talk Using a Co-culture System. In: MISHRA, S. (ed.) *Immunometabolism: Methods and Protocols*. New York, NY: Springer US.
- MONTEIRO, N., MARTINS, A., REIS, R. L. & NEVES, N. 2014. Liposomes in tissue engineering and regenerative medicine. *Journal of the Royal Society, Interface / the Royal Society*, 11, 20140459.
- MOON, J. J., SAIK, J. E., POCHÉ, R. A., LESLIE-BARBICK, J. E., LEE, S.-H., SMITH, A. A., DICKINSON, M. E. & WEST, J. L. 2010. Biomimetic hydrogels with pro-angiogenic properties. *Biomaterials*, 31, 3840-3847.
- MORISSETTE MARTIN, P., SHRIDHAR, A., YU, C., BROWN, C. & FLYNN, L. E. 2018. Decellularized Adipose Tissue Scaffolds for Soft Tissue Regeneration and Adipose-Derived Stem/Stromal Cell Delivery. *Methods Mol Biol*, 1773, 53-71.
- MORITA, A., SUGIMOTO, E. & KITAGAWA, Y. 1985. Post-translational assembly and glycosylation of laminin subunits in parietal endoderm-like F9 cells. *The Biochemical journal*, 229, 259-264.
- MOSQUEIRA, D., MANNHARDT, I., BHAGWAN, J. R., LIS-SLIMAK, K., KATILI, P., SCOTT, E., HASSAN, M., PRONDZYNSKI, M., HARMER, S. C., TINKER, A., SMITH, J. G. W., CARRIER, L., WILLIAMS, P. M., GAFFNEY, D., ESCHENHAGEN, T., HANSEN, A. & DENNING, C. 2018. CRISPR/Cas9 editing in human pluripotent stem cell-cardiomyocytes highlights arrhythmias, hypocontractility, and energy depletion as potential therapeutic targets for hypertrophic cardiomyopathy. *European heart journal*, 39, 3879-3892.
- MOUTAL, A., FRANÇOIS-MOUTAL, L., BRITAIN, J. M., KHANNA, M. & KHANNA, R. 2015. Differential neuroprotective potential of CRMP2 peptide aptamers conjugated to cationic, hydrophobic, and amphipathic cell penetrating peptides. *Frontiers in cellular neuroscience*, 8, 471.
- MOUW, J. K., YUI, Y., DAMIANO, L., BAINER, R. O., LAKINS, J. N., ACERBI, I., OU, G., WIJEKON, A. C., LEVENTAL, K. R., GILBERT, P. M., HWANG, E. S., CHEN, Y.-Y. & WEAVER, V. M. 2014. Tissue mechanics modulate microRNA-dependent PTEN expression to regulate malignant progression. *Nature Medicine*, 20, 360-367.
- MSEKA, T., BAMBURG, J. R. & CRAMER, L. P. 2007. ADF/cofilin family proteins control formation of oriented actin-filament bundles in the cell body to trigger fibroblast polarization. *Journal of cell science*, 120, 4332-4344.
- MUIZNIEKS, L. D. & KEELEY, F. W. 2013. Molecular assembly and mechanical properties of the extracellular matrix: A fibrous protein perspective. *Biochimica et Biophysica Acta (BBA)-Molecular Basis of Disease*, 1832, 866-875.
- MUKHERJEE, J., BARANWAL, A. & SCHADE, K. N. 2016. Classification of Therapeutic and Experimental Drugs for Brown Adipose Tissue Activation: Potential Treatment Strategies for Diabetes and Obesity. *Curr Diabetes Rev*, 12, 414-428.
- MURGIA, M., GIORGI, C., PINTON, P. & RIZZUTO, R. 2009. Controlling metabolism and cell death: at the heart of mitochondrial calcium signalling. *Journal of molecular and cellular cardiology*, 46, 781-788.
- MYERS, B., DUBICK, M., LAST, J. A. & RUCKER, R. B. 1983. Elastin synthesis during perinatal lung development in the rat. *Biochimica et Biophysica Acta (BBA)-General Subjects*, 761, 17-22.

References

- NAGANUMA, T. & TRAVERSA, E. 2014. The effect of cerium valence states at cerium oxide nanoparticle surfaces on cell proliferation. *Biomaterials*, 35, 4441-4453.
- NAGY-SMITH, K., YAMADA, Y. & SCHNEIDER, J. P. 2016. Protein release from highly charged peptide hydrogel networks. *J Mater Chem B*, 4, 1999-2007.
- NAIRN, A. V., KINOSHITA-TOYODA, A., TOYODA, H., XIE, J., HARRIS, K., DALTON, S., KULIK, M., PIERCE, J. M., TOIDA, T., MOREMEN, K. W. & LINHARDT, R. J. 2007. Glycomics of proteoglycan biosynthesis in murine embryonic stem cell differentiation. *Journal of proteome research*, 6, 4374-4387.
- NAKAJIMA, I., ASO, H., YAMAGUCHI, T. & OZUTSUMI, K. 1998. Adipose tissue extracellular matrix: newly organized by adipocytes during differentiation. *Differentiation*, 63, 193-200.
- NAKAJIMA, I., MUROYA, S., TANABE, R. & CHIKUNI, K. 2002a. Extracellular matrix development during differentiation into adipocytes with a unique increase in type V and VI collagen. *Biol Cell*, 94, 197-203.
- NAKAJIMA, I., MUROYA, S., TANABE, R. & CHIKUNI, K. 2002b. Positive effect of collagen V and VI on triglyceride accumulation during differentiation in cultures of bovine intramuscular adipocytes. *Differentiation*, 70, 84-91.
- NAPOLITANO, L. 1963. THE DIFFERENTIATION OF WHITE ADIPOSE CELLS. AN ELECTRON MICROSCOPE STUDY. *J Cell Biol*, 18, 663-79.
- NATH, S. C., HORIE, M., NAGAMORI, E. & KINO-OKA, M. 2017. Size- and time-dependent growth properties of human induced pluripotent stem cells in the culture of single aggregate. *Journal of Bioscience and Bioengineering*, 124, 469-475.
- NEDERGAARD, J. & CANNON, B. 2013. UCP1 mRNA does not produce heat. *Biochimica et Biophysica Acta (BBA) - Molecular and Cell Biology of Lipids*, 1831, 943-949.
- NEUSS, S., STAINFORTH, R., SALBER, J., SCHENCK, P., BOVI, M., KNÜCHEL, R. & PEREZ-BOUZA, A. 2008. Long-Term Survival and Bipotent Terminal Differentiation of Human Mesenchymal Stem Cells (hMSC) in Combination with a Commercially Available Three-Dimensional Collagen Scaffold. *Cell Transplantation*, 17, 977-986.
- NEWCOMB, C. J., SUR, S., ORTONY, J. H., LEE, O.-S., MATSON, J. B., BOEKHOVEN, J., YU, J. M., SCHATZ, G. C. & STUPP, S. I. 2014. Cell death versus cell survival instructed by supramolecular cohesion of nanostructures. *Nature communications*, 5, 3321-3321.
- NICU, C., POPLER, J., BONSELL, L., BHOGAL, R., ANSELL, D. M. & PAUS, R. 2018. A guide to studying human dermal adipocytes in situ. *Experimental Dermatology*, 27, 589-602.
- NIEPEL, M. S., EKAMBARAM, B. K., SCHMELZER, C. E. H. & GROTH, T. 2019. Polyelectrolyte multilayers of poly (l-lysine) and hyaluronic acid on nanostructured surfaces affect stem cell response. *Nanoscale*, 11, 2878-2891.
- NISHINO, M., MATSUZAKI, I., MUSANGILE, F. Y., TAKAHASHI, Y., IWAHASHI, Y., WARIGAYA, K., KINOSHITA, Y., KOJIMA, F. & MURATA, S.-I. 2020. Measurement and visualization of cell membrane surface charge in fixed cultured cells related with cell morphology. *PLOS ONE*, 15, e0236373.
- NIWA, H. 2007. How is pluripotency determined and maintained? *Development*, 134, 635-646.
- NÚRIA MARÍ-BUYÉ, T. L., DANIEL NAVAJAS, AND CARLOS E. SEMINO. 2013. Development of a Three-Dimensional Bone-Like Construct in a Soft Self-Assembling Peptide Matrix. *Tissue Engineering Part A*, 19, 870-881.

References

- NWIGWE, L. 2019. *Embryonic Stem Cell Research: An Ethical Dilemma*. [Online]. *Voices in Bioethics*, 5. : *Voices in Bioethics*. [Accessed 2022].
- NYMAN, J. S., ROY, A., TYLER, J. H., ACUNA, R. L., GAYLE, H. J. & WANG, X. 2007. Age-related factors affecting the postyield energy dissipation of human cortical bone. *Journal of orthopaedic research*, 25, 646-655.
- OEHLKE, J., SCHELLER, A., JANEK, K., WIESNER, B., KRAUSE, E., BEYERMANN, M. & BIENERT, M. 2002. Rapid translocation of amphipathic β helical and β -sheet-forming peptides through plasma membranes of endothelial cells. *In: SHIMONISHI, Y. (ed.) Peptide Science — Present and Future: Proceedings of the 1st International Peptide Symposium*. Dordrecht: Springer Netherlands.
- OGUMA, T., TOYODA, H., TOIDA, T. & IMANARI, T. 2001. Analytical Method for Keratan Sulfates by High-Performance Liquid Chromatography/Turbo-Ionspray Tandem Mass Spectrometry. *Analytical Biochemistry*, 290, 68-73.
- OISHI, Y., MANABE, I., TOBE, K., OHSUGI, M., KUBOTA, T., FUJII, K., MAEMURA, K., KUBOTA, N., KADOWAKI, T. & NAGAI, R. 2008. SUMOylation of Krüppel-like transcription factor 5 acts as a molecular switch in transcriptional programs of lipid metabolism involving PPAR- δ . *Nature Medicine*, 14, 656-666.
- OKAY, O. & DURMAZ, S. 2002. Charge density dependence of elastic modulus of strong polyelectrolyte hydrogels. *Polymer*, 43, 1215-1221.
- OKITA, Y., ZHENG, L., KAWANISHI, K., MIYOSHI, H., YANAGIHARA, K. & KATO, M. 2021. Polyvinyl alcohol scaffolds and supplementation support 3D and sphere culturing of human cancer cell lines by reducing apoptosis and promoting cellular proliferation. *Genes Cells*, 26, 336-343.
- OLDBERG, A. & RUOSLAHTI, E. 1982. Interactions between chondroitin sulfate proteoglycan, fibronectin, and collagen. *Journal of Biological Chemistry*, 257, 4859-4863.
- ONOE, H., GOJO, R., TSUDA, Y., KIRIYA, D. & TAKEUCHI, S. Core-shell gel wires for the construction of large area heterogeneous structures with biomaterials. 2010 IEEE 23rd International Conference on Micro Electro Mechanical Systems (MEMS), 24-28 Jan. 2010. 248-251.
- ONOE, H., OKITSU, T., ITOU, A., KATO-NEGISHI, M., GOJO, R., KIRIYA, D., SATO, K., MIURA, S., IWANAGA, S., KURIBAYASHI-SHIGETOMI, K., MATSUNAGA, Y. T., SHIMOYAMA, Y. & TAKEUCHI, S. 2013. Metre-long cell-laden microfibres exhibit tissue morphologies and functions. *Nat Mater*, 12, 584-90.
- ORI, A., WILKINSON, M. C. & FERNIG, D. G. 2011. A systems biology approach for the investigation of the heparin/heparan sulfate interactome. *J Biol Chem*, 286, 19892-904.
- ORRENIUS, S., ZHIVOTOVSKY, B. & NICOTERA, P. 2003. Regulation of cell death: the calcium–apoptosis link. *Nature Reviews Molecular Cell Biology*, 4, 552-565.
- OSUNA DE LA PEÑA, D., TRABULO, S. M. D., COLLIN, E., LIU, Y., SHARMA, S., TATARI, M., BEHRENS, D., ERKAN, M., LAWLOR, R. T., SCARPA, A., HEESCHEN, C., MATA, A. & LOESSNER, D. 2021. Bioengineered 3D models of human pancreatic cancer recapitulate in vivo tumour biology. *Nature Communications*, 12, 5623.
- ÖZTÜRK, E., ARLOV, Ø., AKSEL, S., LI, L., ORNITZ, D. M., SKJÅK-BRÆK, G. & ZENOBI-WONG, M. 2016. Sulfated Hydrogel Matrices Direct Mitogenicity and Maintenance of Chondrocyte Phenotype through Activation of FGF Signaling. *Advanced Functional Materials*, 26, 3649-3662.

References

- PADHI, A. & NAIN, A. S. 2020. ECM in Differentiation: A Review of Matrix Structure, Composition and Mechanical Properties. *Annals of Biomedical Engineering*, 48, 1071-1089.
- PAKZAD, M., TONCHI, M., TAEI, A., SEIFINEJAD, A., HASSANI, S. N. & BAHARVAND, H. 2010. Presence of a ROCK inhibitor in extracellular matrix supports more undifferentiated growth of feeder-free human embryonic and induced pluripotent stem cells upon passaging. *Stem Cell Rev Rep*, 6, 96-107.
- PANDALA, N., LASCOLA, M. A., HINTON, Z., KORLEY, S. T. J. & LAVIK, E. 2022. Finding the sweet spot: a library of hydrogels with tunable degradation for tissue model development. *J Mater Chem B*, 10, 2194-2203.
- PARK, A., KIM, W. K. & BAE, K.-H. 2014. Distinction of white, beige and brown adipocytes derived from mesenchymal stem cells. *World journal of stem cells*, 6, 33-42.
- PARK, J. B., KWAK, H. J. & LEE, S. H. 2008. Role of hyaluronan in glioma invasion. *Cell Adh Migr*, 2, 202-7.
- PASARICA, M., GOWRONSKA-KOZAK, B., BURK, D., REMEDIOS, I., HYMEL, D., GIMBLE, J., RAVUSSIN, E., BRAY, G. A. & SMITH, S. R. 2009. Adipose tissue collagen VI in obesity. *J Clin Endocrinol Metab*, 94, 5155-62.
- PASCALIS, C. D. & ETIENNE-MANNEVILLE, S. 2017. Single and collective cell migration: the mechanics of adhesions. *Molecular Biology of the Cell*, 28, 1833-1846.
- PATEL, N., LALWANI, D., GOLLMER, S., INJETI, E., SARI, Y. & NESAMONY, J. 2016. Development and evaluation of a calcium alginate based oral ceftriaxone sodium formulation. *Progress in biomaterials*, 5, 117-133.
- PATI, F., JANG, J., HA, D.-H., WON KIM, S., RHIE, J.-W., SHIM, J.-H., KIM, D.-H. & CHO, D.-W. 2014. Printing three-dimensional tissue analogues with decellularized extracellular matrix bioink. *Nature Communications*, 5, 3935.
- PEI, H., YAO, Y., YANG, Y., LIAO, K. & WU, J. R. 2011. Krüppel-like factor KLF9 regulates PPAR γ transactivation at the middle stage of adipogenesis. *Cell Death & Differentiation*, 18, 315-327.
- PELLÁ, M. C. G., LIMA-TENÓRIO, M. K., TENÓRIO-NETO, E. T., GUILHERME, M. R., MUNIZ, E. C. & RUBIRA, A. F. 2018. Chitosan-based hydrogels: From preparation to biomedical applications. *Carbohydrate Polymers*, 196, 233-245.
- PEREL, P., ROBERTS, I., SENA, E., WHEBLE, P., BRISCOE, C., SANDERCOCK, P., MACLEOD, M., MIGNINI, L. E., JAYARAM, P. & KHAN, K. S. 2007. Comparison of treatment effects between animal experiments and clinical trials: systematic review. *Bmj*, 334, 197.
- PETERSEN, T. H., CALLE, E. A., ZHAO, L., LEE, E. J., GUI, L., RAREDON, M. B., GAVRILOV, K., YI, T., ZHUANG, Z. W., BREUER, C., HERZOG, E. & NIKLASON, L. E. 2010. Tissue-engineered lungs for in vivo implantation. *Science (New York, N.Y.)*, 329, 538-541.
- PETZOLD, J. & GENTLEMAN, E. 2021. Intrinsic Mechanical Cues and Their Impact on Stem Cells and Embryogenesis. *Front Cell Dev Biol*, 9, 761871.
- PICKFORD, C. E., HOLLEY, R. J., RUSHTON, G., STAVRIDIS, M. P., WARD, C. M. & MERRY, C. L. 2011. Specific glycosaminoglycans modulate neural specification of mouse embryonic stem cells. *Stem Cells*, 29, 629-40.
- PIETERS, V. M., RJAIBI, S. T., SINGH, K., LI, N. T., KHAN, S. T., NUNES, S. S., DAL CIN, A., GILBERT, P. M. & MCGUIGAN, A. P. 2022. A three-dimensional human adipocyte model of fatty acid-induced obesity. *Biofabrication*, 14, 045009.

References

- PIJUAN-GALITÓ, S., TAMM, C., SCHUSTER, J., SOBOL, M., FORSBERG, L., MERRY, C. L. & ANNERÉN, C. 2016. Human serum-derived protein removes the need for coating in defined human pluripotent stem cell culture. *Nat Commun*, 7, 12170.
- PILKINGTON, A. C., PAZ, H. A. & WANKHADE, U. D. 2021. Beige Adipose Tissue Identification and Marker Specificity-Overview. *Front Endocrinol (Lausanne)*, 12, 599134.
- PLOU, J., JUSTE-LANAS, Y., OLIVARES, V., DEL AMO, C., BORAU, C. & GARCÍA-AZNAR, J. M. 2018. From individual to collective 3D cancer dissemination: roles of collagen concentration and TGF- β . *Sci Rep*, 8, 12723.
- PLOW, E. F., HAAS, T. A., ZHANG, L., LOFTUS, J. & SMITH, J. W. 2000. Ligand Binding to Integrins *. *Journal of Biological Chemistry*, 275, 21785-21788.
- PUIGSERVER, P., WU, Z., PARK, C. W., GRAVES, R., WRIGHT, M. & SPIEGELMAN, B. M. 1998. A cold-inducible coactivator of nuclear receptors linked to adaptive thermogenesis. *Cell*, 92, 829-39.
- PURWANTI, N., PUSFITASARI, E., KHALID, N., FEBRIANTO, E., SURO MARDJAN, S., ANDREAS & KOBAYASHI, I. 2018. Emulsion stability of clove oil in chitosan and sodium alginate matrix. *International Journal of Food Properties*, 21.
- QIU, Y., SUN, Y., XU, D., YANG, Y., LIU, X., WEI, Y., CHEN, Y., FENG, Z., LI, S., REYAD-UL FERDOUS, M., ZHAO, Y., XU, H., LAO, Y. & DING, Q. 2018. Screening of FDA-approved drugs identifies sutent as a modulator of UCP1 expression in brown adipose tissue. *EBioMedicine*, 37, 344-355.
- QU, J., ZHAO, X., MA, P. X. & GUO, B. 2018. Injectable antibacterial conductive hydrogels with dual response to an electric field and pH for localized "smart" drug release. *Acta Biomater*, 72, 55-69.
- QUARATO, G., LLAMBI, F., GUY, C. S., MIN, J., ACTIS, M., SUN, H., NARINA, S., PRUETT-MILLER, S. M., PENG, J., RANKOVIC, Z. & GREEN, D. R. 2022. Ca²⁺-mediated mitochondrial inner membrane permeabilization induces cell death independently of Bax and Bak. *Cell Death & Differentiation*.
- RABKIN, S. W. 2017. The role matrix metalloproteinases in the production of aortic aneurysm. *Progress in molecular biology and translational science*, 147, 239-265.
- RAHAMAN, S. O., GROVE, L. M., PARUCHURI, S., SOUTHERN, B. D., ABRAHAM, S., NIESE, K. A., SCHERAGA, R. G., GHOSH, S., THODETI, C. K., ZHANG, D. X., MORAN, M. M., SCHILLING, W. P., TSCHUMPERLIN, D. J. & OLMAN, M. A. 2014. TRPV4 mediates myofibroblast differentiation and pulmonary fibrosis in mice. *J Clin Invest*, 124, 5225-38.
- RAJANGAM, K., BEHANNA, H. A., HUI, M. J., HAN, X., HULVAT, J. F., LOMASNEY, J. W. & STUPP, S. I. 2006. Heparin Binding Nanostructures to Promote Growth of Blood Vessels. *Nano Letters*, 6, 2086-2090.
- RAMACHANDRAN, G. & KARTHA, G. 1955. Structure of collagen. *Nature*, 176, 593-595.
- RAMSHAW, J. A. M. & GLATTAUER, V. 2019. Biosynthesis and biodegradation of collagen. *Biophysical and Chemical Properties of Collagen: Biomedical Applications*. IOP Publishing.
- RAOF, N. A., PADGEN, M. R., GRACIAS, A. R., BERGKVIST, M. & XIE, Y. 2011. One-dimensional self-assembly of mouse embryonic stem cells using an array of hydrogel microstrands. *Biomaterials*, 32, 4498-505.
- RAPRAEGER, A. C., KRUFKA, A. & OLWIN, B. B. 1991. Requirement of Heparan Sulfate for bFGF-Mediated Fibroblast Growth and Myoblast Differentiation. *Science*, 252, 1705-1708.

References

- REDONDO-GÓMEZ, C., ABDOUNI, Y., BECER, C. R. & MATA, A. 2019. Self-Assembling Hydrogels Based on a Complementary Host–Guest Peptide Amphiphile Pair. *Biomacromolecules*, 20, 2276-2285.
- REICHHELD, S. E., MUIZNIEKS, L. D., LU, R., SHARPE, S. & KEELEY, F. W. 2019. Sequence variants of human tropoelastin affecting assembly, structural characteristics and functional properties of polymeric elastin in health and disease. *Matrix Biology*, 84, 68-80.
- REZAEI LARIJANI, M., SEIFINEJAD, A., POURNASR, B., GAZESTANI, V., HASSANI, S.-N., TONONCHI, M., YOUSEFI, M., SHAMSI, F., SALEKDEH, G. H. & BAHARVAND, H. 2011. Long-Term Maintenance of Undifferentiated Human Embryonic and Induced Pluripotent Stem Cells in Suspension. *Stem cells and development*, 20, 1911-23.
- RICARD-BLUM, S. 2011. The collagen family. *Cold Spring Harb Perspect Biol*, 3, a004978.
- RICHARD, A. J., WHITE, U., ELKS, C. M. & STEPHENS, J. M. 2020. Adipose Tissue: Physiology to Metabolic Dysfunction. In: FEINGOLD, K., ANAWALT, B. & BOYCE, A. (eds.) <http://www.endotext.org/>. South Dartmouth: MDText.com, .
- RIEUSSET, J., ANDREELLI, F., AUBOEUF, D., ROQUES, M., VALLIER, P., RIOU, J. P., AUWERX, J., LAVILLE, M. & VIDAL, H. 1999. Insulin acutely regulates the expression of the peroxisome proliferator-activated receptor-gamma in human adipocytes. *Diabetes*, 48, 699-705.
- RIPPON, H. J. & BISHOP, A. E. 2004a. Embryonic stem cells. *Cell Proliferation*, 37, 23-34.
- RIPPON, H. J. & BISHOP, A. E. 2004b. Embryonic stem cells. *Cell Prolif*, 37, 23-34.
- RISTELI, J., TIMPL, R., BÄCHINGER, H. P., ENGEL, J. & FURTHMAYR, H. 1980. 7-S collagen: characterization of an unusual basement membrane structure. *European journal of biochemistry*, 108, 239-250.
- RODIN, S., ANTONSSON, L., NIAUDET, C., SIMONSON, O. E., SALMELA, E., HANSSON, E. M., DOMOGATSKAYA, A., XIAO, Z., DAMDIMOPOULOU, P., SHEIKHI, M., INZUNZA, J., NILSSON, A. S., BAKER, D., KUIPER, R., SUN, Y., BLENNOW, E., NORDENSKJÖLD, M., GRINNEMO, K. H., KERE, J., BETSHOLTZ, C., HOVATTA, O. & TRYGGVASON, K. 2014. Clonal culturing of human embryonic stem cells on laminin-521/E-cadherin matrix in defined and xeno-free environment. *Nat Commun*, 5, 3195.
- RODIN, S., DOMOGATSKAYA, A., STRÖM, S., HANSSON, E. M., CHIEN, K. R., INZUNZA, J., HOVATTA, O. & TRYGGVASON, K. 2010. Long-term self-renewal of human pluripotent stem cells on human recombinant laminin-511. *Nature Biotechnology*, 28, 611-615.
- ROPER, S. J. & COYLE, B. 2022. Establishing an In Vitro 3D Spheroid Model to Study Medulloblastoma Drug Response and Tumor Dissemination. *Current Protocols*, 2, e357.
- ROSALES, A. M. & ANSETH, K. S. 2016. The design of reversible hydrogels to capture extracellular matrix dynamics. *Nature Reviews Materials*, 1, 15012.
- ROSEN, E. D., HSU, C. H., WANG, X., SAKAI, S., FREEMAN, M. W., GONZALEZ, F. J. & SPIEGELMAN, B. M. 2002. C/EBPalpha induces adipogenesis through PPARgamma: a unified pathway. *Genes Dev*, 16, 22-6.
- ROSIŃCZUK, J., TARADAJ, J., DYMAREK, R. & SOPEL, M. 2016. Mechanoregulation of Wound Healing and Skin Homeostasis. *BioMed Research International*, 2016, 3943481.
- ROTEN, S. V., BHAT, S. & BHAWAN, J. 1996. Elastic fibers in scar tissue. *Journal of Cutaneous Pathology*, 23, 37-42.

References

- ROUGHLEY, P. J., LAMPLUGH, L., LEE, E. R., MATSUMOTO, K. & YAMAGUCHI, Y. 2011. The Role of Hyaluronan Produced by Has2 Gene Expression in Development of the Spine. *Spine*, 36.
- ROUSSELLE, P., LUNSTRUM, G. P., KEENE, D. R. & BURGESSON, R. E. 1991. Kalinin: an epithelium-specific basement membrane adhesion molecule that is a component of anchoring filaments. *The Journal of Cell Biology*, 114, 567-576.
- ROZARIO, T. & DESIMONE, D. W. 2010. The extracellular matrix in development and morphogenesis: a dynamic view. *Dev Biol*, 341, 126-40.
- RUOSLAHTI, E. & PIERSCHBACHER, M. D. 1986. Arg-Gly-Asp: a versatile cell recognition signal. *Cell*, 44, 517-8.
- SAAR, K., LINDGREN, M., HANSEN, M., EIRÍKSDÓTTIR, E., JIANG, Y., ROSENTHAL-AIZMAN, K., SASSIAN, M. & LANGEL, Ü. 2005. Cell-penetrating peptides: A comparative membrane toxicity study. *Analytical Biochemistry*, 345, 55-65.
- SABARATNAM, R. & SVENNINGSEN, P. 2021. Adipocyte-Endothelium Crosstalk in Obesity. *Front Endocrinol (Lausanne)*, 12, 681290.
- SABEH, F., SHIMIZU-HIROTA, R. & WEISS, S. J. 2009. Protease-dependent versus -independent cancer cell invasion programs: three-dimensional amoeboid movement revisited. *J Cell Biol*, 185, 11-9.
- SAKAI, S., HARADA, R. & KOTANI, T. 2021. Freeform 3D Bioprinting Involving Ink Gelation by Cascade Reaction of Oxidase and Peroxidase: A Feasibility Study Using Hyaluronic Acid-Based Ink. *Biomolecules*, 11.
- SAKAI, S., YAMAGUCHI, S., TAKEI, T. & KAWAKAMI, K. 2008. Oxidized Alginate-Cross-Linked Alginate/Gelatin Hydrogel Fibers for Fabricating Tubular Constructs with Layered Smooth Muscle Cells and Endothelial Cells in Collagen Gels. *Biomacromolecules*, 9, 2036-2041.
- SALLOUH, M., JAROCKI, M., SALLOUH, O., DEGEN, P., FAISSNER, A. & WEBERSKIRCH, R. 2017. The Synergistic Effect of Cationic Moieties and GRGDSF-Peptides in Hydrogels on Neural Stem Cell Behavior. *Macromolecular Bioscience*, 17, 1600178.
- SAMUEL, J., FARHADIAN, F., SABRI, A., MAROTTE, F., ROBERT, V. & RAPPAPORT, L. 1994. Expression of fibronectin during rat fetal and postnatal development: an in situ hybridisation and immunohistochemical study. *Cardiovascular research*, 28, 1653-1661.
- SANO, K., ASAHII, M., YANAGIBASHI, M., HASHII, N., ITOH, S., KAWASAKI, N. & OGAWA, H. 2008. Glycosylation and ligand-binding activities of rat plasma fibronectin during liver regeneration after partial hepatectomy. *Carbohydrate Research*, 343, 2329-2335.
- SÁRVÁRI, A. K., DOAN-XUAN, Q. M., BACSÓ, Z., CSOMÓS, I., BALAJTHY, Z. & FÉSÜS, L. 2015. Interaction of differentiated human adipocytes with macrophages leads to trogocytosis and selective IL-6 secretion. *Cell Death & Disease*, 6, e1613-e1613.
- SASAKI, M., KLEINMAN, H. K., HUBER, H., DEUTZMANN, R. & YAMADA, Y. 1988. Laminin, a multidomain protein. The A chain has a unique globular domain and homology with the basement membrane proteoglycan and the laminin B chains. *J. Biol. Chem.*, 263.
- SASAKI, T., FÄSSLER, R. & HOHENESTER, E. 2004. Laminin : the crux of basement membrane assembly. *Journal of Cell Biology*, 164, 959-963.
- SAYED, N., LIU, C. & WU, J. C. 2016. Translation of Human-Induced Pluripotent Stem Cells: From Clinical Trial in a Dish to Precision Medicine. *J Am Coll Cardiol*, 67, 2161-2176.

References

- SCHEGG, B., HÜLSMEIER, A. J., RUTSCHMANN, C., MAAG, C. & HENNET, T. 2009. Core glycosylation of collagen is initiated by two beta(1-O)galactosyltransferases. *Molecular and cellular biology*, 29, 943-952.
- SHELLER, A., OEHLKE, J., WIESNER, B., DATHE, M., KRAUSE, E., BEYERMANN, M., MELZIG, M. & BIENERT, M. 1999. Structural requirements for cellular uptake of α -helical amphipathic peptides. *Journal of Peptide Science*, 5, 185-194.
- SCHERER, P. E., BICKEL, P. E., KOTLER, M. & LODISH, H. F. 1998. Cloning of cell-specific secreted and surface proteins by subtractive antibody screening. *Nat Biotechnol*, 16, 581-6.
- SCHILLEMANS, J. P., VERHEYEN, E., BARENDREGT, A., HENNINK, W. E. & VAN NOSTRUM, C. F. 2011. Anionic and cationic dextran hydrogels for post-loading and release of proteins. *Journal of Controlled Release*, 150, 266-271.
- SCHILLING, J. A. 1976. Wound healing. *Surg Clin North Am*, 56, 859-74.
- SCHINDELIN, J., ARGANDA-CARRERAS, I., FRISE, E., KAYNIG, V., LONGAIR, M., PIETZSCH, T., PREIBISCH, S., RUEDEN, C., SAALFELD, S., SCHMID, B., TINEVEZ, J.-Y., WHITE, D. J., HARTENSTEIN, V., ELICEIRI, K., TOMANCAK, P. & CARDONA, A. 2012. Fiji: an open-source platform for biological-image analysis. *Nature methods*, 9, 676-682.
- SCHMELZER, C. E. H., NAGEL, M. B. M., DZIOMBA, S., MERKHER, Y., SIVAN, S. S. & HEINZ, A. 2016. Prolyl hydroxylation in elastin is not random. *Biochimica et Biophysica Acta (BBA) - General Subjects*, 1860, 2169-2177.
- SCHOONJANS, K., WATANABE, M., SUZUKI, H., MAHFOUDI, A., KREY, G., WAHLI, W., GRIMALDI, P., STAELS, B., YAMAMOTO, T. & AUWERX, J. 1995. Induction of the acyl-coenzyme A synthetase gene by fibrates and fatty acids is mediated by a peroxisome proliferator response element in the C promoter. *J Biol Chem*, 270, 19269-76.
- SCHREIER, S., MALHEIROS, S. V. P. & DE PAULA, E. 2000. Surface active drugs: self-association and interaction with membranes and surfactants. Physicochemical and biological aspects. *Biochimica et Biophysica Acta (BBA) - Biomembranes*, 1508, 210-234.
- SCHULZ, A., KATSEN-GLOBA, A., HUBER, E. J., MUELLER, S. C., KREINER, A., PÜTZ, N., GEPP, M. M., FISCHER, B., STRACKE, F., VON BRIESEN, H., NEUBAUER, J. C. & ZIMMERMANN, H. 2018. Poly(amidoamine)-alginate hydrogels: directing the behavior of mesenchymal stem cells with charged hydrogel surfaces. *J Mater Sci Mater Med*, 29, 105.
- SCHWARZBAUER, J. E. & DESIMONE, D. W. 2011. Fibronectins, their fibrillogenesis, and in vivo functions. *Cold Spring Harb Perspect Biol*, 3.
- SEBO, Z. L. & RODEHEFFER, M. S. 2019. Assembling the adipose organ: adipocyte lineage segregation and adipogenesis in vivo. *Development*, 146.
- SEEWALDT, V. 2014. ECM stiffness paves the way for tumor cells. *Nature Medicine*, 20, 332-333.
- SEMLER, O., REHBERG, M., MEHDIANI, N., JACKELS, M. & HOYER-KUHN, H. 2019. Current and Emerging Therapeutic Options for the Management of Rare Skeletal Diseases. *Paediatr Drugs*, 21, 95-106.
- SEN, B., XIE, Z., CASE, N., MA, M., RUBIN, C. & RUBIN, J. 2008. Mechanical Strain Inhibits Adipogenesis in Mesenchymal Stem Cells by Stimulating a Durable β -Catenin Signal. *Endocrinology*, 149, 6065-6075.

References

- SHAH, R. N., SHAH, N. A., DEL ROSARIO LIM, M. M., HSIEH, C., NUBER, G. & STUPP, S. I. 2010. Supramolecular design of self-assembling nanofibers for cartilage regeneration. *Proc Natl Acad Sci U S A*, 107, 3293-8.
- SHAO, L., GAO, Q., XIE, C., FU, J., XIANG, M. & HE, Y. 2019. Bioprinting of cell-laden microfiber: can it become a standard product? *Advanced healthcare materials*, 8.
- SHARMA, V. S. 2016. *Size controlled retinal differentiation of human induced pluripotent stem cells in shaking microwells*. University College London.
- SHEN, J. X., COUCHET, M., DUFAU, J., DE CASTRO BARBOSA, T., ULBRICH, M. H., HELMSTÄDTER, M., KEMAS, A. M., ZANDI SHAFAGH, R., MARQUES, M.-A., HANSEN, J. B., MEJHERT, N., LANGIN, D., RYDÉN, M. & LAUSCHKE, V. M. 2021. 3D Adipose Tissue Culture Links the Organotypic Microenvironment to Improved Adipogenesis. *Advanced Science*, 8, 2100106.
- SHIDA, M., MIKAMI, T., TAMURA, J.-I. & KITAGAWA, H. 2019. Chondroitin sulfate-D promotes neurite outgrowth by acting as an extracellular ligand for neuronal integrin $\alpha V\beta 3$. *Biochimica et Biophysica Acta (BBA) - General Subjects*, 1863, 1319-1331.
- SHIN, S. J., PARK, J. Y., LEE, J. Y., PARK, H., PARK, Y. D., LEE, K. B., WHANG, C. M. & LEE, S. H. 2007. "On the fly" continuous generation of alginate fibers using a microfluidic device. *Langmuir*, 23, 9104-8.
- SHIWARSKI, D. J., HUDSON, A. R., TASHMAN, J. W. & FEINBERG, A. W. 2021. Emergence of FRESH 3D printing as a platform for advanced tissue biofabrication. *APL Bioeng*, 5, 010904.
- SHOULDERS, M. D. & RAINES, R. T. 2009. Collagen structure and stability. *Annu Rev Biochem*, 78, 929-58.
- SIDHAYE, J. & KNOBLICH, J. A. 2021. Brain organoids: an ensemble of bioassays to investigate human neurodevelopment and disease. *Cell Death & Differentiation*, 28, 52-67.
- SILVA, G. A., CZEISLER, C., NIECE, K. L., BENIASH, E., HARRINGTON, D. A., KESSLER, J. A. & STUPP, S. I. 2004. Selective differentiation of neural progenitor cells by high-epitope density nanofibers. *Science*, 303, 1352-5.
- SIMON-ASSMANN, P., KEDINGER, M., DE ARCANGELIS, A., ROUSSEAU, V. & SIMO, P. 1995. Extracellular matrix components in intestinal development. *Experientia*, 51, 883-900.
- SINGER, II, KAWKA, D. W., SCOTT, S., MUMFORD, R. A. & LARK, M. W. 1987. The fibronectin cell attachment sequence Arg-Gly-Asp-Ser promotes focal contact formation during early fibroblast attachment and spreading. *J Cell Biol*, 104, 573-84.
- SINGH, A. M., ZHANG, L., AVERY, J., YIN, A., DU, Y., WANG, H., LI, Z., FU, H., YIN, H. & DALTON, S. 2020. Human beige adipocytes for drug discovery and cell therapy in metabolic diseases. *Nature Communications*, 11, 2758.
- SINGH, P., CARRAHER, C. & SCHWARZBAUER, J. E. 2010. Assembly of fibronectin extracellular matrix. *Annu Rev Cell Dev Biol*, 26, 397-419.
- SINGLETON, P. A. & BOURGUIGNON, L. Y. W. 2002. CD44v10 interaction with Rho-kinase (ROK) activates inositol 1,4,5-triphosphate (IP3) receptor-mediated Ca²⁺ signaling during hyaluronan (HA)-induced endothelial cell migration. *Cell motility and the cytoskeleton*, 53, 293-316.
- SMIDSRØD, O. & SKJÅK-BRİK, G. 1990. Alginate as immobilization matrix for cells. *Trends in Biotechnology*, 8, 71-78.

References

- SMITH, A. G. 2001. Embryo-Derived Stem Cells: Of Mice and Men. *Annual Review of Cell and Developmental Biology*, 17, 435-462.
- SOLEIMANI, M. & NADRI, S. 2009. A protocol for isolation and culture of mesenchymal stem cells from mouse bone marrow. *Nature Protocols*, 4, 102-106.
- SOLEIMANPOUR, M., MIRHAJI, S. S., JAFARI, S., DERAKHSHANKHAH, H., MAMASHLI, F., NEDAEI, H., KARIMI, M. R., MOTASADIZADEH, H., FATAHI, Y., GHASEMI, A., NEZAMTAHERI, M. S., KHAJEZADE, M., TEIMOURI, M., GOLIAEI, B., DELATTRE, C. & SABOURY, A. A. 2022. Designing a new alginate-fibrinogen biomaterial composite hydrogel for wound healing. *Sci Rep*, 12, 7213.
- SONG, G., JU, Y. & SOYAMA, H. 2008. Growth and proliferation of bone marrow mesenchymal stem cells affected by type I collagen, fibronectin and bFGF. *Materials Science and Engineering: C*, 28, 1467-1471.
- SONG, J., ZHANG, Y., ZHANG, W., CHEN, J., YANG, X., MA, P., ZHANG, B., LIU, B., NI, J. & WANG, R. 2015. Cell penetrating peptide TAT can kill cancer cells via membrane disruption after attachment of camptothecin. *Peptides*, 63, 143-149.
- SOOFI, S. S., LAST, J. A., LILIENSIEK, S. J., NEALEY, P. F. & MURPHY, C. J. 2009. The elastic modulus of Matrigel™ as determined by atomic force microscopy. *Journal of Structural Biology*, 167, 216-219.
- SPANGRUDE, G. J., HEIMFELD, S. & WEISSMAN, I. L. 1988. Purification and characterization of mouse hematopoietic stem cells. *Science*, 241, 58-62.
- SPRADLING, A., NYSTUL, T., LIGHTHOUSE, D., MORRIS, L., FOX, D., COX, R., TOOTLE, T., FREDERICK, R. & SKORA, A. Stem cells and their niches: integrated units that maintain Drosophila tissues. Cold Spring Harbor symposia on quantitative biology, 2008. Cold Spring Harbor Laboratory Press, 49-57.
- STENDAHL, J., RAO, M., GULER, M. & STUPP, S. I. 2006. Intermolecular Forces in the Self-Assembly of Peptide Amphiphile Nanofibers. *Advanced Functional Materials*, 16, 499-508.
- STEVENS, M. M. & GEORGE, J. H. 2005. Exploring and engineering the cell surface interface. *Science*, 310, 1135-8.
- STOCK, K., ESTRADA, M. F., VIDIC, S., GJERDE, K., RUDISCH, A., SANTO, V. E., BARBIER, M., BLOM, S., ARUNKAR, S. C., SELVAM, I., OSSWALD, A., STEIN, Y., GRUENEWALD, S., BRITO, C., VAN WEERDEN, W., ROTTER, V., BOGHAERT, E., OREN, M., SOMMERGRUBER, W., CHONG, Y., DE HOOGT, R. & GRAESER, R. 2016. Capturing tumor complexity in vitro: Comparative analysis of 2D and 3D tumor models for drug discovery. *Sci Rep*, 6, 28951.
- STORRIE, H., GULER, M. O., ABU-AMARA, S. N., VOLBERG, T., RAO, M., GEIGER, B. & STUPP, S. I. 2007. Supramolecular crafting of cell adhesion. *Biomaterials*, 28, 4608-4618.
- STRIEDER-BARBOZA, C., BAKER, N. A., FLESHER, C. G., KARMAKAR, M., PATEL, A., LUMENG, C. N. & O'ROURKE, R. W. 2020. Depot-specific adipocyte-extracellular matrix metabolic crosstalk in murine obesity. *Adipocyte*, 9, 189-196.
- SU, T., XU, M., LU, F. & CHANG, Q. 2022. Adipogenesis or osteogenesis: destiny decision made by mechanical properties of biomaterials. *RSC Advances*, 12, 24501-24510.
- SVENDSEN, O., SANDØE, P. & THORN, N. A. 1997. Laboratory Animal Science, Welfare and Ethics in Pharmacology and Toxicology. *Pharmacology & Toxicology*, 80, 3-5.
- SWEE, M. H., PARKS, W. C. & PIERCE, R. A. 1995. Developmental Regulation of Elastin Production.: EXPRESSION OF TROPOELASTIN PRE-mRNA PERSISTS AFTER

References

- DOWN-REGULATION OF STEADY-STATE mRNA LEVELS (∗). *Journal of Biological Chemistry*, 270, 14899-14906.
- TABAR, V. & STUDER, L. 2014. Pluripotent stem cells in regenerative medicine: challenges and recent progress. *Nat Rev Genet*, 15, 82-92.
- TAKAHASHI, K., TANABE, K., OHNUKI, M., NARITA, M., ICHISAKA, T., TOMODA, K. & YAMANAKA, S. 2007. Induction of Pluripotent Stem Cells from Adult Human Fibroblasts by Defined Factors. *Cell*, 131, 861-872.
- TAKAHASHI, K. & YAMANAKA, S. 2006. Induction of Pluripotent Stem Cells from Mouse Embryonic and Adult Fibroblast Cultures by Defined Factors. *Cell*, 126, 663-676.
- TAM, S. K., DUSSEAULT, J., BILODEAU, S., LANGLOIS, G., HALLÉ, J.-P. & YAHIA, L. H. 2011. Factors influencing alginate gel biocompatibility. *Journal of Biomedical Materials Research Part A*, 98A, 40-52.
- TAN, F., LIU, J., LIU, M. & WANG, J. 2017. Charge density is more important than charge polarity in enhancing osteoblast-like cell attachment on poly(ethylene glycol)-diacrylate hydrogel. *Materials Science and Engineering: C*, 76, 330-339.
- TANABE, Y., KOGA, M., SAITO, M., MATSUNAGA, Y. & NAKAYAMA, K. 2004. Inhibition of adipocyte differentiation by mechanical stretching through ERK-mediated downregulation of PPAR γ . *Journal of Cell Science*, 117, 3605.
- TANAHASHI, K. & MIKOS, A. G. 2003. Protein adsorption and smooth muscle cell adhesion on biodegradable agmatine-modified poly(propylene fumarate-co-ethylene glycol) hydrogels. *Journal of Biomedical Materials Research Part A*, 67A, 448-457.
- TANG, B., ZHANG, B., ZHUANG, J., WANG, Q., DONG, L., CHENG, K. & WENG, W. 2018. Surface potential-governed cellular osteogenic differentiation on ferroelectric polyvinylidene fluoride trifluoroethylene films. *Acta Biomaterialia*, 74, 291-301.
- TANSEY, J., SZTALRYD, C., HLAVIN, E., KIMMEL, A. & LONDOS, C. 2004. The Central Role of Perilipin A in Lipid Metabolism and Adipocyte Lipolysis. *IUBMB Life*, 56, 379-385.
- THAN, M. E., HENRICH, S., HUBER, R., RIES, A., MANN, K., KÜHN, K., TIMPL, R., BOURENKOV, G. P., BARTUNIK, H. D. & BODE, W. 2002. The 1.9-Å crystal structure of the noncollagenous (NC1) domain of human placenta collagen IV shows stabilization via a novel type of covalent Met-Lys cross-link. *Proceedings of the National Academy of Sciences*, 99, 6607-6612.
- THEOCHARIS, A. D., SKANDALIS, S. S., GIALELI, C. & KARAMANOS, N. K. 2016. Extracellular matrix structure. *Advanced Drug Delivery Reviews*, 97, 4-27.
- THERMO FISHER SCIENTIFIC. 2019. *Microplate Protocol for Presto Blue HS and Presto Blue Cell Viability Reagents* [Online]. Thermo Fisher Scientific. Available: https://www.thermofisher.com/uk/en/home/references/protocols/cell-and-tissue-analysis/protocols/prestoblue-cell-viability-reagent-for-microplates-protocol.html?gclid=EAlaIQobChMIIYH8jOXc4wIVwbTtCh0qSwcgEAAYASABEgJ8JvD_BwE&ef_id=EAlaIQobChMIIYH8jOXc4wIVwbTtCh0qSwcgEAAYASABEgJ8JvD_BwE:G:s&s_kwid=AL!3652!3!355223665606!e!!g!!presto%20blue [Accessed 30.07.19 2019].
- THIERY, J. P. 1984. Mechanisms of cell migration in the vertebrate embryo. *Cell Differentiation*, 15, 1-15.
- THOMSON, J. A., ITSKOVITZ-ELDOR, J., SHAPIRO, S. S., WAKNITZ, M. A., SWIERGIEL, J. J., MARSHALL, V. S. & JONES, J. M. 1998. Embryonic stem cell lines derived from human blastocysts. *Science*, 282, 1145-7.

References

- TIAN, C., ZHANG, X. & ZHAO, G. 2019. Vitrification of stem cell-laden core-shell microfibers with unusually low concentrations of cryoprotective agents. *Biomaterials Science*, 7, 889-900.
- TIBBITT, M. W. & ANSETH, K. S. 2009. Hydrogels as extracellular matrix mimics for 3D cell culture. *Biotechnology and bioengineering*, 103, 655-663.
- TO, W. S. & MIDWOOD, K. S. 2011. Plasma and cellular fibronectin: distinct and independent functions during tissue repair. *Fibrogenesis & Tissue Repair*, 4, 21.
- TOMASZEWSKI, C. E., DILILLO, K. M., BAKER, B. M., ARNOLD, K. B. & SHIKANOV, A. 2021. Sequestered cell-secreted extracellular matrix proteins improve murine folliculogenesis and oocyte maturation for fertility preservation. *Acta Biomater*, 132, 313-324.
- TONTONOZ, P., HU, E. & SPIEGELMAN, B. M. 1994. Stimulation of adipogenesis in fibroblasts by PPAR gamma 2, a lipid-activated transcription factor. *Cell*, 79, 1147-56.
- TOOLE, B. P. 2004. Hyaluronan: from extracellular glue to pericellular cue. *Nat Rev Cancer*, 4, 528-39.
- TOOLE, B. P. & GROSS, J. 1971. The extracellular matrix of the regenerating newt limb: Synthesis and removal of hyaluronate prior to differentiation. *Developmental Biology*, 25, 57-77.
- TORABIZADEH, F., FADAIE, M., MIRZAEI, E., SADEGHI, S. & NEJABAT, G. R. 2022. Tailoring structural properties, mechanical behavior and cellular performance of collagen hydrogel through incorporation of cellulose microfibrils and cellulose nanocrystals: A comparative study. *Int J Biol Macromol*.
- TOTONCHI, M., TAEI, A., SEIFINEJAD, A., TABEBORDBAR, M., RASSOULI, H., FARROKHI, A., GOURABI, H., AGHDAMI, N., HOSSEINI-SALEKDEH, G. & BAHARVAND, H. 2010. Feeder- and serum-free establishment and expansion of human induced pluripotent stem cells. *Int J Dev Biol*, 54, 877-86.
- TRAVERS, J. G., KAMAL, F. A., ROBBINS, J., YUTZEY, K. E. & BLAXALL, B. C. 2016. Cardiac Fibrosis: The Fibroblast Awakens. *Circ Res*, 118, 1021-40.
- TRAYHURN, P. & BEATTIE, J. H. 2001. Physiological role of adipose tissue: white adipose tissue as an endocrine and secretory organ. *Proceedings of the Nutrition Society*, 60, 329 - 339.
- TREBBIN, M., STEINHAUSER, D., PERLICH, J., BUFFET, A., ROTH, S. V., ZIMMERMANN, W., THIELE, J. & FÖRSTER, S. 2013. Anisotropic particles align perpendicular to the flow direction in narrow microchannels. *Proceedings of the National Academy of Sciences*, 110, 6706.
- TRZOS, K., PYDYN, N., JURA, J. & KOTLINOWSKI, J. 2022. Selected transgenic murine models of human autoimmune liver diseases. *Pharmacol Rep*, 74, 263-272.
- TSAI, K.-S., KAO, S.-Y., WANG, C.-Y., WANG, Y.-J., WANG, J.-P. & HUNG, S.-C. 2010. Type I collagen promotes proliferation and osteogenesis of human mesenchymal stem cells via activation of ERK and Akt pathways. *Journal of Biomedical Materials Research Part A*, 94A, 673-682.
- TSUI, L. 2022. Adipocyte-based high throughput screening for anti-obesity drug discovery: Current status and future perspectives. *SLAS Discovery*.
- TURNER, P. A., GURUMURTHY, B., BAILEY, J. L., ELKS, C. M. & JANORKAR, A. V. 2017. Adipogenic Differentiation of Human Adipose-Derived Stem Cells Grown as Spheroids. *Process biochemistry (Barking, London, England)*, 59, 312-320.

References

- TYAGI, S., GUPTA, P., SAINI, A. S., KAUSHAL, C. & SHARMA, S. 2011. The peroxisome proliferator-activated receptor: A family of nuclear receptors role in various diseases. *J Adv Pharm Technol Res*, 2, 236-40.
- TZU, J., LI, J. & MARINKOVICH, M. P. 2005. Basement membrane and extracellular matrix molecules in the skin. *Advances in Developmental Biology*. Elsevier.
- TZU, J. & MARINKOVICH, M. P. 2008. Bridging structure with function: structural, regulatory, and developmental role of laminins. *The international journal of biochemistry & cell biology*, 40, 199-214.
- UCHIDA, S., TANAKA, Y., ITO, H., SAITOH-OHARA, F., INAZAWA, J., YOKOYAMA, K., SASAKI, S. & MARUMO, F. 2000. Transcriptional Regulation of the CLC-K1 Promoter by myc-Associated Zinc Finger Protein and Kidney-Enriched Krüppel-Like Factor, a Novel Zinc Finger Repressor. *Molecular and cellular biology*, 20, 7319-31.
- UITTO, J. 1979. Biochemistry of the elastic fibers in normal connective tissues and its alterations in diseases. *Journal of Investigative Dermatology*, 72, 1-10.
- UK GOVERNMENT 2020. Policy paper
- Tackling obesity: empowering adults and children to live healthier lives. In: CARE, D. O. H. A. S. (ed.). Gov.uk: UK Government.
- UMEDA, H., NAKAMURA, F. & SUYAMA, K. 2001. Oxodesmosine and Isooxodesmosine, Candidates of Oxidative Metabolic Intermediates of Pyridinium Cross-Links in Elastin. *Archives of Biochemistry and Biophysics*, 385, 209-219.
- UNSER, A. M., MOONEY, B., CORR, D. T., TSENG, Y.-H. & XIE, Y. 2016a. 3D brown adipogenesis to create "Brown-Fat-in-Microstrands". *Biomaterials*, 75, 123-134.
- UNSER, A. M., MOONEY, B., CORR, D. T., TSENG, Y.-H. & XIE, Y. 2016b. 3D brown adipogenesis to create "Brown-Fat-in-Microstrands". *Biomaterials*, 75, 123-134.
- UNSER, A. M., TIAN, Y. & XIE, Y. 2015. Opportunities and challenges in three-dimensional brown adipogenesis of stem cells. *Biotechnol Adv*, 33, 962-79.
- USSAR, S., LEE, K. Y., DANKEL, S. N., BOUCHER, J., HAERING, M. F., KLEINRIDDERS, A., THOMOU, T., XUE, R., MACOTELA, Y., CYPESS, A. M., TSENG, Y. H., MELLGREN, G. & KAHN, C. R. 2014. ASC-1, PAT2, and P2RX5 are cell surface markers for white, beige, and brown adipocytes. *Sci Transl Med*, 6, 247ra103.
- VABRES, P. 2010. Hyaluronan, embryogenesis and morphogenesis. *Annales de dermatologie et de vénéréologie*, 137 Suppl 1, S9-S14.
- VALAMEHR, B., JONAS, S. J., POLLEUX, J., QIAO, R., GUO, S., GSCHWENG, E. H., STILES, B., KAM, K., LUO, T. J., WITTE, O. N., LIU, X., DUNN, B. & WU, H. 2008. Hydrophobic surfaces for enhanced differentiation of embryonic stem cell-derived embryoid bodies. *Proc Natl Acad Sci U S A*, 105, 14459-64.
- VALLMAJO-MARTIN, Q., BROGUIERE, N., MILLAN, C., ZENOBI-WONG, M. & EHRBAR, M. 2020. PEG/HA Hybrid Hydrogels for Biologically and Mechanically Tailorable Bone Marrow Organoids. *Advanced Functional Materials*, 30, 1910282.
- VAN DEN BRINK, S. C., ALEMANY, A., VAN BATENBURG, V., MORIS, N., BLOTENBURG, M., VIVIÉ, J., BAILLIE-JOHNSON, P., NICHOLS, J., SONNEN, K. F., MARTINEZ ARIAS, A. & VAN OUDENAARDEN, A. 2020. Single-cell and spatial transcriptomics reveal somitogenesis in gastruloids. *Nature*, 582, 405-409.
- VAN GINKEL, J. R. & KROONENBERG, P. M. 2014. Analysis of Variance of Multiply Imputed Data. *Multivariate Behavioral Research*, 49, 78-91.

References

- VAN WINKLE, A. P., GATES, I. D. & KALLOS, M. S. 2012. Mass transfer limitations in embryoid bodies during human embryonic stem cell differentiation. *Cells Tissues Organs*, 196, 34-47.
- VARGHESE, S., HWANG, N. S., CANVER, A. C., THEPRUNGSIRIKUL, P., LIN, D. W. & ELISSEFF, J. 2008. Chondroitin sulfate based niches for chondrogenic differentiation of mesenchymal stem cells. *Matrix Biology*, 27, 12-21.
- VEEVERS-LOWE, J., BALL, S. G., SHUTTLEWORTH, A. & KIELTY, C. M. 2011. Mesenchymal stem cell migration is regulated by fibronectin through $\alpha 5\beta 1$ -integrin-mediated activation of PDGFR- β and potentiation of growth factor signals. *Journal of Cell Science*, 124, 1288-1300.
- VELICHKO, Y. S., STUPP, S. I. & DE LA CRUZ, M. O. 2008. Molecular simulation study of peptide amphiphile self-assembly. *J Phys Chem B*, 112, 2326-34.
- VELICKOVIC, K., LUGO LEIJA, H. A., BLOOR, I., LAW, J., SACKS, H., SYMONDS, M. & SOTTILE, V. 2018. Low temperature exposure induces browning of bone marrow stem cell derived adipocytes in vitro. *Scientific Reports*, 8, 4974.
- VELICKOVIC, K., WAYNE, D., LEIJA, H. A. L., BLOOR, I., MORRIS, D. E., LAW, J., BUDGE, H., SACKS, H., SYMONDS, M. E. & SOTTILE, V. 2019. Caffeine exposure induces browning features in adipose tissue in vitro and in vivo. *Sci Rep*, 9, 9104.
- VENKATESAN, J., BHATNAGAR, I., MANIVASAGAN, P., KANG, K.-H. & KIM, S.-K. 2015. Alginate composites for bone tissue engineering: A review. *International Journal of Biological Macromolecules*, 72, 269-281.
- VENUGOPAL, B., FERNANDEZ, F. B., HARIKRISHNAN, V. S. & JOHN, A. 2017. Post implantation fate of adipogenic induced mesenchymal stem cells on Type I collagen scaffold in a rat model. *Journal of Materials Science: Materials in Medicine*, 28, 28.
- VERNOCHET, C., PERES, S. B., DAVIS, K. E., MCDONALD, M. E., QIANG, L., WANG, H., SCHERER, P. E. & FARMER, S. R. 2009. C/EBP α and the corepressors CtBP1 and CtBP2 regulate repression of select visceral white adipose genes during induction of the brown phenotype in white adipocytes by peroxisome proliferator-activated receptor gamma agonists. *Mol Cell Biol*, 29, 4714-28.
- VICENTE-MANZANARES, M. & HORWITZ, A. R. 2011. Adhesion dynamics at a glance. *Journal of cell science*, 124, 3923-3927.
- VILLA-DIAZ, L. G., KIM, J. K., LAPERLE, A., PALECEK, S. P. & KREBSBACH, P. H. 2016. Inhibition of Focal Adhesion Kinase Signaling by Integrin $\alpha 6\beta 1$ Supports Human Pluripotent Stem Cell Self-Renewal. *Stem Cells*, 34, 1753-64.
- VISCONTI, R. P., BARTH, J. L., KEELEY, F. W. & LITTLE, C. D. 2003. Codistribution analysis of elastin and related fibrillar proteins in early vertebrate development. *Matrix biology*, 22, 109-121.
- VOLZ, A.-C., OMENGO, B., GEHRKE, S. & KLUGER, P. J. 2019. Comparing the use of differentiated adipose-derived stem cells and mature adipocytes to model adipose tissue in vitro. *Differentiation*, 110, 19-28.
- VON DER MARK, K., GAUSS, V., VON DER MARK, H. & MÜLLER, P. 1977. Relationship between cell shape and type of collagen synthesised as chondrocytes lose their cartilage phenotype in culture. *Nature*, 267, 531-532.
- VON PALUBITZKI, L., WANG, Y., HOFFMANN, S., VIDAL-Y-SY, S., ZOBIAK, B., FAILLA, A. V., SCHMAGE, P., JOHN, A., OSORIO-MADRAZO, A., BAUER, A. T., SCHNEIDER, S. W., GOYCOOLEA, F. M. & GORZELANNY, C. 2020. Differences of the tumour cell glycocalyx affect binding of capsaicin-loaded chitosan nanocapsules. *Scientific Reports*, 10, 22443.

References

- VUONG-BRENDER, T. T. K., BEN AMAR, M., PONTABRY, J. & LABOUESSE, M. 2017. The interplay of stiffness and force anisotropies drives embryo elongation. *eLife*, 6, e23866.
- WALDÉN, T. B., HANSEN, I. R., TIMMONS, J. A., CANNON, B. & NEDERGAARD, J. 2012. Recruited vs. nonrecruited molecular signatures of brown, "brite," and white adipose tissues. *Am J Physiol Endocrinol Metab*, 302, E19-31.
- WALTERS, B. D. & STEGEMANN, J. P. 2014. Strategies for directing the structure and function of three-dimensional collagen biomaterials across length scales. *Acta Biomater*, 10, 1488-501.
- WALTERS, N. & GENTLEMAN, E. 2014. Evolving insights in cell-matrix interactions: Elucidating how non-soluble properties of the extracellular niche direct stem cell fate. *Acta Biomaterialia*, 11, 3–16.
- WANG, G., JIA, L., HAN, F., WANG, J., YU, L., YU, Y., TURNBULL, G., GUO, M., SHU, W. & LI, B. 2019a. Microfluidics-Based Fabrication of Cell-Laden Hydrogel Microfibers for Potential Applications in Tissue Engineering. *Molecules*, 24.
- WANG, G., JIA, L. L., HAN, F. X., WANG, J. Y., YU, L., YU, Y. K., TURNBULL, G., GUO, M. Y., SHU, W. M. & LI, B. 2019b. Microfluidics-Based Fabrication of Cell-Laden Hydrogel Microfibers for Potential Applications in Tissue Engineering. *Molecules*, 24, 11.
- WANG, M., BAI, J., SHAO, K., TANG, W., ZHAO, X., LIN, D., HUANG, S., CHEN, C., DING, Z. & YE, J. 2021. Poly(vinyl alcohol) Hydrogels: The Old and New Functional Materials. *International Journal of Polymer Science*, 2021, 2225426.
- WANG, M., LIU, X., LYU, Z., GU, H., LI, D. & CHEN, H. 2017. Glycosaminoglycans (GAGs) and GAG mimetics regulate the behavior of stem cell differentiation. *Colloids and Surfaces B: Biointerfaces*, 150, 175-182.
- WANG, W. & SEALE, P. 2016. Control of brown and beige fat development. *Nat Rev Mol Cell Biol*, 17, 691-702.
- WANG, Y. & JEON, H. 2022. 3D cell cultures toward quantitative high-throughput drug screening. *Trends in Pharmacological Sciences*, 43, 569-581.
- WANG, Y.-X. 2010. PPARs: diverse regulators in energy metabolism and metabolic diseases. *Cell Research*, 20, 124-137.
- WARTIOVAARA, J., LEIVO, I. & VAHERI, A. 1979. Expression of the cell surface-associated glycoprotein, fibronectin, in the early mouse embryo. *Dev Biol*, 69, 247-57.
- WEBBER, M. J., HAN, X., MURTHY, S. N., RAJANGAM, K., STUPP, S. I. & LOMASNEY, J. W. 2010a. Capturing the stem cell paracrine effect using heparin-presenting nanofibres to treat cardiovascular diseases. *J Tissue Eng Regen Med*, 4, 600-10.
- WEBBER, M. J., KESSLER, J. A. & STUPP, S. I. 2010b. Emerging peptide nanomedicine to regenerate tissues and organs. *J Intern Med*, 267, 71-88.
- WEBBER, M. J., TONGERS, J., RENAULT, M.-A., RONCALLI, J. G., LOSORDO, D. W. & STUPP, S. I. 2010c. Development of bioactive peptide amphiphiles for therapeutic cell delivery. *Acta Biomaterialia*, 6, 3-11.
- WEBBER, M. J., TONGERS, J., RENAULT, M. A., RONCALLI, J. G., LOSORDO, D. W. & STUPP, S. I. 2010d. Development of bioactive peptide amphiphiles for therapeutic cell delivery. *Acta Biomater*, 6, 3-11.
- WEDEL, A. & ZIEGLER-HEITBROCK, H. W. 1995. The C/EBP family of transcription factors. *Immunobiology*, 193, 171-85.
- WEI, D., SUN, J., BOLDESON, J., ZHONG, M., DALBY, M. J., CUSACK, M., YIN, H., FAN, H. & ZHANG, X. 2017. Continuous Fabrication and Assembly of Spatial Cell-Laden

References

- Fibers for a Tissue-Like Construct via a Photolithographic-Based Microfluidic Chip. *ACS Applied Materials & Interfaces*, 9, 14606-14617.
- WEI, W., MA, Y., YAO, X., ZHOU, W., WANG, X., LI, C., LIN, J., HE, Q., LEPTIHN, S. & OUYANG, H. 2021. Advanced hydrogels for the repair of cartilage defects and regeneration. *Bioactive Materials*, 6, 998-1011.
- WEISSMAN, I. L. 2000. Stem cells: units of development, units of regeneration, and units in evolution. *cell*, 100, 157-168.
- WEN, X., ZHANG, B., WU, B., XIAO, H., LI, Z., LI, R., XU, X. & LI, T. 2022. Signaling pathways in obesity: mechanisms and therapeutic interventions. *Signal Transduction and Targeted Therapy*, 7, 298.
- WENSTRUP, R. J., FLORER, J. B., BRUNSKILL, E. W., BELL, S. M., CHERVONEVA, I. & BIRK, D. E. 2004. Type V collagen controls the initiation of collagen fibril assembly. *Journal of Biological Chemistry*, 279, 53331-53337.
- WERNIG, M., MEISSNER, A., FOREMAN, R., BRAMBRINK, T., KU, M., HOCHEDLINGER, K., BERNSTEIN, B. E. & JAENISCH, R. 2007. In vitro reprogramming of fibroblasts into a pluripotent ES-cell-like state. *Nature*, 448, 318-24.
- WHATELEY, J. G. & KNOX, P. 1980. Isolation of a serum component that stimulates the spreading of cells in culture. *Biochem J*, 185, 349-54.
- WICHAI, S., CHUYSINUAN, P., CHAIARWUT, S., EKABUTR, P. & SUPAPHOL, P. 2019. Development of bacterial cellulose/alginate/chitosan composites incorporating copper (II) sulfate as an antibacterial wound dressing. *Journal of Drug Delivery Science and Technology*, 51, 662-671.
- WIJELATH, E. S., RAHMAN, S., NAMEKATA, M., MURRAY, J., NISHIMURA, T., MOSTAFAVI-POUR, Z., PATEL, Y., SUDA, Y., HUMPHRIES, M. J. & SOBEL, M. 2006. Heparin-II Domain of Fibronectin Is a Vascular Endothelial Growth Factor-Binding Domain. *Circulation Research*, 99, 853-860.
- WINKLER, J., ABISOYE-OGUNNIYAN, A., METCALF, K. J. & WERB, Z. 2020. Concepts of extracellular matrix remodelling in tumour progression and metastasis. *Nature Communications*, 11, 5120.
- WIPFF, P.-J., RIFKIN, D. B., MEISTER, J.-J. & HINZ, B. 2007. Myofibroblast contraction activates latent TGF- β 1 from the extracellular matrix. *The Journal of cell biology*, 179, 1311-1323.
- WOLF, K., TE LINDERT, M., KRAUSE, M., ALEXANDER, S., TE RIET, J., WILLIS, A. L., HOFFMAN, R. M., FIGDOR, C. G., WEISS, S. J. & FRIEDL, P. 2013. Physical limits of cell migration: Control by ECM space and nuclear deformation and tuning by proteolysis and traction force. *Journal of Cell Biology*, 201, 1069-1084.
- WOLFF, A., FRANK, M., STAEHLKE, S. & PETERS, K. 2022. A Comparative Study on the Adipogenic Differentiation of Mesenchymal Stem/Stromal Cells in 2D and 3D Culture. *Cells*, 11, 1313.
- WOODS, A. 2001. Syndecans: transmembrane modulators of adhesion and matrix assembly. *J Clin Invest*, 107, 935-41.
- WORKMAN, V. L., DUNNETT, S. B., KILLE, P. & PALMER, D. D. 2007. Microfluidic chip-based synthesis of alginate microspheres for encapsulation of immortalized human cells. *Biomicrofluidics*, 1, 14105.
- WU, J., BOSTRÖM, P., SPARKS, L. M., YE, L., CHOI, J. H., GIANG, A. H., KHANDEKAR, M., VIRTANEN, K. A., NUUTILA, P., SCHAART, G., HUANG, K., TU, H., VAN MARKEN LICHTENBELT, W. D., HOEKS, J., ENERBÄCK, S., SCHRAUWEN, P. &

References

- SPIEGELMAN, B. M. 2012. Beige adipocytes are a distinct type of thermogenic fat cell in mouse and human. *Cell*, 150, 366-76.
- WU, J., SRINIVASAN, S., NEUMANN, J. & LINGREL, J. 2005. The KLF2 Transcription Factor Does Not Affect the Formation of Preadipocytes but Inhibits Their Differentiation into Adipocytes †. *Biochemistry*, 44, 11098-105.
- WU, J.-J., WOODS, P. E. & EYRE, D. R. 1992. Identification of cross-linking sites in bovine cartilage type IX collagen reveals an antiparallel type II-type IX molecular relationship and type IX to type IX bonding. *Journal of Biological Chemistry*, 267, 23007-23014.
- WU, M., CRONIN, K. & CRANE, J. S. 2022. *Biochemistry, Collagen Synthesis.*, In: StatPearls [Internet], Treasure Island (FL): StatPearls Publishing.
- WU, Y. & GE, G. 2019. Complexity of type IV collagens: from network assembly to function. *Biol Chem*, 400, 565-574.
- WU, Z., SU, X., XU, Y., KONG, B., SUN, W. & MI, S. 2016. Bioprinting three-dimensional cell-laden tissue constructs with controllable degradation. *Scientific Reports*, 6, 24474.
- WU, Z. & WANG, S. 2013. Role of kruppel-like transcription factors in adipogenesis. *Dev Biol*, 373, 235-43.
- XIONG, X., XIAO, W., ZHOU, S., CUI, R., XU, H. H. K. & QU, S. 2021. Enhanced proliferation and angiogenic phenotype of endothelial cells via negatively-charged alginate and chondroitin sulfate microsphere hydrogels. *Biomedical Materials*, 16, 025012.
- XU, C., INOKUMA, M. S., DENHAM, J., GOLDS, K., KUNDU, P., GOLD, J. D. & CARPENTER, M. K. 2001. Feeder-free growth of undifferentiated human embryonic stem cells. *Nat Biotechnol*, 19, 971-4.
- XU, D., PRESTEGARD, J. H., LINHARDT, R. J. & ESKO, J. D. 2022. Proteins That Bind Sulfated Glycosaminoglycans. . In: HARBOR, C. S. (ed.) *Essentials of Glycobiology [Internet]*. New York: Cold Spring Harbor Laboratory Press.
- XU, X., JHA, A. K., HARRINGTON, D. A., FARACH-CARSON, M. C. & JIA, X. 2012. Hyaluronic Acid-Based Hydrogels: from a Natural Polysaccharide to Complex Networks. *Soft Matter*, 8, 3280-3294.
- XU, X.-D., JIN, Y., LIU, Y., ZHANG, X.-Z. & ZHUO, R.-X. 2010a. Self-assembly behavior of peptide amphiphiles (PAs) with different length of hydrophobic alkyl tails. *Colloids and Surfaces B: Biointerfaces*, 81, 329-335.
- XU, Y., ZHU, X., HAHM, H. S., WEI, W., HAO, E., HAYEK, A. & DING, S. 2010b. Revealing a core signaling regulatory mechanism for pluripotent stem cell survival and self-renewal by small molecules. *Proceedings of the National Academy of Sciences*, 107, 8129-8134.
- YALAK, G., SHIU, J.-Y., SCHOEN, I., MITSU, M. & VOGEL, V. 2019. Phosphorylated fibronectin enhances cell attachment and upregulates mechanical cell functions. *PLOS ONE*, 14, e0218893.
- YAMADA, M., UTOH, R., OHASHI, K., TATSUMI, K., YAMATO, M., OKANO, T. & SEKI, M. 2012. Controlled formation of heterotypic hepatic micro-organoids in anisotropic hydrogel microfibers for long-term preservation of liver-specific functions. *Biomaterials*, 33, 8304-8315.
- YANG, J., SUN, Y., LIU, X., XU, F., LIU, W., HAYASHI, T., IMAMURA, Y., MIZUNO, K., HATTORI, S., TANAKA, K., FUJISAKI, H., TASHIRO, S.-I., ONODERA, S. & IKEJIMA, T. 2019. Silibinin's regulation of proliferation and collagen gene expressions of rat pancreatic β -cells cultured on types I and V collagen involves β -catenin nuclear translocation. *Connective Tissue Research*, 60, 463-476.

References

- YASUAKI, K., SACHIKO, K., IKUYO, N., KAZUAKI, T. & NAKAMURA, F. 2000. Organization of Extracellular Matrix Components during Differentiation of Adipocytes in Long-Term Culture. *In Vitro Cellular & Developmental Biology. Animal*, 36, 38-44.
- YAYON, A., KLAGSBRUN, M., ESKO, J. D., LEDER, P. & ORNITZ, D. M. 1991. Cell surface, heparin-like molecules are required for binding of basic fibroblast growth factor to its high affinity receptor. *Cell*, 64, 841-848.
- YEGANEH, A., STELMACK, G. L., FANDRICH, R. R., HALAYKO, A. J., KARDAMI, E. & ZAHRADKA, P. 2012. Connexin 43 phosphorylation and degradation are required for adipogenesis. *Biochimica et Biophysica Acta (BBA) - Molecular Cell Research*, 1823, 1731-1744.
- YERLY, L., PICH-BAVASTRO, C., DI DOMIZIO, J., WYSS, T., TISSOT-RENAUD, S., CANGKRAMA, M., GILLIET, M., WERNER, S. & KUONEN, F. 2022. Integrated multi-omics reveals cellular and molecular interactions governing the invasive niche of basal cell carcinoma. *Nature Communications*, 13, 4897.
- YOKOMIZO, A., MORIMOTO, Y., NISHIMURA, K. & TAKEUCHI, S. 2019. Temporal Observation of Adipocyte Microfiber Using Anchoring Device. *Micromachines*, 10.
- YOSHIDA, S., MIWA, H., KAWACHI, T., KUME, S. & TAKAHASHI, K. 2020. Generation of intestinal organoids derived from human pluripotent stem cells for drug testing. *Scientific Reports*, 10, 5989.
- YOUNG, D. A., CHOI, Y. S., ENGLER, A. J. & CHRISTMAN, K. L. 2013. Stimulation of adipogenesis of adult adipose-derived stem cells using substrates that mimic the stiffness of adipose tissue. *Biomaterials*, 34, 8581-8588.
- YU, Y.-C., BERNDT, P., TIRRELL, M. & FIELDS, G. B. 1996. Self-Assembling Amphiphiles for Construction of Protein Molecular Architecture. *Journal of the American Chemical Society*, 118, 12515-12520.
- YUAN, C., CHAKRABORTY, S., CHITTA, K. K., SUBRAMANIAN, S., LIM, T. E., HAN, W., BHANU PRAKASH, K. N. & SUGII, S. 2019. Fast Adipogenesis Tracking System (FATS)—a robust, high-throughput, automation-ready adipogenesis quantification technique. *Stem Cell Research & Therapy*, 10, 38.
- YUE, B. 2014. Biology of the Extracellular Matrix: An Overview. *Journal of glaucoma*, 23 Proceedings of the 20th Annual Think Tank: “Exfoliation Syndrome: What We Know and Where We Need To Go” September 19-21, 2013 New York, NY Sponsored by The Glaucoma Foundation (TGF), S20-S23.
- YURCHENCO, P. D., QUAN, Y., COLOGNATO, H., MATHUS, T., HARRISON, D., YAMADA, Y. & O'REAR, J. J. 1997. The alpha chain of laminin-1 is independently secreted and drives secretion of its beta- and gamma-chain partners. *Proceedings of the National Academy of Sciences of the United States of America*, 94, 10189-10194.
- ZELTZ, C. & GULLBERG, D. 2016. The integrin–collagen connection – a glue for tissue repair? *Journal of Cell Science*, 129, 653-664.
- ZEUGOLIS, D. & RAGHUNATH, M. 2011. Collagen: materials analysis and implant uses.
- ZHANG, H. H., KUMAR, S., BARNETT, A. H. & EGGO, M. C. 2000. Ceiling culture of mature human adipocytes: use in studies of adipocyte functions. *J Endocrinol*, 164, 119-28.
- ZHANG, P., WU, W., DU, C., JI, X., WANG, Y., HAN, Q., XU, H., LI, C. & XU, Y. 2022a. RNA-seq profiling of white and brown adipocyte differentiation treated with epigallocatechin gallate. *Scientific Data*, 9, 41.
- ZHANG, S., GREENFIELD, M. A., MATA, A., PALMER, L. C., BITTON, R., MANTEI, J. R., APARICIO, C., DE LA CRUZ, M. O. & STUPP, S. I. 2010. A self-assembly pathway to aligned monodomain gels. *Nature Materials*, 9, 594-601.

References

- ZHANG, X., CHEN, X., HONG, H., HU, R., LIU, J. & LIU, C. 2022b. Decellularized extracellular matrix scaffolds: Recent trends and emerging strategies in tissue engineering. *Bioact Mater*, 10, 15-31.
- ZHANG, X. N., ZHENG, Q. & WU, Z. L. 2022c. Recent advances in 3D printing of tough hydrogels: A review. *Composites Part B: Engineering*, 238, 109895.
- ZHAO, C. 2023. Cell culture: in vitro model system and a promising path to in vivo applications. *Journal of Histotechnology*, 46, 1-4.
- ZHAO, D., PAN, Y., YU, N., BAI, Y., MA, R., MO, F., ZUO, J., CHEN, B., JIA, Q., ZHANG, D., LIU, J., JIANG, G. & GAO, S. 2021. Curcumin improves adipocytes browning and mitochondrial function in 3T3-L1 cells and obese rodent model. *R Soc Open Sci*, 8, 200974.
- ZHENG, J., XIE, Y., YOSHITOMI, T., KAWAZOE, N., YANG, Y. & CHEN, G. 2022. Stepwise Proliferation and Chondrogenic Differentiation of Mesenchymal Stem Cells in Collagen Sponges under Different Microenvironments. *International Journal of Molecular Sciences*, 23, 6406.
- ZHONG, J., YANG, Y., LIAO, L. & ZHANG, C. 2020. Matrix stiffness-regulated cellular functions under different dimensionalities. *Biomaterials Science*, 8, 2734-2755.
- ZHOU, C., DUAN, M., GUO, D., DU, X., ZHANG, D. & XIE, J. 2022. Microenvironmental stiffness mediates cytoskeleton re-organization in chondrocytes through laminin-FAK mechanotransduction. *International Journal of Oral Science*, 14, 15.
- ZHU, M. M., MOLLET, M., HUBERT, R. S., KYUNG, Y. S. & ZHANG, G. G. 2017. Industrial Production of Therapeutic Proteins: Cell Lines, Cell Culture, and Purification. *Handbook of Industrial Chemistry and Biotechnology*, 1639-69.
- ZHUANG, Y., WANG, X., NGUYEN, H. T., ZHUO, Y., CUI, X., FEWELL, C., FLEMINGTON, E. K. & SHAN, B. 2013. Induction of long intergenic non-coding RNA HOTAIR in lung cancer cells by type I collagen. *Journal of Hematology & Oncology*, 6, 35.
- ZIMMERMAN, E., GEIGER, B. & ADDADI, L. 2002. Initial stages of cell-matrix adhesion can be mediated and modulated by cell-surface hyaluronan. *Biophys J*, 82, 1848-57.
- ZOICO, E., RUBELE, S., CARO, A., NORI, N., MAZZALI, G., FANTIN, F., ROSSI, A. & ZAMBONI, M. 2019. Brown and Beige Adipose Tissue and Aging. *Frontiers in Endocrinology*, 10.
- ZOLLINGER, A. J. & SMITH, M. L. 2017. Fibronectin, the extracellular glue. *Matrix Biology*, 60-61, 27-37.
- ZORKO, M. & LANGEL, Ü. 2005. Cell-penetrating peptides: mechanism and kinetics of cargo delivery. *Advanced Drug Delivery Reviews*, 57, 529-545.
- ZUCKER, S. & VACIRCA, J. 2004. Role of matrix metalloproteinases (MMPs) in colorectal cancer. *Cancer Metastasis Rev*, 23, 101-17.

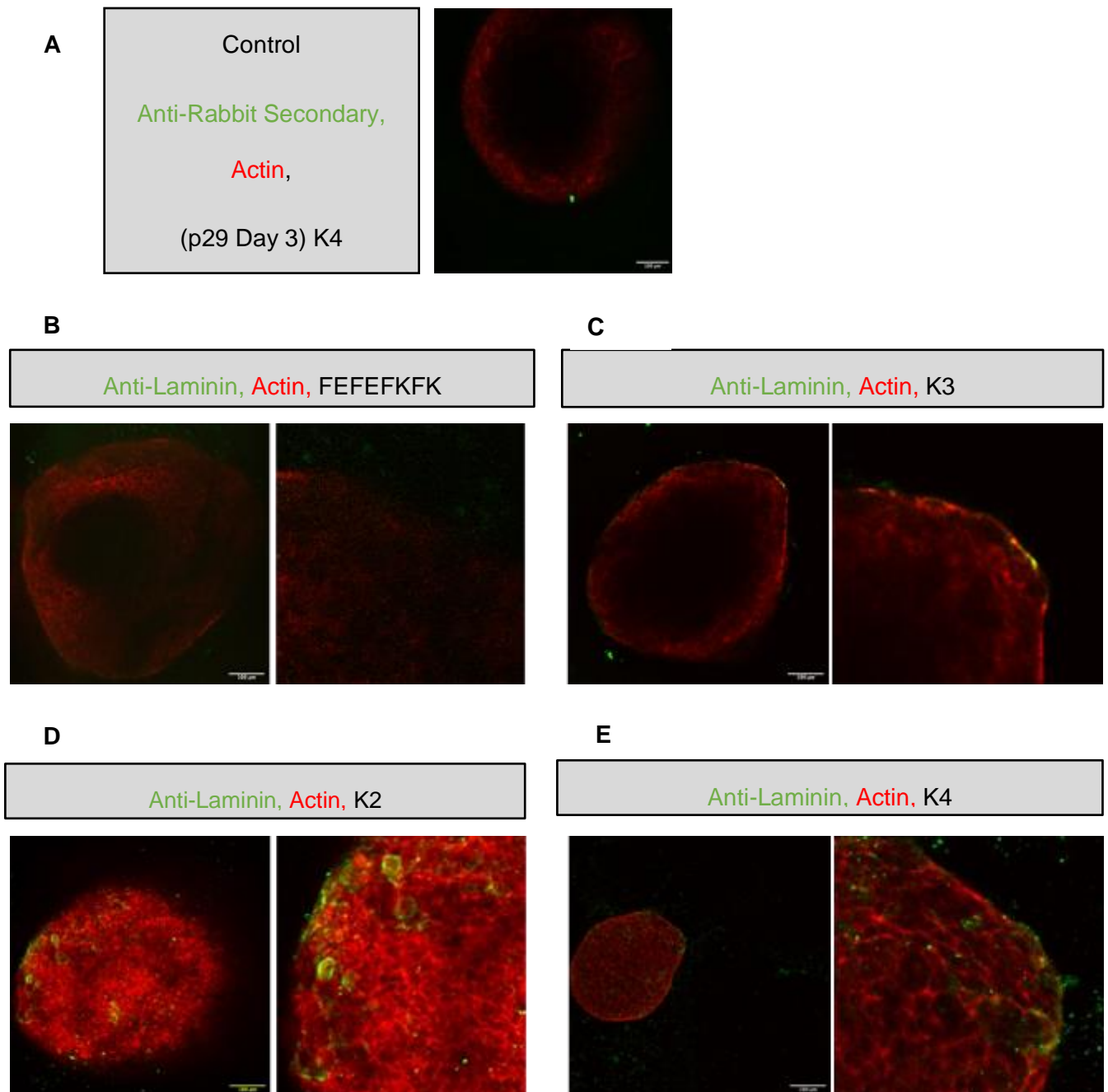
CHAPTER 5. APPENDIX

Figure 61. Anti-laminin immunostaining upon differently charged hydrogels.

The laminin staining was not found to be appropriate for inclusion in results due to the lack of staining. It was impossible to state whether the lack of staining was true result or due to problems during immunostaining. The phalloidin staining (actin) was successful but only present to assist in staining. **A** The assessment of non-specific binding of the secondary antibody. There was no evidence of non-specific binding. **B** there was no presence of the anti-laminin fluorescence on the clusters cultured on the FEFEFKFK hydrogel. **C** The anti-laminin secondary was located around single cells on the clusters upon the K2 hydrogel. **D** There was a negligible level of anti-laminin fluorescence of the clusters on the K3 hydrogel. **E** There was negligible level of anti-laminin fluorescence of the clusters on the K4 hydrogel. N = 1. Clusters were cultured for 3 days.